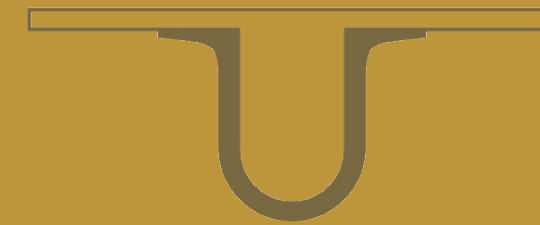




UNIVERSIDADE DE  
COIMBRA



Tânia Firmino Guerra Guerreiro da Cova

**SIMULATION OF SUPRAMOLECULAR SYSTEMS  
FOR DRUG DELIVERY  
BASED ON INCLUSION COMPLEXES**

Tese no âmbito do Doutoramento em Química, ramo de Química Macromolecular orientada pelo Professor Doutor Alberto António Caria Canelas Pais e apresentada ao Departamento de Química da Faculdade de Ciências e Tecnologia da Universidade de Coimbra.

Agosto de 2018

Faculdade de Ciências e Tecnologia

# **Simulation of Supramolecular Systems for Drug Delivery Based on Inclusion Complexes**

Tânia Firmino Guerra Guerreiro da Cova

Tese no âmbito do Doutoramento em Química, ramo de Química Macromolecular orientada pelo Professor Doutor Alberto António Caria Canelas Pais e apresentada ao Departamento de Química da Faculdade de Ciências e Tecnologia da Universidade de Coimbra.

Agosto de 2018



UNIVERSIDADE DE  
COIMBRA





The research work presented in this thesis was developed under the supervision of Professor *Alberto António Caria Canelas Pais* from the Coimbra Chemistry Centre (CQC), Department of Chemistry, Faculty of Sciences and Technology (FCTUC), University of Coimbra.

O trabalho apresentado nesta tese foi desenvolvido sob a orientação científica do Professor Doutor *Alberto António Caria Canelas Pais* do Centro de Química de Coimbra (CQC), Departamento de Química, da Faculdade de Ciências e Tecnologia (FCTUC) da Universidade de Coimbra.



*"Look at situations from all angles, and you will become more open."  
(Dalai Lama)*



# Acknowledgements

The completion of this dissertation is only possible with the support of several people. I would like to express my sincere gratitude to everyone who generously contributed to this work.

First and foremost I want to thank my advisor Professor Alberto António Caria Canelas Pais. It has been an honor to be his Ph.D. student. He has taught me how good data science, computational chemistry and whole science, is done. I appreciate all his dedication, continuous support and contributions to make my Ph.D. experience stimulating and productive. The intrinsic enthusiasm for his research, his students and collaborators, is inspiring, motivational and contagious.

Muito obrigado Professor pelos ensinamentos que me transmitiu ao longo desta maratona. Foi um grande estímulo e incentivo para ultrapassar várias etapas. A recompensa para uma coisa bem feita é tê-la feita! Ficar dependente dos resultados afasta-nos do momento presente. Obrigado também por todos os conhecimentos que me transmitiu, pela paciência e disponibilidade, pelo talento magistral e intelecto admirável. À medida que vamos descobrindo como a nossa mente trabalha começamos a ver que na vida temos aquilo que pensamos, e que temos tendência para conseguir o que o nosso subconsciente espera. No entanto, para termos êxito temos que nos sentir gratos por quem nos ajuda e orienta. Uma atitude de gratidão assegura que a nossa atenção se mantém no que queremos, não perdemos o foco e podemos assim, conseguir atingir o que ambicionamos. Os nossos objectivos são veículos através dos quais podemos vir a ser algo mais do que já somos, não tanto pelo que nos trazem, mas pelo que fazem por nós. Foi um trabalho hercúleo do qual me orgulho e que não teria sido possível sem a ajuda do Professor.

*"Quer pense que terá sucesso, ou não, estará correcto." (Henry Ford)*

Agradeço postumamente ao Professor Doutor Sebastião José Formosinho Sanches Simões, um grande Investigador em diversas áreas. Uma pessoa acessível, sempre disponível, de uma enorme simpatia, que nunca evitou um confronto científico. Um ser humano de exceção, com o qual tive o privilégio



de trabalhar.

*"Espíritos grandiosos sempre encontraram oposição violenta de mentes medíocres." (Albert Einstein)*

Ao Professor Doutor Jorge Luís Gabriel Ferreira da Silva da Costa Pereira com quem iniciei todo este processo, por todos os ensinamentos, incentivo e apoio. Sempre procurou uma solução para me ajudar quando tudo estava mais difícil. Ter objectivos e atingir as metas faz parte da natureza humana, mas também é importante o que aprendemos e o que crescemos durante o percurso.

*"Nenhum dever é mais importante do que a gratidão." (Cícero)*

Ao Professor Doutor Artur José Monteiro Valente pela disponibilidade, confiança e colaboração em vários trabalhos científicos. Sabemos que não se atingem objectivos sem que existam alguns contratempos. No entanto, fazem parte do modo como tudo está planeado, porque alguns só se alcançam através de muitas correcções. Tudo faz parte do mesmo processo de aprendizagem. Não é vergonha falhar, vergonha é nunca ter tentado.

*"A inteligência é a habilidade de se adaptar às mudanças." (Stephen Hawking)*

Ao Professor Doutor J. Sérgio Seixas de Melo e à Doutora Filipa Lã pela simpatia e apoio que sempre manifestaram, pelo dinamismo e interesse em ajudar a encontrar soluções em diversas situações.

Ao Professor Doutor Jorge Manuel Campos Marques, pela simpatia e pela disponibilidade para discutir e analisar questões que a ciência e a investigação muitas vezes nos colocaram ao longo deste percurso.

Ao Professor Doutor Rui Fausto Martins Ribeiro Silva Lourenço e à Professora Doutora Teresa Margarida Vasconcelos Dias Pinho e Melo expresso a minha gratidão pelo acolhimento no Centro de Química de Coimbra e no Departamento de Química da Universidade de Coimbra, por terem proporcionado todas as condições necessárias ao desenvolvimento deste trabalho e pela disponibilidade que sempre demonstraram.

Estendo ainda o meu agradecimento aos restantes Professores e Funcionários do Departamento de Química e da Faculdade de Ciências e Tecnologia da Universidade de Coimbra que contribuíram para o culminar desta etapa, pela simpatia e apoio demonstrados.

À minha Família a quem dedico esta tese. Muito obrigado aos meus pais (Isabel Guerra e Victor Cova) pela dedicação e amor incondicional, pela paciência e apoio, e pelo incentivo nos momentos de maior cansaço. Sempre disponíveis para tudo, obrigado pela confiança e fé que depositaram em mim, sempre acreditando nas minhas capacidades e nunca duvidando do meu sucesso. Sempre me ensinaram que ser feliz é continuar a desejar aquilo que já temos, olhar a vida com optimismo e simplicidade, porque às vezes somos felizes e não sabemos.

Muito obrigado aos meus avós (Vitorina Guerra e Francisco Firmino) pelo exemplo de vida que sempre me deram. Sempre torceram pelo meu sucesso. Como diria *Balzac*: "*Cada idade tem a sua juvenude*", e ambos apesar da idade são dois jovens que muito admiro.

Aos meus Tios e Primos, sempre presentes. Obrigado pelo incentivo, apoio e carinho ao longo destes anos. Um obrigado muito especial à minha Tia, Luísa Firmino, a quem dedico esta frase de *Voltaire*: "*Não é a nossa condição social mas a qualidade da nossa alma que nos torna felizes*". Obrigado pela generosidade e apoio! Sei que a família vem sempre em primeiro lugar, e que para ti o que vale, acima de todas as coisas, é levar um pouco de felicidade aos outros, mas também devemos respeitar o seu direito de viver como querem.

A todos os Amigos e Colegas de trabalho que me ajudaram e apoiaram, criando um ciclo de afecto que facilitou muito a tarefa até ao fim desta etapa. O meu agradecimento vai para todos sem excepção. Como alguém disse e eu subscrevo: "*Um sonho é apenas um sonho se o sonharmos sozinhos, mas se o sonharmos com os nossos Amigos será o início de uma coisa real. Um amigo é alguém que nos ajuda a descobrir a meta que queremos alcançar e nos acompanha durante uma parte do caminho.*"

À Carla Vitorino, Amiga de todas as horas, sempre disponível e disposta a ajudar. Um ser humano excepcional com quem tenho a sorte e o prazer de trabalhar. Uma irmã adoptiva que merece tudo de bom na vida. Uma grande amizade constrói-se com pequenos gestos e momentos partilhados de apoio e afecto.

À Sandra Nunes, ao Zé Gaspar e ao Guilherme, grande amor e alegria de ambos, com quem tenho partilhado muitos momentos de ternura, que só um "Feijãozinho" pode proporcionar. Muito obrigado Sandra pela cumplicidade, disponibilidade e ajuda também no local de trabalho. Acredito que a Colega e a Amiga não existem uma sem a outra, e que uma boa Amizade está acima de qualquer coisa.

À Dulce Gabriel, uma irmã de alma e coração de longa data. Uma Amiga especial com quem passo

momentos hilariantes, alguns imprevisíveis, que só alguém com uma luz muito especial nos pode proporcionar.

À Simone Ferreira pela disponibilidade e simpatia com que sempre me brindou e por quem tenho um enorme carinho.

*"A Amizade consiste em esquecer o que se dá e recordar o que se recebe, fazendo com que a vida valha a pena ser vivida." (Alexandre Dumas).*

Às minhas Colegas e Amigas Anabela, Telma, Cláudia e Andreia, pela disponibilidade e apoio e pela ajuda no momento certo. Sei que posso contar com vocês. Tudo o que temos é o presente e viver o presente significa agir sem nenhum medo das consequências. Vocês merecem estar bem. Aproveitem todos os momentos.

Agradeço ainda à Fundação para a Ciência e a Tecnologia (FCT) pelo financiamento através da atribuição da Bolsa de Doutoramento com a referência SFRH/BD/95459/2013.



# Abstract

The accurate description and quantification of the interaction patterns, energetics and binding affinities of host-guest systems by means of molecular dynamics (MD) and free-energy calculations have gained increasing interest in pharmaceutical technology and drug delivery applications. In spite of its importance, many conceptual and practical aspects are still under intense scrutiny, particularly those related to the molecular origin, strength, and individual/cooperative action of the driving forces governing soft associations in this type of systems. Relevant paradigms of such factors in understanding molecular recognition and binding, in inclusion complexes consisting of cyclic oligosaccharides, including cyclodextrins (Cds), or water-soluble glycoluril-based macrocycles, bambusurils (BUs), and guest molecules of different natures and sizes, are the critical roles of solvent, enthalpy, entropy and conformational contributions. Naphthalene (Np), adamantane (Ad), lycorine, and hyaluronan derivatives (Hy), and also small ionic species are used as models of leading structures of promising therapeutic agents and serve as model building blocks in supramolecular structures and self-assembled systems.

In this context, the work described in this dissertation aims at developing a systematic modeling approach for understanding the factors that govern the formation of supramolecular nanostructures resorting to MD and potential of mean force calculations. The main topics gather different aspects in quantifying host-guest binding. Firstly, self-consistent algorithmic approaches for exploring conformational space and decomposing energy changes are developed and combined with the automated selection of representative molecular structures and inclusion/binding modes, providing the initial conformations for free-energy calculations. The focus is given to the systematic generation of complex delegates covering a wide range of accessible molecular conformations and host-guest interaction modes. This input information is subsequently used for developing binding affinity models and

introducing a broad picture on the structure and dynamics of several molecular systems, suitable as biocompatible platforms for drug delivery. Applications include (i) the prediction of the preferred binding modes and affinities, and the quantification of interaction and energy components guiding complex formation, in water, between  $\beta$ -Cd and several Np derivatives, (ii) the assessment of the effect of guest size, host flexibility and cavity size in supramolecular complexation involving  $\beta$ - and  $\gamma$ -Cds and Np, Ad and lycorine derivatives, (iii) the establishment of thermodynamic signatures and identification of stabilizing/destabilizing noncovalent interaction within the complexes between Hy bearing monomeric  $\beta$ -Cd and Ad moieties, used as models of network junction nodes, (iv) the description of the aggregation process, in water, between Cds in the absence and in the presence of hydrophobic or amphiphilic guests, and finally (v) the study of the caging ability of BUs to anions, also in aqueous media, to focus on a different type of complexes. It is shown that substitution of Np promotes an increase in the complexation constant (up to 100-fold), irrespective of the nature of the substituent. Entropy does not favor inclusion, being the order of magnitude of the binding free-energy given by the enthalpy component, with a dominating host-guest interaction contribution. Complexation is also governed by the available Cd cavity volume, as guest fitting variations and the enthalpy penalty from Cd deformation impact on the binding constants (promoting a reduction of up to  $10^4$ ). The often neglected Cd deformation plays, thus, an important role in the interaction behavior of larger cavity Cd-based systems, being crucial in the recognition phenomena. It corresponds to an increase in energy of up to ca.  $90 \text{ kJ mol}^{-1}$ . Distortion is not significant in  $\beta$ -Cd, and larger guests promote higher binding constants. Complex stability and desolvation of the host cavity and guest backbone are related. Complexes with  $\gamma$ -Cd are generally less stable than those with  $\beta$ -Cd, since deformation in  $\gamma$ -Cd opposes inclusion and binding. It is also observed that structural variations promote major changes in the thermodynamic variables. The presence of amphiphilic chains in both host and guest molecules emphasizes inclusion and drastically increases the binding constant (to ca.  $10^{28}$ ). In what pertains to  $\beta$ -Cd aggregation in water, it is concluded that  $\beta$ -Cds may form dimers with varying arrangements and proximities between one primary portal and one secondary portal, two primary portals, and two secondary portals. The model guest, poly(vinyl alcohol), promotes the formation of Cd dimers and contains both hydrophilic and hydrophobic groups that interact either with the outside part of Cds or form inclusion complexes.

Finally, water-soluble BUs can bind and isolate inorganic anions in the center of the hydrophobic cavity, with high affinity and selectivity. The latter are hermetically sealed inside the cavity, as a result of a concerted action involving conformation and desolvation of both ion and BU cavity.

In summary, the effect of (i) the nature, size and orientation of guest molecules, (ii) non-included guest moieties (iii) substituents in both guest and host molecules, (iv) host conformation, flexibility and cavity size, (v) host and guest desolvation, (vi) nature and strength of host-guest interactions, and (vii) energy contributions, on the stability constants are duly assessed. Comprehensive thermodynamic schemes are provided, in which host-guest interactions, host conformation and size, and solvation play the leading roles. Substantial modulation of the inclusion complexes, as well as the character of the network interaction sites and the formation of small aggregates, can thus be achieved imposing different substituents and arrangements; this has direct implications upon the design of supramolecular structures with tailored properties based on these complexes.

**Keywords:** Supramolecular structures; Inclusion complexes; Host-guest interactions; Molecular simulation; Drug delivery.



# Resumo

Uma descrição precisa e quantificação dos padrões de interação, incluindo energias e afinidades de ligação, dos sistemas hospedeiro-hóspede (H-G) por meio de dinâmica molecular (MD) e cálculos de energia livre têm atraído um crescente interesse devido a aplicações em tecnologia farmacêutica e administração de fármacos. Apesar da sua importância, muitos aspectos conceituais e práticos ainda estão sob intenso escrutínio, incluindo a origem molecular e a dualidade ação individual/cooperativa das forças que governam a associação neste tipo de sistemas. As contribuições do solvente, entalpia, entropia e conformação constituem paradigmas relevantes de tais fatores em complexos de inclusão com oligossacarídeos cíclicos, incluindo ciclodextrinas (Cds) ou macrociclos constituídos por grupos glicolúricos, os bambusurilos (BUs), e moléculas hóspede (G) de diferentes naturezas e tamanhos. Derivados de naftaleno (NP), adamantano (Ad), licorina e ácido hialurônico (Hy) e também pequenas espécies iônicas são usados como modelos de estruturas representativas de uma extensa série de agentes terapêuticos promissores e servem também como blocos de construção em estruturas supramoleculares e sistemas auto-agregados. Neste contexto, o trabalho descrito nesta dissertação visa desenvolver uma modelação sistemática para compreender os fatores que governam a formação de nanoestruturas supramoleculares baseadas em complexos H-G, recorrendo à MD e a cálculos de potencial de força média. O foco principal tem a ver com a quantificação da ligação H-G. São desenvolvidas abordagens algorítmicas auto-consistentes para explorar o espaço conformacional e diferenças de energia em termos resultantes de decomposição sistemática em componentes energéticas relevantes. Estas resultam de uma combinação com uma seleção automatizada de estruturas moleculares representativas e imposição dos modos de inclusão/ligação, fornecendo as conformações iniciais. Estas informações de entrada são usadas para desenvolver modelos de afinidade de ligação e descrever a estrutura e dinâmica de vários sistemas moleculares, adequados como plataformas biocompatíveis para admin-



istração de fármacos. As aplicações incluem (i) a previsão dos modos e afinidades de ligação, e a quantificação de componentes de interação e energia que estabelecem a formação do complexo, em água, entre  $\beta$ -Cds e vários derivados de Np contendo diferentes substituintes, (ii) a avaliação do efeito do tamanho de G, da flexibilidade do H e do tamanho da cavidade na complexação supramolecular, envolvendo derivados  $\beta$ - e  $\gamma$ -Cds, e Np, Ad e licorina (iii) o estabelecimento de grandezas termodinâmicas relevantes e a identificação de interações estabilizadoras/desestabilizadoras dentro dos complexos entre derivados de ácido hialurônico portadores de  $\beta$ -Cd e Ad, usados como modelos de pontos de junção em redes transientes, (iv) a descrição do processo de agregação, em água, entre Cds na ausência e na presença de G hidrofóbicos ou anfifílicos, e finalmente (v) inspecionar a capacidade de inclusão de aniões em BUs, também em meio aquoso, para tornar mais amplo o leque de aplicações. Mostra-se que a substituição do Np promove um aumento na constante de complexação (até 100 vezes), independentemente da natureza do substituinte. A entropia não favorece a inclusão, sendo a ordem de grandeza da energia livre de ligação dada pelo componente entálpico, com uma contribuição dominante da interação H-G. A complexação é também afetada pelo volume disponível na cavidade da Cd, promovendo variações na adaptação de moléculas H e observando-se uma penalização resultante da entalpia de deformação de Cd nas constantes de ligação (que podem diminuir até um fator de  $10^4$ ). A deformação da Cd, tantas vezes negligenciada, desempenha, assim, um papel importante no comportamento de interação de sistemas baseados em Cd de cavidades maiores, sendo crucial em fenômenos associados de reconhecimento molecular. Nos sistemas estudados, pode penalizar a energia de associação até ca.  $90 \text{ kJ mol}^{-1}$ . A distorção não é tão significativa na  $\beta$ -Cd, onde G de maiores dimensões promovem constantes de ligação mais elevadas. A estabilidade do complexo está relacionada com a dessolvatação da cavidade do H e do G. Complexos com  $\gamma$ -Cd são geralmente menos estáveis do que aqueles com  $\beta$ -Cd, já que a deformação em  $\gamma$ -Cd se opõe à inclusão e à ligação. Observa-se também que variações estruturais promovem grandes mudanças nas variáveis termodinâmicas. A presença de cadeias anfifílicas nas moléculas H e G enfatiza a inclusão e aumenta drasticamente a constante de ligação (até  $10^{28}$ ). No que diz respeito à agregação de  $\beta$ -Cd em água, conclui-se que estas moléculas podem formar dímeros com arranjos e proximidades variáveis. Utilizando álcool polivinílico como G, verifica-se que este promove a formação de dímeros de Cd, e que contém grupos hidrofílicos e hidrofóbicos que interagem com a parte externa de Cds ou

formam complexos de inclusão. Finalmente, BUs solúveis em água podem incluir e isolar aniões inorgânicos no centro da cavidade hidrofóbica, com alta afinidade e seletividade. Estes últimos podem ser hermeticamente selados dentro da cavidade, como resultado de uma ação concertada envolvendo modificação na conformação e dessolvatação do ião e da cavidade do BU. Em resumo, (i) a natureza, tamanho e orientação das moléculas hóspedes, (ii) zonas da molécula hóspede não incluídas (iii) substituintes nas moléculas hóspedes e hospedeiras, (iv) conformação do hospedeiro, flexibilidade e tamanho da cavidade, (v) dessolvatação de hospedeiros e hóspedes, (vi) natureza e força das interações hospedeiro-hóspede, e (vi) contribuições dos diversos termos da energia de interação sobre as constantes de estabilidade são fatores estudados em detalhe. Fornecem-se esquemas termodinâmicos abrangentes, nos quais as interações entre hospedeiro-hóspede, conformação e tamanho do hospedeiro e solvatação desempenham os papéis principais. A modulação de complexos de inclusão, controlando a estabilidade dos sítios de interação numa rede transiente e a formação de pequenos agregados, pode ser alcançada impondo diferentes substituições e arranjos. Tal tem implicações diretas no projeto racional de estruturas supramoleculares baseadas nestes complexos.

**Palavras-chave:** Estruturas supramoleculares; Complexos de inclusão; Interações host-guest; Simulação molecular; Administração de fármacos.



# List of Abbreviations

- ABF** – Adaptive biasing force
- ACF** – Autocorrelation functions
- AFM** – Atomic force Microscopy
- Ald** – Aldehydic chain
- AIM** – Theory of Atoms in Molecules
- AmB** – Amphotericin B
- AnB** – Aniline blue
- Anh** – Anhydrolycorine
- APR** – Attach-pull-release method
- BU** – Bambusuril
- BSA** – Bovine serum albumin
- CB** – Cucurbituril
- Cd** – Cyclodextrin
- CHX** – Chlorhexidine digluconate
- CNCs** – Cellulose nanocrystals
- COM** – Center-of-mass
- DFT** – Density Functional Theory
- DLS** – Dynamic-Light Scattering
- DSC** – Differential Scanning Calorimetry
- ELF** – Electron Localization Function
- ESI-MS** – Electrospray mass spectrometry
- FEP** – Free-energy perturbation

**FF** – Force field

**FTIR** – Fourier Transform Infrared Spectroscopy

**5-FU** – 5-fluorouracil

**GO** – Glycosidic oxygen

**HACC** – Modified chitosan

**hAgo2** – Human Argonaute 2

**HEC** – Hydroxyethyl cellulose

**HG** – Host-Guest

**hmCB** – Hemicucurbituril

**HP** – Hydroxypropyl

**HPC** – Hydroxypropyl cellulose

**HPMC** – Hydroxypropylmethyl cellulose

**Hy** – Hyaluronic acid

**IGM** – Independent Gradient Method

**ITC** – Isothermal titration calorimetry

**MAh** – Maleic anhydride

**MD** – Molecular Dynamics

**MC** – Monte Carlo

**MCE** – Methylcellulose

**MFC** – Microfibrillated cellulose

**MM-GBSA** – Generalized Born and Surface Area Continuum Solvation

**MM-PBSA** – Molecular Mechanics Poisson-Boltzmann Surface Area

**MOI** – Principal moments of inertia

**NCI** – Noncovalent interactions

**NPR** – Naphthalene derivatives

**NMR** – Nuclear Magnetic Resonance

**PCS** – Photon Correlation Spectroscopy

**PEO** – Poly(ethylene oxide)

**PME** – Particle mesh Eward

**PMF** – Potential of mean force  
**PS** – Phosphorothioate thymidine  
**PVA** – Poly(vinyl alcohol)  
**QM** – Quantum Mechanical *ab initio*-methods  
**QM/MM** – Quantum Mechanics/Molecular Mechanics  
**RMSD** – Root-mean-square deviation  
**RRHO** – Rigid Rotor Harmonic Oscillator  
**SEB** – Sulfobutylether  
**SEM** – Scanning Electron Microscopy  
**SMD** – Steered Molecular Dynamics  
**TEM** – Transmission Electron Microscopy  
**TGA** – Thermogravimetric Analysis  
**THR** – L-threoninol-thymine  
**TI** – Thermodynamic Integration  
**TST** – Transition State Theory  
**WHAM** – Weighted Histogram Analysis Method  
**XRPD** – X-ray Powder Diffractometry



# Preface

The design, assembly and modeling of soft supramolecular structures based on small building blocks, including cyclodextrin (Cd) inclusion complexes, Cd-based conjugates and bambusurils are revised in **Chapter 1**. The respective applications as biocompatible platforms for drug delivery are also outlined. Prior to specific applications, **Chapter 2** summarizes the entire theoretical background in terms of relevant phenomena, structure and energy quantification in host-guest associations, as well as the molecular dynamics-based methods for free-energy calculations and thermodynamic characterization of the binding process. The designed algorithmic approaches for exploring conformational space and decomposing energy changes, and selecting representative molecular structures and inclusion/binding modes are also described. Relevant aspects for optimizing the procedure in umbrella sampling, construction of the potential of mean force (PMF) profiles, and the analysis of the thermodynamic aspects of inclusion are also presented. In a first application described in **Chapter 3**, the effect of non-included moieties in the stability constants of host-guest complexes is investigated. Bearing in mind that, in most cases, the host cavity cannot fully accommodate the guest, the free-energy oriented approach (described in **Chapter 2**), which is based on Molecular Dynamics, PMF calculations and the "flexible molecule" approximation, is applied for estimating binding constants of inclusion complexes between  $\beta$ -Cd and different naphthalene derivatives with pendant hydrophobic and hydrophilic groups.

**Chapter 4** deals with the question whether (and how) the accessible cavity volume for guest molecules of different natures and sizes determines the intimate conformations and stability of the Cd-based complexes. The interaction patterns and the leading factors affecting the thermodynamic signatures and stability of inclusion complexes between Cds with different cavity sizes, and different model guests are detailed, combining the previously designed MD/PMF-based procedure and the analysis



of the electronic charge density of the binding partners and the respective gradients, which allows visualizing and quantifying regions of stabilizing/destabilizing noncovalent interactions.

The effect of polymer pendant modification over the thermodynamic signatures and association/binding constants of the partner junction sites has not been addressed so far, in the context of network stabilization, being the main focus of **Chapter 5**.

The self-aggregation capability of Cds has also aroused great controversy, being affected, among other aspects, by the type of Cd present in the aqueous solution. While the aggregates of  $\alpha$ -Cd and  $\gamma$ -Cd can be completely removed by conventional filtering, the formation  $\beta$ -Cd dimers or possibly larger aggregates usually persists in solution, displaying fast aggregation kinetics. This suggests that the hydrophilic Cd portals play a definite role in the aggregation process. Additionally, the assembly of Cd molecules in aggregates, in the presence of guest candidates deserves also further attention. These aspects are assessed in **Chapter 6**, in which a timely and critical review on the phenomenon of Cd aggregation and the respective supramolecular properties, including computational rationales are presented. Atomistic simulations are performed to explore the formation of Cd dimers, displaying different arrangements, and to inspect the inclusion behavior, in water, of the complexes between  $\beta$ -Cds and poly(vinyl alcohol) molecules. The relevance of the latter is associated to the ability of the polymer to form hydrogels, exhibiting a high degree of swelling in water, with potential for being used as matrix in drug delivery.

Finally, a challenge on the supramolecular chemistry of bambusurils is to understand the affinity trends of these receptors towards anions. Computer simulations of the bambusuril systems, employing systematic approaches, are almost inexistent and are clearly useful to predict and guide such studies. Other results previously obtained with larger anionic species seem to point towards the feasibility of obtaining interesting supramolecular structures, which further motivates exploring the potential of these macrocycles, particularly some water-soluble derivatives. In this context, one of the first *in silico* studies based on MD for describing the binding affinity of bambusurils is presented in **Chapter 7**. **Chapter 8** summarizes the main findings and provides suggestions for future work.

# Contents

<b>Acknowledgements</b>	<b>7</b>
<b>Abstract</b>	<b>i</b>
<b>Resumo</b>	<b>v</b>
<b>Preface</b>	<b>xiii</b>
<b>1 General Introduction</b>	<b>1</b>
1.1 Context and relevant aspects . . . . .	3
1.1.1 Correlation between structure and energy . . . . .	4
1.2 Host-guest systems based on Cyclodextrins in pharmaceutical technology and drug delivery . . . . .	5
1.2.1 Structure and properties . . . . .	6
1.2.2 Inclusion complexes . . . . .	8
1.2.3 Polymers . . . . .	12
1.2.4 Aggregates . . . . .	21
1.3 Modeling soft supramolecular structures . . . . .	22

1.3.1	Applications	26
1.4	Motivation and aims	33
<b>2</b>	<b>Theory and Methods</b>	<b>55</b>
2.1	Free-energy calculations and rare events	56
2.1.1	Calculating free-energy differences	59
2.2	Potential of mean force	61
2.3	Steered molecular dynamics and umbrella sampling automation	64
2.3.1	Building the PMF profile	68
2.4	Thermodynamics	71
2.4.1	Binding constants and the cylindrical approximation	74
2.5	Visualizing noncovalent interactions	76
<b>3</b>	<b>Free-energy Patterns and The Relevance of Non-included Moieties</b>	<b>95</b>
3.1	Context and relevant issues	96
3.2	Simulation details	96
3.2.1	General setup	97
3.2.2	Reaction coordinate and biasing procedure	98
3.2.3	Equilibrium and references	99
3.2.4	Thermodynamics of inclusion	99
3.3	Results and discussion	99
3.3.1	PMF and preferred orientation	99

---

3.3.2	Equilibrium positioning and degree of inclusion . . . . .	101
3.3.3	Comparison to experiment . . . . .	103
3.3.4	$\beta$ -Cd conformation . . . . .	104
3.3.5	Thermodynamics . . . . .	106
3.3.6	Interaction components . . . . .	111
3.3.7	Inclusion and solvation . . . . .	112
3.3.8	A closer look at the hydroxyl derivatives . . . . .	113
3.4	Overview . . . . .	115
3.5	Concluding remarks . . . . .	116
<b>4</b>	<b>Host Flexibility and Space Filling</b>	<b>125</b>
4.1	Context and relevant issues . . . . .	125
4.1.1	System construction and simulation details . . . . .	129
4.1.2	Visualization of noncovalent interactions . . . . .	132
4.2	Results . . . . .	133
4.2.1	PMF and thermodynamics . . . . .	133
4.2.2	Solvation . . . . .	136
4.2.3	Cd conformation and host-guest contact . . . . .	138
4.3	Discussion . . . . .	144
4.4	Concluding remarks . . . . .	146

<b>5</b>	<b>Network Stabilization</b>	<b>159</b>
5.1	General aspects . . . . .	159
5.2	Model and computational details . . . . .	160
5.2.1	Binding constants . . . . .	161
5.2.2	Charge density interaction analysis . . . . .	162
5.3	Computational methodology . . . . .	163
5.3.1	System components and molecular dynamics simulation setup . . . . .	163
5.3.2	Biasing procedure . . . . .	164
5.3.3	Construction of the free-energy profiles . . . . .	165
5.3.4	Equilibrium, references and energy decomposition . . . . .	165
5.3.5	NCI calculations . . . . .	166
5.4	Results and discussion . . . . .	167
5.4.1	Free-energy profiles and favorable interactions . . . . .	167
5.4.2	Thermodynamics and interaction components . . . . .	172
5.4.3	Analysis of substitution effects . . . . .	174
5.5	Concluding remarks . . . . .	175
<b>6</b>	<b>Aggregation of Cyclodextrins</b>	<b>181</b>
6.1	Controversial experimental evidence . . . . .	181
6.2	Common arrangements in Cd aggregates . . . . .	186
6.3	Applications of Cd aggregates . . . . .	187
6.4	Computational results . . . . .	188

6.5	Concluding remarks . . . . .	193
<b>7</b>	<b>Properties and Patterns in Bambusurils</b>	<b>203</b>
7.1	Anion-receptors: properties and relevant issues . . . . .	203
7.2	Structure and binding affinity . . . . .	206
7.3	Synthesis and properties . . . . .	209
7.4	Complexes . . . . .	215
7.5	Evaluating the ion caging ability . . . . .	221
7.5.1	General procedure . . . . .	222
7.5.2	Free-energy calculations . . . . .	223
7.5.3	Structural stability and cavity size . . . . .	224
7.5.4	Solvation . . . . .	228
7.5.5	Interaction components . . . . .	229
7.6	Concluding remarks . . . . .	232
<b>8</b>	<b>Conclusions and Future Prospects</b>	<b>245</b>



# List of Tables

1.1	Some physical properties of $\alpha$ -, $\beta$ - and $\gamma$ -cyclodextrins. . . . .	7
3.1	Summary of the main features assessed from the PMF profiles of the inclusion complexes between $\beta$ -Cd and naphthalene derivatives, including the minimum depth and position, and width at half height. . . . .	100
3.2	Summary of the total and averaged moment of inertia, $I_1$ , $I_2$ and $I_3$ , and aspect ratio and elongation values for the $\beta$ -cyclodextrin backbone, upon inclusion at the equilibrium state. Standard deviations of the estimated parameters are also provided. . . . .	105
3.3	Binding free energies ( $\text{kJ mol}^{-1}$ ) and association constants characterizing the complexation of NP derivatives by $\beta$ -Cd in aqueous solution. . . . .	107
3.4	Enthalpy and entropy changes ( $\text{kJ mol}^{-1}$ ), for inclusion complex formation of $\beta$ -Cd and NP derivatives at 300 K. . . . .	110
3.5	Individual interaction component change ( $\text{kJ mol}^{-1}$ ) for the inclusion process of naphthalene derivatives in $\beta$ -Cd, considering the most favorable orientation. . . . .	112
4.1	Minimum depth ( $-\Delta G_{PMF}$ ) and position ( $\xi_{z0}$ ), and width at half height (FWHM) extracted from the PMF profiles of the inclusion complexes between $\beta$ - and $\gamma$ -Cd and the model guests (Np, NpAld, Ad, AdAld, NpNH <sub>3</sub> <sup>+</sup> and Anh). . . . .	135
4.2	Binding free energies ( $\text{kJ mol}^{-1}$ ) and binding constants characterizing the complexation of by $\beta$ - and $\gamma$ -Cds in aqueous solution, at 300 K. . . . .	136



4.3	Summary of the total and averaged moments of inertia, $I_1$ , $I_2$ and $I_3$ , and aspect ratio and elongation values for the $\beta$ - and $\gamma$ -Cd backbone, upon inclusion at the equilibrium state. Standard deviations of the estimated parameters are also provided. . . . .	138
5.1	Summary of the main features assessed from the PMF profiles of the inclusion complexes between hyaluronic acid derivatives, including the minimum depth ( $\text{kJ mol}^{-1}$ ) and position (nm), and width at half height. . . . .	170
5.2	Binding free energies, enthalpy and entropy changes ( $\text{kJ mol}^{-1}$ ), and association constants for the complex formation between hyaluronic acid derivatives, at 300K and in aqueous solution. Standard deviations of the estimated association constants are also provided. . . . .	172
5.3	Individual interaction changes ( $\text{kJ mol}^{-1}$ ) for the inclusion process between hyaluronic acid derivatives. . . . .	173
5.4	Coefficient values obtained from a simple factorial design, reflecting the significance of the main substitution effects. . . . .	175
7.1	Lennard-Jones, $\Delta H_{LJ}$ , and Coulombic contributions (Coulombic, $\Delta H_{Coul}$ , and reciprocal sum, $\Delta H_{Coul_{rec}}$ ) ( $\text{kJ mol}^{-1}$ ) for the interaction between $(\text{BnCOO}^-)_{12}\text{BU}[6]$ and chloride ion. . . . .	231

# List of Figures

1.1	Chemical (left) and 3D structures (right) of $\alpha$ -, $\beta$ - and $\gamma$ -cyclodextrins. . . . .	7
1.2	Phase-solubility profiles for the solubilization of a drug as a function of the Cd host concentration. Also included is the classification of Cd-drug complexes according to Higuchi and Connors . . . . .	10
1.3	Schematic illustration of the formation of supramolecular micelles from MCE, $\beta$ -Cd and MAh/ $\beta$ -Cd. . . . .	15
1.4	Schematic representation of the mechanism for the adsorption of AnB in the hydrogels. . . . .	17
1.5	Schematic representation of the different scenarios for explaining the release mechanism involving $\beta$ -Cds and chlorhexidine digluconate (CHX), and the respective inclusion complexes. . . . .	20

- 1.6 (A) Schematic representation of the two inclusion pathways along which AmB approximates to  $\beta$ - or  $\gamma$ - cyclodextrins. (B) PMF profiles for the inclusion of AmB with  $\beta$ - and  $\gamma$ -cyclodextrins considering the two orientations. (C) Equilibrium configuration of the complex between AmB and  $\beta$ -cyclodextrin (orientation I) followed by a representation of the hydrogen bonds formed between host and guest molecules and the respective averaged number ( $\text{O-H}\cdots\text{O}$  angle  $> 135^\circ$  and  $\text{O}\cdots\text{O}$  distance  $< 3.5$  Å), as a function of the simulation time. (D) Decomposition of the PMFs into van der Waals and electrostatic host-guest and host-solvent contributions, for the complexes between AmB and  $\beta$ - and  $\gamma$ -cyclodextrin in orientation I, and AmB and  $\gamma$ -cyclodextrin in orientation II. . . . . 27
- 1.7 Schematic representation of the association coordinate for the 2:1 complex between a  $\beta$ - cyclodextrin dimer and daidzein. (Bottom) PMF profiles and representative configurations of the 2:1 complexes between the specific BHHP arrangement of  $\beta$ - cyclodextrin dimer and three different model drugs. . . . . 29
- 1.8 (A) Structural arrangement of a polyrotaxane formed formed by a poly(ethylene glycol chain included in multiple  $\alpha$ -cyclodextrins, (B) definition of the reaction coordinate,  $\xi$ , in wich both the geometrically restrained (cyan) and free (red) cyclodextrins are presented. (C) Three possible conformations (HH, HT and TT) showing different spatial arrangements of two consecutive  $\alpha$ -cyclodextrin molecules. (D-F) Free-energy profiles corresponding to the dimerization of  $\alpha$ -cyclodextrins on the poly(ethylene glycol chain, for the HH, HT and TT conformations. (G-I) Individual cyclodextrin-cyclodextrin, cyclodextrin-water, and cyclodextrin-thread energy contributions for the total free-energy, in the three conformations. . . . . 30

- 1.9 Representative conformation of the complex between PAZ domain of the human argonaute 2 (hAgo2) and the chemically modified siRNAs at 3' overhang, obtained from the last nanoseconds of the MD production runs. Panel A illustrates the relative positioning of domains and interdomain linker of the hAgo2 (using the crystal coordinates of PDB ID: 4F3T) and the positioning of the siRNA antisense strand. Panels B and C show the most representative structures of the complexes formed between PAZ domain and siRNAs, modified with phosphorothioate thymidine (PS) and L-threoninol-thymine (THR), respectively. PS and THR correspond to the second-last residues of the modified siRNAs while PS3' and THR3' correspond to the last one. Hydrogen-bonding interactions between the siRNA nucleotides and the PAZ amino acid residues are represented in black dash lines. The phosphorus, oxygen, nitrogen, hydrogen and sulphur atoms are colored in yellow, red, blue, white, and green respectively. Panels D and E correspond to the occupancies of the most prominent hydrogen bonds formed between the PAZ binding pocket and 2-nt modified nucleotides with PS and THR, respectively. The analysis of the instantaneous hydrogen bond formation was obtained using an in-house algorithm. . . . . 32
- 2.1 Illustration of the umbrella sampling method used to overcome energy barriers between stable states of the system. . . . . 63
- 2.2 Schematic representation of an AFM experiment (panel a) in which the host or guest molecules are anchored to a surface, while the binding counterparts are attached to a force sensor (micron-sized cantilever). The host-guest complex is dissociated by increasing the distance between the surface and the force sensor. In constant velocity SMD (panel b) a harmonic potential is used to displace the guest molecule along the reaction coordinate. The free end of the spring is moved at constant velocity, while the guest atoms attached to the other end of the spring are subject to the steering force. 65
- 2.3 Illustrative representation of the pulling process using the position setting, along the z-axis. . . . . 66

- 2.4 Schematic representation of the umbrella sampling procedure applied to a system along the pathway for the association/dissociation of a model guest with a host cavity. 69
- 2.5 Schematic representations of a reversible noncovalent association/dissociation process of a guest molecule (green) and a host (orange) molecule, possessing a certain binding energy difference ( $\Delta G_{bind}$ ) between the associated and dissociated states. . . . 71
- 2.6 Illustrative representation of a typical model reflecting the cylindrical approximation. The cylindrical channel, shown in brown, is embedded in the Cd cavity. When the guest molecule (green circle) enters the Cd cavity (orange truncated cone), the sampled volume for the guest is restrained to the cylinder defined by the area accessible for guest movement in the  $xy$  plane. The average radius of that cylinder,  $r_{cyl}$ , is obtained from COM positions of the guest at each sampling window. . . . . 76
- 2.7 Host-guest complexation between curcubituril and the dodecyl serine-based monomeric cationic surfactant 12SerTFAC. (Left) Reduced density gradient,  $s = 0.4$ , isosurface colored by value of  $sign(\lambda_2)\rho$  ( $-0.03 \leq sign(\lambda_2)\rho \leq 0.03$  a.u.). Blue: stabilizing, red: destabilizing and green weak interactions. . . . . 79
- 2.8 Host-guest complexation between curcubituril and 12serTFAC surfactant. (Left) IGM  $\delta g^{inter} = 0.01$  a.u. isosurface colored by value of  $sign(\lambda_2)\rho$  ( $-0.03 \leq sign(\lambda_2)\rho \leq 0.03$  a.u.). Blue: stabilizing, red: destabilizing and green: weak interactions. (Right) Scatter plot of  $\delta g^{inter}$  and  $sign(\lambda_2)\rho$  values. . . . . 80
- 3.1 Schematic representation of two pathways along which naphthalene derivative is pulled. The pathways were named according to orientation (O1 and O2) and initial position (from portal P1 or portal P2). The red point indicate where the steering force is applied. 98
- 3.2 Free energy profiles for the inclusion of naphthalene derivatives in  $\beta$ -cyclodextrin along the model reaction coordinate  $\xi$ , in two orientations: solid lines, orientation 1, dashed lines, orientation 2. . . . . 100

- 3.3 The two possible conformations of the complex between  $\beta$ -Cd and naphthalene: axial inclusion (left) and equatorial inclusion (right). Two additional axes defined by the centers of mass of the two Cd portals and corresponding to the centers of mass of the C2-C3 and C7-C8 pairs of carbons in the NP backbone are also included and used for inspecting the relative alignment between host and guest molecules. . . . . 102
- 3.4 Typical conformations (accounting for more than 50% of the occurrences) for the inclusion complexes (1:1) of  $\beta$ -Cd and naphthalene derivatives in aqueous solution, sampled during the MD simulations (using the GROMACS package and the amber99sb forcefield) at 300 K, and identified by geometric cluster analysis. The occurrence of each type of conformation is also included. Starting geometries optimized by the semi-empirical Antechamber/SQM method. Electrostatic charges obtained from AM1-BCC calculations. . . . . 102
- 3.5 Free-energy ( $\Delta G$ ), enthalpy ( $\Delta H$ ) and entropy ( $T\Delta S$ ) contributions for the complex formation of  $\beta$ -Cd with NP derivatives for the most favorable orientations (2,3-NP(OH)<sub>2</sub>, 2-NPCH<sub>3</sub>, 2-NPOH and 2-NPNH<sub>3</sub><sup>+</sup>, O1; 2-NPSO<sub>3</sub><sup>-</sup>, O2). . . . . 109
- 3.6 Coordination number for water molecules from the center of the  $\beta$ -Cd cavity in aqueous solution and in the corresponding binary systems. . . . . 112
- 3.7 Running coordination number of water molecules per substituent group as a function of distance. . . . . 113
- 3.8 Distribution of distances between hydrogen atoms of adjacent hydroxyl groups in 2,3-NP(OH)<sub>2</sub>. Dominant conformations (accounting for more than 95% of the occurrences) of 2,3-NP(OH)<sub>2</sub> in solution or included in the  $\beta$ -Cd cavity for both orientations, are depicted in the inset. These conformations were sampled during the MD simulations in the equilibrium state, at 300 K, and identified by geometric cluster analysis. . . . . 114

- 4.1 Free-energy profiles for the formation of  $\beta$ - and  $\gamma$ -Cd based inclusion complexes calculated from the integration of the mean forces (solid curves) and from the WHAM procedure (dashed curves). The curves are vertically aligned to have the Cd cavity positioned at  $\xi_z = 0.0$  nm. The error bars represent the statistical uncertainties estimated with bootstrap analysis. Also included are the structures of the complexes sampled from the A-F and A'-F' minima in the PMFs. . . . . 134
- 4.2 Coordination number for water molecules from the center of the (a)  $\beta$ -Cd and (b)  $\gamma$ -Cd cavities in aqueous solution and in the corresponding inclusion complexes. . . . 136
- 4.3 Running coordination number of water molecules relative to each guest molecule as a function of distance. . . . . 137
- 4.4 Illustrative representation of a typical model reflecting the calculation of the moments of inertia, denoted as  $I_1$ ,  $I_2$  and  $I_3$ , which are averaged over the course of the simulations. The cavities of  $\beta$ - and  $\gamma$ -Cds are positioned symmetrically along the z-component,  $I_3$ . Also described are the aspect ratio and the elongation parameters, used for evaluating the distortion degree of Cds based on  $I_1$  and  $I_2$ . . . . . 139
- 4.5 A composed view of the IGMPLOT isosurfaces and 2D scatter plots for each  $\beta$ - and  $\gamma$ -Cd complex, corresponding to structures in lower energy states (local minima sampled from the PMF profiles). Stabilizing/destabilizing noncovalent interactions are represented in blue/red and van der Waals forces are colored in green (volume cutoff of  $\delta g_{inter} = 0.05$ ; color coding:  $-0.1 \leq \text{sign}(\lambda_2)\rho \leq 0.1$ ). . . . . 141
- 4.6 An overview of the individual atomic contributions to the Cd-guest noncovalent interactions discriminated in the iso-surfaces included in Figure 4.5. A relative score (%) is attributed to each atom, which is colored using a gray-to-red color gradient, according to this percentage. Gray: no contribution to the noncovalent interaction, red: significant relative contribution to the Cd-guest interaction. . . . . 143

- 4.7 Stability constants ( $M^{-1}$ ) extracted from ([Ciobanu2013]), showing that 1:1 complexes between  $\beta$ -Cd and several terpenes are, in general, more stable than those with  $\gamma$ -Cd. . . . . 144
- 4.8 Schematic illustration of the proposed thermodynamic cycle corresponding to the formation of 1:1 complexes between  $\beta$ - and  $\gamma$ -Cds and adamantane. The estimated energy differences were estimated using the hybrid DFT TPSS0 level with D3 dispersion corrections and PCM water. The triple-zeta polarized Def2-TZVP (a) and the related Def2-TZVPP (b) with further polarization functions are the two large basis sets used to check the convergence of the energies. . . . . 145
- 5.1 Schematic representation of the system components including (top) the targeted networks in which Cd/Ad complexes play the role of junction points and (bottom) the chemical structure of the hyaluronic acid derivatives. Also included (right) are the inclusion complexes used as models of the network junction points, with increasing structural complexity. The Cd:Ad complex is used as a reference system. . . . . 161
- 5.2 (Top) Free energy profiles for the formation of inclusion complexes involving non-substituted Ad moieties: (A) Cd:Ad and (B) CdHy:Ad, calculated from the integration of the mean forces (solid curves) and from the WHAM approach (dashed curves), both presenting a high degree of overlap. All curves are vertically aligned to have the Cd cavity positioned at  $\xi_z = 0.0$  nm. The error bars represent the statistical uncertainties estimated with bootstrap analysis. (Bottom) IGMPLOT isosurfaces (side and top views) for the (A) reference system, Cd:Ad, and (B) CdHy:Ad, for complex structures sampled from the A/B minima in the upper plot. Blue/red indicates stabilizing/destabilizing noncovalent interactions and green indicates weak vdW-type interactions (volume cut-off of  $\delta g_{inter} = 0.05$ , color coding:  $-0.1 \leq \text{sign}(\lambda_2)\rho \leq 0.1$ ). 168



5.3	A composed view of the PMF profiles for the inclusion complexes between (orange) natural Cd and substituted guest AdHy, Cd:AdHy, and (red) substituted host and guest molecules, CdHy:AdHy. Also included are the 3D molecular images for the equilibrium states of Cd:AdHy (C and C') and CdHy:AdHy (D and D') complexes, showing different types and strengths of noncovalent interactions between host and guest molecules (for details see Figure 5.2). . . . .	169
5.4	IGMPlot isosurfaces (top) and 2D scatter plots (bottom) for the CdHy:AdHy system, corresponding to the deepest minimum (left) and to the higher-lying local minimum (right) of the corresponding PMF profiles, depicted in Figure 5.3, D and D', respectively.	171
5.5	Estimated $\Delta\Delta G_{bind}$ differences between the inclusion complexes corresponding to the reference system Cd:Ad (NN), Cd:AdHy (NS), CdHy:Ad (SN) and CdHy:AdHy (SS).	175
6.1	Schematic representation of packing structures of (a) cage-type; (b) layer-type Cd; and (c) head-to-tail channel-type Cd crystals. . . . .	187
6.2	Schematic illustration of the pairwise initial arrangements of $\beta$ -Cds, with facing primary and secondary portals (PS), two primary portals (PP), and two secondary portals (SS), with the colors used to distinguish $\beta$ -Cd molecules. . . . .	190
6.3	Distribution of distances between the centers of mass of $\beta$ -Cd molecules, defined by the oxygen atoms of the secondary portals. Right panels illustrate the final conformations for the imposed PS, PP and SS initial arrangements of $\beta$ -Cd molecules, in aqueous solution, sampled during the MD simulations at 300 K and identified by geometric cluster analysis. The colour codes for Cd molecules are as in Figure 6.2, while the initial arrangements are represented in black, green and red, for PS, PP and SS, respectively . . . . .	191
6.4	Cyclodextrin structures ( $\alpha$ -Cd, n=6; $\beta$ -Cd, n=7 and $\gamma$ -Cd, n=8). . . . .	192
6.5	Average autocorrelation function of C2-D bond for Cd molecules in the monomeric and dimeric states, in water at 300 K. (black and orange curves, respectively). . . . .	192

- 6.6 Summary of the MD simulations between  $\beta$ -Cd and PVA molecules. Left panels present the measured distances between the center of mass of the groups formed by (i) each  $\beta$ -Cd in the dimer ( $Dm_{AB}$ ), (ii) the secondary-secondary portals (SS), the primary-primary portals ( $Dm_{AB/PP}$ ), the secondary-primary portals (PS),  $Dm_{AB}$ -PVA,  $Dm_{AB}$ -PVB,  $Cd_A$ -PVA,  $Cd_A$ -PVB,  $Cd_B$ -PVA,  $Cd_B$ -PVB,  $Dm_{AB}$ -PVA aggregate ( $Ag(4PVA)$ ),  $Cd_A$ - $Ag(4PVA)$ ,  $Cd_B$ - $Ag(4PVA)$ , and  $Ag(4PVA)$  - 6 separated PVA molecules ( $Sg(6PVA)$ ). Right panels illustrate the 3 dominant conformations (accounting for more than 50 %, panel a, and 90 %, panels b and c, of the occurrences) sampled during the equilibrated parts of the production runs, at 300 K, in aqueous solution. The force field F-85 was used for the Cds. The electrostatic charges of PVA were calculated using the R.E.D. server and the remaining terms generated by acpype. 194
- 7.1 (a) Molecular structures of bare CB[6] (left), hmCB[6] (middle) and BU[6] (right) molecules. The shaded parts highlight one of the repeating units. (b) Electrostatic potential profiles of CB[6] (left), hmCB[6] (middle) and BU[6]. ESPs are mapped on electron density isosurfaces at the HF/6-31G(d) level of theory. The carbonyl oxygen atoms of the macrocycles are negatively charged and are colored in red, while positive regions are depicted in blue. (c) Lowest unoccupied molecular orbitals of CB[6] (left), hmCB[6] (middle) and BU[6] (right). (d) Optimized structures of a halide encapsulated in CB[6] (left), hmCB[6] (middle) and BU[6] (right) (color code: yellow refers to oxygen, bright blue to carbon, green to nitrogen, brown to halide ion and pale white to hydrogen). . . . . 208
- 7.2 Crystal structure of the complex between BU[6] and iodide including the measured (b) diameters and (c) heights. The glycoluril units of the host displayed on the upper (blue) and lower positions (yellow) are symmetric related and are at the same distance to the central anion. . . . . 209
- 7.3 General synthesis of bambusuril derivatives from the acidic-catalyzed condensation between 2,4-disubstituted glycoluril (c') and formaldehyde (d). . . . . 211

- 7.4 Representative structures of some derivatives and analogues of bambusurils. All structures were optimized at the HF/6-31G(d) level, except for the larger molecules (Bn<sub>8</sub> BU[4] and Bn<sub>12</sub>BU[6]), in which the AM1 semiempirical method was employed. Color code: red refers to oxygen; gray to carbon; blue to nitrogen and orange to sulfur atoms. . . . . 213
- 7.5 Electrostatic potential maps (left) and structure of the HOMO and LUMO (middle) and binding geometries (right) of the different complexes involving glycoluril analogs, 2a-e. Calculations were performed at the M06-2X/6-311+G\*\* level of theory. The electrostatic potential surfaces are presented in kcal mol<sup>-1</sup>, ranging from red (R) to blue (B). . . . . 220
- 7.6 Schematic representation of the pathway along which chloride ion is pulled along the z-component, with umbrella sampling. The purple circle indicates where the steering force is applied. . . . . 224
- 7.7 Typical conformations for the bare Me<sub>12</sub>BU[6], Bn<sub>12</sub>BU[6], (BnCOOH)<sub>12</sub>BU[6] hosts in aqueous solution, sampled during the MD simulations. The occurrence of each type of conformation is also included. . . . . 225
- 7.8 Schematic illustration of the structural symmetry present in the bare BU-hosts and reflected by the final arrangement of the six glycoluril units and the methyl (Me<sub>12</sub>BU[6]), phenyl (Bn<sub>12</sub>BU[6]) and carboxybenzyl ((BnCOOH)<sub>12</sub>BU[6]) substituents relative to the plane defined by the cavity methylene-linked groups. . . . . 225
- 7.9 Distribution of distances from cavity-carbon CA to cavity-carbon CB in Me<sub>12</sub>BU[6] (green), Bn<sub>12</sub>BU[6] (orange), (BnCOOH)<sub>12</sub>BU[6] (purple) and (BnCOO)<sub>12</sub>-BU[6]-Cl (magenta). The cavity-carbon atoms considered for each host, to define the relevant distances, are depicted in the structure of each molecule. . . . . 226
- 7.10 Dominant conformation (accounting for more than 94 % of the occurrences) sampled during the last 5 ns of the production run, at 298 K, for the inclusion complex of (BnCOO)<sub>12</sub>BU[6]:Cl (1:1) in aqueous solution (for details see Figure 7.7). . . . . 227

7.11	Distribution of the distances between the center of mass of the groups formed by the two oxygen atoms in each carboxybenzyl group, and the cavity center of $(\text{BnCOO}^-)_{12}\text{BU}[6]$ . Panel (a) and (b) refer to portals P1 and P2 in the hydrated host. Panels (c) and (d) correspond to the same portals in the 1:1 $(\text{BnCOO})_{12}\text{BU}[6]:\text{Cl}$ complex. A schematic illustration of the arrangement of each carboxybenzyl group is included in panel (c) and (d), with the colors used to represent the corresponding oxygen atoms. Right panel illustrates the measured distances referred in panels (a)-(d). . . . .	228
7.12	Time evolution of RMSD for the simulation of the hydrated $(\text{BnCOO})_{12}\text{BU}[6]:\text{Cl}$ complex, panel (a). Red lines represent the RMSD considering all atoms of the host; orange lines refer to the RMSD considering only the atoms of the cavity backbone. Panel (b) shows the normalized statistical distributions for the RMSD values considering the cavity-backbone and all atoms of the host. . . . .	229
7.13	Running coordination number of water molecules, calculated from the center of the BUs cavity. The average cavity radius is indicated as a dashed line in each curve. . . .	230



# Chapter 1

## General Introduction

In the past three decades, atomistic simulations and free-energy calculations have emerged as indispensable tools to tackle deep chemical and biological questions that experiment has left unresolved. To fully understand the vast majority of chemical and biological processes, it is often necessary to examine their underlying free-energy behavior. [1] This is the case, for instance, of phase diagrams, protein-ligand and drug binding affinities, drug partitioning, reaction rates, equilibrium constants, acid-base equilibria, solvation contributions, or confinement energies. The prediction of these quantities, with relevance in the field of computer-aided drug design requires knowledge of the related free-energy changes. [2, 3] Often the research topics involving molecular modeling and simulation, with free-energy calculations, stem from pharmaceutical applications. [1, 4, 5] Those methods have provided insight into the time evolution of host-guest systems and protein-ligand interactions [2, 5] and have revealed the respective dynamic behavior in water, thus establishing relevant recognition and affinity patterns. However, the formation of inclusion complexes is frequently used as a drug solubilizing approach, aiming at better therapeutic outcomes. This makes results sparse and focused on individual systems, lacking a comprehensive characterization for assessing the factors that govern, for example, the inclusion process. Despite the continuous progress and development of improved algorithms, the estimation of binding free-energies by molecular dynamics (MD) simulations still requires significant computational efforts due to the mathematical complexity imposed by the solvated systems, often composed by myriads of atoms. [4] Several (more or less accurate) strategies for estimating free-energies and host-guest binding affinities have been developed, and are discussed in Chapter 2. The common feature in these strategies is that only a small part of space representing the

most favorable host-guest complexation is considered.

In addition to several reviews (see e.g. [6, 7]), including many dealing with specific host-guest systems [5, 7–12], a large number of research papers are available on this subject, including some focused on mechanistic aspects of the inclusion phenomena (see e.g. refs. [3, 13–15]) In fact, both the efficiency and accuracy of free-energy calculations have been greatly improved by a wide variety of methods. [16] However, it is increasingly difficult for researchers to find their way through the maze of available computational techniques. Why are there so many methods? Are they conceptually related? Do they differ in efficiency and accuracy? Why do methods that appear to be very similar carry different names? Which method is the best for a specific problem? How to choose the most relevant method to tackle the system at hand? These questions may leave researchers in the field confused and looking for clear guidelines. However, answers to these questions are not straightforward. A distinction has been made between two classes of free-energy transformations, namely those of alchemical and geometrical nature. [17] While the former exploit the malleability of the potential energy function and the virtually infinite possibilities of computer simulations to transform between chemically distinct states, the latter include positional, orientational, and conformational changes in macromolecules and complexes thereof. At the practical level, such transformations are achieved using a variety of approaches, which can be separated into four main groups, (i) probability distributions and histograms, (ii) perturbation theory, (iii) non-equilibrium work and (iv) gradient-based methods. [18] One recurrent question concerns the selection of the most relevant approach to tackle the problem at hand, which can be reworded in terms of the best-suited, cost-effective method to obtain a reliable answer. To a large extent, this question can be addressed by considering the actual nature of the transformation, alchemical, or geometrical, and subsequently by deciding which one, among the aforementioned methods, is more likely to yield the desired free-energy change at a minimal computational effort.

A detailed overview of the concepts and fundamentals of the available methods for estimating free-energies is given in ref. [16]. The guiding principle is that most of these are based on a few fundamental assumptions, devised by some pioneers in the field. [19–23] With some exceptions, more recent contributions are not based on innovative fundamental principles, but are "*astute and ingenious ways of applying those already known*". [16]

## 1.1 Context and relevant aspects

In the context of supramolecular chemistry, the establishment of intermolecular noncovalent interactions between two or more entities allows creating organized structures or aggregates. These interactions are the basis of relevant chemical and biological processes, such as binding between hosts (receptors) and guests (substrates), cellular recognition, assembly of protein-based complexes, intermolecular reading of the genetic code, among others. [24, 25] The design of artificial host molecules capable of binding specific guests with high affinity and selectivity, and forming host-guest complexes and supramolecular assemblies of tailored structures and multiple functions, arises from the need to emulate weak noncovalent interactions ubiquitous in the natural systems. Hosts are commonly large molecules or aggregates (e.g. enzymes or synthetic cyclic compounds, e.g. cyclodextrins) and guest species are small organic molecules (e.g. drugs and other pharmaceutical active compounds, surfactants, organic pollutants), simple inorganic ions or more complex molecules, such as hormones. The resulting complexes have been defined as "complexes that are composed of two or more molecules or ions held together in unique structural relationships by intermolecular forces". [26, 27] These forces include individual or cooperative hydrophobic/hydrophilic attraction, electrostatic interactions, hydrogen bonds,  $\pi$ - $\pi$  interactions, van der Waals attractive forces and also solvent effects.

Host-guest chemistry is based on three fundamental principles: (i) the selective binding must involve attraction or mutual affinity between host and guest (ii) binding must be selective, involving a steric fit in which the guest has a geometric complementary size or shape relative to the host (molecular recognition), and (iii) molecular binding is the trigger for molecular activity. [10, 28]

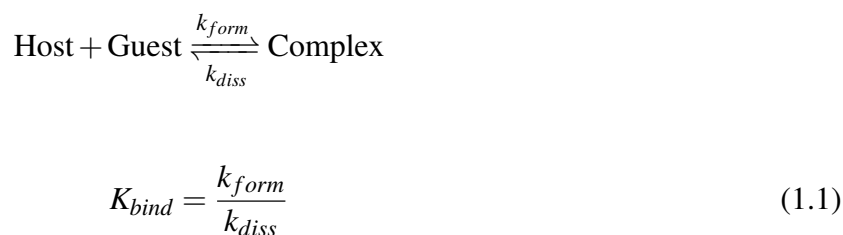
Extensive progress has been made on characterizing and quantifying the affinity of host molecules towards specific guests allowing to infer on the nature and strength of the noncovalent interactions. Controlling these supramolecular interactions allows modulating of specific chemical and biological processes. When compared to routine covalent procedures, noncovalent approaches are considered inexpensive and environmentally safe, avoiding the use of multiple organic synthetic steps. [29]



### 1.1.1 Correlation between structure and energy

The stabilizing energy of noncovalent complexes involves both host and guest molecules and also the respective environment, and generally consists of several energy terms, including electrostatics, induction, dispersion (van der Waals forces), repulsion and charge transfer. Hydrophobic interactions are also important driving forces in supramolecular complexation of guests containing hydrophobic moieties. The latter display low water solubility and tend to avoid the aqueous surrounding. Hydrophobic effects are commonly decoupled into enthalpic and entropic energy components.

Host affinity and selectivity towards specific guests depends on the host-guest binding equilibrium. A kinetically labile complex formation allowing a rapid guest exchange is thus required, considering also an upper limit for the binding constant and the free-energy of binding. In host-guest complexation the equilibrium (binding) constant  $K_{bind}$  can be determined from the ratio of the rate constants corresponding to the complex formation ( $k_{form}$ ) and dissociation ( $k_{diss}$ ) reactions,



where the dissociation rate is defined by

$$v = k_{diss}[\text{complex}] \quad (1.2)$$

and the dissociation half time by

$$\tau_{1/2} = \frac{\ln 2}{k_{diss}} \quad (1.3)$$

Solvent effects play also a critical role in host-guest design, as the net free-energy associated to the complex formation depends strongly on the solvent features, which may favor or oppose host-guest binding and complex stability. [3, 13, 30] Only recently, these components involving host, guest and

solvent effects, have been taken into account for characterizing the structure-energy relationship in host-guest systems. The Gibbs free-energy ( $\Delta G^0$ ) is a combination of the enthalpic and entropic components following the Gibbs-Helmholtz equation,  $\Delta G^0 = \Delta H^0 - T\Delta S^0$  and may change slightly with the host structure as a result of the enthalpy-entropy compensation. [3] A detailed understanding of the individual contributions of the energetic parameters allows determining the nature of the complex formation, i.e., whether the process is governed by enthalpy or entropy changes ( $\Delta H^0$  or  $\Delta S^0$  respectively).

The assessment of the interplay between the various components of this structure-energy relationship is one of the main purposes of the present dissertation. Different factors affecting the binding strength are also evaluated including the nature and size of guest, the presence of substituents in both host and guest, the size and suitability of the host cavity and the flexibility of the host backbone.

## **1.2 Host-guest systems based on Cyclodextrins in pharmaceutical technology and drug delivery**

The number of publications dealing with cyclodextrins (Cds) and the respective properties have increased ca. 55% in the last decade when compared with the previous decade (Web of Science, accessed at 20.07.2018). Such attractiveness can be explained by the ability of the Cd cavity to include a large range of hydrophobic guest molecules, such as drugs[31, 32], surfactants [33], dyes[34], polymers[35], while the hydrophilic exterior renders Cds water soluble[33]. In 2016 Cds were reported in over 2300 patents and patent applications, many of which directed to pharmaceutical applications. [36, 37]

Inclusion complexes based on Cds have been successfully used to improve the water solubility of drugs, aiming at better therapeutic efficacy. Such host-guest systems are capable of modifying the properties of the guest molecules, in particular those related with chemical reactivity and photochemical/thermal degradation, altering the chemical activity of the delivered drugs, and releasing them in a controlled manner, upon competitive binding or external stimulus (e.g. temperature and pH). Their potential for aggregation have also lead to the manufacture of nanoparticles [38, 39] and films [40],

paving the way to applications involving separation processes [41], drug delivery [42–44], tissue engineering [45], among others.

### 1.2.1 Structure and properties

Cyclodextrins are cyclic oligosaccharides that belong to a group of structurally related natural materials, formed during bacterial digestion of cellulose. [46] These consist of ( $\alpha$ -1,4)-linked  $\alpha$ -D-glucopyranose units and possess a hydrophobic cavity and a hydrophilic outer surface. Typical Cds are constituted by six ( $\alpha$ -Cd), seven ( $\beta$ -Cd), and eight ( $\gamma$ -Cd) glucopyranoside units. Recently [47], these macromolecules, and especially  $\alpha$ -Cd, have also been recognized as potential kinetic surrogates for cellulose, comparing the glycosidic bond cleavage of  $\alpha$ -Cd exhibited at low and high temperature kinetic regimes with cellulose hydrolysis. The first reference to what would later prove to be Cds was published in 1891 by Villiers. [48] From the digestion of starch by *Bacillus amylobacter*, Villiers obtained a crystalline substance at which he named "cellulosine" due to its similarity towards cellulose, with respect to the acid resistance and the absence of reducing properties. The author has also found two different distinct forms of cellulosine, which could be related with the occurrence of  $\alpha$ - and  $\beta$ -Cd forms. One decade later, two different crystalline products resulting from the digestion of potato starch by *Bacillus macerans* were reported by Schardinger [49]; these compounds were further characterized by using triiodide solutions and were known as by Schardinger dextrin. The ability of these compounds to complex with organic compounds was firstly reported by Prignsheim [50] and, in the following decades, it was found that the Schradinger dextrins are a family of natural oligosaccharides formed by 6, 7, or 8  $\alpha$ -(1,4) linked glucopyranose units (see Figure 1.1), denoted as  $\alpha$ -,  $\beta$ -, or  $\gamma$ -Cd, respectively [51, 52]. However, the work carried out by Szejtli [53] has been considered a landmark for the large scale use of Cds, in particular for their ability to form inclusion (host-guest) supramolecular complexes with a large variety of molecular guests. [46] Such interest is a direct consequence of the structure of Cds. Each of the chiral glucose units in the Cd molecules is in the rigid  $4C_1$ -chair conformation, giving the macrocycle the shape of a truncated cone with internal cavity diameter ranging from 6 to 10 Å (see Table 1.1). [46] The Cd cavity is lined by the hydrogen atoms and the glycosidic oxygen bridges. The nonbonding electron pairs of the glycosidic oxygen bridges are directed toward

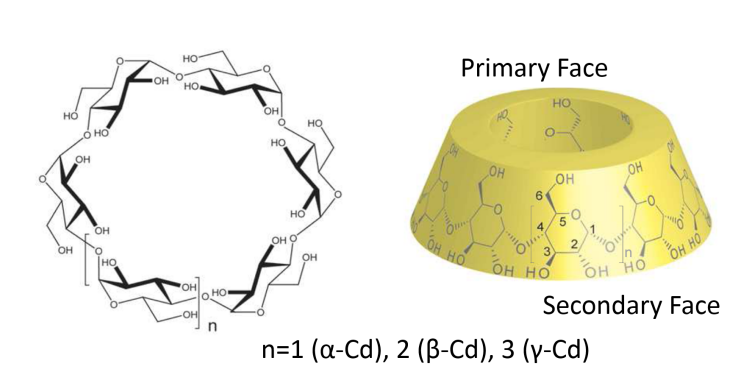


Figure 1.1: Chemical (left) and 3D structures (right) of  $\alpha$ -,  $\beta$ - and  $\gamma$ -cyclodextrins. Adapted from ref. [54]

the cavity interior, conferring some Lewis base character. Simultaneously, the hydroxyl groups are positioned outside at the edges of the truncated cone. [46] The secondary hydroxyls are responsible for intramolecular hydrogen bonds between adjacent glucopyranose unities and as consequence cannot rotate. The intramolecular hydrogen bonding of secondary hydroxyls, resulting in relatively rigid chains, may contribute for the low solubility of  $\beta$ -Cd (Table 1.1), when compared to  $\alpha$ - and  $\gamma$ -Cd. In fact, the formed secondary hydrogen bond ring is incomplete in the  $\alpha$ -Cd (only 4 hydrogen bonds out of 6 are formed); on the other hand the  $\gamma$ -Cd is non-planar being both the more flexible and the more soluble of all three natural Cds. [46]

Table 1.1: Some physical properties of  $\alpha$ -,  $\beta$ - and  $\gamma$ -cyclodextrins. [46]

Property	$\alpha$ -Cd	$\beta$ -Cd	$\gamma$ -Cd
Nb. glucose unities	6	7	8
MW ( $\text{g mol}^{-1}$ )	972	1135	1297
Solubility in water ( $\text{g L}^{-1}$ )	145	18.5	232
Outer diameter cavity (wide end) ( $\text{\AA}$ )	13.7	15.3	16.9
Inner diameter cavity (wide end) ( $\text{\AA}$ )	5.7	7.8	9.5
Volume cavity ( $\text{\AA}^3$ )	174	262	427
Nb. water molecules inside cavity*	5.8	8.7	14.2
Heat capacity ( $C_p$ ) of bound water molecules	59	71	70

\*Assuming a volume of a water molecule equal to  $30 \text{\AA}^3$ .

From the Cd spatial arrangement, the cavity shows a relatively hydrophobic character while the external surface is hydrophilic. The hydrophobic cavity enables the thread of a broad range of hydrophobic guests such as the alkyl chains of surfactants [33, 55] or aromatic compounds [55], forming highly stable host-guest complexes, and contributing for the improvement of guest properties, including solubility enhancement and volatility and antioxidant control [56, 57]. These properties, complemented with their non-toxicity to humans make these compounds very attractive for a wide range of industrial

applications [58] involving pharmaceutical technology [59, 60]. Native Cds are, naturally, interesting hosts. They can be, however, modified in order to change the respective symmetry, or introduce specific groups in an effort to expand the respective range of applications. Modifications in Cds are, however, relatively difficult because of the similarity between the hydroxyl groups in which these modifications can be introduced. These have been carried out resorting to specific substitutions in the wide and narrow rims. A variety of derivatives has been obtained and, for example, Cd derivatives of pharmaceutical interest include the hydroxypropyl derivatives (HP) of  $\beta$ - and  $\gamma$ -Cds, the randomly methylated  $\beta$ -Cd, sulfobutylether  $\beta$ -Cd, and also branched Cds. [61]

### 1.2.2 Inclusion complexes

Inclusion complexes and host-guest interactions based on Cds and Cd derivatives have been largely investigated both from a very fundamental, physical-chemical, point of view, and from a very practical, applied, perspective. In this context, it should be noted that more than 70% of new chemical drugs are poorly soluble in water, which is a limitation both in pharmaceutical development and therapeutic outcome.[11, 62, 63] The formulation of poorly water-soluble drugs relies often in a successful and largely implemented strategy based on the complexation with Cds forming inclusion complexes. [64, 65] However, the fact that inclusion complexes are frequently used aiming at solubilizing drugs, makes results sparse and directed at individual systems and, e.g. the comparison between experimental and simulation results lacks a comprehensive approach, so that the factors governing the inclusion phenomena may be assessed. [3]

In drug delivery systems, the formation of a host-guest complexes is a reversible process, suitable for drug encapsulation and controlled release. It also allows altering the biodistribution, absorption and bioavailability of drugs. Several molecular interactions determine the molecular recognition and inclusion behavior. Typical host molecules for inclusion/encapsulation of drugs are cyclic macromolecules, such as Cds, which possess the capability of accommodating drugs as guest molecules into their cavities. In these Cd complexes, no covalent bonds are formed or disrupted during the complex formation, and drug molecules in the complex are in rapid equilibrium with the free molecules in the solution. [66] The formation of Cd inclusion complexes in aqueous solutions have been evalu-

ated by several physicochemical methods. These include solubility studies [67], spectroscopic methods, such as UV/VIS spectroscopy [68], fluorescence spectroscopy [69], circular dichroism spectroscopy [70] and nuclear magnetic resonance (NMR) spectroscopy. [71] Other techniques such as pH-potentiometric titration [72], microcalorimetry and surface tension [71] can be also used. Specifically, UV/Vis spectroscopy is used for measuring drug solubility enhancement by complexation. In Nuclear Magnetic Resonance (NMR) spectroscopy,  $^1\text{H-NMR}$  is a suitable method for the evaluation of noncovalent interactions at the molecular level (including the two-dimensional NMR spectroscopy NOESY or ROESY). It allows establishing the relative positioning of host and guest molecules in the complex and assessing the including degree. It also provides estimates for the association constants of the complexes.

In Thermogravimetric Analysis (TGA)/Differential Scanning Calorimetry (DSC), the TGA profiles describe the weight losses of pure host and guest components and the complexes, and DSC is performed to characterize the solid-state interactions for the inclusion complexes as compared to the melting points. Fourier Transform Infrared (FTIR) spectroscopy is employed for analyzing the vibrational changes upon the inclusion of drugs in the Cd host. X-ray Powder Diffractometry (XRPD) is used for comparing the powder diffraction patterns of drugs and the respective complexes. Scanning Electron Microscopy (SEM) allows investigating the surface morphology of the pure and complexed form and evaluating the Cd-drug interactions. Electrospray mass spectrometry (ESI-MS) allows determining the molecular association of noncovalent bonding. The appropriate binding mode for the Cd-drug complex can be derived from computational simulations. [63, 71]

Among the methods for analyzing Cd-guest complexes, phase-solubility studies, in which the drug solubility (in moles/liter) is represented as a function of the molar Cd host concentration, are commonly employed. [36] Figure 1.2 displays the effects Cd host concentration on the enhancement of drug solubility and the classification of the profiles of the Cd-drug complexes, according to Higuchi and Connors [67] ( $A_P$ ,  $A_L$ ,  $A_N$ ,  $B_S$ , or  $B_i$ ). The profiles pertaining to the A type indicate that the apparent solubility of drugs increases as a function of Cd host concentration, while the B type characterizes systems in which complexes with limited solubility are formed (usually observed with  $\beta$ -Cd). In the latter type,  $B_S$  is derived from the initial soluble complex and insoluble complex at the maximum point.  $B_i$  indicates that the complex is too insoluble to increase the isotherm. In the A type,

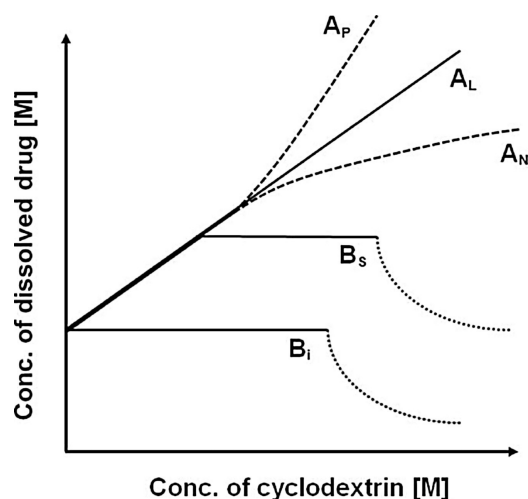


Figure 1.2: Phase-solubility profiles for the solubilization of a drug as a function of the Cd host concentration. Also included is the classification of Cd-drug complexes according to Higuchi and Connors [67]. Reproduced from ref. [36] with permission from Elsevier.

$A_L$  suggests a linear increase in solubility,  $A_P$  and  $A_N$  indicate a positive and negative deviation from linearity, respectively, and  $A_P$  suggests the formation of a higher-order structure. In  $A_L$  type, a profile corresponding to the drug concentration vs. host concentration for the formation of the complex gives a linear profile with the intercept and the slope defined as

$$slope = \frac{mKS_0^m}{(1 + KS_0^m)} \quad (1.4)$$

Where the K value can be calculated from the slope and intercept ( $S_0$ , the intrinsic solubility of the drug in water), if  $m$  is known. In a 1:1 Cd:drug ratio, the complexation is an equilibrium governed by an equilibrium constant ( $K_{1:1}$ ) calculated based on the linear phase-solubility profiles ( $A_L$  type) using

$$K_{1:1}(M^{-1}) = \frac{slope}{S_0(1 - slope)} \quad (1.5)$$

in which the slope is less than unity. In the case of 1:2 Cd:drug complexation, the slope of the  $A_L$  type diagram is less than two, and the association constant ( $K_{1:2}$ ) is determined by

$$K_{1:2}(M^{-1}) = \frac{slope}{S_0^2(2 - slope)} \quad (1.6)$$

As previously mentioned, in aqueous solution drug molecules included in a Cd complex are in dynamic equilibrium with the free solvated molecules, and the complexes are constantly being formed

and disassembled. The typical values of association and dissociation rate constants are in the range of  $10^7$ - $10^8$   $\text{M}^{-1} \text{s}^{-1}$  and  $10^5$   $\text{s}^{-1}$ , respectively, irrespective of the  $K_{1:1}$  value. The  $K_{1:1}$  values for lipophilic and poorly water-soluble drugs are within the range of  $10^2$ - $10^3$   $\text{M}^{-1}$ . The exceptions are some drug candidates containing adamantane moieties that fit suitably in the  $\beta$ -Cd cavity ( $K_{1:1}$  values commonly reported are between  $10^4$  and  $10^5$   $\text{M}^{-1}$ ), and also a designed  $\gamma$ -Cd derivative, sugammadex, for binding of rocuronium ( $K_{1:1}=2.5 \times 10^7$   $\text{M}^{-1}$ ). [30, 63, 71] The mechanism of drug release relies on dissociation/dilution, competitive displacement of drugs from the complex and subsequent Cd host elimination, protein binding and tissue uptake of drugs. Cds can also be ultimately digested by bacteria in the gastrointestinal tract or colon yielding monosaccharides or gases, including carbon dioxide, hydrogen, and methane. Ternary complexes based on small amounts of carbohydrates (e.g.  $\beta$ -Cd) and organic acids (e.g. ascorbic, citric and tartaric acids) can be more efficient for the solubility and bioavailability of drugs. These modifiers are used to modulate the pH under aqueous conditions, affecting the solubility and stability simultaneously.

Another relevant technique is Atomic force Microscopy (AFM), a tool generally used for measuring the interaction between two materials at the atomic scale. [73–77] In host-guest systems, this technique enables differentiating inclusion complexes from their host molecules by mapping local mechanical properties of these soft samples. AFM has been successfully used to evaluate, in aqueous solutions, the rupture forces of host-guest complexes between cyclodextrins and several surface-confined guests, under thermodynamic equilibrium. [75] Changes in the intermolecular interaction between cyclodextrins and guest molecules/materials are thus estimated by measuring the adhesion forces and are dependent on the type of complexes and on the structural deformation promoted by guest molecules (for details see refs. [75]).

Multiple intermolecular forces are involved in the formation of Cd-based complexes. These are weak forces, i.e., weak enough to allow releasing the guest and strong enough to enable the formation of stable complexes. The relative importance depends on the type of guest and in most cases, the formation and stabilization of the complexes result from the cooperative action between several driving forces, including the release of high-energy water and of conformational strain, van der Waals forces, London dispersion forces, hydrogen bonding and dipole-dipole interactions. Solvent (water for most applications) also provides a driving force for complexation. In fact, the hydrophobic cavity of Cd



provides a more thermodynamically favorable environment for the hydrophobic guest or hydrophobic guest moiety than the aqueous environment. Temperature also impacts on the rate of complex formation. Optimal temperatures for complexation must be determined for each guest. As the temperature increases, the solubility of Cd and guest increases, thus increasing the probability of Cd-guest contact. However, the positive effect of increasing solubility must be balanced with the negative effect of complex dissociation promoted by high destabilizing temperatures. [78] One or two Cd molecules can also entrap one or more guest molecules resulting in 1:1, 1:2, 2:1, and 2:2 Cd:guest complexes, or in even more complex association complexes, with higher order equilibria. However, the simplest and most frequent case of Cd:guest ratio is 1:1 because of the molecular encapsulation by  $\alpha$ - and  $\beta$ -Cds. Due to the respective cavity sizes and volumes, the entry of a second guest molecule is hampered (Table 1.1). In these cases only a single molecule can be accommodated through the secondary or primary Cd portals. The displacement of water molecules from the hydrophobic cavity of Cds and the subsequent increase of the number of hydrogen-bonds in the bulk, the reduction of the repulsive interactions between the hydrophobic guest and the aqueous environment, and the increase of the Cd-guest hydrophobic interactions, are some of the possible interactions that favor inclusion and complex formation. [79]

### 1.2.3 Polymers

Polymers based on inclusion complexes and composed of multiple Cd molecules threaded on the chain have attracted great attention in recent years for developing supramolecular materials. [46, 80] The use of inclusion complexes as building blocks for these materials has already reached a high level of complexity, providing an important and convenient route to the construction of targeted controlled-release drug delivery systems. [81–87] This has been realized and improved by supramolecular chemistry and amphiphilic interactions without requiring complicated modification processes. [88, 89] Several research groups have thus opened the way for future progress through innovative applications of Cds combined with other polysaccharides (e.g. hyaluronan, chitosan and cellulose) directed towards physical and organic chemistry, materials design, and pharmaceutical technology. These contributions have been recently reviewed in ref. [46].

In light of the importance of understanding the relationship between structure and properties, selective modifications have been performed, providing new insights on potential applications, since the type of functionalization and substituents affect the resulting physical properties. A deep understanding of these properties is crucial for designing intelligent systems, especially for drug delivery. Among the three native cyclodextrins,  $\beta$ -cyclodextrin is often used because of its availability and suitable cavity size for a widest range of guest molecules, including drugs and hydrocarbon amphiphiles. [89–91] The interaction of Cd with guest molecules has been extensively investigated [92], but there is no assessment of the effect of amphiphilic substituents when moving towards supramolecular Cd assemblies, in which host-guest inclusion complexes act as junction nodes. [89] A quantitative understanding of the effect of substitution on the complex stability is still missing. [3] The effect of polymer pendant modification over the thermodynamic signatures and association/binding constants of the partner junction sites, has not been addressed so far, in the context of network stabilization. Hyaluronic acid (Hy) derivatives bearing monomeric Cd and adamantane (Ad) moieties have been recently used [30] as models for these junctions. Among the potential guest molecules, Ad possesses one of the greatest affinities for Cd (with binding constants up to ca.  $10^5 \text{ M}^{-1}$ ) due to its hydrophobic nature and snug fit within the Cd cavity. [93–95]. Cd-Ad molecular recognition is particularly useful for the formation of supramolecular structures. [96–98] Modification of natural polymers with amphiphilic guest and host groups, either as terminal or pendant modifications, has allowed construction of supramolecular networks based on specific Cd-guest interactions. Because of its unique viscoelastic properties and biological performances, Hy has become an attractive building block for the development of new delivery systems. [99–102] Hy derivatives have been used as carriers and targeting reagents in drug delivery systems due to their biocompatibility, biodegradability, easy modification, high water retention capacity, and specific binding with CD44 cellular receptors over expressed on the surface of cancer cells of solid tumors, such as breast, pancreatic and lung cancers. [103–108]

The binary association of systems formed by conjugating Cd and Ad to hyaluronic acid, chitosan, and other polymers as pendant groups has been investigated from an experimental point of view. [84, 91] The relevance of multivalent and inter-polymer interactions on the inter-partner affinity and network stability has also been emphasized by complementary theoretical and experimental studies. [98, 109] Recently, our group [3] demonstrated the relevance of non-included moieties in the stability con-

stants of several Cd-based complexes using molecular dynamics (MD) simulations and free-energy calculations. This approach includes an automated umbrella-sampling and a "flexible molecule" approximation for the calculation of binding constants.

Cds can also be covalently attached to the surface of polysaccharides, such as cellulose, so that the cavity of the former is accessible to the guest molecules. [46] Cellulose derivatives are optimal guest polymers for the design of novel Cd-containing supramolecular complexes. The host-guest chemistry of Cd/cellulose derivatives in aqueous solutions has been widely explored, especially, in drug delivery systems. These materials are also used for separation and isolation purposes, being employed as sorbents for different compounds, in solution and in gas phase. [41, 46]. An exhaustive account of the wide range of works published in the early years of cellulose and Cd derivatives falls beyond the scope of this section. The reader is referred to refs. [46, 110, 111] for a full description of these efforts.

In the last few years, the utilization of Cd and cellulose derivatives has seen a rapid increase for different pharmaceutical applications. One of the major reasons for this increase lies in the need for achieving critical and desired tunable properties such as biocompatibility, reduced or no toxicity, bioavailability and biodegradability. Pharmaceutical excipients derived from these two molecules have thus been extensively used (see e.g. refs. [46, 112] due to their "green" and specific binding properties, suitable for controlled and sustained drug delivery systems. This requires modifying the morphology and structure of cellulose for attaining the desired properties. In contrast to pure cellulose, which possesses some limitations, the most relevant being poor solubility, bad plasticity and stability, and absence of antibacterial activity, cellulose derivatives have been explored as potential materials for developing several dosage forms and drug delivery systems, aiming at achieving better therapeutic outcomes. In these systems, the gelling and solubility behavior of drugs can be modified, providing different mechanisms for controlling the respective release profiles.

In the following, recent advances on drug delivery applications of Cd/cellulose-based systems are briefly presented, covering some preparation and functionalization methods, as well as addressing relevant characteristics of the drug product, including the release behavior.

Current research on the application of Cds and cellulose for drug delivery encompasses the formulation of nanoparticles [113], microparticles [114], tablets [110], hydrogels [115], and transdermal drug

delivery systems. [110] For instance methylcellulose (MCE) has been compared with Cds in terms of hydrophobicity, displaying affinity to the cavity of  $\beta$ -Cd and forming amphiphilic supramolecular polymers. [80] Du and co-workers [116] have constructed supramolecular polymer micelles based on maleic anhydride (MAh) modified cyclodextrin (MAh/ $\beta$ -Cd) and MCE, using a one-pot self-assembly procedure (Figure 1.3). The micelles displayed regular spherical shapes (with  $25 \pm 5$  nm diameters), possessing a MCE-based core and a hydrophilic shell based on  $\beta$ -Cd and MAh/ $\beta$ -Cd (critical micelle concentrations of  $15.13$  and  $20.89 \text{ mg L}^{-1}$  for MCE/ $\beta$ -Cd and MAh/ $\beta$ -Cd:MCE, respectively). The *in vitro* drug release behaviors of the micelles were established using prednisone acetate as a model drug. It was concluded that the MAh/ $\beta$ -Cd:MCE micelles possessed drug-enrichment cores and exceptional sustaining release time (ca. 700 h).

In a more recent study, Guo and co-workers [117] have described a simple and ecological route for the synthesis of Cd carbamates and production of cellulose-containing supramolecular polymer micelles. The respective drug release behavior was assessed using prednisone acetate, as a model drug. It was shown that the micelles derived from Cd carbamate/cellulose were suitable for long time drug release. The  $\beta$ -Cd:MCE micelles displayed an accumulated release of ca. 100% within 200 h, while in the other micelles, based on  $\gamma$ -Cd and ethyl cellulose or cellulose acetate, the sustained release of the drug was 500 h. [117] Cappello and co-workers [118] have developed topical formulations of rufloxacin

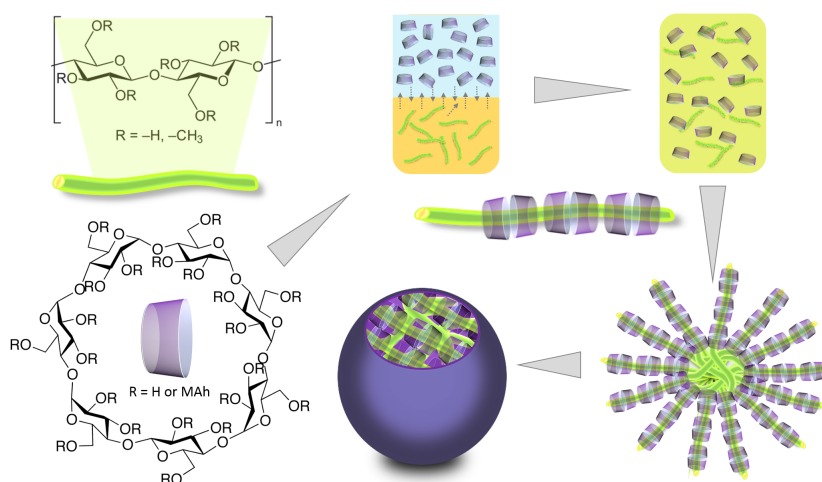


Figure 1.3: Schematic illustration of the formation of supramolecular micelles from MCE,  $\beta$ -Cd and MAh/ $\beta$ -Cd. Reproduced from ref. [46].

resorting to hydroxypropylmethyl cellulose (HPMC) and Cds. The latter were used to improve the

solubility and ocular bioavailability of the drug. HP- $\beta$ -Cd formed the most soluble inclusion complex with rifloxacin. Specifically, the addition of 0.25% HPMC to the solutions containing HP- $\beta$ -Cd increased the solubilizing effect of Cd, reducing the amount of Cds necessary for solubilization of the drug. The most promising formulation was then composed by 0.3% (w/v) of rifloxacin, 6.4% (w/v) of HP- $\beta$ -Cd and 0.25% (w/v) of HPMC. [118]

Host-guest complexes between modified cellulose nanocrystals (CNCs) and  $\beta$ Cd has been used for surface coating purposes [119] and for preparing supramolecular hydrogels, with polymers, such as Pluronic. Lin and Dufresne [120] have used doxorubicin hydrochloride as a model drug for characterizing the release behavior in these gels. Interestingly, a special drug release mechanism was observed upon fitting the release curves into the Ritger-Peppas equation. In fact, drug release followed a Fickian diffusion, when using a neat Pluronic/ $\alpha$ Cd:doxorubicin hydrogel system. However, an anomalous transport release mechanism was observed for the in situ CNCs/CdPluronicdoxorubicin hydrogels. [110, 120]

In another study [121] different proportions of  $\beta$ -Cd, CMC, acrylic acid and  $N'N'$ -methylene bis-acrylamide were used for the preparation of hydrogels via free radical polymerization, directed at controlling the delivery of antiviral drugs (e.g. acyclovir). The successful grafting of the components into the polymeric and thermodynamically stable network was confirmed using FTIR and a thermal/morphological characterization. The obtained hydrogel allowed a controlled release of acyclovir. However, a maximum of 96.15% of cumulative drug release was attained at pH 7.4, from the hydrogel containing the highest acrylic acid concentration, optimum  $\beta$ -Cd and CMC and low  $N'N'$ -methylenebis-acrylamide concentrations, while exhibiting a pH dependent swelling profile [121].

Ndong Ntoutoume et al. [122] have synthesized curcumin-Cd/CNC complexes by functionalizing CNC with cationic  $\beta$ -Cd. This was carried out by ionic association of CNC and Cd and encapsulation of curcumin into the Cd/CNC complexes. It was shown that these complexes displayed an antiproliferative effect on prostatic and colo-rectal cancer cell lines.

Mucoadhesive nasal gels of oxybutynin chloride have also been prepared using many different mucoadhesive polymers, including HPC carbopol and MCE. *In vivo-in situ* models have been used for evaluationg  $\beta$ -Cd, EDTA and bile salts as potential nasal drug adsorption optimizers. [123] Formulations containing  $\beta$ -Cd and chitosan based matrices and EC have been prepared for the release of

ibuprofen. The effect of digestive enzymes on the physicochemical properties of those formulations was studied aiming at assessing the protective role of polysaccharides in gastrointestinal media. The most stable carrier systems were obtained using formulations composed of equal amounts of ethyl cellulose and  $\beta$ -Cd, allowing a slow release of the drug until 24 h (maximum drug release of  $101.04 \pm 0.65\%$ , in which  $83.08 \pm 0.89\%$  of ibuprofen was released in colonic medium). [124]  $\beta$ -Cd/cellulose hydrogels have also been prepared by Zhang et al. [125], in a basic solution (NaOH/urea), using epichlorohydrin as crosslinker and in the presence of 5-fluorouracil (5-FU), bovine serum albumin (BSA) and aniline blue (AnB) (see Figure 1.4). It was found that an increase of the  $\beta$ -Cd content

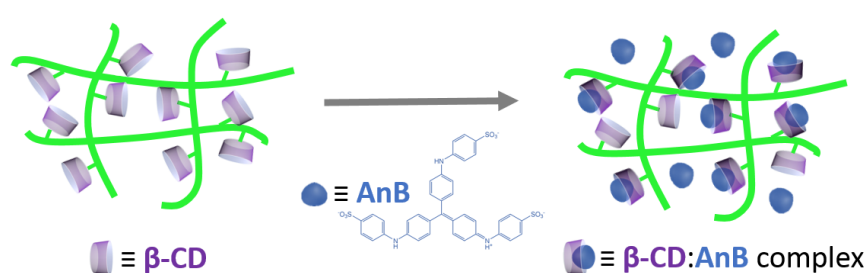


Figure 1.4: Schematic representation of the mechanism for the adsorption of AnB in the hydrogels. Reproduced from ref. [46].

led to a decrease of the swelling degree and the water uptake of the hydrogels. Different drug release behaviors were observed for 5-FU and BSA. Weak interactions were observed between BSA and  $\beta$ -Cd, while the formation of  $\beta$ -Cd:5-FU complexes inhibited the controlled release. AnB was adsorbed by the hydrogels leading to a fluorescence enhancement, which was explained by the formation of  $\beta$ -Cd:AnB complexes. These results also confirmed the usefulness of this type of hydrogels as pharmaceutical excipients for hydrophobic drugs. [125]

Recently, Marcos et al. [126] have developed supramolecular gels based on poloxamer, hydroxyethyl cellulose (HEC) and  $\alpha$ -Cd for improving the solubilization and sustained release of griseofulvin, an antifungal drug for topical application. The authors evaluated the effects of the  $\alpha$ -Cd concentration (from 0 to 10% w/w), on the phase behavior of mixtures of Pluronic P123 (14% w/w) and HEC (2% w/w), at different temperatures. Both components, poly(ethylene oxide) (PEO) blocks of Pluronic and HEC, were able to form supramolecular complexes with Cd, avoiding the phase separation and improving the solubilization of the drug. The rheological and bioadhesive properties of the gels, in the presence and absence of the drug, were tuned using different proportions of the poly-

mers. Furthermore, the addition of HEC to form P123/ $\alpha$ -Cd gels, enhanced the viscosity at 25°C and enabled optimizing the release of griseofulvin at 37 °C. In addition to these features, these ternary supramolecular gels displayed favored biocompatibility and activity against *T. mentagrophytes* and *T. rubrum*, being thus considered a suitable platform for the topical treatment of dermatophytosis and also to be incorporated in formulations for long-term sustained release of several drugs.

Han and co-workers [127] have obtained a hydrogel with three-dimensional double network structures, in which electrostatic and host-guest interactions play the leading roles. HEC and a modified chitosan (HACC) were cross-linked using one-pot reaction for preparing the spherical cage. HACC provided a positive charge core to attract sulfobutylether- $\beta$ -Cd (SEB- $\beta$ -Cd), the negative host molecule. The method of weight increment and photometric titration was implemented to determine the amount of SEB- $\beta$ -Cd loaded (ca. 50.3%). It was shown that the hydrophobic guest substance in the SEB- $\beta$ -Cd@hydrogel was released in a sustained manner in buffer solution and the controlled release of SEB- $\beta$ -Cd by ion-exchange method provided new insights on the rapid release of hydrophobic guest substances. [127]

A zero-order release kinetics of glipizide, used as model drug, from compression-coated tablets for oral administration, was observed by Huang and co-workers [128], using hydroxypropyl cellulose (HPC) as the coating layer. Those tablets were able to form a hydrogel, when in contact with the gastrointestinal fluid, which decreased the drug release rate. It was found that such release rate was controlled by the erosion of the gel matrix. Similarly to previous observations, the formation of host-guest complexes allowed enhancing the solubility of the drug in different pH conditions, thus increasing the dissolution rate of the compression-coated dosage form. It was concluded that different properties, such as the viscosity of HPC and the distribution of the drug between the outer layer and the core of the matrix, can be used for controlling the release behavior. [128]

The use of  $\beta$ -Cd derivatives proved a powerful resource to increase the solubility of chemotherapeutic agents, such as benznidazole. HPMC has been the basis for guiding the release of such agents from solid Cd-based host-guest complexes, ensuring the drug bioavailability. In turn, HP- $\beta$ -Cd produced a significant improvement in drug solubility being often selected for the development of solid systems. [129] New solid dosage forms with improved physicochemical properties and oral bioavailability have been developed, containing HP- $\beta$ -Cd and hydrophilic additives, obtained from supercritical

antisolvent processes. HP- $\beta$ -Cd NPs loading dutasteride formed aggregates within the nanoscale (a mean particle size of ca. 160 nm and a specific surface area over 100 m<sup>2</sup> g<sup>-1</sup>). It was shown that the type of hydrophilic additive influence the maximum achieved supersaturation and also the drug precipitation rate. A maximum solubility and extended supersaturation was observed for the drug-loaded HP- $\beta$ -Cd nanostructures with HPC. The bioavailability of these nanoparticles was comparable to that of the commercially available formulation. [130]

The inclusion of ciprofloxacin by grafting  $\beta$ -Cd on cellulose fibers has been reported by Dong et al. [131]. The  $\beta$ -Cd-grafted cellulose was prepared by the formation of citric acid- $\beta$ -Cd, which was obtained via dehydration of the two adjacent carboxyl groups of the citric acid to form a cyclic anhydride which reacts with the hydroxyl groups of the  $\beta$ -Cd portals. The grafted ratio of  $\beta$ -Cd onto cellulose fibers was 9.7%, under [citric acid- $\beta$ -Cd] = 300 g L<sup>-1</sup>, pH 3.4, 15 min, and 160°C conditions. The release behavior of the encapsulated ciprofloxacin hydrochloride from cellulose fibers was also investigated. The Cd-grafted cellulose showed a higher cumulative release (ca. 90% in half-hour) of the biocide, when compared with the native fibers. The same level was attained with the modified fibers after 240 min, as a consequence of the formation of host-guest complexes. However, the presence of  $\beta$ -Cd and biocide contributed for an increase in the disorder of the cellulose microstructure, affecting the respective mechanical properties. Comparing to pure fibers, the bacterial activity against *E. coli* and *S. aureus* of the grafted chains, loading ciprofloxacin, was significantly higher. [131]

Lavoine et al. [132] have developed a high-performance delivery system using  $\beta$ -Cd containing microfibrillated cellulose (MFC)-coated papers. A model antibacterial drug, chlorhexidine digluconate (CHX) was used in a suspension of MFC, a  $\beta$ -Cd solution, or mixed with both MFC and  $\beta$ -Cd, before coating onto a cellulosic substrate (see Figure 1.5). The proposed scenarios for explaining the release mechanism suggested that (i) the  $\beta$ -Cd:CHX complexes are linked to cellulose via  $\beta$ -Cd/cellulose interaction, being associated to a longer release of the drug, (ii) the interaction with cellulose can be done through the CHX moiety protruding from the  $\beta$ -Cd macrocycles, which are firstly released, followed by the CHX molecules, (iii) either CHX or  $\beta$ -Cd, in the supramolecular form, are concomitantly linked to cellulose. In the latter scenario, the complexes are released at a low kinetic rate, as a consequence of the chemical interactions between the  $\beta$ -Cd:CHX and cellulose. Comparing the  $\beta$ -Cd and MFC releases of CHX, the former promotes a continuous and longer release profile, due



to the formation of the inclusion complex with CHX. Furthermore, when the two compounds were combined a complementary action was observed. The  $\beta$ CD:CHX-coated sample released the lowest amounts of CHX for more 10 h than the CHX/MFC-coated sample. MFC promotes the burst effect, while  $\beta$ -Cd controls the amount of drug released over time. It was concluded that the combination of  $\beta$ -Cd and MFC is suitable for the rapid delivery of CHX, promoting the sustained release of active compounds. [46, 132] Other approaches have been tested for prolonging the drug release in aque-

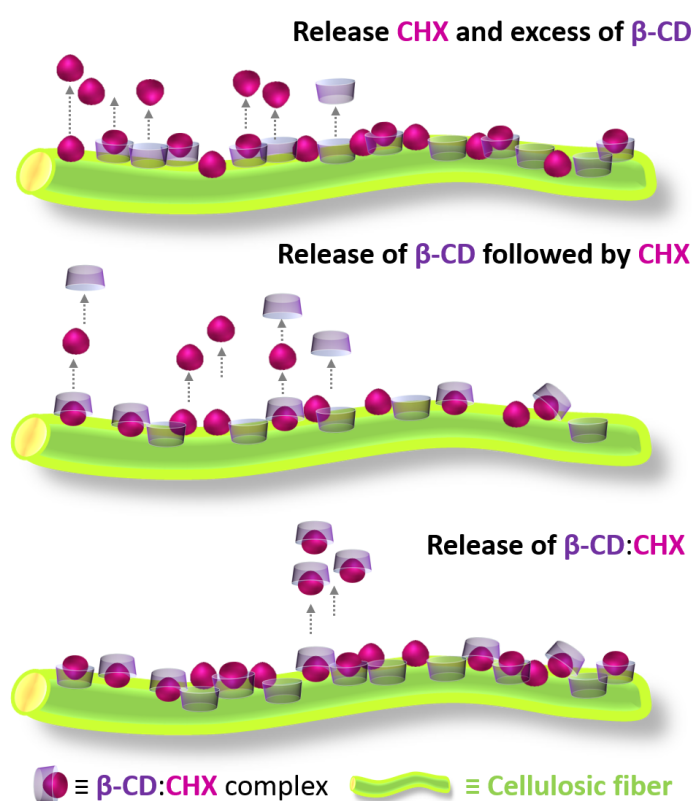


Figure 1.5: Schematic representation of the different scenarios for explaining the release mechanism involving  $\beta$ -CDs and chlorhexidine digluconate (CHX), and the respective inclusion complexes. Reproduced from ref. [46].

ous solutions. These include recent works on the use of electrospun fibers composed by HPC and complexes of HP- $\beta$ -Cd-sulfisoxazole. These components were encapsulated in poly( $\epsilon$ -caprolactone) nanofibers which allowed a more sustained drug release. [133]

### 1.2.4 Aggregates

After a long period in which it has been neglected, Cd aggregation is now a hot-topic, and one far from gathering consensus. [134] This is duly discussed in Chapter 6. The aggregation of amphiphilic molecules in solution, including Cds, can be considered as a microphase separation between polar and non-polar phases. This involves both the hydrophobic and hydrophilic moieties of such molecules and induces the formation and growth of the so-called self-assembled structures. This is a spontaneous process in which the system components form ordered aggregates, typically involving an enthalpy gain in solvation, due to hydrogen bond formation, and possibly a gain in the entropy of bulk water (hydrophobic effect). [11, 135] The process is promoted by balanced attractive and repulsive interactions between molecules, or specific moieties, occurring from a less organized state (e.g. a solution or a disordered aggregate) to a final ordered state (e.g. a crystal). These soft interactions are generally weak, comparable to thermal energies, and noncovalent, with typical strengths varying from less than  $5 \text{ kJ mol}^{-1}$  for van der Waals forces to ca.  $120 \text{ kJ mol}^{-1}$  for hydrogen bonds. [136]

Other relevant factors, such as the reversibility and flexibility, the interaction with the respective environment, and the mobility of the system components, determine the success of the molecular self-assembly process.

Despite a substantial amount of data is available on the thermodynamic aspects of assembly processes, the information on the Cd aggregation behavior and detailed mechanisms of formation and dissociation is scarce. In particular, little is known about the cooperative nature of individual contributions of components for the Cd aggregation/assembly process. This is clearly a topic requiring fundamental research, with direct implications for improving the supramolecular assembly design and fostering new formulation opportunities in this type of systems.

Cds have been used for functionalization of organic and inorganic materials and for the synthesis of nano- and micro-sized aggregates. [137, 138] This process is, in general, driven by hydrophobic interactions, and is affected by a number of factors such as the concentration of reactants, temperature, nature of solvent and the addition of neutral or ionic co-solutes. [139]

One of the most intriguing properties of Cds is the respective solubility. It should be noted that the solubility in water does not follow a common trend, with  $\beta$ -Cd being much less soluble than the other

two. [46, 140] Such behavior has attracted researchers for several years, and different explanations have been proposed, based on the rigidity of the Cd ring and intramolecular hydrogen bonding, or Cd self-aggregation. [141] The formation of aggregates can be enhanced upon formation of inclusion complexes, but in general negligible amounts of aggregates (of ca. 200-300 nm in size) are formed in pure Cd solutions. The extent of aggregation may also increase with increasing Cd concentration. [142] A wide range of experimental data generated on Cd aggregation has been reviewed (see e.g. ref. [143]). However, the mechanisms of Cd aggregation and Cd complex aggregation have not yet been fully understood. [134]

Cd aggregation was originally recognized based on random observations and deviations from theoretical expectations. Several analytical techniques are now being optimized to specifically detect and characterize Cd aggregates. In Cd solutions, dynamic light scattering (DLS) [144, 145] and transmission electron microscopy (TEM) [145] have provided reliable evidence of the aggregation phenomenon. The latter has been recognized by several research groups that have identified aggregates of different shapes, including spherical and elongated particles, welded fibers and rods. [11, 134] A significant amount of microscopic data [146] and information from dynamic light scattering (DLS), nuclear magnetic resonance spectroscopy (NMR), and dialysis membrane permeation methods, have been reported. [11, 146] However, the full characterization of the Cd aggregation behavior by these techniques has been hampered by the poor stability of the aggregates, which makes them sensitive to disruptive side effects. [11, 145]

### 1.3 Modeling soft supramolecular structures

There is a surprising number of studies supporting the use of computational models for mimicking supramolecular systems and studying the underlying patterns of molecular recognition and binding, in multi-dimensional approaches. [147] Based on physical properties and mathematical concepts, these models are able to provide rationales for the conformation, solvation and thermodynamic characterization of this type of systems. Molecular dynamics, including free-energy calculations, yield a direct coupling between experimental and computational investigation.

Host-guest systems have emerged as useful models for assessing the accuracy of simulation meth-

ods. This can be explained by the fact that these systems display interesting features comparable to protein-ligand binding, including hydrogen bonds, conformational restriction and desolvation, and also possess an adequate size for conducting more precise thermodynamic calculations. This is the case of Cd host-guest systems, which mimic several characteristics of protein-ligand binding with the advantage of being much more accessible due to their small size. These characteristics also facilitate the selection of the force field (FF) based on the attribution of the level of accuracy.

Specifically, the combination of MD and free-energy calculations with experimental results have revealed the relevant interaction patterns in the formation of inclusion complexes between several host (e.g. cyclodextrins [3, 148], cucurbiturils [149] and bambusurils [150]) and guest molecules (e.g. antitumor and antiviral drugs [151], steroids [152], flavonoids [153] and small ionic species [150]). These small aggregates, comprising typically two (in 1:1 host-guest complexes) or three molecules (in 1:2 complexes) have been the basis of fundamental developments for establishing what governs associations in soft-matter and stability in larger supramolecular nanostructures, such as nanogels and targeted nanoparticles.

Despite significant advances in molecular modeling techniques and the comparative simplicity of host-guest systems, there is still a need for a tractable and theoretically sound computational method to interpret experimental data and help with the design of new hosts for targeted molecular guests. Similarly to other macromolecular systems, host-guest systems exhibit marked entropy-enthalpy compensation. Such property has been observed for noncovalent interactions in both water and organic solvents. Among the wide applications of alchemical transformations, host-guest chemistry occupies the most prominent position. [154] A fundamental aspect to be understood is the precise manner in which the guest molecule binds to the host. MD simulations have greatly contributed to understanding molecular binding phenomena as a fully dynamical process. However, these simulations are limited by the time scales that can be routinely sampled. The introduction of special-purpose machines and the evolution of parallel codes, has increased enormously the time scales accessible by fully atomistic MD. However, guest molecules (e.g. drugs) with long residence times are common, and the respective association/dissociation from a host or receptor cannot be observed by conventional MD calculations even when specialized hardware is employed. This well-recognized limitation of MD has led to the development of various algorithms to enhance the sampling of the high free-energy states and rare

events, associated to high free-energy barriers.

Enhanced sampling methods can speed up conformational sampling by various means and represent an effective alternative to access with high accuracy the thermodynamics and possibly the kinetics that underlie these processes. Steered MD and umbrella sampling [155], with potential of mean force estimation (PMF) [156] allows inspecting the free-energy profile and the mechanistic aspects involved in formation of host-guest complexes. [3] In recent years, other strategies aimed at the same goal have been proposed. Replica exchange [157] metadynamics [158, 159], accelerated MD [160], milestone sampling [161], transition path sampling [162], and combinations of these are among the most widely used methods to enhance conformational sampling. For instance, the replica exchange methodology has been used in the atomistic simulations, as well as in a number of coarse-grained simulations (see e.g. [158]). This method has been applied to study free-energy landscape and folding mechanisms of several peptides and proteins [157], through several variants of the traditional temperature dependent scheme, available in some of the most popular MD packages, such as AMBER [163], GROMACS [164] and NAMD [165]. Among the enhanced sampling methods that fully explore the binding mechanism, metadynamics, especially in the well-tempered formulation, has emerged as a powerful approach for accelerating rare events. [159] This has been applied in drug docking to protein and enzymes, systems involving big conformational changes and relevant solvation effects. Directed dynamics such as the adaptive biasing force (ABF) and hyperdynamics were also derived from the same principles as adopted by metadynamics. [159] The implementation of metadynamics in MD codes, such as NAMD and GROMACS, have promoted a broad range of applications of the method, ranging from solid state physics to biological systems.

The adaptive biasing force algorithm (ABF) has also emerged as a promising strategy for mapping complex free-energy landscapes [166, 167], as it combines both constrained and unconstrained simulations into a highly efficient scheme, providing an uniform sampling of the order parameter. Briefly, as a simulation progresses, a continuously updated biasing force is added to the equations of motion, such that in the long-time limit it produces a Hamiltonian devoid of an average force acting along the transition coordinate of interest. In contrast to umbrella sampling schemes, based on probability distribution functions, ABF uses forces, which can be readily estimated without the need to sample broad ranges of the order parameter.

Another relevant problem in the early estimations of free-energy is related to the strong dependence on system size, in the presence of significant electrostatic interactions. [168] Once long-range corrections using Ewald lattice summation or the reaction field are included in molecular simulations, size effects in neutral systems decrease markedly. The problem, however, persists in charged systems, for example in determining the free-energy of charging a neutral species in solution. In this context, it has been demonstrated that system-size dependence can be largely eliminated in these cases by careful treatment of the self-interaction term, which is associated with interactions of charged particles with their periodic images and a uniform neutralizing charge background. [168] The ability to decouple relevant energy contributions from individual components is also far from a simple solution, being the basis of alchemical free-energy methods [19, 20], such as the thermodynamic integration (TI) [17, 168, 169], free-energy perturbation (FEP) [20] and molecular mechanics-Poisson-Boltzmann surface area (MM-PBSA). [170] The feasibility of the estimated binding free-energy depends on the correct estimation of thermodynamic quantities and the concerted interaction components (enthalpy, entropy and solvent contributions). [15, 171] For instance, the quantification of these interaction components have been directed at inclusion complexes between cyclodextrins and its derivatives and different model drugs (see refs. [13, 15, 172]). However, only a few studies (e.g. [3, 13]) have introduced technical and practical directions to investigate the energy components underlying the stability of these complexes. Spoel and co-workers [13] have emphasized the role of solvent contribution resorting to steered molecular dynamics and PMF calculations. The latter techniques have also been used by Pais and co-workers [3] for assessing the relevance of non-included guest moieties in the binding constants of cyclodextrin inclusion complexes, estimating the weight of enthalpic and entropic contributions to the free-energy. In this context, MD and PMF calculations allow the modulation of the formation processes in inclusion complexes, along which the free-energy profiles are derived from an umbrella sampling procedure. [3] This approach has been employed in the characterization of the inclusion of a wide range of drugs on cyclodextrins, and also in the aggregation of host units either in dimerization [15, 172] or in rotaxanes formation. [173, 174] Other hybrid approaches [175], including quantum mechanics/molecular mechanics (QM/MM) [153] methods have also provided insight on the formation of inclusion complexes at a molecular level.

### 1.3.1 Applications

This section presents some examples in which MD or Monte Carlo (MC) simulations are used for establishing the contributions of noncovalent interactions (NCI) (e.g. electrostatic, hydrophobic and hydrogen-bond interactions) to the free-energy, in systems in which these are the main source of recognition, assembly, and stability. These include, for instance, host-guest complexes, polyelectrolytes and proteins.

MD and free-energy calculations have provided insight on relevant aspects including the effect of substituents, the role of solvation, and rationales for the conformation and thermodynamic characterization of the systems under investigation. Among several studies on the topic, available in the literature, only a few are briefly reviewed. For instance, MD simulations in water, with PMF estimation based on both TI and constraint force methods, have been used for inspecting the thermodynamic properties of binding of some inorganic ions, such as  $\text{ClO}_4^-$  and  $\text{SO}_4^{2-}$ , and ferrocenyl alkanethiols with both free and gold-surface confined  $\beta$ -cyclodextrins. [14, 176]

In general, the association process between the host and guest molecules is analyzed along the reaction coordinate defined by the distance between the centers of mass of both host and guest, along a reference coordinate (e.g. z-axis). In these particular systems, electrostatic interactions and hydrogen bonding have played a major role on the binding process. For instance, simulations have elucidated the association mode of sulfate anion with free and grafted  $\beta$ -cyclodextrin. For the latter system, a small minimum in the PMF profile, positioned at a larger distance relative to the cavity of surface-grafted cyclodextrin, suggested the formation of a noninclusion complex (see refs. [14, 147] for details). The ion binds to the host by forming hydrogen bonds with the free-cyclodextrin portal. Also relevant is the individual energy contributions to the cyclodextrin-ion interaction, which is governed by electrostatic interactions. However, this favorable electrostatic contribution is not sufficient to compensate desolvation of the anion, considering the respective hydration energy. [14]

The release and transport of drugs mediated by cyclodextrin-based carriers, have also been investigated [177] systematically using MD and free-energy calculations, showing the preferred inclusion modes of such drugs for cyclodextrins. One example (see Figure 1.6), refers to the binding of amphotericin B (AmB), which possesses two sites, within the respective prolonged macrolide, with higher

binding affinity to  $\gamma$ -cyclodextrin. The decomposition of the PMFs into free-energy contributions have suggested that van der Waals and electrostatic interactions are the main driving forces responsible for the formation of this type of complexes. [177]

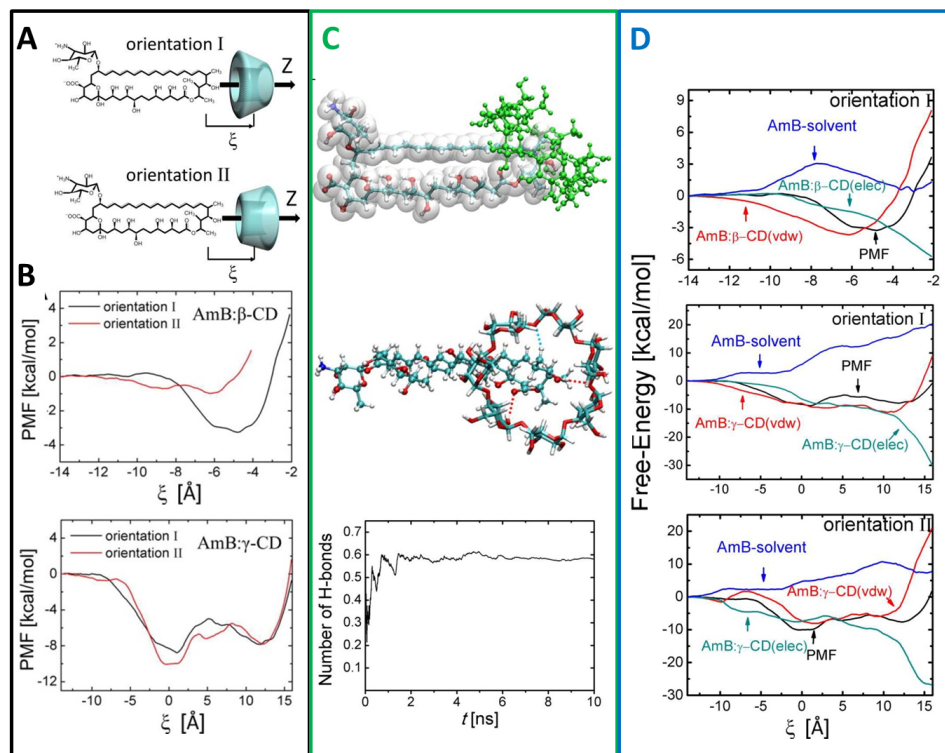


Figure 1.6: (A) Schematic representation of the two inclusion pathways along which AmB approximates to  $\beta$ - or  $\gamma$ - cyclodextrins. (B) PMF profiles for the inclusion of AmB with  $\beta$ - and  $\gamma$ -cyclodextrins considering the two orientations. (C) Equilibrium configuration of the complex between AmB and  $\beta$ -cyclodextrin (orientation I) followed by a representation of the hydrogen bonds formed between host and guest molecules and the respective averaged number ( $\text{O-H}\cdots\text{O}$  angle  $> 135^\circ$  and  $\text{O}\cdots\text{O}$  distance  $< 3.5 \text{ \AA}$ ), as a function of the simulation time. (D) Decomposition of the PMFs into van der Waals and electrostatic host-guest and host-solvent contributions, for the complexes between AmB and  $\beta$ - and  $\gamma$ -cyclodextrin in orientation I, and AmB and  $\gamma$ -cyclodextrin in orientation II. Adapted with permission from ref. [177]. Copyright (2018) American Chemical Society.

Recently, Pais and co-workers [3] (see Chapter 3) have demonstrated the relevance of non-included moieties in the stability constants of several cyclodextrin-based complexes. The binding constants for naphthalene derivatives forming complexes with  $\beta$ -Cd were calculated (ranging from 128 to  $2.1 \times 10^4$ ), pointing out the important effects of the substituents. Substitution of naphthalene promoted an increase in the binding constant (up to 100-fold), irrespective of the nature of the substituent, the latter comprising small hydrophobic and hydrophilic, including charged, groups. Enthalpic and entropic contributions were separated in order to estimate their weight in the free-energy. Also, the preferred



orientation of the guest molecules within the cyclodextrin was established. In a completely different system [150], the same strategy was used for exploring the ion caging ability of bambusurils in aqueous media. Specifically, new insights on the conformation, hydration and energy changes involved in the complexation process between the water-soluble benzoyl-substituted bambus[6]uril and chloride ion were provided. The structural features of three single bambusuril derivatives, and the relative energy contributions to the formation of the benzoyl-substituted bambus[6]uril-chloride complex were computed. The estimated standard free-energy of binding and the respective binding constant were found to be  $-11.7 \text{ kJ mol}^{-1}$  and 112, respectively. Binding occurred with complete desolvation of both guest and host cavity. One of the most interesting observation was that chloride was hermetically sealed inside the host cavity, as a result of a concerted action of both conformation change and desolvation. [150]

Solvent contributions to the thermodynamics of binding have been scrutinized [13], emphasizing the importance of using explicit models for the accurate calculation of binding thermodynamics. A detailed analysis on the energetics of the host-guest complexation between  $\beta$ -cyclodextrin and several model drugs (e.g. puerarin, daidzin, daidzein, and nabumetone) have demonstrated that the flexibility of the binding partners and solvation-related enthalpy and entropy changes must be included explicitly for the precise estimation of thermodynamic parameters involved in molecular association. In this study, it was also demonstrated that implicit models are not suitable to provide detailed information on how free-energy is decomposed into enthalpy and entropy. [13, 178]

The dimerization of Cds has also been recognized as a relevant step in the construction of nanostructured materials. [134] Only a few studies (see e.g. refs. [15, 172]) involving umbrella sampling simulations and PMF calculations have been carried out for investigating the binding affinity of dimers in the presence/absence of a guest molecule, and the preferred orientation of interglucopyranose hydrogen bonds, at the cyclodextrin portals. These include  $\beta$ -cyclodextrin monomers and dimers in aqueous and nonaqueous media. [172] Polar solvents with stronger hydrogen bond accepting abilities can easily disrupt intermolecular hydrogen bonds, decreasing the stability of the dimers. In the same environment, higher binding affinities are achieved if guest molecules are included in the channel-type cavity of such dimers. These results allowed concluding that the formation of dimers is solvent-dependent and guest-modulated. [172] In another related study [15], it was shown that the cooperative

binding of cyclodextrin cavities to guest molecules can facilitate the dimerization process, favoring the overall stability and assembly of nanostructures. Different dimerization modes yielded different binding strengths. This has been demonstrated in systems consisting of isoflavone drug analogues used as drug templates, and cyclodextrins (Figure 1.7). A detailed quantification of host, guest and solvent contributions to the thermodynamics of binding has revealed that head-to-head dimerization promotes the most stable complexes, which can be used as building blocks for template-stabilized nanostructures. Desolvation of cyclodextrin dimers and entropy changes upon complexation also affect significantly the cooperative binding. [15]

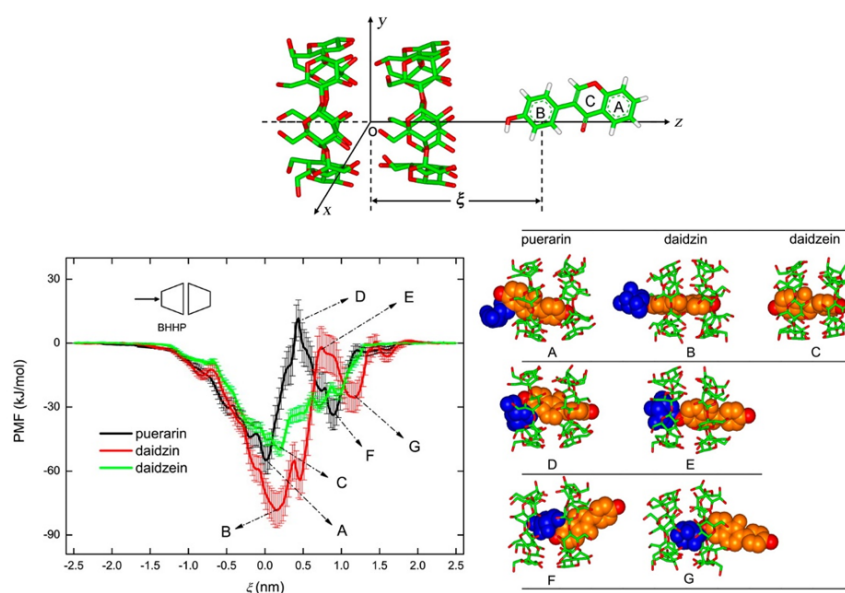


Figure 1.7: Schematic representation of the association coordinate for the 2:1 complex between a  $\beta$ - cyclodextrin dimer and daidzein. (Bottom) PMF profiles and representative configurations of the 2:1 complexes between the specific BHHP arrangement of  $\beta$ - cyclodextrin dimer and three different model drugs. Reprinted from ref. [15] with permission of the American Chemical Society (available from <https://pubs.acs.org/doi/abs/10.1021/jp412041d>).

Other strategies have been adopted resorting to both MD and MC simulations. As an example of application [179], free-energy calculations and lattice chain MC simulations have been used for understanding the formation of polyrotaxanes (Figure 1.8), including the identification of the most favorable conformations of cyclodextrin molecules in a polyrotaxane and the quantification of dimerization free-energies, related to different spatial arrangements of two consecutive cyclodextrin molecules. It has been suggested, that the binary association is controlled by the formation of hydrogen bonds between two adjacent molecules, promoting an overall structural stabilization. [179]

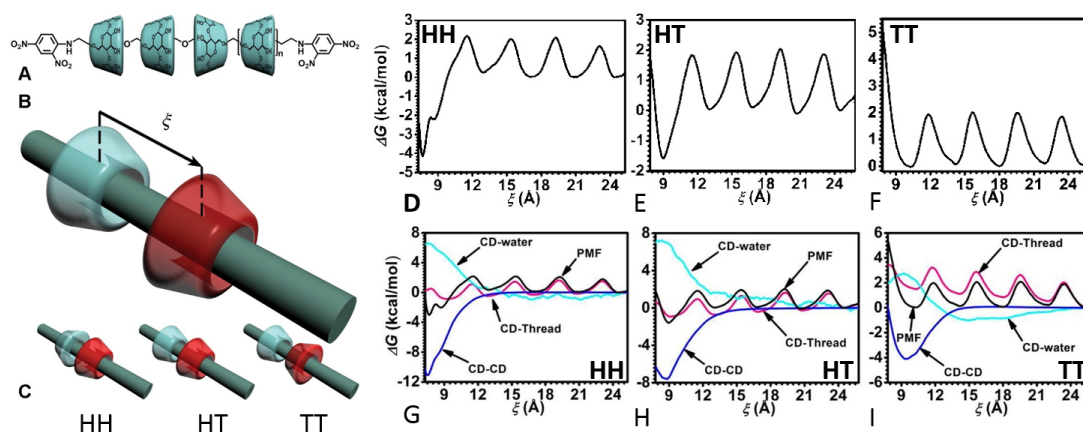


Figure 1.8: (A) Structural arrangement of a polyrotaxane formed by a poly(ethylene glycol) chain included in multiple  $\alpha$ -cyclodextrins, (B) definition of the reaction coordinate,  $\xi$ , in which both the geometrically restrained (cyan) and free (red) cyclodextrins are presented. (C) Three possible conformations (HH, HT and TT) showing different spatial arrangements of two consecutive  $\alpha$ -cyclodextrin molecules. (D-F) Free-energy profiles corresponding to the dimerization of  $\alpha$ -cyclodextrins on the poly(ethylene glycol) chain, for the HH, HT and TT conformations. (G-I) Individual cyclodextrin-cyclodextrin, cyclodextrin-water, and cyclodextrin-thread energy contributions for the total free-energy, in the three conformations. Reprinted with permission from ref. [179]. Copyright (2018) American Chemical Society.

The thermodynamic cost of confining polyelectrolytes spherical cells of different radii can also be quantified by free-energy calculations, resorting to TI. [180] Simulation studies of polyelectrolytes, based on MC and MD, have been precluded by the respective chain lengths and the need of large concentrations of compacting agents. The conformational and energetic changes in DNA delivery systems have been studied computationally by some of the authors. [180, 181] For instance, a coarse-grained model was proposed [180] for exploring structural and thermodynamics aspects of confining polyions in spherical cavities, with different linear charge densities and with counterions of different valences. The free-energy of the confined polyion and counterions were estimated as a function of the sphere radius, from a dilute solution corresponding to the largest sphere. A positive free-energy difference was found for all systems and was associated to the compression. This means that the system containing the polyion with the largest linear charge density and monovalent counterions displays the largest resistance to being compressed. The penalty is thus largest for the polyion with the largest linear charge density and monovalent counterions. The replacement of the monovalent counterions with trivalent ones induced a compactation of the polyion, as a consequence of the stronger electrostatic polyion-counterion attraction. This leads to a nearly full compensation of the ideal and electrostatic

contributions to the free-energy of their confinement.

Other interesting example of application relates to protein-ligand interactions [182–186], which are typically pursued by significant conformational and energetic changes. These changes often occur on time scales that make direct atomic-level simulations useless. One possible alternative relies on the assumption that the change in the binding free-energy resulting, for e.g. from a mutation of a ligand bounded to a protein, complies a linear response scheme [183], with parameters estimated from training sets of protein–ligand complexes, and used for predicting binding affinities of new ligands. Another strategy is the computational design of the ligand in free and bound states. In this type of systems, the emergence of some reliable implicit solvation models and classical statistical–mechanical approaches have been part of the solution. These include, for instance, the use of the molecular mechanics Poisson–Boltzmann surface area (MM-PBSA) model. [170] A theoretical study, recently published [187], encompasses MD and free-energy calculations for evaluating the structural and thermodynamic signatures involved in the interaction of siRNA molecules, bearing chemical modifications at 3'-overhang, with the PAZ domain of human Argonaute (Figure 1.9). In these systems, a reduction of the complex binding affinity has been observed upon siRNA modification, being explained by the hampering of hydrogen bond formation in the active site of PAZ. Analyses of free-energy, achieved from simulations based on the Generalized Born and surface area continuum solvation (MM-GBSA) method, and of hydrogen bonds, have provided a complete identification of the most relevant residues for PAZ-siRNA interaction (see Figure 1.9). This data will contribute to the improved design of synthetic nucleotide analogues, circumventing some of the intrinsic siRNA drawbacks.

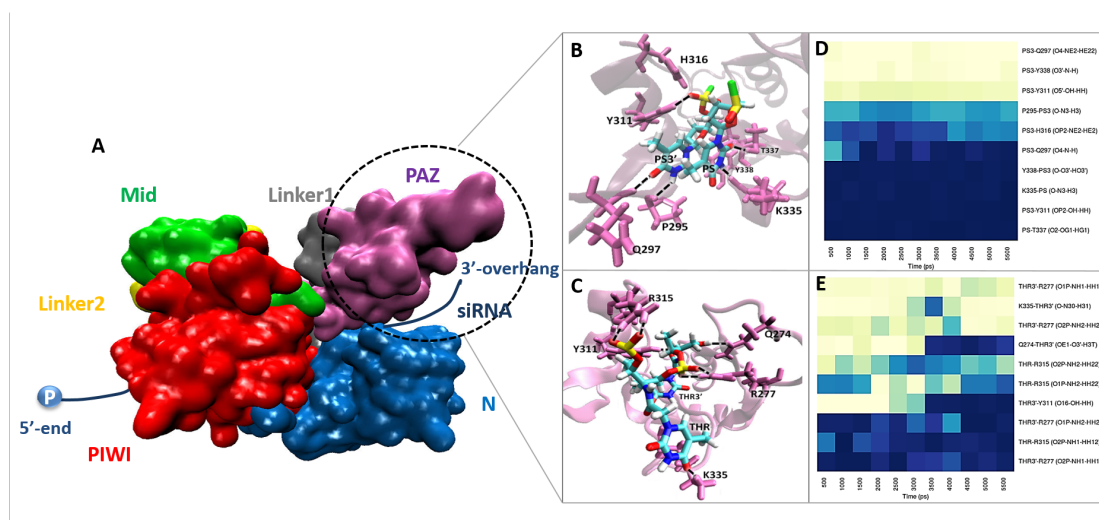


Figure 1.9: Representative conformation of the complex between PAZ domain of the human argonaute 2 (hAgo2) and the chemically modified siRNAs at 3' overhang, obtained from the last nanoseconds of the MD production runs. Panel A illustrates the relative positioning of domains and interdomain linker of the hAgo2 (using the crystal coordinates of PDB ID: 4F3T) and the positioning of the siRNA antisense strand. Panels B and C show the most representative structures of the complexes formed between PAZ domain and siRNAs, modified with phosphorothioate thymidine (PS) and L-threoninol-thymine (THR), respectively. PS and THR correspond to the second-last residues of the modified siRNAs while PS3' and THR3' correspond to the last one. Hydrogen-bonding interactions between the siRNA nucleotides and the PAZ amino acid residues are represented in black dash lines. The phosphorus, oxygen, nitrogen, hydrogen and sulphur atoms are colored in yellow, red, blue, white, and green respectively. Panels D and E correspond to the occupancies of the most prominent hydrogen bonds formed between the PAZ binding pocket and 2-nt modified nucleotides with PS and THR, respectively. The analysis of the instantaneous hydrogen bond formation was obtained using an in-house algorithm. Adapted from Ref. [187]. Published by The Royal Society of Chemistry.

## 1.4 Motivation and aims

The use of host-guest complexes is widespread in terms of practical applications, including the solubilization of insoluble drugs, the preservation of flavors and scents, and the design of more complex supramolecular structures. This wide range of applications tends to generate work, both computational and experimental, that is made on individual systems, and for which the systematic understanding of the factors governing the inclusion process does not constitute the main goal.

*In silico* approaches are generally more cost-effective and less demanding than laboratory experiments, particularly when the *a priori* development of synthetic procedures and binding assays are required. Often, computational methods also provide the only access to risk appraisals of new chemical compounds. They are also the tool of choice to provide a deeper insight and the rationales for both simulation and experimental results, thus allowing for a broader generalization. This dissertation deals with the computational quest for the characterization and quantification of host-guest binding affinities, using various imposed features and models of host-guest systems, which are crucial for the design and incorporation of supramolecular nanostructures in suitable platforms for drug delivery. The features are systematically varied, and include host and guest modifications, host size, inspection of potential transient-gel nodes, and two types of hosts, cyclodextrins and bambusurils.

Two main goals are pursued: understand the factors that govern inclusion, and develop the tools that allow a molecular-dynamics simulation, in-depth study, of these systems. For the first aim, a large number of aspects are examined: these include solvation, conformation, overall and decomposed interaction energy patterns, and the thermodynamic signatures. For the latter, a strict validation procedure based on experimental evidence is used, and the more adequate statistical-mechanical procedure used in an automated fashion, so as to increase throughput. The inspection also focuses on building blocks of larger supramolecular assemblies in various facets, from gel nodes to host aggregates. Finally, other types of complexes are addressed, in which different interactions are highlighted.

## References

- [1] Robert Abel et al. “Advancing Drug Discovery through Enhanced Free Energy Calculations”. *Accounts of Chemical Research* 50.7 (2017), pp. 1625–1632. ISSN: 0001-4842. DOI: [10.1021/acs.accounts.7b00083](https://doi.org/10.1021/acs.accounts.7b00083).
- [2] David L. Mobley and Michael K. Gilson. “Predicting Binding Free Energies: Frontiers and Benchmarks”. *Annual Review of Biophysics* 46.1 (2017), pp. 531–558. DOI: [10.1146/annurev-biophys-070816-033654](https://doi.org/10.1146/annurev-biophys-070816-033654).
- [3] Tânia F. G. G. Cova, Sandra C. C. Nunes, and Alberto A. C. C. Pais. “Free-energy patterns in inclusion complexes: the relevance of non-included moieties in the stability constants”. *Physical Chemistry Chemical Physics* 19.7 (2017), pp. 5209–5221. ISSN: 1463-9076. DOI: [10.1039/C6CP08081B](https://doi.org/10.1039/C6CP08081B).
- [4] Aravindhan Ganesan, Michelle L. Coote, and Khaled Barakat. “Molecular dynamics-driven drug discovery: leaping forward with confidence”. *Drug Discovery Today* 22.2 (2017), pp. 249–269. ISSN: 1359-6446. DOI: <https://doi.org/10.1016/j.drudis.2016.11.001>.
- [5] Zhao Qianqian et al. “Research Advances in Molecular Modeling in Cyclodextrins”. *Current Pharmaceutical Design* 23.3 (2017), pp. 522–531. ISSN: 1381-6128/1873-4286. DOI: <http://dx.doi.org/10.2174/1381612822666161208142617>.
- [6] Hans-Jörg Schneider. “Binding Mechanisms in Supramolecular Complexes”. *Angewandte Chemie International Edition* 48.22 (2009), pp. 3924–3977. ISSN: 1521-3773. DOI: [10.1002/anie.200802947](https://doi.org/10.1002/anie.200802947).
- [7] Frank Biedermann, Werner M. Nau, and Hans-Jörg Schneider. “The Hydrophobic Effect Revisited-Studies with Supramolecular Complexes Imply High-Energy Water as a Noncovalent Driving Force”. *Angewandte Chemie International Edition* 53.42 (2014), pp. 11158–11171. ISSN: 1521-3773. DOI: [10.1002/anie.201310958](https://doi.org/10.1002/anie.201310958).
- [8] Tânia F. G. G. Cova et al. “Properties and patterns in anion-receptors: A closer look at bambusurils”. *Journal of Molecular Liquids* 242.Supplement C (2017), pp. 640–652. ISSN: 0167-7322. DOI: <https://doi.org/10.1016/j.molliq.2017.07.065>.

- [9] Azizeh Abdolmaleki, Fatemeh Ghasemi, and Jahan B. Ghasemi. “Computer-aided drug design to explore cyclodextrin therapeutics and biomedical applications”. *Chemical Biology & Drug Design* 89.2 (2017), pp. 257–268. ISSN: 1747-0285. DOI: [10.1111/cbdd.12825](https://doi.org/10.1111/cbdd.12825).
- [10] Bernhard V. K. J. Schmidt and Christopher Barner-Kowollik. “Dynamic Macromolecular Material Design-The Versatility of Cyclodextrin-Based Host-Guest Chemistry”. *Angewandte Chemie International Edition* 56.29 (2017), pp. 8350–8369. ISSN: 1521-3773. DOI: [10.1002/anie.201612150](https://doi.org/10.1002/anie.201612150).
- [11] Alexey Ryzhakov et al. “Self-Assembly of Cyclodextrins and Their Complexes in Aqueous Solutions”. *Journal of Pharmaceutical Sciences* 105.9 (2016), pp. 2556–2569. ISSN: 0022-3549. DOI: <https://doi.org/10.1016/j.xphs.2016.01.019>.
- [12] Xian Jun Loh. “Supramolecular host-guest polymeric materials for biomedical applications”. *Materials Horizons* 1.2 (2014), pp. 185–195. ISSN: 2051-6347. DOI: [10.1039/C3MH00057E](https://doi.org/10.1039/C3MH00057E).
- [13] Haiyang Zhang et al. “Quantification of Solvent Contribution to the Stability of Noncovalent Complexes”. *Journal of Chemical Theory and Computation* 9.10 (2013), pp. 4542–4551. ISSN: 1549-9618. DOI: [10.1021/ct400404q](https://doi.org/10.1021/ct400404q).
- [14] G. Filippini, C. Bonal, and P. Malfreyt. “How does the dehydration change the host-guest association under homogeneous and heterogeneous conditions?” *Physical Chemistry Chemical Physics* 16.18 (2014), pp. 8667–8674. ISSN: 1463-9076. DOI: [10.1039/C4CP00108G](https://doi.org/10.1039/C4CP00108G).
- [15] Haiyang Zhang et al. “Cooperative Binding of Cyclodextrin Dimers to Isoflavone Analogues Elucidated by Free Energy Calculations”. *The Journal of Physical Chemistry C* 118.13 (2014), pp. 7163–7173. ISSN: 1932-7447. DOI: [10.1021/jp412041d](https://doi.org/10.1021/jp412041d).
- [16] Christophe Chipot and Andrew Pohorille. *Free energy calculations*. Springer, 2007. ISBN: 3540736174.
- [17] Abel Robert et al. “A Critical Review of Validation, Blind Testing, and Real- World Use of Alchemical Protein-Ligand Binding Free Energy Calculations”. *Current Topics in Medicinal Chemistry* 17.23 (2017), pp. 2577–2585. ISSN: 1568-0266/1873-4294. DOI: <http://dx.doi.org/10.2174/1568026617666170414142131>.



- [18] Christophe Chipot. “Frontiers in free-energy calculations of biological systems”. *Wiley Interdisciplinary Reviews: Computational Molecular Science* 4.1 (2014), pp. 71–89. ISSN: 1759-0884. DOI: [10.1002/wcms.1157](https://doi.org/10.1002/wcms.1157).
- [19] John G. Kirkwood. “Statistical Mechanics of Fluid Mixtures”. *The Journal of Chemical Physics* 3.5 (1935), pp. 300–313. ISSN: 0021-9606. DOI: [10.1063/1.1749657](https://doi.org/10.1063/1.1749657).
- [20] Robert W. Zwanzig. “HighTemperature Equation of State by a Perturbation Method. I. Nonpolar Gases”. *The Journal of Chemical Physics* 22.8 (1954), pp. 1420–1426. ISSN: 0021-9606. DOI: [10.1063/1.1740409](https://doi.org/10.1063/1.1740409).
- [21] B. Widom. “Some Topics in the Theory of Fluids”. *The Journal of Chemical Physics* 39.11 (1963), pp. 2808–2812. ISSN: 0021-9606. DOI: [10.1063/1.1734110](https://doi.org/10.1063/1.1734110).
- [22] G. M. Torrie and J. P. Valleau. “Nonphysical sampling distributions in Monte Carlo free-energy estimation: Umbrella sampling”. *Journal of Computational Physics* 23.2 (1977), pp. 187–199. ISSN: 0021-9991. DOI: [https://doi.org/10.1016/0021-9991\(77\)90121-8](https://doi.org/10.1016/0021-9991(77)90121-8).
- [23] Charles H. Bennett. “Efficient estimation of free energy differences from Monte Carlo data”. *Journal of Computational Physics* 22.2 (1976), pp. 245–268. ISSN: 0021-9991. DOI: [https://doi.org/10.1016/0021-9991\(76\)90078-4](https://doi.org/10.1016/0021-9991(76)90078-4).
- [24] Pavel Hobza and Jan Rezac. “Introduction: Noncovalent Interactions”. *Chemical Reviews* 116.9 (2016), pp. 4911–4912. DOI: [10.1021/acs.chemrev.6b00247](https://doi.org/10.1021/acs.chemrev.6b00247).
- [25] M.L. Moraes and L. Caseli. “2 - Supramolecular Systems”. *Nanostructures*. Ed. by Alessandra L. Da Róz et al. William Andrew Publishing, 2017, pp. 33–52. ISBN: 978-0-323-49782-4. DOI: <https://doi.org/10.1016/B978-0-323-49782-4.00002-4>.
- [26] Donald J Cram. “Molecular container compounds”. *Nature* 356.6364 (1992), p. 29.
- [27] Donald J. Cram. “Preorganization-From Solvents to Spherands”. *Angewandte Chemie International Edition in English* 25.12 (1986), pp. 1039–1057. DOI: [10.1002/anie.198610393](https://doi.org/10.1002/anie.198610393).
- [28] Xing Ma and Yanli Zhao. “Biomedical Applications of Supramolecular Systems Based on Host-Guest Interactions”. *Chemical Reviews* 115.15 (2015), pp. 7794–7839. DOI: [10.1021/cr500392w](https://doi.org/10.1021/cr500392w).

- [29] Naji Al-Dubaili, Khaled El-Tarabily, and Nail Saleh. “Host-guest complexes of imazalil with cucurbit[8]uril and  $\beta$ -cyclodextrin and their effect on plant pathogenic fungi”. *Scientific reports* 8.1 (2018), p. 2839.
- [30] Tânia F. G. G. Cova et al. “Drastic Stabilization of Junction Nodes in Supramolecular Structures Based on Host-Guest Complexes”. *Macromolecules* 51.7 (2018), pp. 2732–2741. DOI: [10.1021/acs.macromol.8b00154](https://doi.org/10.1021/acs.macromol.8b00154).
- [31] Ana Figueiras et al. “Interaction of omeprazole with a methylated derivative of beta-cyclodextrin: phase solubility, NMR spectroscopy and molecular simulation”. *Pharmaceutical Research* 24.2 (2007), pp. 377–389. ISSN: 0724-8741. DOI: [10.1007/s11095-006-9161-8](https://doi.org/10.1007/s11095-006-9161-8).
- [32] Ana Figueiras et al. “Molecular interaction governing solubility and release profiles in supramolecular systems containing fenbufen, pluronics and cyclodextrins”. *Journal of Inclusion Phenomena and Macrocyclic Chemistry* 81.3-4 (2015), pp. 395–407. ISSN: 1388-3127.
- [33] Artur J.M. Valente and Olle Soderman. “The formation of host-guest complexes between surfactants and cyclodextrins”. *Advances in Colloid and Interface Science* 205 (2014). Special Issue in honor of Bjorn Lindman, pp. 156–176. ISSN: 0001-8686. DOI: <https://doi.org/10.1016/j.cis.2013.08.001>.
- [34] Mhejabeen Sayed and Haridas Pal. “Supramolecularly assisted modulations in chromophoric properties and their possible applications: an overview”. *Journal of Materials Chemistry C* 4 (14 2016), pp. 2685–2706. DOI: [10.1039/C5TC03321G](https://doi.org/10.1039/C5TC03321G).
- [35] Gerhard Wenz, Bao-Hang Han, and Axel Müller. “Cyclodextrin Rotaxanes and Polyrotaxanes”. *Chemical Reviews* 106.3 (2006), pp. 782–817. DOI: [10.1021/cr970027+](https://doi.org/10.1021/cr970027+).
- [36] Phatsawee Jansook, Noriko Ogawa, and Thorsteinn Loftsson. “Cyclodextrins: structure, physicochemical properties and pharmaceutical applications”. *International Journal of Pharmaceutics* 535.1 (2018), pp. 272–284. ISSN: 0378-5173. DOI: <https://doi.org/10.1016/j.ijpharm.2017.11.018>.
- [37] Sunil S. Jambhekar and Philip Breen. “Cyclodextrins in pharmaceutical formulations I: structure and physicochemical properties, formation of complexes, and types of complex”. *Drug*

- Discovery Today* 21.2 (2016), pp. 356–362. ISSN: 1359-6446. DOI: <https://doi.org/10.1016/j.drudis.2015.11.017>.
- [38] Taishi Higashi, Keiichi Motoyama, and Hidetoshi Arima. “Cyclodextrin-Based Drug Carriers for Low Molecular Weight Drugs, Proteins, and Nucleic Acids”. *Nanomaterials in Pharmacology*. Ed. by Zheng-Rong Lu and Shinji Sakuma. New York, NY: Springer New York, 2016, pp. 27–45. ISBN: 978-1-4939-3121-7. DOI: [10.1007/978-1-4939-3121-7\\_2](https://doi.org/10.1007/978-1-4939-3121-7_2).
- [39] A. Lalatsa and E. Barbu. “Chapter Four - Carbohydrate Nanoparticles for Brain Delivery”. *Nanotechnology and the Brain*. Ed. by Khuloud T. Al-Jamal. Vol. 130. International Review of Neurobiology. Academic Press, 2016, pp. 115–153. DOI: <https://doi.org/10.1016/bs.irn.2016.05.004>.
- [40] Hanna Thomsen et al. “Delivery of cyclodextrin polymers to bacterial biofilms - An exploratory study using rhodamine labelled cyclodextrins and multiphoton microscopy”. *International Journal of Pharmaceutics* 531.2 (2017), pp. 650–657. ISSN: 0378-5173. DOI: <https://doi.org/10.1016/j.ijpharm.2017.06.011>.
- [41] Salvatore Fanali. “Nano-liquid chromatography applied to enantiomers separation”. *Journal of Chromatography A* 1486 (2017). Editors’ Tribute to Professor Hanfa Zou, pp. 20–34. ISSN: 0021-9673. DOI: <https://doi.org/10.1016/j.chroma.2016.10.028>.
- [42] Gilles Brackman et al. “Dressings Loaded with Cyclodextrin-Hamamelitannin Complexes Increase Staphylococcus aureus Susceptibility Toward Antibiotics Both in Single as well as in Mixed Biofilm Communities”. *Macromolecular Bioscience* 16.6 (), pp. 859–869. DOI: [10.1002/mabi.201500437](https://doi.org/10.1002/mabi.201500437).
- [43] Edgardo Rivera-Delgado and Horst A. von Recum. “Using Affinity To Provide Long-Term Delivery of Antiangiogenic Drugs in Cancer Therapy”. *Molecular Pharmaceutics* 14.3 (2017), pp. 899–907. DOI: [10.1021/acs.molpharmaceut.6b01109](https://doi.org/10.1021/acs.molpharmaceut.6b01109).
- [44] Jianxiang Zhang and Peter X. Ma. “Cyclodextrin-based supramolecular systems for drug delivery: Recent progress and future perspective”. *Advanced Drug Delivery Reviews* 65.9 (2013), pp. 1215–1233. ISSN: 0169-409X.

- [45] Ji Sheng Yang and Li Yang. “Preparation and application of cyclodextrin immobilized polysaccharides”. *J. Mater. Chem. B* 1 (7 2013), pp. 909–918. DOI: [10.1039/C2TB00107A](https://doi.org/10.1039/C2TB00107A).
- [46] Tânia FGG Cova et al. “Combining cellulose and cyclodextrins: fascinating designs for materials and pharmaceuticals”. *Frontiers in chemistry* 6 (2018), p. 271.
- [47] Cheng Zhu et al. “Energetics of cellulose and cyclodextrin glycosidic bond cleavage”. *React. Chem. Eng.* 2 (2 2017), pp. 201–214. DOI: [10.1039/C6RE00176A](https://doi.org/10.1039/C6RE00176A).
- [48] A Villiers. “Sur la fermentation de la fécule par l’action du ferment butyrique”. *Compt. Rend. Acad. Sci* 112 (1891), pp. 536–538.
- [49] Fr Schardinger. “Bacillus macerans, ein Aceton bildender Rottebacillus”. *Zbl Bakteriol Parasitenkd Infektionskr Hyg Abt II* 14 (1905), pp. 772–781.
- [50] Hans Pringsheim, Cleveland Abbe, et al. “chemistry of the monosaccharides and the polysaccharides” (1932).
- [51] Karl Freudenberg, Hans Boppel, and Margot Meyer-Delius. “Beobachtungen an der Stärke”. *Naturwissenschaften* 26.8 (1938), pp. 123–124.
- [52] Dexter French. “The schardinger dextrans”. *Advances in carbohydrate chemistry*. Vol. 12. Elsevier, 1957, pp. 189–260.
- [53] Jozsef Szejtli. “Introduction and general overview of cyclodextrin chemistry”. *Chemical reviews* 98.5 (1998), pp. 1743–1754.
- [54] Tomoki Ogoshi and Akira Harada. “Chemical Sensors Based on Cyclodextrin Derivatives”. *Sensors* 8.8 (2008), pp. 4961–4982. ISSN: 1424-8220. DOI: [10.3390/s8084961](https://doi.org/10.3390/s8084961). URL: <http://www.mdpi.com/1424-8220/8/8/4961>.
- [55] Zhongxiang Fang and Bhesh Bhandari. “Encapsulation of polyphenols - a review”. *Trends in Food Science & Technology* 21.10 (2010), pp. 510–523. ISSN: 0924-2244. DOI: <https://doi.org/10.1016/j.tifs.2010.08.003>.
- [56] Seo Yeong Gim et al. “Application of  $\beta$ -cyclodextrin, chitosan, and collagen on the stability of tocopherols and the oxidative stability in heated oils”. *European Journal of Lipid Science and Technology* 119.10 (), p. 1700124. DOI: [10.1002/ejlt.201700124](https://doi.org/10.1002/ejlt.201700124).

- [57] Zeynep Aytac et al. “Antioxidant electrospun zein nanofibrous web encapsulating quercetin/cyclodextrin inclusion complex”. *Journal of Materials Science* 53.2 (2018), pp. 1527–1539. ISSN: 1573-4803. DOI: [10.1007/s10853-017-1580-x](https://doi.org/10.1007/s10853-017-1580-x).
- [58] E. M. Martin Del Valle. “Cyclodextrins and their uses: a review”. *Process Biochemistry* 39.9 (2004), pp. 1033–1046. ISSN: 1359-5113. DOI: [https://doi.org/10.1016/S0032-9592\(03\)00258-9](https://doi.org/10.1016/S0032-9592(03)00258-9).
- [59] Thorsteinn Loftsson and Marcus E. Brewster. “Pharmaceutical applications of cyclodextrins: basic science and product development”. *Journal of Pharmacy and Pharmacology* 62.11 (), pp. 1607–1621. DOI: [10.1111/j.2042-7158.2010.01030.x](https://doi.org/10.1111/j.2042-7158.2010.01030.x).
- [60] Agnieszka Popielec and Thorsteinn Loftsson. “Effects of cyclodextrins on the chemical stability of drugs”. *International Journal of Pharmaceutics* 531.2 (2017), pp. 532–542. ISSN: 0378-5173. DOI: <https://doi.org/10.1016/j.ijpharm.2017.06.009>.
- [61] Thorsteinn Loftsson et al. “Cyclodextrins in drug delivery”. *Expert Opinion on Drug Delivery* 2.2 (2005), pp. 335–351. DOI: [10.1517/17425247.2.1.335](https://doi.org/10.1517/17425247.2.1.335).
- [62] Arik Dahan et al. “The solubility-permeability interplay and oral drug formulation design: Two heads are better than one”. *Advanced Drug Delivery Reviews* 101 (2016). Understanding the challenges of beyond-rule-of-5 compounds, pp. 99–107. ISSN: 0169-409X. DOI: <https://doi.org/10.1016/j.addr.2016.04.018>.
- [63] Eunae Cho and Seunho Jung. “Supramolecular Complexation of Carbohydrates for the Bioavailability Enhancement of Poorly Soluble Drugs”. *Molecules* 20.10 (2015), pp. 19620–19646. ISSN: 1420-3049. DOI: [10.3390/molecules201019620](https://doi.org/10.3390/molecules201019620).
- [64] Ajay Semalty. “Cyclodextrin and phospholipid complexation in solubility and dissolution enhancement: a critical and meta-analysis”. *Expert Opinion on Drug Delivery* 11.8 (2014), pp. 1255–1272. DOI: [10.1517/17425247.2014.916271](https://doi.org/10.1517/17425247.2014.916271).
- [65] Sandeep Kalepu and Vijaykumar Nekkanti. “Insoluble drug delivery strategies: review of recent advances and business prospects”. *Acta pharmaceutica Sinica. B* 5.5 (2015), pp. 442–453. ISSN: 2211-3835. DOI: [10.1016/j.apsb.2015.07.003](https://doi.org/10.1016/j.apsb.2015.07.003).

- [66] Katsuhiko Ariga. “2.2 - Supramolecules”. *Biomaterials Nanoarchitectonics*. Ed. by Mitsuhiro Ebara. William Andrew Publishing, 2016, pp. 25–40. ISBN: 978-0-323-37127-8. DOI: <https://doi.org/10.1016/B978-0-323-37127-8.00003-0>.
- [67] T. Higuchi. “A phase solubility technique”. *Advances in Analytical Chemistry and Instrumentation* 4 (1965), pp. 117–211.
- [68] Benguo Liu et al. “Physiochemical Properties of the Inclusion Complex of Puerarin and Glucosyl- $\beta$ -Cyclodextrin”. *Journal of Agricultural and Food Chemistry* 60.51 (2012), pp. 12501–12507. DOI: [10.1021/jf304447x](https://doi.org/10.1021/jf304447x).
- [69] Emilio Aicart and Elena Junquera. “Complex Formation between Purine Derivatives and Cyclodextrins: A Fluorescence Spectroscopy Study”. *Journal of Inclusion Phenomena and Macrocyclic Chemistry* 47.3 (2003), pp. 161–165. ISSN: 1573-1111. DOI: [10.1023/B:JIPH.0000011786.89533.0e](https://doi.org/10.1023/B:JIPH.0000011786.89533.0e).
- [70] Y. Nagase et al. “Improvement of some pharmaceutical properties of DY-9760e by sulfobutyl ether  $\beta$ -cyclodextrin”. *International Journal of Pharmaceutics* 229.1 (2001), pp. 163–172. ISSN: 0378-5173. DOI: [https://doi.org/10.1016/S0378-5173\(01\)00851-1](https://doi.org/10.1016/S0378-5173(01)00851-1).
- [71] Paola Mura. “Analytical techniques for characterization of cyclodextrin complexes in the solid state: A review”. *Journal of Pharmaceutical and Biomedical Analysis* 113 (2015), pp. 226–238. ISSN: 0731-7085. DOI: <https://doi.org/10.1016/j.jpba.2015.01.058>.
- [72] Szabolcs Béni et al. “Cyclodextrin/imatinib complexation: Binding mode and charge dependent stabilities”. *European Journal of Pharmaceutical Sciences* 30.2 (2007), pp. 167–174. ISSN: 0928-0987. DOI: <https://doi.org/10.1016/j.ejps.2006.10.008>.
- [73] Silvia Munoz-Botella et al. “Differentiating inclusion complexes from host molecules by tapping-mode atomic force microscopy”. *Biophysical Journal* 71.1 (1996), pp. 86–90.
- [74] Shigeo Oyama et al. “Interactive Force between Cyclodextrin Inclusion Complexes Studied by Atomic Force Microscopy”. *Japanese Journal of Applied Physics* 40.6S (2001), p. 4419.
- [75] Tommaso Auletta et al. “ $\beta$ -Cyclodextrin Host-Guest Complexes Probed under Thermodynamic Equilibrium: Thermodynamics and AFM Force Spectroscopy”. *Journal of the American Chemical Society* 126.5 (2004), pp. 1577–1584. DOI: [10.1021/ja0383569](https://doi.org/10.1021/ja0383569).

- [76] R. Periasamy, S. Kothainayaki, and K. Sivakumar. “Encapsulation of dicinnamalacetone in  $\beta$ -cyclodextrin: A physicochemical evaluation and molecular modeling approach on 1:2 inclusion complex”. *Journal of Macromolecular Science, Part A* 53.9 (2016), pp. 546–556. DOI: [10.1080/10601325.2016.1201750](https://doi.org/10.1080/10601325.2016.1201750).
- [77] Katherine Lozano et al. “Electrochemical and associated techniques for the study of the inclusion complexes of thymol and  $\beta$ -cyclodextrin and its interaction with DNA”. *Journal of Solid State Electrochemistry* 22.5 (2018), pp. 1483–1493. ISSN: 1433-0768. DOI: [10.1007/s10008-017-3805-y](https://doi.org/10.1007/s10008-017-3805-y).
- [78] Allan Hedges. “Chapter 22 - Cyclodextrins: Properties and Applications”. *Starch (Third Edition)*. Ed. by James BeMiller and Roy Whistler. Third Edition. Food Science and Technology. San Diego: Academic Press, 2009, pp. 833–851. ISBN: 978-0-12-746275-2. DOI: <https://doi.org/10.1016/B978-0-12-746275-2.00022-7>.
- [79] Gerhard Wenz and Eric Monflier. “Superstructures with cyclodextrins: chemistry and applications III”. *Beilstein Journal of Organic Chemistry* 12 (2016), pp. 937–938. ISSN: 1860-5397. DOI: [10.3762/bjoc.12.91](https://doi.org/10.3762/bjoc.12.91).
- [80] Amornrat Klaewklod et al. “Characterization of supramolecular gels based on  $\beta$ -cyclodextrin and polyethyleneglycol and their potential use for topical drug delivery”. *Materials Science and Engineering: C* 50 (2015), pp. 242–250. ISSN: 0928-4931. DOI: <https://doi.org/10.1016/j.msec.2015.02.018>.
- [81] Yang Yang et al. “Targeted Polysaccharide Nanoparticle for Adamplatin Prodrug Delivery”. *Journal of Medicinal Chemistry* 56.23 (2013), pp. 9725–9736. DOI: [10.1021/jm4014168](https://doi.org/10.1021/jm4014168).
- [82] Qi-Da, Gu-Ping Tang, and Paul K. Chu. “Cyclodextrin-Based Host-Guest Supramolecular Nanoparticles for Delivery: From Design to Applications”. *Accounts of Chemical Research* 47.7 (2014), pp. 2017–2025. DOI: [10.1021/ar500055s](https://doi.org/10.1021/ar500055s).
- [83] Ran Namgung et al. “Poly-cyclodextrin and poly-paclitaxel nano-assembly for anticancer therapy.” *Nature Communications* 5.3702 (2014), pp. 1–12. DOI: [10.1038/ncomms4702](https://doi.org/10.1038/ncomms4702).
- [84] Yang Yang et al. “Polysaccharide-based Noncovalent Assembly for Targeted Delivery of Taxol”. *Scientific Reports* 6.19212 (2016), pp. 559–567. DOI: [10.1038/srep19212](https://doi.org/10.1038/srep19212).

- [85] Chutimon Muankaew and Thorsteinn Loftsson. “Cyclodextrin-Based Formulations: A Non-Invasive Platform for Targeted Drug Delivery”. *Basic & Clinical Pharmacology & Toxicology* 122.1 (2017), pp. 46–55. DOI: [10.1111/bcpt.12917](https://doi.org/10.1111/bcpt.12917).
- [86] Dennis H. Schwarz, Annegret Engelke, and Gerhard Wenz. “Solubilizing steroidal drugs by beta-cyclodextrin derivatives”. *International Journal of Pharmaceutics* 531.2 (2017), pp. 559–567. DOI: [10.1016/j.ijpharm.2017.07.046](https://doi.org/10.1016/j.ijpharm.2017.07.046).
- [87] Qingqing Xiong et al. “A supramolecular nanoparticle system based on  $\beta$ -cyclodextrin-conjugated poly-l-lysine and hyaluronic acid for co-delivery of gene and chemotherapy agent targeting hepatocellular carcinoma”. *Colloids and Surfaces B: Biointerfaces* 155.3 (2017), pp. 93–103. DOI: [10.1016/j.colsurfb.2017.04.008](https://doi.org/10.1016/j.colsurfb.2017.04.008).
- [88] Gamze Varan et al. “Amphiphilic cyclodextrin nanoparticles”. *International Journal of Pharmaceutics* 531.2 (2017), pp. 457–469. DOI: [10.1016/j.ijpharm.2017.06.010](https://doi.org/10.1016/j.ijpharm.2017.06.010).
- [89] Ruslan R. Kashapov et al. “Controlling the binding of hydrophobic drugs with supramolecular assemblies of  $\beta$ -cyclodextrin”. *Colloids and Surfaces A: Physicochemical and Engineering Aspects* 527 (2017), pp. 55–62. DOI: [10.1016/j.colsurfa.2017.05.026](https://doi.org/10.1016/j.colsurfa.2017.05.026).
- [90] Aurélie Charlot et al. “Controlled synthesis and inclusion ability of a hyaluronic acid derivative bearing beta-cyclodextrin molecules”. *Biomacromolecules* 7.3 (2006), pp. 907–913. DOI: [10.1021/bm0507094](https://doi.org/10.1021/bm0507094).
- [91] Aurélie Charlot and Rachel Auzély-Velty. “Synthesis of Novel Supramolecular Assemblies Based on Hyaluronic Acid Derivatives Bearing Bivalent  $\beta$ -Cyclodextrin and Adamantane Moieties”. *Macromolecules* 40.4 (2007), pp. 1147–1158. DOI: [10.1021/ma062322e](https://doi.org/10.1021/ma062322e).
- [92] Wanda Sliwa and Tomasz Girek, eds. *Cyclodextrins: Properties and Applications*. 1st ed. Germany: Wiley-VCH, 2017.
- [93] Mikhail V. Rekharsky and Yoshihisa Inoue. “Complexation Thermodynamics of Cyclodextrins”. *Chemical Reviews* 98.5 (1998), pp. 1875–1918. DOI: [10.1021/cr970015o](https://doi.org/10.1021/cr970015o).
- [94] Christopher B. Rodell, Joshua E. Mealy, and Jason A. Burdick. “Supramolecular Guest-Host Interactions for the Preparation of Biomedical Materials”. *Bioconjugate Chemistry* 26.12 (2015), pp. 2279–2289. DOI: [10.1021/acs.bioconjchem.5b00483](https://doi.org/10.1021/acs.bioconjchem.5b00483).



- [95] Keivan Sadrerafi, Ellen Moore, and Mark Lee. “Association constant of  $\beta$ -cyclodextrin with carboranes, adamantane, and their derivatives using displacement binding technique”. *Journal of Inclusion Phenomena and Macrocyclic Chemistry* 83.1-2 (2015), pp. 159–166. DOI: [10.1007/s10847-015-0552-5](https://doi.org/10.1007/s10847-015-0552-5).
- [96] Diem N. Tran et al. “Cyclodextrin-adamantane conjugates, self-inclusion and aggregation versus supramolecular polymer formation”. *Organic Chemistry Frontiers* 1 (2014), pp. 703–706. DOI: [10.1039/C4QO00104D](https://doi.org/10.1039/C4QO00104D).
- [97] Yang et al. “Nanoassemblies driven by cyclodextrin-based inclusion complexation”. *Chemical Communications* 50.76 (2014), pp. 11083–11092. DOI: [10.1039/C4QO00104D](https://doi.org/10.1039/C4QO00104D).
- [98] Iurii Antoniuk et al. “Host-guest interaction and structural ordering in polymeric nanoassemblies: Influence of molecular design”. *International Journal of Pharmaceutics* 531.2 (2017), pp. 433–443. DOI: [10.1016/j.ijpharm.2017.02.061](https://doi.org/10.1016/j.ijpharm.2017.02.061).
- [99] Xiaoqian Yang et al. “MDR1 siRNA loaded hyaluronic acid-based CD44 targeted nanoparticle systems circumvent paclitaxel resistance in ovarian cancer”. *Scientific Reports* 8509 (2015), pp. 1–8. DOI: [10.1038/srep08509](https://doi.org/10.1038/srep08509).
- [100] Helena Knopf-Marques et al. “Hyaluronic Acid and Its Derivatives in Coating and Delivery Systems: Applications in Tissue Engineering, Regenerative Medicine and Immunomodulation”. *Advanced Healthcare Materials* 5.22 (2016), pp. 2841–2855. DOI: [10.1002/adhm.201600316](https://doi.org/10.1002/adhm.201600316).
- [101] Sindhu Doppalapudi et al. “Biodegradable polymers for targeted delivery of anti-cancer drugs”. *Expert Opinion on Drug Delivery* 13.6 (2016), pp. 891–909. DOI: [10.1517/17425247.2016.1156671](https://doi.org/10.1517/17425247.2016.1156671).
- [102] Abdulaziz Almalik et al. “Hyaluronic Acid Coated Chitosan Nanoparticles Reduced the Immunogenicity of the Formed Protein Corona”. *Scientific Reports* 10542 (2017), pp. 1–6. DOI: [10.1038/s41598-017-10836-7](https://doi.org/10.1038/s41598-017-10836-7).
- [103] George Mattheolabakis et al. “Hyaluronic acid targeting of CD44 for cancer therapy: from receptor biology to nanomedicine”. *Journal of Drug Targeting* 23.7-8 (2015), pp. 605–618. DOI: [10.3109/1061186X.2015.10520729](https://doi.org/10.3109/1061186X.2015.10520729).

- [104] H. S. Han et al. “Bioreducible core-crosslinked hyaluronic acid micelle for targeted cancer therapy”. *Journal of Controlled Release* 200 (2015), pp. 158–166. DOI: [10.1016/j.jconrel.2014.12.032](https://doi.org/10.1016/j.jconrel.2014.12.032).
- [105] David Naor. “Interaction Between Hyaluronic Acid and Its Receptors (CD44, RHAMM) Regulates the Activity of Inflammation and Cancer”. *Frontiers in Immunology* 7.39 (2016), Editorial. DOI: [10.3389/fimmu.2016.00039](https://doi.org/10.3389/fimmu.2016.00039).
- [106] Giuliana Manzi et al. ““Click” hyaluronan based nanohydrogels as multifunctionalizable carriers for hydrophobic drugs”. *Carbohydrate Polymers* 174 (2017), pp. 706–715. DOI: [10.1016/j.carbpol.2017.07.003](https://doi.org/10.1016/j.carbpol.2017.07.003).
- [107] M. Barbarisi et al. “Novel nanohydrogel of hyaluronic acid loaded with quercetin alone and in combination with temozolomide as new therapeutic tool, CD44 targeted based, of glioblastoma multiforme”. *Journal of Cellular Physiology* (2017). DOI: [10.1002/jcp.26238](https://doi.org/10.1002/jcp.26238).
- [108] Mehmet S. Eroglu et al. “Sugar Based Biopolymers in Nanomedicine; New Emerging Era for Cancer Imaging and Therapy”. *Current Topics in Medicinal Chemistry* 17.13 (2017), pp. 1507–1520. DOI: [10.2174/1568026616666161222101703](https://doi.org/10.2174/1568026616666161222101703).
- [109] Yoshinori Takashima et al. “Supramolecular Materials Cross-Linked by Host-Guest Inclusion Complexes: The Effect of Side Chain Molecules on Mechanical Properties”. *Macromolecules* 50.8 (2017), pp. 53254–3261. DOI: [10.1021/acs.macromol.7b00266](https://doi.org/10.1021/acs.macromol.7b00266).
- [110] Mohammad Jawaid and Faruq Mohammad. *Nanocellulose and Nanohydrogel Matrices: Biotechnological and Biomedical Applications*. John Wiley & Sons, 2017. ISBN: 978-3-527-34172-6.
- [111] Pranjali Yadav et al. “Gold laced bio-macromolecules for theranostic application”. *International Journal of Biological Macromolecules* 110 (2018). *Biological Macromolecules for Delivery, Imaging & Therapy (BMDIT-2018)*, pp. 39–53. ISSN: 0141-8130. DOI: <https://doi.org/10.1016/j.ijbiomac.2017.10.124>.
- [112] Chutimon Muankaew, Phatsawee Jansook, and Thorsteinn Loftsson. “Evaluation of  $\gamma$ -cyclodextrin effect on permeation of lipophilic drugs: application of cellophane/fused octanol membrane”. *Pharmaceutical Development and Technology* 22.4 (2017), pp. 562–570. DOI: [10.1080/10837450.2016.1180394](https://doi.org/10.1080/10837450.2016.1180394).

- [113] Murali Mohan Yallapu et al. “Design of curcumin loaded cellulose nanoparticles for prostate cancer”. *Current drug metabolism* 13.1 (2012), pp. 120–128. ISSN: 1389-2002/1875-5453. DOI: [10.2174/138920012798356952](https://doi.org/10.2174/138920012798356952).
- [114] Xianqiang Li et al. “Preparation, characterization and pharmacokinetics of doxycycline hydrochloride and florfenicol polyvinylpyrrolidone microparticle entrapped with hydroxypropyl- $\beta$ -cyclodextrin inclusion complexes suspension”. *Colloids and Surfaces B: Biointerfaces* 141 (2016), pp. 634–642. ISSN: 0927-7765. DOI: <https://doi.org/10.1016/j.colsurfb.2016.02.027>.
- [115] Nan Sun, Ting Wang, and Xiufeng Yan. “Self-assembled supermolecular hydrogel based on hydroxyethyl cellulose: Formation, in vitro release and bacteriostasis application”. *Carbohydrate Polymers* 172 (2017), pp. 49–59. ISSN: 0144-8617. DOI: <https://doi.org/10.1016/j.carbpol.2017.05.026>.
- [116] Jiaojiao Du et al. “Biopolymer-based supramolecular micelles from  $\beta$ -cyclodextrin and methylcellulose”. *Carbohydrate Polymers* 90.1 (2012), pp. 569–574. ISSN: 0144-8617. DOI: <https://doi.org/10.1016/j.carbpol.2012.05.079>.
- [117] “Host-guest chemistry of cyclodextrin carbamates and cellulose derivatives in aqueous solution”. *Carbohydrate Polymers* 98.1 (2013), pp. 982–987. ISSN: 0144-8617. DOI: <https://doi.org/10.1016/j.carbpol.2013.06.075>.
- [118] Brunella Cappello et al. “Formulation and Preliminary in vivo Testing of Rufloxacin-Cyclodextrin Ophthalmic Solutions”. *Journal of Inclusion Phenomena and Macrocyclic Chemistry* 44.1 (2002), pp. 173–176. ISSN: 1573-1111. DOI: [10.1023/A:1023050814697](https://doi.org/10.1023/A:1023050814697).
- [119] Ambar S Jimenez et al. “Effect of surface organic coatings of cellulose nanocrystals on the viability of mammalian cell lines”. *Nanotechnology, Science and Applications* 10 (2017), p. 123.
- [120] Ning Lin and Alain Dufresne. “Supramolecular Hydrogels from In Situ Host-Guest Inclusion between Chemically Modified Cellulose Nanocrystals and Cyclodextrin”. *Biomacromolecules* 14.3 (2013), pp. 871–880. DOI: [10.1021/bm301955k](https://doi.org/10.1021/bm301955k).

- [121] Nadia Shamshad Malik, Mahmood Ahmad, and Muhammad Usman Minhas. “Cross-linked  $\beta$ -cyclodextrin and carboxymethyl cellulose hydrogels for controlled drug delivery of acyclovir”. *PloS one* 12.2 (2017), e0172727.
- [122] Gautier M.A. Ndong Ntoutoume et al. “Development of curcumin-cyclodextrin/cellulose nanocrystals complexes: New anticancer drug delivery systems”. *Bioorganic & Medicinal Chemistry Letters* 26.3 (2016), pp. 941–945. ISSN: 0960-894X. DOI: <https://doi.org/10.1016/j.bmcl.2015.12.060>.
- [123] S.A. El-Gizawy et al. “Nasal Drug Delivery of a Mucoadhesive Oxybutynin Chloride Gel: In Vitro Evaluation and In Vivo in Situ Study in Experimental Rats”. *Journal of Drug Delivery Science and Technology* 23.6 (2013), pp. 569–575. ISSN: 1773-2247. DOI: [https://doi.org/10.1016/S1773-2247\(13\)50086-4](https://doi.org/10.1016/S1773-2247(13)50086-4).
- [124] K Rehman, MCIM Amin, and S Muda. “Influence of beta-cyclodextrin and chitosan in the formulation of a colon-specific drug delivery system”. *Drug Res* 63 (2013), pp. 657–662. DOI: [10.1055/s-0033-1349129](https://doi.org/10.1055/s-0033-1349129).
- [125] Lingzhi Zhang, Jinping Zhou, and Lina Zhang. “Structure and properties of  $\beta$ -cyclodextrin/cellulose hydrogels prepared in NaOH/urea aqueous solution”. *Carbohydrate Polymers* 94.1 (2013), pp. 386–393. ISSN: 0144-8617. DOI: <https://doi.org/10.1016/j.carbpol.2012.12.077>.
- [126] Xelhua Marcos et al. “Poloxamer-hydroxyethyl cellulose- $\alpha$ -cyclodextrin supramolecular gels for sustained release of griseofulvin”. *International Journal of Pharmaceutics* 500.1 (2016), pp. 11–19. ISSN: 0378-5173. DOI: <https://doi.org/10.1016/j.ijpharm.2016.01.015>.
- [127] Shuai Han et al. “Building a bio-based hydrogel via electrostatic and host-guest interactions for realizing dual-controlled release mechanism”. *International Journal of Biological Macromolecules* 105 (2017), pp. 377–384. ISSN: 0141-8130. DOI: <https://doi.org/10.1016/j.ijbiomac.2017.07.049>.
- [128] Haiqin Huang et al. “Compression-coated tablets of glipizide using hydroxypropylcellulose for zero-order release: In vitro and in vivo evaluation”. *International Journal of Pharmaceutics* 446.1 (2013), pp. 211–218. ISSN: 0378-5173. DOI: <https://doi.org/10.1016/j.ijpharm.2013.01.039>.

- [129] L. C. L. Sá-Barreto et al. “Modulated dissolution rate from the inclusion complex of antichagasic benzimidazole and cyclodextrin using hydrophilic polymer”. *Pharmaceutical Development and Technology* 18.5 (2013), pp. 1035–1041. DOI: [10.3109/10837450.2011.644299](https://doi.org/10.3109/10837450.2011.644299).
- [130] Min-Soo Kim. “Influence of hydrophilic additives on the supersaturation and bioavailability of dutasteride-loaded hydroxypropyl- $\beta$ -cyclodextrin nanostructures”. *International journal of nanomedicine* 8 (2013), p. 2029.
- [131] Chao Dong et al. “Preparation of antimicrobial cellulose fibers by grafting  $\beta$ -cyclodextrin and inclusion with antibiotics”. *Materials Letters* 124 (2014), pp. 181–183. ISSN: 0167-577X. DOI: <https://doi.org/10.1016/j.matlet.2014.03.091>.
- [132] Nathalie Lavoine et al. “Elaboration of a new antibacterial bio-nano-material for food-packaging by synergistic action of cyclodextrin and microfibrillated cellulose”. *Innovative Food Science & Emerging Technologies* 26 (2014), pp. 330–340. ISSN: 1466-8564. DOI: <https://doi.org/10.1016/j.ifset.2014.06.006>.
- [133] Alejandro Costoya, Angel Concheiro, and Carmen Alvarez-Lorenzo. “Electrospun Fibers of Cyclodextrins and Poly(cyclodextrins)”. *Molecules* 22.2 (2017). ISSN: 1420-3049. DOI: [10.3390/molecules22020230](https://doi.org/10.3390/molecules22020230).
- [134] Tânia F.G.G. Cova et al. “Aggregation of Cyclodextrins: Fundamental Issues and Applications”. *Cyclodextrin*. Ed. by Poonam Arora and Neelima Dhingra. Rijeka: IntechOpen, 2018. Chap. 2. DOI: [10.5772/intechopen.73532](https://doi.org/10.5772/intechopen.73532).
- [135] Phennapha Saokham et al. “The self-assemble of natural cyclodextrins in aqueous solutions: Application of miniature permeation studies for critical aggregation concentration (cac) determinations”. *International Journal of Pharmaceutics* 505.1 (2016), pp. 187–193. ISSN: 0378-5173. DOI: <https://doi.org/10.1016/j.ijpharm.2016.03.049>.
- [136] George M. Whitesides and Mila Boncheva. “Beyond molecules: Self-assembly of mesoscopic and macroscopic components”. *Proceedings of the National Academy of Sciences* 99.8 (2002), pp. 4769–4774. ISSN: 0027-8424. DOI: [10.1073/pnas.082065899](https://doi.org/10.1073/pnas.082065899).

- [137] Thorsteinn Loftsson. “Self-assembled cyclodextrin nanoparticles and drug delivery”. *Journal of Inclusion Phenomena and Macrocyclic Chemistry* 80.1 (2014), pp. 1–7. ISSN: 1573-1111. DOI: [10.1007/s10847-013-0375-1](https://doi.org/10.1007/s10847-013-0375-1).
- [138] Martin Messner et al. “Self-assembled cyclodextrin aggregates and nanoparticles”. *International Journal of Pharmaceutics* 387.1 (2010), pp. 199–208. ISSN: 0378-5173. DOI: <https://doi.org/10.1016/j.ijpharm.2009.11.035>.
- [139] Frederico B. De Sousa et al. “Superstructure based on small beta-CD self-assembly induced by a small guest molecule”. *Physical Chemistry Chemical Physics* 14.6 (2012), pp. 1934–1944. ISSN: 1463-9076. DOI: [10.1039/C2CP22768A](https://doi.org/10.1039/C2CP22768A).
- [140] Edvaldo Sabadini, Terence Cosgrove, and Fernanda do Carmo. “Solubility of cyclomaltooligosaccharides (cyclodextrins) in  $H_2O$  and  $D_2O$ : a comparative study”. *Carbohydrate Research* 341.2 (2006), pp. 270–274. ISSN: 0008-6215. DOI: <https://doi.org/10.1016/j.carres.2005.11.004>.
- [141] Wensheng Cai et al. “Can the anomalous aqueous solubility of small beta-cyclodextrin be explained by its hydration free energy alone?” *Physical Chemistry Chemical Physics* 10.22 (2008), pp. 3236–3243. ISSN: 1463-9076. DOI: [10.1039/B717509D](https://doi.org/10.1039/B717509D).
- [142] G. González-Gaitano et al. “The Aggregation of Cyclodextrins as Studied by Photon Correlation Spectroscopy”. *Journal of Inclusion Phenomena and Macrocyclic Chemistry* 44.1 (2002), pp. 101–105. ISSN: 1573-1111. DOI: [10.1023/A:1023065823358](https://doi.org/10.1023/A:1023065823358).
- [143] Guosong Chen and Ming Jiang. “Cyclodextrin-based inclusion complexation bridging supramolecular chemistry and macromolecular self-assembly”. *Chem. Soc. Rev.* 40 (5 2011), pp. 2254–2266. DOI: [10.1039/C0CS00153H](https://doi.org/10.1039/C0CS00153H).
- [144] Hadar Zaman et al. “Characterisation of aggregates of cyclodextrin-drug complexes using Taylor Dispersion Analysis”. *International Journal of Pharmaceutics* 522.1 (2017), pp. 98–109. ISSN: 0378-5173. DOI: <https://doi.org/10.1016/j.ijpharm.2017.02.012>.
- [145] Jef Stappaerts et al. “The impact of guest compounds on cyclodextrin aggregation behavior: A series of structurally related parabens”. *International Journal of Pharmaceutics* 529.1 (2017), pp. 442–450. ISSN: 0378-5173. DOI: <https://doi.org/10.1016/j.ijpharm.2017.07.026>.

- [146] Sergey V. Kurkov and Thorsteinn Loftsson. “Cyclodextrins”. *International Journal of Pharmaceutics* 453.1 (2013). Poorly Soluble Drugs, pp. 167–180. ISSN: 0378-5173. DOI: <https://doi.org/10.1016/j.ijpharm.2012.06.055>.
- [147] Tânia F. Cova et al. “Modeling Soft Supramolecular Nanostructures by Molecular Simulations”. *Molecular Dynamics*. Ed. by Alexander Vakhrushev. Rijeka: IntechOpen, 2018. Chap. 2. DOI: [10.5772/intechopen.74939](https://doi.org/10.5772/intechopen.74939).
- [148] Qianqian Zhao et al. “Research advances in molecular modeling in cyclodextrins”. *Current Pharmaceutical Design* 23.3 (2017), pp. 522–531.
- [149] Lama D. Malhis et al. “Molecular dynamics simulation of a cucurbituril based molecular switch triggered by pH changes”. *Computational and Theoretical Chemistry* 1066.Supplement C (2015), pp. 104–112. ISSN: 2210-271X. DOI: <https://doi.org/10.1016/j.comptc.2015.05.010>.
- [150] Tânia F. G. G. Cova et al. “Bambusurils as effective ion caging agents: Does desolvation guide conformation?” *Chemical Physics Letters* 672.Supplement C (2017), pp. 89–96. ISSN: 0009-2614. DOI: <https://doi.org/10.1016/j.cplett.2017.01.029>.
- [151] Ruyin Cao and Shanshan Wu. “In silico properties characterization of water-soluble  $\gamma$ -cyclodextrin bi-capped C60 complex: Free energy and geometrical insights for stability and solubility”. *Carbohydrate Polymers* 124.Supplement C (2015), pp. 188–195. ISSN: 0144-8617. DOI: <https://doi.org/10.1016/j.carbpol.2015.02.014>.
- [152] Wensheng Cai et al. “Inclusion Mechanism of Steroid Drugs into  $\beta$ -Cyclodextrins. Insights from Free Energy Calculations”. *The Journal of Physical Chemistry B* 113.22 (2009), pp. 7836–7843. ISSN: 1520-6106. DOI: [10.1021/jp901825w](https://doi.org/10.1021/jp901825w).
- [153] Matias I. Sancho et al. “Theoretical and Experimental Study of Inclusion Complexes of  $\beta$ -Cyclodextrins with Chalcone and 2',4'-Dihydroxychalcone”. *The Journal of Physical Chemistry B* 120.12 (2016), pp. 3000–3011. ISSN: 1520-6106. DOI: [10.1021/acs.jpccb.5b11317](https://doi.org/10.1021/acs.jpccb.5b11317).
- [154] Edoardo Giovannelli et al. “Binding Free Energies of Host-Guest Systems by Nonequilibrium Alchemical Simulations with Constrained Dynamics: Theoretical Framework”. *Journal of*

- Chemical Theory and Computation* 13.12 (2017), pp. 5874–5886. ISSN: 1549-9618. DOI: [10.1021/acs.jctc.7b00594](https://doi.org/10.1021/acs.jctc.7b00594).
- [155] R. Vijayaraj et al. “Molecular Dynamics and Umbrella Sampling Study of Stabilizing Factors in Cyclic Peptide-Based Nanotubes”. *The Journal of Physical Chemistry B* 116.33 (2012), pp. 9922–9933. ISSN: 1520-6106. DOI: [10.1021/jp303418a](https://doi.org/10.1021/jp303418a).
- [156] Benoît Roux. “The calculation of the potential of mean force using computer simulations”. *Computer Physics Communications* 91.1 (1995), pp. 275–282. ISSN: 0010-4655. DOI: [https://doi.org/10.1016/0010-4655\(95\)00053-I](https://doi.org/10.1016/0010-4655(95)00053-I).
- [157] Rafael C. Bernardi, Marcelo C. R. Melo, and Klaus Schulten. “Enhanced sampling techniques in molecular dynamics simulations of biological systems”. *Biochimica et Biophysica Acta (BBA) - General Subjects* 1850.5 (2015), pp. 872–877. ISSN: 0304-4165. DOI: <https://doi.org/10.1016/j.bbagen.2014.10.019>.
- [158] Cameron Abrams and Giovanni Bussi. “Enhanced Sampling in Molecular Dynamics Using Metadynamics, Replica-Exchange, and Temperature-Acceleration”. *Entropy* 16.1 (2014), p. 163. ISSN: 1099-4300.
- [159] Andrea Cavalli et al. “Investigating Drug-Target Association and Dissociation Mechanisms Using Metadynamics-Based Algorithms”. *Accounts of Chemical Research* 48.2 (2015), pp. 277–285. ISSN: 0001-4842. DOI: [10.1021/ar500356n](https://doi.org/10.1021/ar500356n).
- [160] Donald Hamelberg, John Mongan, and J. Andrew McCammon. “Accelerated molecular dynamics: A promising and efficient simulation method for biomolecules”. *The Journal of Chemical Physics* 120.24 (2004), pp. 11919–11929. ISSN: 0021-9606. DOI: [10.1063/1.1755656](https://doi.org/10.1063/1.1755656).
- [161] Anton K. Faradjian and Ron Elber. “Computing time scales from reaction coordinates by milestoning”. *The Journal of Chemical Physics* 120.23 (2004), pp. 10880–10889. ISSN: 0021-9606. DOI: [10.1063/1.1738640](https://doi.org/10.1063/1.1738640).
- [162] Peter G. Bolhuis et al. “Transition Path Sampling: Throwing Ropes Over Rough Mountain Passes, in the Dark”. *Annual Review of Physical Chemistry* 53.1 (2002), pp. 291–318. DOI: [10.1146/annurev.physchem.53.082301.113146](https://doi.org/10.1146/annurev.physchem.53.082301.113146).



- [163] David A. Pearlman et al. “AMBER, a package of computer programs for applying molecular mechanics, normal mode analysis, molecular dynamics and free energy calculations to simulate the structural and energetic properties of molecules”. *Computer Physics Communications* 91.1 (1995), pp. 1–41. ISSN: 0010-4655. DOI: [https://doi.org/10.1016/0010-4655\(95\)00041-D](https://doi.org/10.1016/0010-4655(95)00041-D).
- [164] Mark James Abraham et al. “GROMACS: High performance molecular simulations through multi-level parallelism from laptops to supercomputers”. *SoftwareX* 1-2 (2015), pp. 19–25. ISSN: 2352-7110. DOI: <https://doi.org/10.1016/j.softx.2015.06.001>.
- [165] James C. Phillips et al. “Scalable molecular dynamics with NAMD”. *Journal of Computational Chemistry* 26.16 (2005), pp. 1781–1802. ISSN: 1096-987X. DOI: [10.1002/jcc.20289](https://doi.org/10.1002/jcc.20289).
- [166] Jeffrey Comer et al. “The Adaptive Biasing Force Method: Everything You Always Wanted To Know but Were Afraid To Ask”. *The Journal of Physical Chemistry B* 119.3 (2015), pp. 1129–1151. ISSN: 1520-6106. DOI: [10.1021/jp506633n](https://doi.org/10.1021/jp506633n).
- [167] Tanfeng Zhao et al. “The Extended Generalized Adaptive Biasing Force Algorithm for Multidimensional Free-Energy Calculations”. *Journal of Chemical Theory and Computation* 13.4 (2017), pp. 1566–1576. ISSN: 1549-9618. DOI: [10.1021/acs.jctc.7b00032](https://doi.org/10.1021/acs.jctc.7b00032).
- [168] T. P. Straatsma and H. J. C. Berendsen. “Free energy of ionic hydration: Analysis of a thermodynamic integration technique to evaluate free energy differences by molecular dynamics simulations”. *The Journal of Chemical Physics* 89.9 (1988), pp. 5876–5886. ISSN: 0021-9606. DOI: [10.1063/1.455539](https://doi.org/10.1063/1.455539).
- [169] Silvia A. Martins et al. “Prediction of Solvation Free Energies with Thermodynamic Integration Using the General Amber Force Field”. *Journal of Chemical Theory and Computation* 10.8 (2014), pp. 3570–3577. ISSN: 1549-9618. DOI: [10.1021/ct500346y](https://doi.org/10.1021/ct500346y).
- [170] Samuel Genheden and Ulf Ryde. “The MM/PBSA and MM/GBSA methods to estimate ligand-binding affinities”. *Expert Opinion on Drug Discovery* 10.5 (2015), pp. 449–461. ISSN: 1746-0441 1746-045X. DOI: [10.1517/17460441.2015.1032936](https://doi.org/10.1517/17460441.2015.1032936).

- [171] Jia He et al. “Cooperative Recruitment of Amphotericin B Mediated by a Cyclodextrin Dimer”. *The Journal of Physical Chemistry C* 118.41 (2014), pp. 24173–24180. ISSN: 1932-7447. DOI: [10.1021/jp507325j](https://doi.org/10.1021/jp507325j).
- [172] Haiyang Zhang et al. “Molecular Recognition in Different Environments:  $\beta$ -Cyclodextrin Dimer Formation in Organic Solvents”. *The Journal of Physical Chemistry B* 116.42 (2012), pp. 12684–12693. ISSN: 1520-6106. DOI: [10.1021/jp308416p](https://doi.org/10.1021/jp308416p).
- [173] Scott Loethen, JongMok Kim, and David H. Thompson. “Biomedical Applications of Cyclodextrin Based Polyrotaxanes”. *Polymer Reviews* 47.3 (2007), pp. 383–418. ISSN: 1558-3724. DOI: [10.1080/15583720701455145](https://doi.org/10.1080/15583720701455145).
- [174] Yanmin Yu et al. “Spatial Arrangement of  $\alpha$ -Cyclodextrins in a Rotaxane. Insights from Free-Energy Calculations”. *The Journal of Physical Chemistry B* 112.17 (2008), pp. 5268–5271. ISSN: 1520-6106. DOI: [10.1021/jp711413a](https://doi.org/10.1021/jp711413a).
- [175] Sugita Masatake and Hirata Fumio. “Predicting the binding free energy of the inclusion process of 2-hydroxypropyl-  $\beta$  -cyclodextrin and small molecules by means of the MM/3D-RISM method”. *Journal of Physics: Condensed Matter* 28.38 (2016), p. 384002. ISSN: 0953-8984.
- [176] Gaëlle Filippini et al. “Host-Guest Complexation in the Ferrocenyl Alkanethiols-Thio  $\beta$ -Cyclodextrin Mixed Self-Assembled Monolayers”. *The Journal of Physical Chemistry C* 118.6 (2014), pp. 3102–3109. ISSN: 1932-7447. DOI: [10.1021/jp4114128](https://doi.org/10.1021/jp4114128).
- [177] Jia He et al. “Cyclodextrin-Mediated Recruitment and Delivery of Amphotericin B”. *The Journal of Physical Chemistry C* 117.22 (2013), pp. 11750–11756. ISSN: 1932-7447. DOI: [10.1021/jp3128324](https://doi.org/10.1021/jp3128324).
- [178] Haiyang Zhang et al. “Investigation of the Inclusions of Puerarin and Daidzin with beta-Cyclodextrin by Molecular Dynamics Simulation”. *Journal of Physical Chemistry B* 114.14 (2010), pp. 4876–4883. ISSN: 1520-6106.
- [179] Peng Liu et al. “How Do  $\alpha$ -Cyclodextrins Self-Organize on a Polymer Chain?” *The Journal of Physical Chemistry C* 116.33 (2012), pp. 17913–17918. ISSN: 1932-7447. DOI: [10.1021/jp304035q](https://doi.org/10.1021/jp304035q).

- [180] A. A. C. C. Pais et al. “Polyelectrolytes confined to spherical cavities”. *The Journal of Chemical Physics* 117.3 (2002), pp. 1385–1394. DOI: [10.1063/1.1483857](https://doi.org/10.1063/1.1483857).
- [181] Rita Dias and Bjorn Lindman. *DNA interactions with polymers and surfactants*. John Wiley & Sons, 2008. ISBN: 0470286350.
- [182] Gerolamo Vettoretti et al. “Molecular Dynamics Simulations Reveal the Mechanisms of Allosteric Activation of Hsp90 by Designed Ligands”. *Scientific Reports* 6 (2016), p. 23830. DOI: [10.1038/srep23830](https://doi.org/10.1038/srep23830).
- [183] Akash Khandelwal and Stefan Balaz. “Improved estimation of ligand-macromolecule binding affinities by linear response approach using a combination of multi-mode MD simulation and QM/MM methods”. *Journal of Computer-Aided Molecular Design* 21.1 (2007), pp. 131–137. ISSN: 1573-4951. DOI: [10.1007/s10822-007-9104-4](https://doi.org/10.1007/s10822-007-9104-4).
- [184] Luciano A. Abriata and Matteo Dal Peraro. “Assessing the potential of atomistic molecular dynamics simulations to probe reversible protein-protein recognition and binding”. *Scientific Reports* 5 (2015), p. 10549. DOI: [10.1038/srep10549](https://doi.org/10.1038/srep10549).
- [185] Matthew Carter Childers and Valerie Daggett. “Insights from molecular dynamics simulations for computational protein design”. *Molecular Systems Design & Engineering* 2.1 (2017), pp. 9–33. DOI: [10.1039/C6ME00083E](https://doi.org/10.1039/C6ME00083E).
- [186] Bernd Kuhn et al. “Prospective Evaluation of Free Energy Calculations for the Prioritization of Cathepsin L Inhibitors”. *Journal of Medicinal Chemistry* 60.6 (2017), pp. 2485–2497. ISSN: 0022-2623. DOI: [10.1021/acs.jmedchem.6b01881](https://doi.org/10.1021/acs.jmedchem.6b01881).
- [187] Adele Alagia et al. “Exploring PAZ/3’-overhang interaction to improve siRNA specificity. A combined experimental and modeling study”. *Chemical Science* 9 (8 2018), pp. 2074–2086. DOI: [10.1039/C8SC00010G](https://doi.org/10.1039/C8SC00010G).

# Chapter 2

## Theory and Methods

Molecular modeling and simulation are powerful tools for the quantitative understanding of the driving forces that govern molecular recognition and binding in host-guest systems. [1–7] However, the energetic description of the binding process requires high accuracy potential energy, transposable between different chemical and physical environments. Also, the flexibility of host, guest and solvent molecules introduces several degrees of freedom that preclude an adequate exploration of the configuration space by standard molecular dynamics approaches. [8–12] These are the most prominent and challenging tasks for the accurate computation of binding free-energies by molecular simulations. Describing computationally the free-energy behavior of relatively small molecules (such as cyclodextrins) and guests, practical shortcomings can be better identified and amended for proceeding the calculation of binding free-energies in larger systems. [1, 8, 13] With increasing complexity in host-guest systems, adequate sampling over the binding process by conventional methods becomes limited due to the computational cost. The simulation and estimation of rare events are among the most challenging topics in molecular dynamics, as the equations of motion are high-dimensional. [11, 12, 14–19]

Several innovative applications of free-energy methods towards physical and organic chemistry, as well as structural biology have been proposed. An exhaustive account of the wide range of works published in the early years of free-energy calculations falls beyond the scope of this chapter. References [17] and [20] provide a full description of these efforts. A complete thermodynamic characterization of the binding process implies the knowledge of the enthalpy and entropy of association. [21] This is one of the key element in identifying the stabilizing factors and understanding how

guest and host assemble. Standard molecular simulation methods have reproduced the absolute thermodynamic properties of binding (standard free-energy, enthalpy and entropy) between host-guest systems. [22] The absolute binding free-energy can be expressed as the sum of separate free-energy contributions corresponding to a step-by-step process describing the association process between the host and guest. [23] This can be accomplished by calculating the PMF profile along a specific reaction coordinate characterizing the association process (e.g. the distance between the center of mass of the host and that of the guest). [13, 23–33] Different methodologies have been successfully applied for the calculation of the PMF profile. Among them, free-energy perturbation (FEP) [30, 34–36], thermodynamic integration (TI) [30, 37], umbrella sampling [38], with the weighted histogram analysis method (WHAM) [23, 39] and force constraint methods [17] are the most commonly used in chemically and biologically relevant systems.

## 2.1 Free-energy calculations and rare events

The conformational changes of macromolecules, host-guest associations/dissociations, chemical reactions, and nucleation phenomena during protein folding, are relevant processes involving rare events. [11, 12, 14–19] These require unusual large thermal fluctuations for driving the system over energy barriers separating intrinsic conformations, and often occur on time scales much larger than the microsecond. The respective study by conventional molecular dynamics simulations is thus hindered by the wide separation of time scales. A deep characterization and understanding of the underlying free-energy states inherent to these molecular mechanisms has been the subject of intense debate in both theoretical and practical contexts. [21, 26, 27, 40–43] Free-energy provides the most measurable coupling between experimental and *in silico* approaches. Calculating *a priori* free-energy differences with high accuracy allows assessing the quality of the designed models. This is the basis for the development of a extensive list of methods, over the last thirty years. [17] Specifically, a physical phase transition among two or more thermodynamically stable, or metastable, states separated by free-energy barriers is a rare event, associated to a long system delay for crossing the high-energy region in the phase space. [44] Determining the free-energy of those states and the respective free-energy barriers allows describing rare dynamic events. [17, 21] The Helmholtz free energy,  $A$ , particularly

useful for the condition of constant volume, is given by

$$A = -k_B T \ln Q \quad (2.1)$$

and

$$A = -k_B T \ln \left\langle e^{-\frac{H(\mathbf{p}^{3N}, \mathbf{r}^{3N})}{k_B T}} \right\rangle \quad (2.2)$$

In these equations  $k_B$  refers to the Boltzmann's constant,  $T$  is the absolute temperature in Kelvin units and  $\langle \rangle$  represents the canonical ensemble average.

Free-energy is generally expressed as the Helmholtz function ( $A$ ) under the  $NVT$  ensemble or the Gibbs function ( $G$ ) under the  $NPT$  ensemble. The Helmholtz free-energy  $A$  is commonly represented as a phase space integral (Eq. 2.1). Theoretically,  $A$  can be calculated resorting to MD or MC sampling methods using Eq. 2.2, but in practice the result is misleading due to (i) the exponentially increasing function in the integrand of the equation, which inflates the contribution of some rarely accessed regions in the phase space to the entire integral, and also to (ii) the complex and high dimensional character of the phase space, which difficult sampling the space ergodically, when using standard sampling approaches, such as those of MD and MC. If the coordinates of the system are collectively denoted as  $\mathbf{x}$  and the respective energy function is  $E(\mathbf{x})$ , then the partition function,  $Q$ , is given by the configurational integral

$$Q = N \int d\mathbf{x} e^{-\beta E(\mathbf{x})} \quad (2.3)$$

where  $\beta = (k_B T)^{-1}$  and the constant  $N$  are introduced to represent  $Q$  unitless, i.e. the respective value does not have any significance in this case. The average energy of the system is

$$\langle E \rangle = \int d\mathbf{x} E(\mathbf{x}) \rho(\mathbf{x}) \quad (2.4)$$

in which  $\rho(\mathbf{x})$ , the equilibrium probability density in  $\mathbf{x}$ , is

$$\rho(\mathbf{x}) = \frac{e^{-\beta E(\mathbf{x})}}{\int d\mathbf{x} e^{-\beta E(\mathbf{x})}} \quad (2.5)$$

In contrast to the calculation of absolute free-energy, the relative term is easier to determine. Transition state theory (TST) [44, 45] allows evaluating the occurrence of rare events with a simplistic approach. Assuming that a molecule has two meta-stable states A and B, and considering the ergodic hypothesis, in which the time average equals the ensemble average, it is possible to perform longer simulations and collect the probability of both states, A and B, and thus obtain the free-energy difference between the states using

$$\Delta G = -k_B T \ln \frac{P_A}{P_B} \quad (2.6)$$

However, in the presence of a large energy barrier between A and B, a long time transition from A to B is expected, leading to a cryptic result,  $P_B = 0$  and  $\Delta G = -\infty$ . The general algorithm of umbrella sampling was developed to solve this issue. [46–48] From umbrella sampling an imposed coordinate, which is a function of the system, able to monotonically discriminate states A and B, and the saddle point, is found, allowing to impose an external potential to the coordinate and coercing the system to sample a specific phase region. The free-energy associated to the imposed coordinate can thus be obtained by histogram analysis. In real systems, this scheme possesses limitations in practical conformational change situations, as rugged potential energy landscapes and several local points of low energy, between states A and B can be identified. A series of transition path based theories and methods have been developed [47] for dealing with these aspects. Determination of reliable free-energy changes by numerical simulations based on the basic principles of statistical mechanics is currently available and the methodological advances, as well as the extended computational capacity for dealing with complex systems and increased numerical processing, have simultaneously contributed to transform free-energy calculations in robust and well-defined modeling tools and to expand the respective applications.

### 2.1.1 Calculating free-energy differences

The free-energy difference is the driving force of any process with applications ranging from solid-state and catalytic reactions to biochemical processes and rational drug design. The transition state theory can be used for calculating reaction rates from free-energy barriers. [46] Free-energy contains entropy, a measure for the available space. Mapping the available space in complex systems requires extensive sampling. [21] The canonical partition function  $Q$  of a system can be determined along the integral over the whole phase space, i.e. configuration space and momentum space. If the potential energy  $E$  is independent of the momentum, the integral over the latter is a multiplicative constant to  $Q$ , which can be neglected.  $Q$  can be obtained from

$$Q = \int e^{-\beta E(r)} d^N r \quad (2.7)$$

where  $N$  corresponds to the number of degrees of freedom of the system. As already stated, the free (Helmholtz) energy  $A$  is related to  $Q$  from  $A = -1/\beta \ln Q$ . The canonical partition function involves a constant number of particles, constant volume, and a constant temperature. If the pressure, rather than the volume, is kept constant, the Gibbs free-energy ( $G$ ) is obtained. Apart from the change in the ensemble, the following formalisms and derivations are equivalent for  $A$  and  $G$ . In the condensed phase, which is relevant for most applications, the systems are incompressible, so  $A$  and  $G$  are numerically similar.

Free-energy differences between two states are crucial in chemical reactions. If the two states differ geometrically (e.g. a reactant and product of a reaction) the integration in Eq. 2.7 is performed partially over the coordinate space, for each state. The reaction coordinate ( $\xi$ ) is, in general, a continuous (one or multi dimensional) parameter defined for discriminating two thermodynamic states. Often,  $\xi$  is defined based on geometric grounds, such as distance, torsion, or the difference between root mean square deviations from two reference states. [17, 46, 49] The probability distribution of the system along  $\xi$  can thus be calculated by integration of all degrees of freedom using

$$Q(\xi) = \frac{\int \delta[\xi(r) - \xi] e^{-\beta E} d^N r}{\int e^{-\beta E} d^N r} \quad (2.8)$$



$Q(\xi)d\xi$  can be interpreted as the probability of finding the system in a small interval  $d\xi$  around  $\xi$ . This allows calculating the free-energy along the reaction coordinate. In  $A(\xi) = -1/\beta \ln Q(\xi)$ ,  $A(\xi)$  also reflects the potential of mean force (PMF). It should be noted that the direct phase-space integrals used in Eqs. 2.7 and 2.8 are impossible to calculate in computer simulations. However, if the system is ergodic, i.e., if every point in phase space is visited during the simulation,  $Q(\xi)$  is equal to  $P(\xi)$ ,

$$P(\xi) = \lim_{t \rightarrow \infty} \frac{1}{t} \int_0^t \rho(\xi(t')) dt \quad (2.9)$$

i.e., the ensemble average  $Q(\xi)$  becomes equal to the time average  $P(\xi)$  for infinite sampling in an ergodic system. In Eq. 2.9,  $t$  denotes the time and  $\rho$  simply counts the occurrence of  $\xi$  in a given interval.  $A(\xi)$  can be directly obtained from MD simulations by monitoring  $P(\xi)$ , the distribution of the system along the reaction coordinate.  $P(\xi)$  refers to the normalized frequency of finding the system in the vicinity of a given value of  $\xi$ . If  $P(\xi)$  is obtained from an exact ensemble average rather than a sampled quantity,  $P(\xi)$  corresponds to a probability density. However, simulations are performed for running finite times. Regions in configuration space around a minimum in  $E(r)$  are generally well-sampled, in contrast to those regions of higher energy, which are less probable. For these rare events, those with an energy barrier significantly larger than  $k_B T$ , direct sampling is unfeasible. Successfully constructing the  $A(\xi)$  profile requires also taking these high-energy regions into account. Different approaches have been developed to sample such rare events, including equilibrium or non-equilibrium sampling methods, and those that introduce additional degrees of freedom, along which the free-energy is derived. In equilibrium/non-equilibrium methods a global sampling can be achieved considering two different scenarios: (i) the interaction path is divided into several independent sampled windows, each of which covers a small region of  $\xi$ , and the results from the different windows are then combined to produce a global free-energy profile  $A(\xi)$ , and (ii) a procedure based on multiple simulations in which the system is driven from one state to other state, considering in each run different paths, and including averaging over the simulations.

## 2.2 Potential of mean force

Potential of mean force calculations play a considerable role in understanding how chemical species recognize and associate. [1] One might argue that they actually provide a more satisfactory picture of these phenomena than alchemical free-energy calculations, because they follow the molecules of interest from their free, unbound state, to the bound state of the complex. This point of view is obviously misleading, as the model reaction coordinate followed to describe association/dissociation bears certain arbitrariness. Furthermore, PMF have helped to decode complex recognition and association phenomena in thermodynamic signatures with a detailed atomic description of the underlying processes. A detailed description of the theoretical basis of PMF calculation is given in ref. [17] Only a few methods for calculating the potential of mean force can be efficiently combined with computer simulations. Those relied on obtaining the probability density function,  $P(\xi_1, \dots, \xi_p)$ , of finding the system at values  $\xi_1, \dots, \xi_p$  of the  $p$  selected coordinates allow estimating the potential of mean force,  $A(\xi_1, \dots, \xi_p)$  as

$$A(\xi_1, \dots, \xi_p) = -k_B T \log P(\xi_1, \dots, \xi_p) \quad (2.10)$$

Another, general, method for calculating the potential of mean force requires calculating the derivatives  $\partial A / \partial \xi$  in a series of calculations, in which  $\xi_i$  is constrained to fixed values distributed along  $[\xi_{imin}, \xi_{imax}]$  in the range of interest. In such an approach the potential of mean force is obtained by numerical integration. The derivative of the free energy is related to the constraint force required to keep the system at the imposed value of  $\xi_i$ . The exact nature of this relationship has been the subject of some debate as described in ref. [50]. It should be noted that there are several problems that transcend the fiability of force-fields, and produce some impact in the results. Firstly, the restrictions for the sampling, along the inclusion coordinate, often fail. This happens because the inclusion potential is usually steep, and, when summed with the common harmonic potential restriction makes this latter useless. [23]

PMF calculation based on stratified umbrella sampling is nowadays conducted routinely for inclusion complexes. Determination based on experimental techniques can also be conducted routinely and, for instance, association constants and interaction/geometrical parameters can be, respectively, obtained

by techniques such as  $^1\text{H NMR}$ , isothermal titration calorimetry (ITC) and solubility experiments. The PMF,  $W(\xi)$  may be interpreted as the potential that is produced by the average forces over all the configurations of a given system, in which a set of molecules is kept fixed (at a certain value of a reaction coordinate,  $\xi$ ). This quantity was devised by Kirkwood [46, 51] and can be defined based on the average distribution function,  $\rho(\xi)$ , along the coordinate  $\xi$ , obtained from a Boltzmann weighted average,

$$\langle \rho(\xi) \rangle = \frac{\int dr \delta(\xi'(r) - \xi) e^{\left(\frac{-U(r)}{k_B T}\right)}}{\int dr e^{\left(\frac{-U(r)}{k_B T}\right)}} \quad (2.11)$$

$$W(\xi) = W(\xi^*) - K_B T \ln \left[ \frac{\langle \rho(\xi) \rangle}{\langle \rho(\xi^*) \rangle} \right] \quad (2.12)$$

where  $W(\xi^*)$  and  $\xi^*$  are arbitrary reference values,  $\delta(\xi'(r) - \xi)$  corresponds to the Dirac delta function for the coordinate  $\xi$ ,  $U(r)$  represents the total energy of the system as a function of the coordinates  $r$ , and  $\xi'(r)$  is a function depending on the number of degrees of freedom, such as an angle, a distance or a more complex function of the cartesian coordinates of the system. The chosen coordinate  $\xi$  is, in the systems studied, a geometrical coordinate  $\xi(r)$ , although  $\xi$  may be defined differently. The PMF is a central quantity in theoretical and computational studies of macromolecular systems, and may be interpreted as the potential that is produced by the average forces over all the configurations of a given system, in which a set of molecules is kept fixed (at a certain value of  $\xi$ ).

The PMF values can vary by several  $k_B T$  over the relevant range of  $\xi(r)$ . In this case, the distribution function  $\langle \rho(\xi) \rangle$  cannot be computed by standard Monte Carlo (MC) or molecular dynamics (MD) simulations, due to low sampling frequency in higher-energy configurations. Specific sampling techniques (non-Boltzmann sampling) have been designed to calculate a PMF along a coordinate  $\xi$ , from a molecular dynamics trajectory. The umbrella sampling technique, proposed in the 1970's by Torrie and Valeau [48, 52], is one of these approaches, and is used to overcome the difficulty of sampling rare events, by modifying the potential function so that the unfavorable states are sampled appropriately (see Figure 2.1). [53] The system is simulated in the presence of an artificial biasing window potential,  $w(\xi)$ , introduced to enhance the sampling in the vicinity of a focused region  $\xi$  of the configurational space. This window potential, often of quadratic form, is used to improve the sampling in the region defined by the coordinate  $\xi$ , whose variations within a small interval are restricted. In

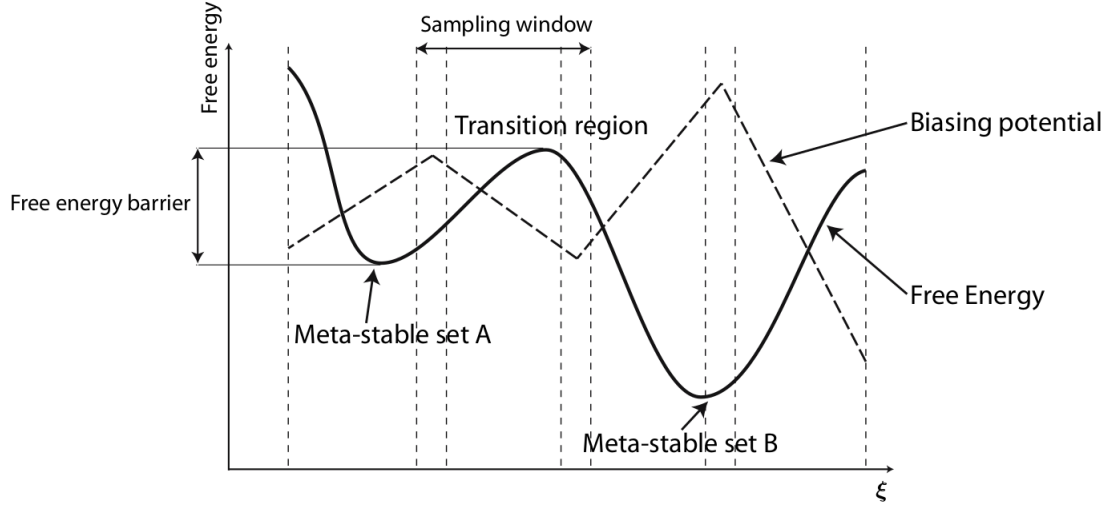


Figure 2.1: Illustration of the umbrella sampling method used to overcome energy barriers between stable states of the system. Reproduced from ref. [53] with permission from Springer Nature.

general, the potential energy ( $U(r) + w(\xi)$ ) is used to generate the biased simulations. The harmonic functions defined as  $w_i(\xi) = \frac{1}{2}K(\xi - \xi_i)^2$  and centered at subsequent values of  $\xi_i$ , are used to produce the biased ensembles. Several biased window simulations are required to obtain the PMF over the whole target region ( $\xi$ ). The final estimate  $W(\xi)$  is obtained combining the results of the set of windows, previously unbiased. Specifically, the information from these different biased simulations is converted into local probability histograms, which are then merged to produce an unbiased Boltzmann statistical probability. The weighted histogram analysis method (WHAM) [39] can be used to obtain a proper unbiased estimate of the PMF from the biased simulation data and to calculate the PMF. These last steps are the most important in the umbrella sampling procedure. [38, 46, 51, 54] According to Eq. 2.11, the biased distribution function obtained from the  $i$ th biased ensemble is

$$\langle \rho(\xi) \rangle_{(i)} = e^{-w_i(\xi)/k_B T} \langle \rho(\xi) \rangle \langle e^{-w_i(\xi)/k_B T} \rangle^{-1} \quad (2.13)$$

The unbiased PMF from  $i$ th windows is

$$W_i(\xi) = W(\xi^*) - k_B T \ln \left[ \frac{\langle \rho(\xi) \rangle_{(i)}}{\langle \rho(\xi^*) \rangle} \right] - w_i(\xi) + F_i, \quad (2.14)$$

where the undetermined constant  $F_i$  derived from

$$e^{-F_i/k_B T} = \langle e^{-w_i(\xi)/k_B T} \rangle, \quad (2.15)$$

corresponds to the free-energy associated with the window potential. Several efforts have been made for establishing enhanced solutions for unbiasing and recombining the information from umbrella sampling. [23, 38, 51]

## 2.3 Steered molecular dynamics and umbrella sampling automation

Association and dissociation processes in host-guest complexes, are ruled by rare transitions between the two equilibrium states. By applying an external force (force bias) to the guest molecule, these transitions can be induced at faster rates than in the natural processes. This has been conducted experimentally resorting to atomic force microscopy (AFM) [55–60], and computer simulations [1, 13, 23, 24, 28, 54, 60–64]. In the latter, conventional MD simulation provides detailed information on structural changes, but is limited for describing the complete association/dissociation of the binding partners, as the progress can not be monitored at the time scale of standard MD.

Steered molecular dynamics (SMD) allows mimicking AFM experiments, providing relevant insights on the molecular mechanisms underlying such processes by focusing on selected degrees of freedom. In AFM studies, the tip of an elastic cantilever applies an external mechanical force to a host-complex complex, for inducing complex dissociation. This force is measured by monitoring the position of the tip (see Figure 2.2, panel a). The experiments are typically realized over time scales in the range of  $1 \text{ ms}^{-1} \text{ s}$ , and the spring constants,  $k$ , of the cantilevers are ca.  $1 \text{ pN}/\text{\AA}$ , so that the variation in the position of the attached guest,  $(k_B T/k)^{1/2}$ , are large on the atomic scale. From these approximation, the peak force reflects the rupture force, leading to a crude and poorly detailed interpretation of the process.

SMD is an effective method to explore the association/dissociation mechanism allowing to construct

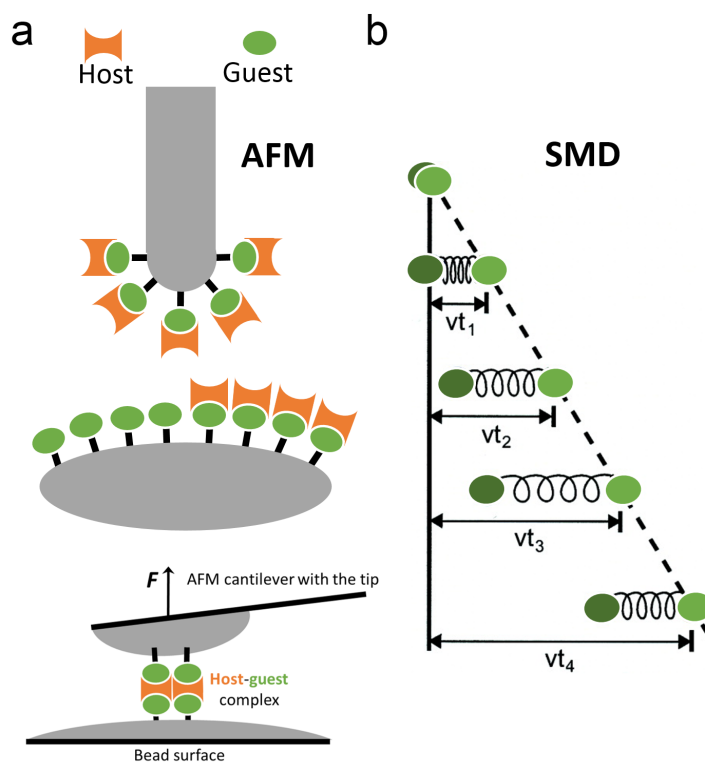


Figure 2.2: Schematic representation of an AFM experiment (panel a) in which the host or guest molecules are anchored to a surface, while the binding counterparts are attached to a force sensor (micron-sized cantilever). The host-guest complex is dissociated by increasing the distance between the surface and the force sensor. In constant velocity SMD (panel b) a harmonic potential is used to displace the guest molecule along the reaction coordinate. The free end of the spring is moved at constant velocity, while the guest atoms attached to the other end of the spring are subject to the steering force. Adapted from ref. [65] with permission from the American Association for the Advancement of Science.

within its framework the PMF profiles of the system under study. It simulates a host-guest system under the influence of an applied force bias ( $\vec{F}_{fb}$ ) to a single atom or a group of atoms (through their center of mass) of the guest molecule, employing harder springs than those used in AFM experiments. This provides a detailed information on the interaction energies and finer spatial resolution. The time scales of the simulations are typically  $10^6$  times shorter than those of AFM. Steering forces are thus applied to accelerate processes affected by energy barriers. This method is reviewed in refs. [38, 63, 66, 67]. A typical SMD simulation steers the system by applying a constraint, such as a harmonic potential, that moves along a defined path in the configuration space. This is illustrated in Figure 2.2 (panel b). A constant velocity SMD is schematically represented, in which a harmonic potential (spring) induces motion along the reaction coordinate. The extension of the spring determines the force applied, which can be monitored over the course of the simulation. The principle of SMD is

based on the hypothesis that the larger is the force required to separate a guest from a host the higher the respective binding affinity.

Specifically, to probe the binding affinity of host and guest molecules, one applies the steering force to pull guest from or towards the cavity of the host, without restricting the guest atoms (see see Figure 2.3). Under the force loaded with a constant rate the total energy ( $E$ ) of the host-guest complex is

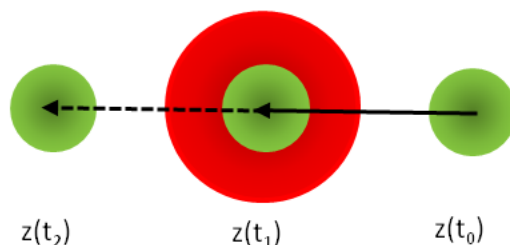


Figure 2.3: Illustrative representation of the pulling process using the position setting, along the  $z$ -axis. Reproduced from ref. [23] with permission from the PCCP Owner Societies

$$E = E_{host} + E_{guest} + E_{host-guest} + E_{force}, \quad (2.16)$$

$$E_{force} = \frac{k}{2}(x - vt)^2 \quad (2.17)$$

in which each energy term corresponds to interaction energies of host, guest and host-guest, respectively. [63] The respective forms are dependent on the force fields used to describe the binding process. In AFM, the spring constant of the cantilever tip  $k$  is typically in the range of 10-1000 pN nm<sup>-1</sup>. In Eq. 2.17,  $x$  refers to the displacement relative to the initial position of the guest atom in which the force is applied,  $v$  corresponds to the pulling velocity, and  $kv$  is the force ( $F$ ) experienced by the guest,  $F = kv$ .

All-atom MD simulations allow running simulation up to 1  $\mu$ s and the pulling of a guest molecule can be at least 10<sup>4</sup> times faster than in AFM. SMD involves high pulling velocities or large constant forces, and have been routinely implemented in several softwares, including GROMACS [68, 69], AMBER [70], CHARMM [71] and NAMD [72].

However, higher pulling velocities result in non-equilibrium situations, which introduces significant error into the simulation results. To mimic AFM the pulling velocity should be as small as possible.

The value of the spring force varies significantly with the pulling velocity and also with the spring constant applied to the system. The latter must be large enough to enable measuring the local potential and low enough to avoid background noise. [63] SMD is an irreversible approach based on the Jarzynski equality  $\langle e^{-W/k_B T} \rangle = e^{-\Delta G/k_B T}$  where  $W$  is the total nonreversible work done on the system by the force bias,  $\vec{F}_{fb}$ , during a nonequilibrium transition between two states connected by a reaction coordinate  $\xi$ . The free-energy difference between these two states is given by  $\Delta G \equiv \Delta G(\xi)$ . The angular brackets represents the ensemble average taken by repeating the simulation several times along the path connecting the initial and final states,  $\xi_i$  and  $\xi_f$ . The Jarzynski equality allows a direct connection between the work done in a nonequilibrium process to the change in the equilibrium free-energy difference.

The direction of  $\vec{F}_{fb}$  can be defined as  $\vec{r}_{fb}$  and all other degrees of freedom are allowed to react freely to  $\vec{F}_{fb}$ . The system is thus driven by a harmonic force  $\vec{F}_{fb}(\xi) = k(\xi)(\vec{r}_{fb} - \vec{r}_{cm})$  where  $k$  is the force constant and  $\vec{r}_{cm}$  is the center of mass. A force bias with a fixed value of  $k$  is introduced with  $\xi$  increasing from zero to one at a continuous pulling rate along the simulation. [54]

It should be noted that SMD is essentially umbrella sampling if the velocity of pulling is very small. In the following chapters, SMD is combined with umbrella sampling with the aim of describing detailed thermodynamics and exploring the conformational space of host-guest complexes based on cyclodextrins and bambusurils. SMD are nonequilibrium simulations that allow generating different configurations of the systems. These configurations are then used as starting points for the equilibrium umbrella sampling simulations, as described below.

Umbrella sampling allows estimating the free-energy difference between two states from a set of equilibrated simulations. Similarly to SMD, a force bias is imposed. However, in umbrella sampling the system configuration is equilibrated at each position of the reaction coordinate, corresponding to umbrella windows. In these approach the value of the harmonic force constant imposed in each window is independent and can be estimated for optimizing the efficiency with which the phase space is sampled. This means that the force constant and the positions of the reaction coordinate must be selected adequately for ensuring that the phase space sampled by neighboring windows overlaps sufficiently, forming a continuous pathway between  $\xi_i$  and  $\xi_f$ . The complete thermodynamic evolution along the reaction coordinate can be provided by combining the results from all umbrella windows



resorting to the weighted histogram analysis method (WHAM). [39, 73]

### 2.3.1 Building the PMF profile

Umbrella sampling is commonly used to describe simulations in which an imposed coordinate connecting the initial and final ensembles is divided into mutually overlapping regions, or windows, which are sampled using non-Boltzmann weights. [25, 32, 61, 73, 74] To explain briefly, several independent simulations are performed in each of the imposed regions of the reaction coordinate (Figure 2.4, bottom), using a bias potential to constrain the simulations to adjacent windows. Such initial configurations are generated, each corresponding to a location wherein the guest molecule is restrained and centered at subsequent values of  $\xi_i$ , corresponding to decreasing or increasing center-of-mass (COM) distances from the center of the host cavity, using an umbrella biasing potential,  $w(\xi)$ , often of quadratic form,  $w_i(\xi) = 0.5K(\xi - \xi_i)^2$ . This restraint allows the guest molecule to sample the configurational space in a defined region along the association/dissociation coordinate. Then the biased system (Figure 2.4 middle) will sample configurations close to a defined position,  $z_0$ , even when these would not be sampled in the unbiased system. In general, the potential energy ( $U(r) + w(\xi)$ ) is used to generate the biased simulations. The mean force, as a function of position, is calculated in each window, and the respective potentials,  $W(\xi)$ , are derived using an unbiasing procedure. Statistical techniques, such as WHAM [39, 73] are used to remove the umbrella bias and combine the local distributions, allowing free-energy to be computed (Figure 2.4, top). WHAM is the basic tool for constructing free-energy profiles from distributions derived through stratification, for which the path connecting the reference and the target states is separated into intermediate states. The respective equations have also been used as the core of adaptive umbrella sampling approaches [75], in which the efficiency of free-energy calculations are improved through refinement of the biasing potentials as the simulation progressed. There are several ways to calculate the PMF in GROMACS, probably the most common is to make use of the pulling code. To sum up, the main steps for obtaining a PMF using umbrella sampling, which allows for sampling of statistically-improbable states, are: (i) generate a series of configurations along a reaction coordinate from a SMD simulation, (ii) extract frames from the trajectory in step (i) that corresponds to the desired center of mass spacing,

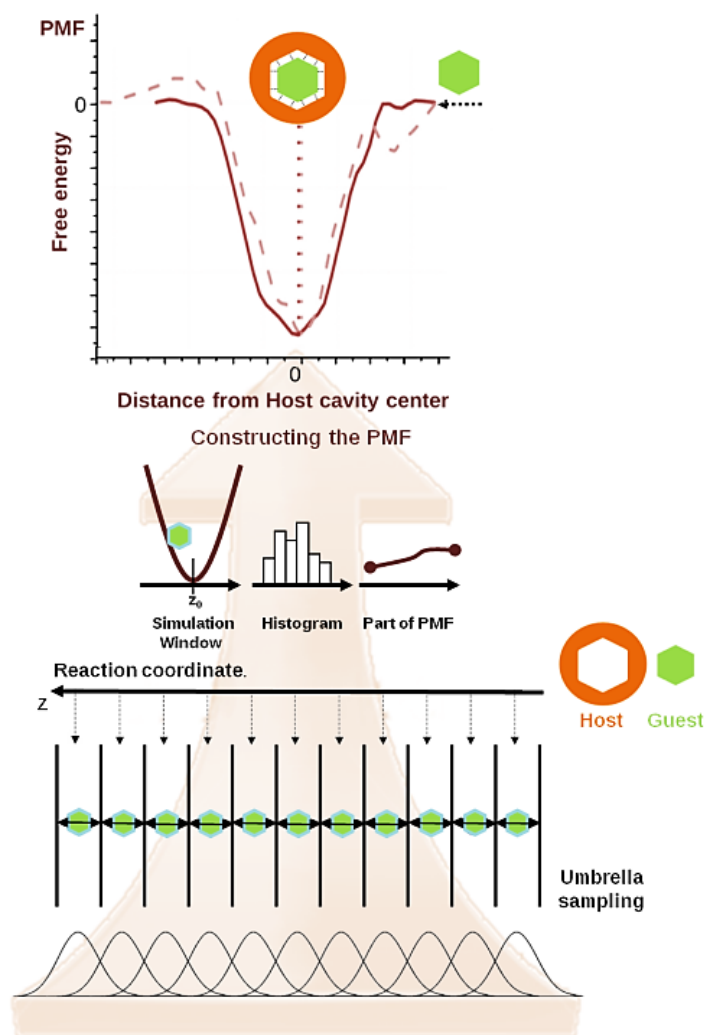


Figure 2.4: Schematic representation of the umbrella sampling procedure applied to a system along the pathway for the association/dissociation of a model guest with a host cavity. Reproduced from ref. [1].

(iii) use umbrella sampling to restrain these configurations within sampling windows, and (iv) use the Weighted Histogram Analysis Method to reconstruct a PMF profile and calculate  $\Delta G_{bind}$ .

### *Estimating force constants*

In order to automatically extract the configurations and estimate the force constant values to be used in umbrella sampling, relevant code was developed (available in [UPonIncluSys](#)). [23] These configurations should be as closer as possible of an equilibrated state, in order to maximize the respective usefulness. In practical terms, these configurations are obtained via a previous pulling step, within the SMD scheme. Pulling force constants of  $1000 \text{ kJ mol}^{-1} \text{ nm}^{-2}$  and  $2000 \text{ kJ mol}^{-1} \text{ nm}^{-2}$  were used in

the studied systems. These values were optimized in conjunction with the pulling rate i.e., the velocity at which the restriction travels along the reaction coordinate. This velocity also defines the length of the simulation within this pulling process, after the traveling path is defined. Results from pulling were used both to establish the initial configurations and to estimate the force constants to be applied in each window in the actual umbrella sampling. Note that these require a sufficient restriction to approximately maintain an imposed host/guest relative position, and also a sufficient overlap with the nearest sampling windows. The force constants were simply estimated from the equality between the value of the force imposed in the limits of the window, and that resulting from the difference between the position imposed in the pull and that actually determined

$$k(z_{wl} - z_{wc}) = k_{pull}(z_r - z_{wc}) \quad (2.18)$$

In the above equation,  $z_{wl}$  corresponds to the point common to two sequential windows, such that the displacement in the left-hand side is half the window width,  $z_{wc}$  is the coordinate at the central point of each window and defined by a regular interval established in the pulling process,  $z_r$  is the coordinate actually found in the pulling,  $k$  is the force constant to be imposed in each window and  $k_{pull}$  is the force constant in the pulling process, which is maintained throughout this process. In simple terms, the value imposed in the frontier of each window corresponds to that required to restrain the host/guest distance when the system drifts from the imposed location during the pull. This is a trivial step, but allows to build an automated sequence in which the imposed distances are given by the usual expression for each sequential window

$$z_{wc}^{(i)} = z_{init} + t^{(i)} v_{pull} \quad (2.19)$$

where  $t^{(i)}$  is the time to attain window ( $i$ ) and pull rate is a constant velocity, corresponding to the displacement of the harmonic restriction. Positions  $z$  are compared to those actually found for the respective configurations, and the values of  $k$  estimated. These are subsequently used for calculating each restricted window in the umbrella sampling, which are automatically launched. This avoids time consuming and cumbersome repetitions to correct deficiencies in the sampling.

## 2.4 Thermodynamics

The determination of binding affinities for host-guest complexes arising from the noncovalent association of two molecules is of paramount importance in different fields, including drug discovery. The host-guest binding affinity is related to the difference in Gibbs free energies of binding ( $\Delta G_{bind}$ ) corresponding to the associated and dissociated states of the system under study (see Figure 2.5).  $\Delta G_{bind}$



Figure 2.5: Schematic representations of a reversible noncovalent association/dissociation process of a guest molecule (green) and a host (orange) molecule, possessing a certain binding energy difference ( $\Delta G_{bind}$ ) between the associated and dissociated states. Reproduced from ref. [1].

is composed of enthalpic and entropic terms. While the enthalpic contribution reflects changes in the inner energy of the systems, i.e. energies related to atomic motions and interactions, entropic contributions are also related with conformational changes upon binding. [17] The common methods for binding affinity estimation include very fast but less accurate similarity-based regression models and scoring functions and accurate but computationally demanding physical methods, which require a large number of MD (or Monte Carlo) simulations. [76] This suggests that the most convenient methods and algorithms are those that offer a good balance between computational costs and accuracy. Most accurate strategies provide estimates for thermodynamic quantities, with intrinsic difficulties associated to fundamental aspects. The quantification of atomic or ionic interactions, associated to repulsive and attractive forces, requires physical models assigned to different force fields (FF). The latter can be detailed using quantum mechanical (QM) *ab-initio* methods. However, a quantum mechanical representation of solvated biological systems, such as membranes and proteins consisting of large amounts of atoms is difficult to obtain, even with alternatives, such as the density functional theory (DFT). [77, 78] Relevant considerations have been made [19] on the accuracy of FF for the calculation of binding thermodynamics. Some FF combinations may provide the most accurate binding enthalpies but the least accurate binding free energies, with implications in the development of new FF. These have been evaluated for a wide range of host-guest complexes and water models, using

different partial charge assignment methods and host FF parameters, and resorting to the attach-pull-release (APR) method [19], which allows computing the absolute binding free energies, from a series of umbrella sampling simulations. In the latter, restraints controlling the host-guest complex are activated cumulatively for separating host and guest molecules, and then released to leave the guest at standard concentration.

In fact, the selection of FF and setup parameters (e.g. protonation states and slow motions) can be a difficult task, as new variants primarily concerned to the treatment of proteins, are constantly being produced. There are standard options such as OPLS [79], AMBER [70], CHARMM [80] and GRO-MOS [81] and other more specific FF, such as the Kirkwood-Buff [82] FF, directed at aromatic amino acids, the CHARMM polarizable FF, based on the classical Drude oscillator [83, 84], the induced dipole [85], for modeling polarization in proteins and protein-ligand complexes, the Jorgensen's approach [86] for parameterization by atoms-in-molecule electron density partitioning, AMOEBA [87] and GEM\* [88], among many others. [89–91] Additionally, several water models such as TIP3P [92], TIP4Pew [93], and SPC/E [94], and the recently introduced OPC [95], TIP3P-FB and TIP4P-FB [96], TIP4P-D [97], and iAMOEBA [98] are also available. It is worth mentioning that the assessment of the ability of these FF to reproduce experimental data is not systematic, and based on the free-energy of hydration of small molecules [99], and on the structure of nucleic acids [100] and proteins [101]. With regard to explicit solvent methods, only a few studies have focused on thermodynamic data from noncovalent binding for validating the FF. Recently [102, 103], the binding free energies of cyclodextrin host-guest complexes were also used, but in the context of implicit solvent models.

It is worth to note that there are other issues in this type of systems that transcend the accuracy of the selected FF, and affect the simulation results. These are related to restrictions for the sampling and estimation of reliable thermodynamic quantities, including the respective binding constants. The latter can be determined from experimental techniques such as  $^1\text{H}$  NMR, isothermal titration calorimetry and solubility experiments. The calculations of binding constants that provide a convenient counterpart to the experimental observations in inclusion complexes is sometimes addressed using a "flexible molecule" approximation [23], instead of the conventional rigid rotor harmonic oscillator (RRHO). [21, 104, 105] The available volume for a guest molecule is described in terms of a cylindrical, PMF weighted region, in which the respective motion is measured by the positioning of

the center of mass. The "flexible molecule" approximation is not as widespread as might be expected, and relatively recent publications [21, 106] both divulge the approximation and highlight controversies on the topic.

In fact, noncovalent binding is the basis of host-guest and supramolecular chemistry. Statistical thermodynamics provides the required mapping of these interactions to macroscopically observable binding affinities, and the theoretical foundations of binding thermodynamics seem to be well established. [21] However, both experimental and theoretical characterization of binding, often relies on inaccurate frameworks, leading to ambiguous or contradictory outcomes, still remaining a topic of active debate, especially in the decomposition and establishment of individual contributions to entropic and entropic changes.

To formulate the statistical thermodynamics of noncovalent binding, expressions for the partition functions of the free host and guest molecules are needed. The first approach is to use the approximation based on RRHO. This approximation was first formulated in order to treat, with quantum mechanics, the molecular motions. Considering a molecule as rigid, the respective internal motions encompass only vibrations of small amplitude, allowing to approximate the energy contributions (both kinetic and potential) of its translational, rotational and vibrational motions as separated terms. A complete description of the formulation of the molecular partition function according to the RRHO approximation is given in ref. [21] The second approach, although not new, is still poorly understood. Surprisingly it has been recently discussed (see refs. [21, 106]) and the first definition as "flexible molecule" approach appears in 2009. [106] This is supported by classical statistical thermodynamics, routinely used in MC and MD simulations. In the classical approximation, the kinetic energy of each atom makes a fixed contribution to the partition function that is independent of conformation and potential energy. There is no alteration of these kinetic energy contributions to the partition function and no influence on the binding free-energy, when host and guest molecules bind to form a noncovalent complex, i.e., kinetic energy can be completely neglected in the classical calculations of the binding constant, yielding to results that are independent of the atomic masses. Each atom contributes thus with a factor  $(1/h)^3$  to the multiplicative constant  $N$  in the partition function, so the binding free-energy is also independent of  $N$  and of Planck's constant  $h$  (see ref. [21] for details).

By neglecting the kinetic energy contribution to the partition function, the configurational integral

over spatial coordinates is obtained. The approximation of fixed moments of inertia becomes unnecessary so the unrealistic rigid rotor approximation can be discarded. However, it is necessary to separate the  $n$  spatial coordinates of the molecule into 3 coordinates for overall translation, 3 more for overall rotation, and  $3n - 6$  internal coordinates. In general, the contribution of translation to the configuration integral, reflects the total volume (a factor of  $V$ ), and rotation contributes with a factor of  $8\pi^2$ . The internal contribution can thus be described as

$$Q_{in} = \int d\mathbf{x} J(\mathbf{x}) e^{-\beta E(x)} \quad (2.20)$$

where  $x$  corresponds to internal coordinates, and  $J(\mathbf{x})$  is a Jacobian factor, which depends on the selected internal coordinates. As the multiplicative constant  $N$  has no influence on the final binding free-energy  $\Delta G_{bind}$  it is omitted. The partition function of the molecule is defined as

$$Q = 8\pi^2 V \int d\mathbf{x} J(\mathbf{x}) e^{-\beta E(\mathbf{x})} \quad (2.21)$$

It should be noted, that according to the classical approximation the conformational changes of any amplitude and form can be considered, so that the "flexible molecule" approach is not restricted to the small amplitude, vibrational model of internal motion as in the RRHO treatment. This flexible model is by far more suitable for flexible molecules, such as cyclodextrins. For this reason, and due to its simplicity, the following developments in the studied systems rely on the "flexible molecule" approach for estimating the binding constants of the host-guest complexes.

### 2.4.1 Binding constants and the cylindrical approximation

Experimental studies on host-guest interactions usually provide information on stoichiometry and affinity, and/or estimates of free energy, enthalpy, entropy changes and heat capacity. Such changes in binding interactions involve low probability events identified as changes in affinity, as a consequence of the enthalpy-entropy compensation, from which the enthalpy released from an improved favorable association is offset by an entropic penalty. However, such changes can be inspected by measuring the binding enthalpy. The thermodynamics of inclusion is described essentially by two components

of the standard Gibbs free energy,  $\Delta G_{bind}^0$ , the standard enthalpy,  $\Delta H_{bind}^0$ , and the standard entropy  $\Delta S_{bind}^0$ , which are determined for the entire inclusion process. In the present work, the binding affinity is derived numerically from the association constant,  $K_{bind}$ . [23, 26] The latter can be estimated by integrating the PMF values,  $\Delta G_{PMF}^0$ , along the reaction coordinate  $\xi$ ,

$$K_{bind} = \pi N_A \int r(\xi)^2 e^{\left(\frac{-\Delta G_{PMF}(\xi)}{RT}\right)} d\xi \quad (2.22)$$

where  $\Delta G_{PMF}$  refers to the values of the free energy profiles obtained from PMF calculations,  $N_A$  and  $R$  are the Avogadro and the ideal gas constants, respectively, and  $r$  corresponds to the average radius of the cross section in each sampling window, which is also a function of  $\xi$ . The interval over which host and guest molecules associate and dissociate provides the limits of integration. Eq.(2.22) weighs each value of the inclusion coordinate and the complex volume, established on the basis of the COM positioning related to each guest backbone inside the cavity. The values of  $K_{bind}$  for the complexes are computed using a cylindrical approximation [23], illustrated in Figure 2.6. The cylindrical approximation allows determination of the available volume for the guests upon inclusion. This volume is constrained to a small cylinder able to sample most of the movements of guest molecules along the  $xy$  plane of the host (e.g. cyclodextrin) cavity. The PMF is thus defined in the cylindrical region where the  $\xi_z$  coordinate is oriented along the axis of the cavity and the cylinder (Figure 2.6). Integrating the PMF over  $z$  is equivalent to integrating over the whole cylinder. It is also possible to calculate the standard free-energy of binding,  $\Delta G_{bind}^0$ , from

$$\Delta G_{bind}^0 = -RT \ln(K_{bind}) \quad (2.23)$$

while the standard enthalpy,  $\Delta H_{bind}^0$ , and entropy  $T\Delta S_{bind}^0$  are obtained from

$$\Delta H_{bind}^0 = RT^2 \frac{d}{dT} \ln(K_{bind}) = \frac{\int r(\xi)^2 \Delta G_{PMF}(\xi) e^{\frac{-\Delta_{PMF}(\xi)}{RT}} d\xi}{\int r(\xi)^2 e^{\frac{-\Delta_{PMF}(\xi)}{RT}} d\xi} \quad (2.24)$$

$$-T\Delta S_{bind}^0 = \Delta G_{bind}^0 - \Delta H_{bind}^0 \quad (2.25)$$



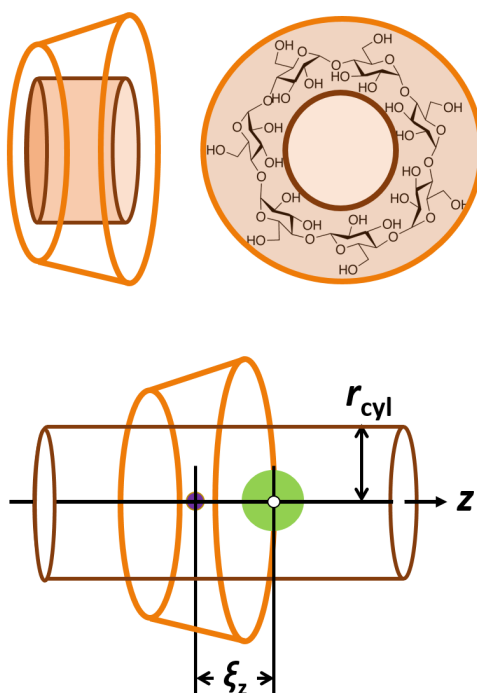


Figure 2.6: Illustrative representation of a typical model reflecting the cylindrical approximation. The cylindrical channel, shown in brown, is embedded in the Cd cavity. When the guest molecule (green circle) enters the Cd cavity (orange truncated cone), the sampled volume for the guest is restrained to the cylinder defined by the area accessible for guest movement in the  $xy$  plane. The average radius of that cylinder,  $r_{cyl}$ , is obtained from COM positions of the guest at each sampling window. Reproduced with permission from ref. [13]. Copyright (2018) American Chemical Society.

## 2.5 Visualizing noncovalent interactions

The key factors affecting the thermodynamic signatures in host-guest systems can also be assessed along with an accurate description of the NCI including their spatial features. This can be carried out resorting to a recently developed Independent Gradient Method (IGM) of Lefebvre and co-workers [107], which allows the visualization of regions of low charge density corresponding to stabilizing/destabilizing NCI, based on the analysis of the electronic charge density of the interacting molecules and the respective gradients. Although the original NCI method of Johnson and co-workers [108] provides a very similar qualitative analysis of NCI, the reduced density gradient,  $s$ , used to identify the interaction types is a dimensionless quantity and therefore difficult the evaluation of the respective strengths. The new IGM allows for a quantitative comparison of the strength of NCI through the calculation of the IGM descriptor,  $\delta g$ , which corresponds directly to the charge density gradient(s) in real-space.

The topological features of the electronic charge density have played an important part in several schemes aiming to provide a route to understanding molecular structure from first principles, that is, without resorting to any form of empirical or approximate models (other than the physically justified approximations underlying the electronic structure methods employed). Methods such as the theory of Atoms in Molecules (AIM) [109] and the Electron Localization Function (ELF) [110–112] can provide great insight into features of the density. Both AIM and the ELF are useful for studying strong interactions such as covalent or ionic bonding but are not as useful in the analysis of very weak interactions of the type that are important for subjects as diverse as protein structure, drug design, catalysis, materials self-assembly, and many more. To address this, Johnson et al. [108, 113] introduced the NCI analysis method. This approach is based on the electronic charge density,  $\rho$ , and its derivatives. The first derivative  $\nabla\rho$  enters into the expression for the reduced density gradient,  $s$ ,

$$s = \frac{1}{(2(3\pi^2))^{1/3}} \frac{|\nabla\rho|}{\rho^{4/3}} \quad (2.26)$$

In regions of low  $\rho$  such as the density tails far from a molecule the gradient remains large and so  $s$  displays high values. However, in regions of low  $\rho$  between atoms where weak NCI occur the gradient (and therefore  $s$ ) drop to zero. In order to differentiate between stabilizing attractive interactions and those that are unfavorable and destabilize the system it is necessary to analyze the second derivative (Laplacian) of the charge density  $\nabla^2\rho$ . Decomposition of  $\nabla^2\rho$  into the three eigenvalues representing the axes of maximal variation

$$\nabla^2\rho = \lambda_1 + \lambda_2 + \lambda_3 \quad (\lambda_1 \leq \lambda_2 \leq \lambda_3) \quad (2.27)$$

provides information on the nature of the interactions at a given point in space.  $\lambda_2$  displays negative values in stabilizing/bonding regions (charge is flowing into this region indicating a local build-up of  $\rho$ ) whilst in destabilizing/repulsive regions it is positive (charge flowing out, indicating a local depletion of  $\rho$ ). Plotting  $s$  against  $\text{sign}(\lambda_2)\rho$  will therefore permit the identification of NCI in regions where  $s$  and  $\text{sign}(\lambda_2)\rho \rightarrow 0$ . Although these quantities can be readily obtained with first-principles electronic structure methods, such calculations remain too computationally expensive for the large systems of interest in biological or materials science applications. In such cases it is possible to ap-

proximate the charge density with a sum of atomic densities providing a pro-molecular density,  $\rho^{pro}$ . This approximate density does not include relaxation of the atomic densities as would happen in self-consistent calculations for bonded systems. Fortunately, the largest deviation of  $\rho^{pro}$  from the fully relaxed density occurs in covalent bonding regions and has a minimal effect on the (low-density) NCI regions.

Substituting  $\rho^{pro}$  into the equations above has been found to have very little impact on the resulting NCI analysis. For purposes of interfacing with the results of molecular dynamics simulations, pro-molecular densities have the additional advantages that they are readily computed for both finite and extended/periodic systems and the fact that this approach requires orders of magnitude less computational time than the method based on first-principles electronic structure calculations. A recent development of the NCI method that makes use of the pro-molecular route to building the charge density of the system under study is IGM of Lefebvre et al.[90] As with the NCI method, IGM employs in addition to  $\rho$  quantities related to the first and second derivatives of the density. However, in IGM the reduced density gradient,  $s$ , is replaced with the descriptor  $\delta g^{inter}$ , defined as the difference between the first derivatives of the charge densities for the total system and the fragments

$$\delta g^{inter} = |\nabla \rho^{IGM,inter}| - |\nabla \rho| \quad (2.28)$$

$\delta g^{inter} > 0$  indicates the presence of noncovalent interactions and the magnitude of the descriptor at a point in space gives an indication of the strength of the interaction.

$$\left( \frac{\delta \rho}{\delta x} \right)^{IGM,inter} = \left| \sum_{i=1}^{N_A} \frac{\delta \rho_i}{\delta x} \right| + \left| \sum_{i=1}^{N_B} \frac{\delta \rho_i}{\delta x} \right| \quad (2.29)$$

The IGM approach has the attractive feature that  $\delta g^{inter}$  allows for a more facile comparison of the strength of the weak interactions than the quantity  $s$  in the original NCI. [107] This is due to the fact that the presence of significant noncovalent interactions is indicated when  $s \rightarrow 0$  making interpretation difficult whereas the magnitude of the IGM quantity  $\delta g^{inter}$  increases in proportion to the strength of the interaction.

An illustrative example of the use of the NCI and IGM methods is given in Figures 2.7 and 2.8. The host-guest complex shown is between curcurbit[7]uril and the dodecyl serine-based monomeric

cationic surfactant 12SerTFAC [114] (to make the example more accessible to the reader only a single configuration is shown). Calculation of the NCI and IGM descriptors was performed using IGMPlot version 1.0. [107] As can be seen from the molecular structure images, both the  $s$  and  $\delta g^{inter}$  surfaces provide qualitatively similar information and display the general distribution of the most significant host-guest interactions. Similarly, the color-coding provided by the value of  $sign(\lambda_2)\rho$  can be seen to predict that the interactions are largely of the weak van der Waals type with the exception of a single blue region denoting the hydrogen bond between the serine hydroxyl group and the host. A significant difference between the  $s$  and  $\delta g^{inter}$  surfaces is that the latter also contains information on the strength of the interactions through the volumes of the isosurface regions at a given point.

The IGM approach therefore provides an important extra source of information on the nature of the interactions. The intrinsic difference between the two methods is even more clearly seen in the adjacent scatter plots. In the IGM plot (Figure 2.8, right) peaks of different magnitude corresponding to different strengths of interaction can be seen which give rise to the differing isosurface volumes. The NCI plot (Figure 2.7, right), however, displays all spikes in the noncovalent interaction region  $-0.025 \leq \delta g^{inter} \leq 0.025$  in a very similar manner and makes interpretation much less easy. For this reason, despite very similar computational requirements for both methods making them equally suitable for analysis of large (ensembles of) systems such as those arising from MD simulations it is likely that the future will see the newer IGM method being used much more extensively than the original NCI one.

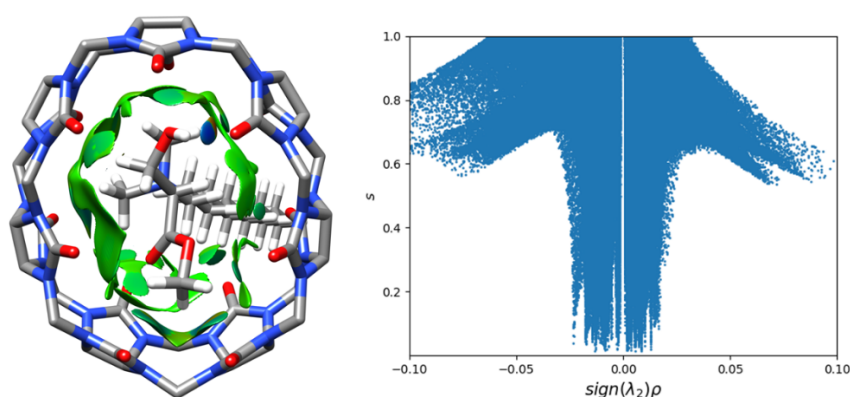


Figure 2.7: Host-guest complexation between curcubituril and the dodecyl serine-based monomeric cationic surfactant 12SerTFAC. (Left) Reduced density gradient,  $s=0.4$ , isosurface colored by value of  $sign(\lambda_2)\rho$  ( $-0.03 \leq sign(\lambda_2)\rho \leq 0.03$  a.u.). Blue: stabilizing, red: destabilizing and green weak interactions. (Right) Scatter plot of  $s$  and  $sign(\lambda_2)\rho$  values. Reproduced from ref. [1].

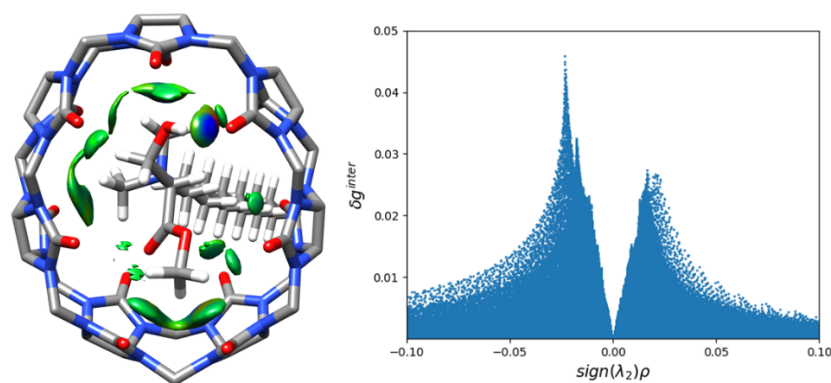


Figure 2.8: Host-guest complexation between curcubituril and 12serTFAC surfactant. (Left) IGM  $\delta g^{inter} = 0.01$  a.u. isosurface colored by value of  $sign(\lambda_2)\rho$  ( $-0.03 \leq sign(\lambda_2)\rho \leq 0.03$  a.u.). Blue: stabilizing, red: destabilizing and green: weak interactions. (Right) Scatter plot of  $\delta g^{inter}$  and  $sign(\lambda_2)\rho$  values. Reproduced from ref. [1].

## References

- [1] Tânia F. Cova et al. “Modeling Soft Supramolecular Nanostructures by Molecular Simulations”. *Molecular Dynamics*. Ed. by Alexander Vakhrushev. Rijeka: IntechOpen, 2018. Chap. 2. DOI: [10.5772/intechopen.74939](https://doi.org/10.5772/intechopen.74939).
- [2] Samikannu Prabu et al. “Preparation, characterization and molecular modeling studies of the inclusion complex of Caffeine with Beta-cyclodextrin”. *Journal of Molecular Structure* 1099 (2015), pp. 616–624. ISSN: 0022-2860. DOI: <https://doi.org/10.1016/j.molstruc.2015.07.018>.
- [3] Paula dos Passos Menezes et al. “Molecular Modeling and Physicochemical Properties of Supramolecular Complexes of Limonene with  $\alpha$ - and  $\beta$ -Cyclodextrins”. *AAPS PharmSciTech* 18.1 (2017), pp. 49–57. DOI: [10.1208/s12249-016-0516-0](https://doi.org/10.1208/s12249-016-0516-0).
- [4] K. Sivakumar et al. “Preparation, characterization and molecular modeling studies of the beta-cyclodextrin inclusion complex with benzoguanamine and its analytical application as chemosensor for the selective sensing of  $Ce^{4+}$ ”. *Spectrochimica Acta Part A: Molecular and Biomolecular Spectroscopy* 200 (2018), pp. 212–225. ISSN: 1386-1425. DOI: <https://doi.org/10.1016/j.saa.2018.04.034>.

- [5] Myungshim Kang, Kaushik Chakraborty, and Sharon M. Loverde. “Molecular Dynamics Simulations of Supramolecular Anticancer Nanotubes”. *Journal of Chemical Information and Modeling* 58.6 (2018), pp. 1164–1168. DOI: [10.1021/acs.jcim.8b00193](https://doi.org/10.1021/acs.jcim.8b00193).
- [6] Xiangze Zeng et al. “Harnessing complexity in molecular self-assembly using computer simulations”. *Physical Chemistry Chemical Physics* 20 (10 2018), pp. 6767–6776. DOI: [10.1039/C7CP06181A](https://doi.org/10.1039/C7CP06181A).
- [7] Maali Saad Mokhtar, FakhrEldin O. Suliman, and Abdalla A. Elbashir. “Experimental and molecular modeling investigations of inclusion complexes of imazapyr with 2-hydroxypropyl( $\beta/\gamma$ ) cyclodextrin”. *Journal of Molecular Liquids* 262 (2018), pp. 504–513. ISSN: 0167-7322. DOI: <https://doi.org/10.1016/j.molliq.2018.04.088>.
- [8] Wen Sheng Cai et al. “Free Energy Calculations for Cyclodextrin Inclusion Complexes”. *Current Organic Chemistry* 15.6 (2011), pp. 839–847. ISSN: 1385-2728. DOI: [doi:10.2174/138527211794518853](https://doi.org/10.2174/138527211794518853).
- [9] Cameron Abrams and Giovanni Bussi. “Enhanced Sampling in Molecular Dynamics Using Metadynamics, Replica-Exchange, and Temperature-Acceleration”. *Entropy* 16.1 (2014), p. 163. ISSN: 1099-4300.
- [10] Andrea Cavalli et al. “Investigating Drug-Target Association and Dissociation Mechanisms Using Metadynamics-Based Algorithms”. *Accounts of Chemical Research* 48.2 (2015), pp. 277–285. ISSN: 0001-4842. DOI: [10.1021/ar500356n](https://doi.org/10.1021/ar500356n).
- [11] Alessandro Laio and Francesco L Gervasio. “Metadynamics: a method to simulate rare events and reconstruct the free energy in biophysics, chemistry and material science”. *Reports on Progress in Physics* 71.12 (2008), p. 126601.
- [12] Yong Wang et al. “Frequency adaptive metadynamics for the calculation of rare-event kinetics”. *The Journal of Chemical Physics* 149.7 (2018), p. 072309. DOI: [10.1063/1.5024679](https://doi.org/10.1063/1.5024679).
- [13] Tânia F. G. G. Cova et al. “Drastic Stabilization of Junction Nodes in Supramolecular Structures Based on Host-Guest Complexes”. *Macromolecules* 51.7 (2018), pp. 2732–2741. DOI: [10.1021/acs.macromol.8b00154](https://doi.org/10.1021/acs.macromol.8b00154).

- [14] Baron Peters. “Chapter 22 - Free energy relationships”. *Reaction Rate Theory and Rare Events Simulations*. Ed. by Baron Peters. Amsterdam: Elsevier, 2017, pp. 601–613. ISBN: 978-0-444-56349-1. DOI: <https://doi.org/10.1016/B978-0-44-456349-1.00022-2>.
- [15] Yukun Wang et al. “Applications of Rare Event Dynamics on the Free Energy Calculations for Membrane Protein Systems”. *Advance in Structural Bioinformatics*. Ed. by Dongqing Wei et al. Dordrecht: Springer Netherlands, 2015, pp. 71–82. ISBN: 978-94-017-9245-5. DOI: [10.1007/978-94-017-9245-5\\_6](https://doi.org/10.1007/978-94-017-9245-5_6).
- [16] Jens Smiatek, Niels Hansen, and Johannes Kastner. “Chapter 6 - Free Energy Calculation Methods and Rare Event Sampling Techniques for Biomolecular Simulations”. *Simulating Enzyme Reactivity: Computational Methods in Enzyme Catalysis*. The Royal Society of Chemistry, 2017, pp. 185–214. ISBN: 978-1-78262-429-5. DOI: [10.1039/9781782626831-00185](https://doi.org/10.1039/9781782626831-00185).
- [17] Christophe Chipot and Andrew Pohorille. *Free energy calculations*. Springer, 2007. ISBN: 3540736174.
- [18] David R. Bell et al. “Calculating binding free energies of host-guest systems using the AMOEBA polarizable force field”. *Physical Chemistry Chemical Physics* 18 (44 2016), pp. 30261–30269. DOI: [10.1039/C6CP02509A](https://doi.org/10.1039/C6CP02509A).
- [19] Niel M. Henriksen and Michael K. Gilson. “Evaluating Force Field Performance in Thermodynamic Calculations of Cyclodextrin Host-Guest Binding: Water Models, Partial Charges, and Host Force Field Parameters”. *Journal of Chemical Theory and Computation* 13.9 (2017), pp. 4253–4269. ISSN: 1549-9618. DOI: [10.1021/acs.jctc.7b00359](https://doi.org/10.1021/acs.jctc.7b00359).
- [20] Peter Kollman. “Free energy calculations: Applications to chemical and biochemical phenomena”. *Chemical Reviews* 93.7 (1993), pp. 2395–2417. ISSN: 0009-2665. DOI: [10.1021/cr00023a004](https://doi.org/10.1021/cr00023a004).
- [21] Huan-Xiang Zhou and Michael K. Gilson. “Theory of Free Energy and Entropy in Noncovalent Binding”. *Chemical Reviews* 109.9 (2009), pp. 4092–4107. ISSN: 0009-2665. DOI: [10.1021/cr800551w](https://doi.org/10.1021/cr800551w).

- [22] Aziz Ghoufi and Patrice Malfreyt. “Calculation of the absolute thermodynamic properties of association of host-guest systems from the intermolecular potential of mean force”. *The Journal of Chemical Physics* 125.22 (2006), p. 224503. ISSN: 0021-9606. DOI: [10.1063/1.2402165](https://doi.org/10.1063/1.2402165).
- [23] Tânia F. G. G. Cova, Sandra C. C. Nunes, and Alberto A. C. C. Pais. “Free-energy patterns in inclusion complexes: the relevance of non-included moieties in the stability constants”. *Physical Chemistry Chemical Physics* 19.7 (2017), pp. 5209–5221. ISSN: 1463-9076. DOI: [10.1039/C6CP08081B](https://doi.org/10.1039/C6CP08081B).
- [24] Tânia F. G. G. Cova et al. “Bambusurils as effective ion caging agents: Does desolvation guide conformation?” *Chemical Physics Letters* 672.Supplement C (2017), pp. 89–96. ISSN: 0009-2614. DOI: <https://doi.org/10.1016/j.cplett.2017.01.029>.
- [25] Haiyang Zhang et al. “Molecular Recognition in Different Environments:  $\beta$ -Cyclodextrin Dimer Formation in Organic Solvents”. *The Journal of Physical Chemistry B* 116.42 (2012), pp. 12684–12693. ISSN: 1520-6106. DOI: [10.1021/jp308416p](https://doi.org/10.1021/jp308416p).
- [26] Haiyang Zhang et al. “Quantification of Solvent Contribution to the Stability of Noncovalent Complexes”. *Journal of Chemical Theory and Computation* 9.10 (2013), pp. 4542–4551. ISSN: 1549-9618. DOI: [10.1021/ct400404q](https://doi.org/10.1021/ct400404q).
- [27] Haiyang Zhang et al. “Cooperative Binding of Cyclodextrin Dimers to Isoflavone Analogues Elucidated by Free Energy Calculations”. *The Journal of Physical Chemistry C* 118.13 (2014), pp. 7163–7173. ISSN: 1932-7447. DOI: [10.1021/jp412041d](https://doi.org/10.1021/jp412041d).
- [28] Julio Caballero et al. “Study of the interaction between progesterone and beta-cyclodextrin by electrochemical techniques and steered molecular dynamics”. *Journal of Physical Chemistry B* 112.33 (2008), pp. 10194–10201. ISSN: 1520-6106.
- [29] G. Filippini, C. Bonal, and P. Malfreyt. “How does the dehydration change the host-guest association under homogeneous and heterogeneous conditions?” *Physical Chemistry Chemical Physics* 16.18 (2014), pp. 8667–8674. ISSN: 1463-9076. DOI: [10.1039/C4CP00108G](https://doi.org/10.1039/C4CP00108G).



- [30] Jia He et al. “Cooperative Recruitment of Amphotericin B Mediated by a Cyclodextrin Dimer”. *The Journal of Physical Chemistry C* 118.41 (2014), pp. 24173–24180. ISSN: 1932-7447. DOI: [10.1021/jp507325j](https://doi.org/10.1021/jp507325j).
- [31] Matias I. Sancho et al. “Theoretical and Experimental Study of Inclusion Complexes of  $\beta$ -Cyclodextrins with Chalcone and 2',4'-Dihydroxychalcone”. *The Journal of Physical Chemistry B* 120.12 (2016), pp. 3000–3011. ISSN: 1520-6106. DOI: [10.1021/acs.jpcc.5b11317](https://doi.org/10.1021/acs.jpcc.5b11317).
- [32] Ruyin Cao and Shanshan Wu. “In silico properties characterization of water-soluble  $\gamma$ -cyclodextrin bi-capped C60 complex: Free energy and geometrical insights for stability and solubility”. *Carbohydrate Polymers* 124.Supplement C (2015), pp. 188–195. ISSN: 0144-8617. DOI: <https://doi.org/10.1016/j.carbpol.2015.02.014>.
- [33] Baiping Ren et al. “In Silico understanding of the cyclodextrin-phenanthrene hybrid assemblies in both aqueous medium and bacterial membranes”. *Journal of Hazardous Materials* 285 (2015), pp. 148–156. ISSN: 0304-3894. DOI: <https://doi.org/10.1016/j.jhazmat.2014.12.001>.
- [34] Yanmin Yu et al. “Spatial Arrangement of  $\alpha$ -Cyclodextrins in a Rotaxane. Insights from Free-Energy Calculations”. *The Journal of Physical Chemistry B* 112.17 (2008), pp. 5268–5271. ISSN: 1520-6106. DOI: [10.1021/jp711413a](https://doi.org/10.1021/jp711413a).
- [35] Michelle L. Lamb and William L. Jorgensen. “Computational approaches to molecular recognition”. *Current Opinion in Chemical Biology* 1.4 (1997), pp. 449–457. ISSN: 1367-5931. DOI: [https://doi.org/10.1016/S1367-5931\(97\)80038-5](https://doi.org/10.1016/S1367-5931(97)80038-5).
- [36] Wensheng Cai et al. “Can the anomalous aqueous solubility of small beta-cyclodextrin be explained by its hydration free energy alone?” *Physical Chemistry Chemical Physics* 10.22 (2008), pp. 3236–3243. ISSN: 1463-9076. DOI: [10.1039/B717509D](https://doi.org/10.1039/B717509D).
- [37] Silvia A. Martins et al. “Prediction of Solvation Free Energies with Thermodynamic Integration Using the General Amber Force Field”. *Journal of Chemical Theory and Computation* 10.8 (2014), pp. 3570–3577. ISSN: 1549-9618. DOI: [10.1021/ct500346y](https://doi.org/10.1021/ct500346y).
- [38] Johannes Kästner. “Umbrella sampling”. *Wiley Interdisciplinary Reviews: Computational Molecular Science* 1.6 (2011), pp. 932–942. DOI: [10.1002/wcms.66](https://doi.org/10.1002/wcms.66).

- [39] Jochen S. Hub, Bert L. de Groot, and David van der Spoel. “ $q_w$ ham-A Free Weighted Histogram Analysis Implementation Including Robust Error and Autocorrelation Estimates”. *Journal of Chemical Theory and Computation* 6.12 (2010), pp. 3713–3720. ISSN: 1549-9618. DOI: [10.1021/ct100494z](https://doi.org/10.1021/ct100494z).
- [40] Andrew Pohorille, Christopher Jarzynski, and Christophe Chipot. “Good Practices in Free-Energy Calculations”. *The Journal of Physical Chemistry B* 114.32 (2010), pp. 10235–10253. DOI: [10.1021/jp102971x](https://doi.org/10.1021/jp102971x).
- [41] Niels Hansen and Wilfred F. van Gunsteren. “Practical Aspects of Free-Energy Calculations: A Review”. *Journal of Chemical Theory and Computation* 10.7 (2014), pp. 2632–2647. DOI: [10.1021/ct500161f](https://doi.org/10.1021/ct500161f).
- [42] Pavel V. Klimovich, Michael R. Shirts, and David L. Mobley. “Guidelines for the analysis of free energy calculations”. *Journal of Computer-Aided Molecular Design* 29.5 (2015), pp. 397–411. ISSN: 1573-4951. DOI: [10.1007/s10822-015-9840-9](https://doi.org/10.1007/s10822-015-9840-9).
- [43] Hagai Meirovitch, Srinath Chelvaraja, and Ronald P White. “Methods for calculating the entropy and free energy and their application to problems involving protein flexibility and ligand binding”. *Current Protein and Peptide Science* 10.3 (2009), pp. 229–243.
- [44] Peter G. Bolhuis et al. “Transition Path Sampling: Throwing Ropes Over Rough Mountain Passes, in the Dark”. *Annual Review of Physical Chemistry* 53.1 (2002), pp. 291–318. DOI: [10.1146/annurev.physchem.53.082301.113146](https://doi.org/10.1146/annurev.physchem.53.082301.113146).
- [45] Keith J. Laidler and M. Christine King. “Development of transition-state theory”. *The Journal of Physical Chemistry* 87.15 (1983), pp. 2657–2664. DOI: [10.1021/j100238a002](https://doi.org/10.1021/j100238a002).
- [46] John G. Kirkwood. “Statistical Mechanics of Fluid Mixtures”. *The Journal of Chemical Physics* 3.5 (1935), pp. 300–313. ISSN: 0021-9606. DOI: [10.1063/1.1749657](https://doi.org/10.1063/1.1749657).
- [47] Liangzhen Zheng et al. “Molecular Dynamics and Simulation”. *Reference Module in Life Sciences*. Elsevier, 2018. ISBN: 978-0-12-809633-8. DOI: <https://doi.org/10.1016/B978-0-12-809633-8.20284-7>. URL: <http://www.sciencedirect.com/science/article/pii/B9780128096338202847>.

- [48] G. M. Torrie and J. P. Valleau. “Nonphysical sampling distributions in Monte Carlo free-energy estimation: Umbrella sampling”. *Journal of Computational Physics* 23.2 (1977), pp. 187–199. ISSN: 0021-9991. DOI: [https://doi.org/10.1016/0021-9991\(77\)90121-8](https://doi.org/10.1016/0021-9991(77)90121-8).
- [49] Christophe Chipot. “Frontiers in free-energy calculations of biological systems”. *Wiley Interdisciplinary Reviews: Computational Molecular Science* 4.1 (2014), pp. 71–89. ISSN: 1759-0884. DOI: [10.1002/wcms.1157](https://doi.org/10.1002/wcms.1157).
- [50] Eric Darve and Andrew Pohorille. “Calculating free energies using average force”. *The Journal of Chemical Physics* 115.20 (2001), pp. 9169–9183. DOI: [10.1063/1.1410978](https://doi.org/10.1063/1.1410978).
- [51] Benoît Roux. “The calculation of the potential of mean force using computer simulations”. *Computer Physics Communications* 91.1 (1995), pp. 275–282. ISSN: 0010-4655. DOI: [https://doi.org/10.1016/0010-4655\(95\)00053-I](https://doi.org/10.1016/0010-4655(95)00053-I).
- [52] G. M. Torrie and J. P. Valleau. “Monte-Carlo Free-Energy Estimates Using Non-Boltzmann Sampling - Application to Subcritical Lennard-Jones Fluid”. *Chemical Physics Letters* 28.4 (1974), pp. 578–581. ISSN: 0009-2614.
- [53] Eric Darve. “Numerical Methods for Calculating the Potential of Mean Force”. *New Algorithms for Macromolecular Simulation*. Ed. by Benedict Leimkuhler et al. Berlin, Heidelberg: Springer Berlin Heidelberg, 2006, pp. 213–249. ISBN: 978-3-540-31618-3. DOI: [10.1007/3-540-31618-3\\_13](https://doi.org/10.1007/3-540-31618-3_13).
- [54] Jean-Fran St-Pierre et al. “Use of Umbrella Sampling to Calculate the Entrance/Exit Pathway for Z-Pro-Prolinal Inhibitor in Prolyl Oligopeptidase”. *Journal of Chemical Theory and Computation* 7.6 (2011), pp. 1583–1594. DOI: [10.1021/ct1007058](https://doi.org/10.1021/ct1007058).
- [55] Silvia Munoz-Botella et al. “Differentiating inclusion complexes from host molecules by tapping-mode atomic force microscopy”. *Biophysical journal* 71.1 (1996), pp. 86–90.
- [56] Shigeo Oyama et al. “Interactive Force between Cyclodextrin Inclusion Complexes Studied by Atomic Force Microscopy”. *Japanese Journal of Applied Physics* 40.6S (2001), p. 4419.
- [57] Tommaso Auletta et al. “ $\beta$ -Cyclodextrin Host-Guest Complexes Probed under Thermodynamic Equilibrium: Thermodynamics and AFM Force Spectroscopy”. *Journal of the American Chemical Society* 126.5 (2004), pp. 1577–1584. DOI: [10.1021/ja0383569](https://doi.org/10.1021/ja0383569).

- [58] R. Periasamy, S. Kothainayaki, and K. Sivakumar. “Encapsulation of dicinnamalacetone in  $\beta$ -cyclodextrin: A physicochemical evaluation and molecular modeling approach on 1:2 inclusion complex”. *Journal of Macromolecular Science, Part A* 53.9 (2016), pp. 546–556. DOI: [10.1080/10601325.2016.1201750](https://doi.org/10.1080/10601325.2016.1201750).
- [59] Katherine Lozano et al. “Electrochemical and associated techniques for the study of the inclusion complexes of thymol and  $\beta$ -cyclodextrin and its interaction with DNA”. *Journal of Solid State Electrochemistry* 22.5 (2018), pp. 1483–1493. ISSN: 1433-0768. DOI: [10.1007/s10008-017-3805-y](https://doi.org/10.1007/s10008-017-3805-y).
- [60] J Strzelecki et al. “AFM force spectroscopy and steered molecular dynamics simulation of protein contactin 4”. *Acta Physica Polonica A* 116.CONF (2009).
- [61] P. Virnau and M. Muller. “Calculation of free energy through successive umbrella sampling”. *Journal of Chemical Physics* 120.23 (2004), pp. 10925–10930. ISSN: 0021-9606.
- [62] Justin R Gullingsrud, Rosemary Braun, and Klaus Schulten. “Reconstructing potentials of mean force through time series analysis of steered molecular dynamics simulations”. *Journal of Computational Physics* 151.1 (1999), pp. 190–211.
- [63] Mai Suan Li and Binh Khanh Mai. “Steered molecular dynamics-a promising tool for drug design”. *Current Bioinformatics* 7.4 (2012), pp. 342–351.
- [64] Sanghyun Park and Klaus Schulten. “Calculating potentials of mean force from steered molecular dynamics simulations”. *The Journal of Chemical Physics* 120.13 (2004), pp. 5946–5961. DOI: [10.1063/1.1651473](https://doi.org/10.1063/1.1651473).
- [65] EL Florin, VT Moy, and HE Gaub. “Adhesion forces between individual ligand-receptor pairs”. *Science* 264.5157 (1994), pp. 415–417. ISSN: 0036-8075. DOI: [10.1126/science.8153628](https://doi.org/10.1126/science.8153628).
- [66] C.L. Ramírez, M.A. Martí, and A.E. Roitberg. “Chapter 6 - Steered Molecular Dynamics Methods Applied to Enzyme Mechanism and Energetics”. *Computational Approaches for Studying Enzyme Mechanism Part B*. Ed. by Gregory A. Voth. Vol. 578. *Methods in Enzymology*. Academic Press, 2016, pp. 123–143. DOI: <https://doi.org/10.1016/bs.mie.2016.05.029>.

- [67] Francesco Di Palma, Francesco Colizzi, and Giovanni Bussi. “Chapter 6 - Using Reweighted Pulling Simulations to Characterize Conformational Changes in Riboswitches”. *Computational Methods for Understanding Riboswitches*. Ed. by Shi-Jie Chen and Donald H. Burke-Aguero. Vol. 553. Methods in Enzymology. Academic Press, 2015, pp. 139–162. DOI: <https://doi.org/10.1016/bs.mie.2014.10.055>.
- [68] Mark James Abraham et al. “GROMACS: High performance molecular simulations through multi-level parallelism from laptops to supercomputers”. *SoftwareX* 1-2 (2015), pp. 19–25. ISSN: 2352-7110. DOI: <https://doi.org/10.1016/j.softx.2015.06.001>.
- [69] Berk Hess et al. “GROMACS 4: Algorithms for highly efficient, load-balanced, and scalable molecular simulation”. *Journal of Chemical Theory and Computation* 4.3 (2008), pp. 435–447. ISSN: 1549-9618.
- [70] D.A. Case et al. *AMBER. 16*. Aggregated Database. 2016.
- [71] Bernard R Brooks et al. “CHARMM: the biomolecular simulation program”. *Journal of computational chemistry* 30.10 (2009), pp. 1545–1614.
- [72] James C. Phillips et al. “Scalable molecular dynamics with NAMD”. *Journal of Computational Chemistry* 26.16 (2005), pp. 1781–1802. ISSN: 1096-987X. DOI: [10.1002/jcc.20289](https://doi.org/10.1002/jcc.20289).
- [73] S. Kumar et al. “The Weighted Histogram Analysis Method for Free-Energy Calculations on Biomolecules .1. The Method”. *Journal of Computational Chemistry* 13.8 (1992), pp. 1011–1021. ISSN: 0192-8651.
- [74] M. Souaille and B. Roux. “Extension to the weighted histogram analysis method: combining umbrella sampling with free energy calculations”. *Computer Physics Communications* 135.1 (2001), pp. 40–57. ISSN: 0010-4655.
- [75] Jeffrey Comer et al. “The Adaptive Biasing Force Method: Everything You Always Wanted To Know but Were Afraid To Ask”. *The Journal of Physical Chemistry B* 119.3 (2015), pp. 1129–1151. ISSN: 1520-6106. DOI: [10.1021/jp506633n](https://doi.org/10.1021/jp506633n).
- [76] Bjorn O. Brandsdal et al. “Free Energy Calculations and Ligand Binding”. *Advances in Protein Chemistry*. Vol. 66. Academic Press, 2003, pp. 123–158. DOI: [https://doi.org/10.1016/S0065-3233\(03\)66004-3](https://doi.org/10.1016/S0065-3233(03)66004-3).

- [77] Gino A. DiLabio and Alberto Otero-de-la-Roza. “Noncovalent Interactions in Density Functional Theory”. *Reviews in Computational Chemistry*. John Wiley & Sons, Inc, 2016, pp. 1–97. ISBN: 9781119148739. DOI: [10.1002/9781119148739.ch1](https://doi.org/10.1002/9781119148739.ch1).
- [78] Jack Simons. “An experimental chemist’s guide to ab initio quantum chemistry”. *The Journal of Physical Chemistry* 95.3 (1991), pp. 1017–1029. ISSN: 0022-3654.
- [79] Michael J. Robertson, Julian Tirado-Rives, and William L. Jorgensen. “Improved Peptide and Protein Torsional Energetics with the OPLS-AA Force Field”. *Journal of Chemical Theory and Computation* 11.7 (2015), pp. 3499–3509. ISSN: 1549-9618. DOI: [10.1021/acs.jctc.5b00356](https://doi.org/10.1021/acs.jctc.5b00356).
- [80] K. Vanommeslaeghe et al. “CHARMM general force field: A force field for drug-like molecules compatible with the CHARMM all-atom additive biological force fields”. *Journal of Computational Chemistry* 31.4 (2010), pp. 671–690. ISSN: 1096-987X. DOI: [10.1002/jcc.21367](https://doi.org/10.1002/jcc.21367).
- [81] Maria M. Reif, Philippe H. Hünenberger, and Chris Oostenbrink. “New Interaction Parameters for Charged Amino Acid Side Chains in the GROMOS Force Field”. *Journal of Chemical Theory and Computation* 8.10 (2012), pp. 3705–3723. ISSN: 1549-9618. DOI: [10.1021/ct300156h](https://doi.org/10.1021/ct300156h).
- [82] Elizabeth A. Ploetz and Paul E. Smith. “A Kirkwood-Buff force field for the aromatic amino acids”. *Physical Chemistry Chemical Physics* 13.40 (2011), pp. 18154–18167. ISSN: 1463-9076. DOI: [10.1039/C1CP21883B](https://doi.org/10.1039/C1CP21883B).
- [83] Christopher M. Baker, Victor M. Anisimov, and Alexander D. MacKerell. “Development of CHARMM Polarizable Force Field for Nucleic Acid Bases Based on the Classical Drude Oscillator Model”. *The Journal of Physical Chemistry B* 115.3 (2011), pp. 580–596. ISSN: 1520-6106. DOI: [10.1021/jp1092338](https://doi.org/10.1021/jp1092338).
- [84] Justin A. Lemkul and Alexander D. MacKerell. “Balancing the Interactions of Mg<sup>2+</sup> in Aqueous Solution and with Nucleic Acid Moieties For a Polarizable Force Field Based on the Classical Drude Oscillator Model”. *The Journal of Physical Chemistry B* 120.44 (2016), pp. 11436–11448. ISSN: 1520-6106. DOI: [10.1021/acs.jpcc.6b09262](https://doi.org/10.1021/acs.jpcc.6b09262).

- [85] Zhi-Xiang Wang et al. “Strike a balance: Optimization of backbone torsion parameters of AMBER polarizable force field for simulations of proteins and peptides”. *Journal of Computational Chemistry* 27.6 (2006), pp. 781–790. ISSN: 1096-987X. DOI: [10.1002/jcc.20386](https://doi.org/10.1002/jcc.20386).
- [86] Daniel J. Cole et al. “Biomolecular Force Field Parameterization via Atoms-in-Molecule Electron Density Partitioning”. *Journal of Chemical Theory and Computation* 12.5 (2016), pp. 2312–2323. ISSN: 1549-9618. DOI: [10.1021/acs.jctc.6b00027](https://doi.org/10.1021/acs.jctc.6b00027).
- [87] Yue Shi et al. “Polarizable Atomic Multipole-Based AMOEBA Force Field for Proteins”. *Journal of Chemical Theory and Computation* 9.9 (2013), pp. 4046–4063. ISSN: 1549-9618. DOI: [10.1021/ct4003702](https://doi.org/10.1021/ct4003702).
- [88] Robert E. Duke et al. “GEM\*: A Molecular Electronic Density-Based Force Field for Molecular Dynamics Simulations”. *Journal of Chemical Theory and Computation* 10.4 (2014), pp. 1361–1365. ISSN: 1549-9618. DOI: [10.1021/ct500050p](https://doi.org/10.1021/ct500050p).
- [89] Stefan Grimme. “A General Quantum Mechanically Derived Force Field (QMDFFF) for Molecules and Condensed Phase Simulations”. *Journal of Chemical Theory and Computation* 10.10 (2014), pp. 4497–4514. ISSN: 1549-9618. DOI: [10.1021/ct500573f](https://doi.org/10.1021/ct500573f).
- [90] Susanna Monti et al. “Exploring the conformational and reactive dynamics of biomolecules in solution using an extended version of the glycine reactive force field”. *Physical Chemistry Chemical Physics* 15.36 (2013), pp. 15062–15077. ISSN: 1463-9076. DOI: [10.1039/C3CP51931G](https://doi.org/10.1039/C3CP51931G).
- [91] Jiali Gao et al. “Explicit Polarization: A Quantum Mechanical Framework for Developing Next Generation Force Fields”. *Accounts of Chemical Research* 47.9 (2014), pp. 2837–2845. ISSN: 0001-4842. DOI: [10.1021/ar5002186](https://doi.org/10.1021/ar5002186).
- [92] William L. Jorgensen et al. “Comparison of simple potential functions for simulating liquid water”. *The Journal of Chemical Physics* 79.2 (1983), pp. 926–935. ISSN: 0021-9606. DOI: [10.1063/1.445869](https://doi.org/10.1063/1.445869).
- [93] Hans W. Horn et al. “Development of an improved four-site water model for biomolecular simulations: TIP4P-Ew”. *The Journal of Chemical Physics* 120.20 (2004), pp. 9665–9678. ISSN: 0021-9606. DOI: [10.1063/1.1683075](https://doi.org/10.1063/1.1683075).

- [94] H. J. C. Berendsen, J. R. Grigera, and T. P. Straatsma. “The missing term in effective pair potentials”. *The Journal of Physical Chemistry* 91.24 (1987), pp. 6269–6271. ISSN: 0022-3654. DOI: [10.1021/j100308a038](https://doi.org/10.1021/j100308a038).
- [95] Saeed Izadi, Ramu Anandakrishnan, and Alexey V. Onufriev. “Building Water Models: A Different Approach”. *The Journal of Physical Chemistry Letters* 5.21 (2014), pp. 3863–3871. ISSN: 1948-7185. DOI: [10.1021/jz501780a](https://doi.org/10.1021/jz501780a).
- [96] Lee-Ping Wang, Todd J. Martinez, and Vijay S. Pande. “Building Force Fields: An Automatic, Systematic, and Reproducible Approach”. *The Journal of Physical Chemistry Letters* 5.11 (2014), pp. 1885–1891. ISSN: 1948-7185. DOI: [10.1021/jz500737m](https://doi.org/10.1021/jz500737m).
- [97] Stefano Piana et al. “Water Dispersion Interactions Strongly Influence Simulated Structural Properties of Disordered Protein States”. *The Journal of Physical Chemistry B* 119.16 (2015), pp. 5113–5123. ISSN: 1520-6106. DOI: [10.1021/jp508971m](https://doi.org/10.1021/jp508971m).
- [98] Lee-Ping Wang et al. “Systematic Improvement of a Classical Molecular Model of Water”. *The Journal of Physical Chemistry B* 117.34 (2013), pp. 9956–9972. ISSN: 1520-6106. DOI: [10.1021/jp403802c](https://doi.org/10.1021/jp403802c).
- [99] David L. Mobley et al. “Small Molecule Hydration Free Energies in Explicit Solvent: An Extensive Test of Fixed-Charge Atomistic Simulations”. *Journal of Chemical Theory and Computation* 5.2 (2009), pp. 350–358. ISSN: 1549-9618. DOI: [10.1021/ct800409d](https://doi.org/10.1021/ct800409d).
- [100] Rodrigo Galindo-Murillo et al. “Assessing the Current State of Amber Force Field Modifications for DNA”. *Journal of Chemical Theory and Computation* 12.8 (2016), pp. 4114–4127. ISSN: 1549-9618. DOI: [10.1021/acs.jctc.6b00186](https://doi.org/10.1021/acs.jctc.6b00186).
- [101] James A. Maier et al. “ff14SB: Improving the Accuracy of Protein Side Chain and Backbone Parameters from ff99SB”. *Journal of Chemical Theory and Computation* 11.8 (2015), pp. 3696–3713. ISSN: 1549-9618. DOI: [10.1021/acs.jctc.5b00255](https://doi.org/10.1021/acs.jctc.5b00255).
- [102] Lauren Wickstrom et al. “Large Scale Affinity Calculations of Cyclodextrin Host-Guest Complexes: Understanding the Role of Reorganization in the Molecular Recognition Process”. *Journal of Chemical Theory and Computation* 9.7 (2013), pp. 3136–3150. ISSN: 1549-9618. DOI: [10.1021/ct400003r](https://doi.org/10.1021/ct400003r).

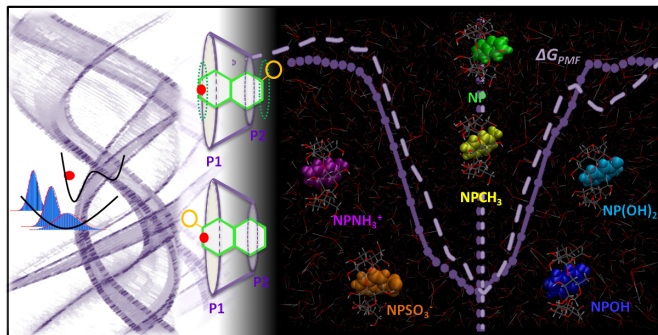


- [103] Haiyang Zhang et al. “Evaluation of Generalized Born Models for Large Scale Affinity Prediction of Cyclodextrin Host-Guest Complexes”. *Journal of Chemical Information and Modeling* 56.10 (2016), pp. 2080–2092. ISSN: 1549-9596. DOI: [10.1021/acs.jcim.6b00418](https://doi.org/10.1021/acs.jcim.6b00418).
- [104] Tianyi Yang et al. “Virtual Screening Using Molecular Simulations”. *Proteins* 79.6 (2011). 21491494[pmid] *Proteins*, pp. 1940–1951. ISSN: 0887-3585 1097-0134. DOI: [10.1002/prot.23018](https://doi.org/10.1002/prot.23018).
- [105] Dimas Suárez and Natalia Díaz. “Conformational and entropy analyses of extended molecular dynamics simulations of  $\alpha$ -,  $\beta$ - and  $\gamma$ -cyclodextrins and of the  $\beta$ -cyclodextrin/nabumetone complex”. *Physical Chemistry Chemical Physics* 19 (2 2017), pp. 1431–1440. DOI: [10.1039/C6CP06107A](https://doi.org/10.1039/C6CP06107A).
- [106] Djurre H. De Jong et al. “Determining equilibrium constants for dimerization reactions from molecular dynamics simulations”. *Journal of Computational Chemistry* 32.9 (2011), pp. 1919–1928. ISSN: 1096-987X. DOI: [10.1002/jcc.21776](https://doi.org/10.1002/jcc.21776).
- [107] Corentin Lefebvre et al. “Accurately extracting the signature of intermolecular interactions present in the NCI plot of the reduced density gradient versus electron density”. *Physical Chemistry Chemical Physics* 19.27 (2017), pp. 17928–17936. ISSN: 1463-9076. DOI: [10.1039/C7CP02110K](https://doi.org/10.1039/C7CP02110K).
- [108] Contreras-García Julia et al. “NCIPLLOT: A Program for Plotting Noncovalent Interaction Regions”. *Journal of Chemical Theory and Computation* 7.3 (2011), pp. 625–632. DOI: [10.1021/ct100641a](https://doi.org/10.1021/ct100641a).
- [109] Richard F.W. Bader. *Atoms in Molecules: A Quantum Theory*. Vol. 1. Oxford: Clarendon Press, 1994, p. 456. ISBN: 9780198558651.
- [110] A. D. Becke and K. E. Edgecombe. “A simple measure of electron localization in atomic and molecular systems”. *The Journal of Chemical Physics* 92.9 (1990), pp. 5397–5403. ISSN: 0021-9606. DOI: [10.1063/1.458517](https://doi.org/10.1063/1.458517).
- [111] B. Silvi and A. Savin. “Classification of chemical bonds based on topological analysis of electron localization functions”. *Nature* 371 (1994), p. 683. DOI: [10.1038/371683a0](https://doi.org/10.1038/371683a0).

- [112] T. Burnus, M. A. L. Marques, and E. K. U. Gross. “Time-dependent electron localization function”. *Physical Review A* 71.1 (2005). PRA, p. 010501.
- [113] Erin R. Johnson et al. “Revealing Noncovalent Interactions”. *Journal of the American Chemical Society* 132.18 (2010), pp. 6498–6506. ISSN: 0002-7863. DOI: [10.1021/ja100936w](https://doi.org/10.1021/ja100936w).
- [114] Rodrigo O. Brito et al. “Enhanced interfacial properties of novel amino acid-derived surfactants: Effects of headgroup chemistry and of alkyl chain length and unsaturation”. *Colloids and Surfaces B: Biointerfaces* 86.1 (2011), pp. 65–70. ISSN: 0927-7765. DOI: <https://doi.org/10.1016/j.colsurfb.2011.03.017>.



## Chapter 3



# Free-energy Patterns and The Relevance of Non-included Moieties

Inclusion complexes play a definite role in a variety of applications, ranging from drug solubilization to smart materials. This chapter presents a series of studies based on MD, including PMF calculations, and aiming at understanding the factors that govern inclusion. The procedure (described in Chapter 2) is designed for quantification of interaction and energy components guiding the complex formation, in water, between  $\beta$ -Cd and several naphthalene derivatives (NPR) containing hydrophobic and hydrophilic substituents, including charged groups. A series of umbrella sampling MD simulations is performed to calculate the free-energy profiles and derive the thermodynamic parameters and stability constants from a flexible model approach. The total enthalpy and entropy changes are inspected and individual components are further decomposed in order to get information on the relative weight of each component in the inclusion process.

The host and guest molecules are chosen as models of simple precursors or building blocks for designing more complex structures for pharmaceutical applications.  $\beta$ -Cd is used due to its appropriate size and stabilized circular structure. Naphthalene provides a rigid hydrophobic backbone, which allows to explore the individual effect of guest functionalization in the inclusion process.

It is observed that the substitution of naphthalene promotes an increase in the complexation constant (up to 100-fold), irrespective of the nature of the substituent, the latter comprising small hydrophobic and hydrophilic (including charged) groups. It is also seen that entropy does not favor inclusion, being the order of magnitude of the binding free energy given by the enthalpic component, with a

dominating guest-host interaction contribution. Desolvation penalizes the inclusion process, and is not observed in the vicinity of the hydrophilic and charged groups, which remain exposed to the solvent. The estimated thermodynamic quantities contribute to explain the effects of using imposed features (e.g. the nature and size of substituents of the guest molecules) in the conformation, solvation and complexation behavior of Cd-based systems, with direct transposition for the modulation of properties in supramolecular structures based on these complexes.

### 3.1 Context and relevant issues

Inclusion complexes have been suggested as building blocks for supramolecular structures such as polyrotaxanes[1, 2] and hydrogels.[3–5] This often implies that the guest molecule is modified, so as to produce a dimer for connecting host-grafted chains, complementary host and guest-grafted chains, and other alterations to the basic structure. It is therefore useful to predict the effect that an alteration in a guest molecule produces for a known inclusion complex. Naturally, the same happens if the host is altered, but this will be addressed in Chapters 4 and 5. Herein, a model molecule is used, naphthalene, and different substituents are attached to this molecule. Naphthalene is a small, symmetric and hydrophobic molecule and has been the subject of several experimental studies. The substituents include hydrophobic and hydrophilic moieties. For each case, the potential of mean force, association constant and thermodynamic parameters for inclusion are to be calculated. Also, guest positioning and hydration are inspected along the inclusion coordinate. Where possible, the results are contrasted with experimental observations.

### 3.2 Simulation details

This section presents some preliminary steps for optimizing the overall procedure in umbrella sampling, followed by a systematic analysis on PMF and thermodynamic aspects of inclusion. Focus will also be directed at solvation effects.

A pulling force constant of  $1000 \text{ kJ mol}^{-1} \text{ nm}^{-2}$  is used. This value was optimized in conjunction with

the pulling rate i.e., the velocity at which the restriction travels along the reaction coordinate. Results from pulling were used for establishing the initial configurations and estimating the force constants to be applied in each umbrella window (for details see Chapter 2).

### 3.2.1 General setup

The starting geometries of NPR molecules (2-methylnaphthalene, 2-NPCH<sub>3</sub>, 2-naphthol, 2-NPOH, 2,3-dinaphthol, 2,3-NP(OH)<sub>2</sub>, 2-naphthalenesulfonate, 2-NPSO<sub>3</sub><sup>-</sup> and 2-aminonaphthalene, 2-NPNH<sub>3</sub><sup>+</sup>) were constructed resorting to Pymol (Version 1.7.7.2) and optimized by the semi-empirical Antechamber/SQM method. The initial coordinates of the  $\beta$ -Cd were extracted from the RCSB protein data bank (PDB code: 1DMB) and partial charges were generated using the R.E.D.D. Server.[6] MD simulations were performed with the GROMACS package (version 4.6.5)[7, 8] using the all-atom amber99sb[9, 10] forcefield and the TIP3P water model. The selected forcefield has been validated for use in the GROMACS suite[11, 12] and was used to describe both  $\beta$ -Cd and NPR molecules. Periodic boundary conditions were used in combination with a NPT ensemble. A coupling constant of 0.5 ps was used to maintain the temperature at 300 K and a coupling constant of 1 ps was applied to keep the pressure at 1 bar. Prior to each production run an equilibration of 500 ps in which the pressure was maintained at 1 bar with the Berendsen barostat was performed. The box size was kept unchanged with no pressure coupling, during the production runs. A cutoff of 0.9 nm was used for calculating the Lennard-Jones interactions. Electrostatic interactions were evaluated using the particle mesh Ewald method.[13, 14] Constraints were applied for bond lengths of host and guest molecules with the LINCS algorithm.[15] Long-range electrostatic interactions were treated using the particle mesh Ewald (PME) method. Further details of the simulation procedure are presented in ref. [13]. Each system containing one  $\beta$ -Cd molecule and one NP derivative were solvated with approximately 13000 water molecules in a cubic box of 7.5×7.5×7.5 nm<sup>3</sup>. The host molecule was centered in the simulation box with the cavity axis of  $\beta$ -Cd parallel to the z-axis.

### 3.2.2 Reaction coordinate and biasing procedure

The distance between the COM of the NP backbone and that of the seven glycosidic oxygens of  $\beta$ -Cd along the  $z$ -axis was defined as the reaction coordinate  $\xi$  (Figure 3.1). The initial (i) and final (f) values of the reaction coordinate were set to  $\xi_i = 0.8$  nm and  $\xi_f = -1.6$  nm, respectively. After equilibration, a periodic pulling simulation was carried out allowing the distance to be larger than half the box size, to modulate a formation process of 1:1  $\beta$ -Cd:NPR complexes. The center of mass of the

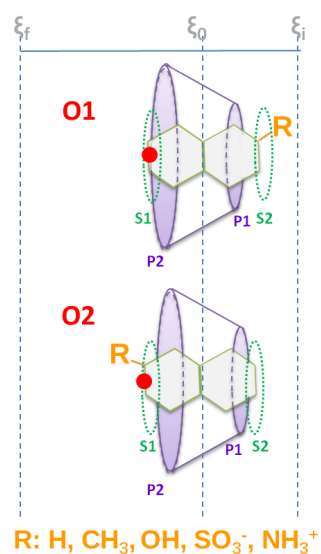


Figure 3.1: Schematic representation of two pathways along which naphthalene derivative is pulled. The pathways were named according to orientation (O1 and O2) and initial position (from portal P1 or portal P2). The red point indicate where the steering force is applied. Reproduced from ref. [16] with permission from the PCCP Owner Societies.

$\beta$ -Cd backbone was harmonically restrained with an isotropic force constant of  $1000 \text{ kJ}\cdot\text{mol}^{-1}\text{nm}^{-2}$  and used as an immobile reference for pulling simulations. The NP backbone was pulled through the  $\beta$ -Cd cavity from the primary or secondary portal (see the arrangements presented in Figure 3.1, respectively), along the  $z$ -axis over 360 ps with a harmonic force constant of  $1000 \text{ kJ mol}^{-1}\text{nm}^{-2}$  and a pulling rate of  $0.01 \text{ nm ps}^{-1}$ . The guest molecules were sampled approximately 2.4 nm covering the entire  $[\xi_i, \xi_f]$  interval. In this interval ca. 80 windows were selected, with an imposed distance of 0.03 nm between adjacent positions. and used as starting configuration for umbrella sampling simulations. A total of 12 PMF profiles were constructed based on six guest molecules with two different arrangements, following the same scheme.

### 3.2.3 Equilibrium and references

At equilibrium, NPR molecules are included in the  $\beta$ -Cd cavity. In order to obtain appropriate references for free-energy calculations and subsequent energy decomposition, 12 independent simulations were performed, corresponding to the equilibrium state of 1:1  $\beta$ -Cd:NPR complexes and the completely separate state between  $\beta$ -Cd and each NPR molecule. Equilibrium properties, structure and dynamics of the systems were calculated over the 5ns simulation runs after the systems were equilibrated for 500ps.

### 3.2.4 Thermodynamics of inclusion

The association constant,  $K_{bind}$ , is a key indicator to describe the binding affinity which can be determined both experimentally and computationally [13, 17–21]. In the latter, when NP guests inserts into the Cd cavity, the available volume for the guest can be constrained to a small cylinder, which should be able to sample most of the movements of NP guests in the cavity along x or y axes.  $K_{bind}$  can be estimated here by integrating the PMF values (depicted as  $\Delta G(\xi)$  according to Eq. (2.22). The standard thermodynamic indicators of binding,  $\Delta G^0$ ,  $\Delta H^0$  and  $T\Delta S^0$ , can be obtained from Equations 2.23, 2.24 and 2.25, defined in Chapter 2. The interval over which  $\beta$ -Cd and NP molecules associate and dissociate, limits the integration.

## 3.3 Results and discussion

### 3.3.1 PMF and preferred orientation

In what follows, the analysis of PMF profiles presented in Figure 3.2 will allow the comparison of the different systems under focus. Naphthalene will serve as a reference, while the substituted molecules will help to assess the different features that are imposed. It should be recalled that derivatives include hydrophobic and hydrophilic groups. Table 3.1 summarizes the characteristics of these profiles, and includes the minimum depth and position, and the width at half height. These values are presented



for two different orientations of the guest as represented in Figures 3.1 and 3.2. In O1 the group  $-R$  is oriented to the smaller portal P1 while in O2 the group points to the larger Cd portal, P2.

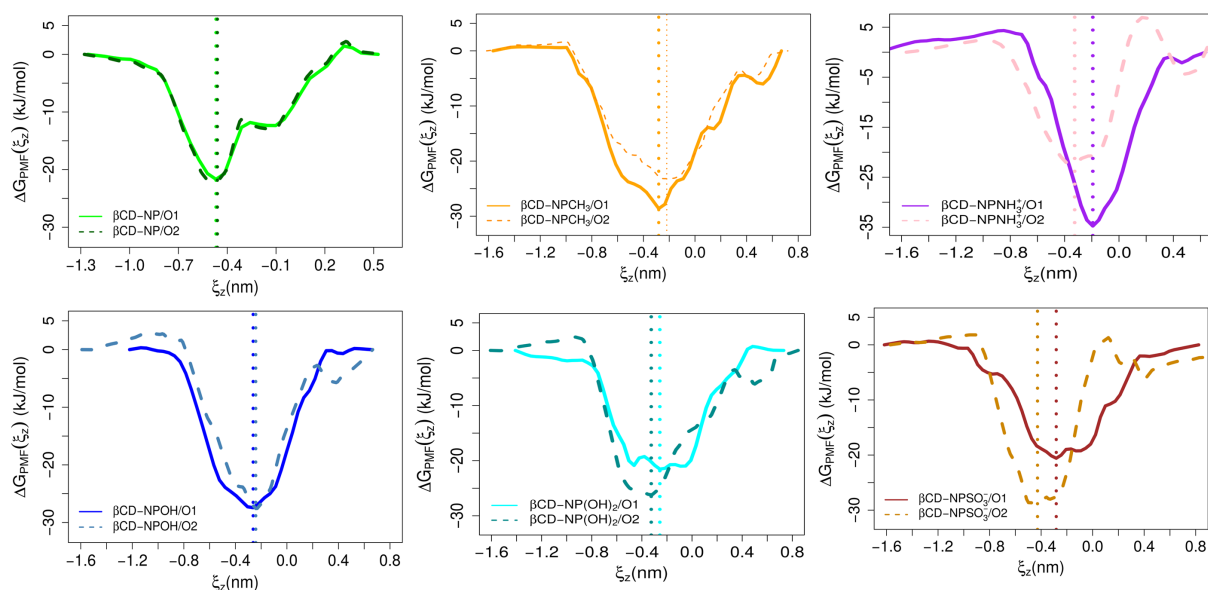


Figure 3.2: Free energy profiles for the inclusion of naphthalene derivatives in  $\beta$ -cyclodextrin along the model reaction coordinate  $\xi$ , in two orientations: solid lines, orientation 1, dashed lines, orientation 2. Reproduced from ref. [16] with permission from the PCCP Owner Societies.

Table 3.1: Summary of the main features assessed from the PMF profiles of the inclusion complexes between  $\beta$ -Cd and naphthalene derivatives, including the minimum depth and position, and width at half height. Reproduced from ref. [16] with permission from the PCCP Owner Societies.

Complex	$-\Delta G_{\text{PMF}}^{O1}$	$-\Delta G_{\text{PMF}}^{O2}$	$FWHM_{O1}$	$FWHM_{O2}$	$\xi_z^{O1}$	$\xi_z^{O2}$
$\beta$ -Cd:NP	23.1	23.1	0.630	0.630	-0.469	-0.461
$\beta$ -Cd:NP(OH) <sub>2</sub>	22.3	23.2	0.782	0.629	-0.257	-0.326
$\beta$ -Cd:NPCH <sub>3</sub>	29.4	25.9	0.856	0.845	-0.281	-0.219
$\beta$ -Cd:NPOH	27.8	25.2	0.698	0.609	-0.262	-0.242
$\beta$ -Cd:NPSO <sub>3</sub> <sup>-</sup>	21.2	29.9	0.763	0.576	-0.282	-0.428
$\beta$ -Cd:NPNH <sub>3</sub> <sup>+</sup>	34.8	22.5	0.480	0.594	-0.193	-0.326

The range of profile depths is 21-35 kJ mol<sup>-1</sup>, with the extreme values corresponding to the charged derivatives, 2-NPSO<sub>3</sub><sup>-</sup> and 2-NPNH<sub>3</sub><sup>+</sup>, both in orientation 1. It is clear that substituents affect the PMF profile, with some tendency to make it deeper relative to that of NP. In fact, there are three exceptions, 2-NPSO<sub>3</sub><sup>-</sup> in orientation 1, 2,3-NP(OH)<sub>2</sub> in orientation 1 and 2-NPNH<sub>3</sub><sup>+</sup> in orientation 2, in ascending order of well depth.

If, for each system, the orientation with the deeper PMF curve (see Figure 3.2 and Table 3.1) is selected, well depths arranged in increasing order are NP < 2,3-NP(OH)<sub>2</sub> < 2-NPOH < 2-NPCH<sub>3</sub>

$< 2\text{-NPSO}_3^- < 2\text{-NPNH}_3^+$ . These observations point to molecules with substitutions based on a charged group as those forming inclusion complexes with the strongest interaction, followed by the hydrophobically substituted ones. The complex with 2-NPOH promotes a deeper PMF than that formed with 2,3-NP(OH)<sub>2</sub>. In fact, and somewhat counterintuitively at first sight, the latter minimum is very close to that found for naphthalene. The most favorable orientation (based solely on the PMF) is, excluding 2-NPSO<sub>3</sub><sup>-</sup> and 2,3-NP(OH)<sub>2</sub>, O1 in which the group is closer to the primary portal (P1). Naturally, for NP the two orientations are equivalent. In what follows, discussion will be centered, in the most favorable orientation for each system.

### 3.3.2 Equilibrium positioning and degree of inclusion

Overall shape and width of the PMF curve are also affected by substitution. The naphthalene system displays a pronounced feature (formally a local minimum) at ca.  $\xi_z = -0.1$  nm, upon inclusion of a first ring, followed by a deeper minimum at  $\xi_z = -0.47$  nm. In the latter, configurations in which one ring is partially exposed to the solvent coexist with others in which both rings are included in the Cd. The former is normally associated to some rotation of the double ring inside the host and the molecule may, although seldom, attain an equatorial alignment[22, 23] (see Figure 3.3). This behavior may be quantified inspecting the alignment of host and guest molecules. This can be defined as the average angle ( $\alpha_{al}$ ) between two axes: one defined by the centers of mass of the two Cd portals and the other corresponding to the axis between the centers of mass of the C2-C3 and C7-C8 pairs of carbons in the NP backbone. In the complex with naphthalene, the alignment is given by  $\alpha_{al} = 38$  deg, which is compatible with a large amplitude motion within the host. In general, the minima in the PMF for the substituted molecules are located close to  $\xi_z = -0.3$  nm, which points to a degree of exposure of the double ring to the solvent lower than that found for naphthalene. In other words, *substitution induces the protection of the hydrophobic backbone of NP*.

Examining the PMF profiles for each complex in more detail, and considering the most prevailing (>50%) structures in the equilibrium state, Figure 3.4, it is seen that, in general, the hydrophobic backbone of the guest molecules is embedded within the Cd cavity, although displaying different inclusion depths and alignments related to the Cd axis. In the complex with 2,3-NP(OH)<sub>2</sub>, the double

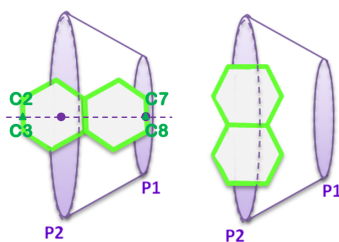


Figure 3.3: The two possible conformations of the complex between  $\beta$ -Cd and naphthalene: axial inclusion (left) and equatorial inclusion (right). Two additional axes defined by the centers of mass of the two Cd portals and corresponding to the centers of mass of the C2-C3 and C7-C8 pairs of carbons in the NP backbone are also included and used for inspecting the relative alignment between host and guest molecules. Reproduced from ref. [16] with permission from the PCCP Owner Societies.

ring is typically inside the cavity ( $\xi_z^{O2} = -0.33$  nm), and aligned with the Cd axis ( $\alpha_{al.} = 20.6$  deg). The complex with 2-NPOH displays a minimum located for similar values of the inclusion coordinate ( $\xi_z^{O1} = -0.26$  nm and  $\xi_z^{O2} = -0.24$  nm). The guest molecule displays a high degree of inclusion. For 2-NPCH<sub>3</sub>, the double ring is also found deep inside the  $\beta$ -Cd ( $\xi_z^{O1} = -0.28$  nm and  $\alpha_{al.} = 21$  deg). It should be noted that the results, in terms of degree of inclusion and angle, indicate that the hydroxyl group is located at the primary portal P1 while the methyl group is found outside this portal. In

Conformation [ $\beta$ -CD:NP]	NP	NPCH <sub>3</sub>	NPNH <sub>3</sub> <sup>+</sup>	NPOH	NP(OH) <sub>2</sub>	NPSO <sub>3</sub> <sup>-</sup>
Side1						
Side2						
Top1						
Top2						
Prevalence (%)	57.5	69.4	73.2	62.2	75.4	52.6

Figure 3.4: Typical conformations (accounting for more than 50% of the occurrences) for the inclusion complexes (1:1) of  $\beta$ -Cd and naphthalene derivatives in aqueous solution, sampled during the MD simulations (using the GROMACS package and the amber99sb forcefield) at 300 K, and identified by geometric cluster analysis.[24] The occurrence of each type of conformation is also included. Starting geometries optimized by the semi-empirical Antechamber/SQM method. Electrostatic charges obtained from AM1-BCC[25, 26] calculations. Reproduced from ref. [16] with permission from the PCCP Owner Societies.

turn, for 2-NPSO<sub>3</sub><sup>-</sup>, the tendency to expose the charged group (and also the carbon backbone) is especially marked in O2 ( $\xi_z^{O1} = -0.43$  nm and  $\alpha_{al.} = 24$  deg) in which sulfonate is placed outside of the secondary portal P2. Finally, for the complex including 2-NPNH<sub>3</sub><sup>+</sup>, a deeper and well-defined minimum at  $\xi_z = -0.19$  is observed in O1. In this conformation, the NP backbone is deeply included and aligned with the  $\beta$ -Cd axis upon complexation ( $\alpha_{al.} = 22$  deg) and the charged group is positioned outside of the primary portal P1.

A summary of the observations can now be done for each system, in terms of how they deviate from a central positioning of the double ring structure ( $\xi_z \approx -0.2$ ) inside the Cd cavity. The general tendency is to have the systems *displaced towards the larger portal*, which can be interpreted in terms of higher mobility and specific interaction effects. As such, a central positioning of the backbone means, in fact, that the included molecule is pushed into the cavity. The charged molecules expose their groups to the solvent, 2-NPNH<sub>3</sub><sup>+</sup> is in O1, while 2-NPSO<sub>3</sub><sup>-</sup> prefers O2. However, 2-NPCH<sub>3</sub> tends to avoid contact between the group and the solvent. As such, the structure is slightly deviated towards the secondary portal (in O1). Finally, 2-NPOH is deeply included into the cavity (O1), and 2,3-NP(OH)<sub>2</sub> slightly less (O2 from the PMF curve, or O1 in  $\Delta G_{bind}$ , see below).

### 3.3.3 Comparison to experiment

An excellent agreement between simulations and experiment is found for the structural features of the inclusion complexes between  $\beta$ -Cd and NP derivatives. In fact, the conformation found for the complex with 2-NPCH<sub>3</sub> is consonant with observations reported previously[27], in which some inclusion models were proposed based on the magnitude of the estimated association constants, indicating O1 as preferred.

The structural characteristics of inclusion complexes formed between native and modified  $\beta$ -Cd and hydroxyl substituted naphthalenes have also been characterized using NMR data.[28] Based on the results with native  $\beta$ -Cd, it is confirmed that the hydroxyl group of 2-NPOH is positioned at the primary portal P1 of the Cd molecule.

Experimental evidence[28, 29] have also suggested a structure with the hydroxyl groups of 2,3-NP(OH)<sub>2</sub> placed at the primary portal P1 of  $\beta$ -Cd. However, other plausible structures with modified

$\beta$ -Cd present a reversed orientation of 2,3-NP(OH)<sub>2</sub>[28]. It should be noted that the present results indicate that the energy difference between the two orientations, in terms of PMF minimum, is the lowest of those found within the naphthalene derivatives.

For 2-NPSO<sub>3</sub><sup>-</sup>, the structure of the complex is consistent with sulfonate being positioned close to the secondary portal of  $\beta$ -Cd, and displaying an axial alignment, as previously described.[30]. Experimental data pertaining to 2-NPNH<sub>3</sub><sup>+</sup> inclusion are not available, but a recent study[31] on the inclusion mechanism involving natural amino acids and cyclodextrins ( $\alpha$  and  $\beta$ -Cds) in aqueous solution, supports the feasibility of the structure found for 2-NPNH<sub>3</sub><sup>+</sup>, with the charged terminal group (NH<sub>3</sub><sup>+</sup>) of L-arginine in contact with the solvent from P1.

Considering the possible pathways for inclusion (from P1 or P2), it is seen that only the charged substituents promote significant barriers in the PMF upon entrance. This helps suggesting a more probable inclusion mode. For 2-NPSO<sub>3</sub><sup>-</sup>, similarly to what was observed for other systems[30], the insertion of the guest molecule considering the most favorable orientation, is expected from the wider rim of the Cd molecule (P2); this maximizes the degree of inclusion and contact of the hydrophobic backbone with the Cd cavity, a situation frequently supported by NMR data.[30] For 2-NPNH<sub>3</sub><sup>+</sup>, entrance is more probable through P1.

### 3.3.4 $\beta$ -Cd conformation

Another fundamental aspect to be understood is the conformational change of the  $\beta$ -Cd backbone upon complexation. For that purpose, the centers of mass of the carbon pairs at the glucose units of the Cd backbone were defined as reference points for evaluating distorted structures over the course of the simulation.

The overall conformation of  $\beta$ -Cd, free in solution or in the complex is summarized in Table 3.2. From this Table, a detailed analysis of the deformation of the  $\beta$ -Cd cavity is possible by inspecting the principal moments of inertia (MOI), denoted as  $I_1$ ,  $I_2$  and  $I_3$ [32, 33]. As expected, the values of the  $z$ -component ( $\langle I_3 \rangle$ ) averaged over the course of the simulation, are higher than  $x$ - and  $y$ - components ( $\langle I_1 \rangle$  and  $\langle I_2 \rangle$ ), respectively. The cavity of  $\beta$ -Cd is positioned symmetrically along this higher component, at the center of the doughnut-like shape, being three MOI ratios found for the different

systems of 1:1.2:2.1, 1:1.2:2.2 and 1:1.3:2.2 (see Table 3.2). In the absence of a guest molecule, the host cavity presents a similar deformation degree as that observed for the complexes with methyl and hydroxyl derivatives (1:1.2:2.1). For the complexes with NP, 2,3-NP(OH)<sub>2</sub>, 2-NPSO<sub>3</sub><sup>-</sup> and 2-NPNH<sub>3</sub><sup>+</sup>, the values slightly differ, with the less balanced ratio attributed to 2-NPNH<sub>3</sub><sup>+</sup>. The distortion of the Cd cavity has been previously pointed out, using other force-fields[34]. As described earlier[35], the cavity of β-Cd can be compressed and stretched due to specific guests and different binding modes. Inclusion complexes in equilibrium that display a larger deformation of the host cavity (close to elliptically distorted conformations) are characterized by a higher degree of inclusion and stronger host-guest interactions. In contrast, complexes with less distorted Cd structures (displaying at least two similar components) present less favorable interactions. The former situation occurs in complexes with 2-NPSO<sub>3</sub><sup>-</sup> and 2-NPNH<sub>3</sub><sup>+</sup>, which were identified previously, as the ones possessing deeper PMF wells. Deformation of the host cavity can be further characterized by inspecting the aspect ratio and the elongation values[32, 33], also included in Table 3.2. These properties provide

Table 3.2: Summary of the total and averaged moment of inertia,  $I_1$ ,  $I_2$  and  $I_3$ , and aspect ratio and elongation values for the β-cyclodextrin backbone, upon inclusion at the equilibrium state. Standard deviations of the estimated parameters are also provided. Reproduced from ref. [16] with permission from the PCCP Owner Societies.

Complex	$I_{tot}$	$\langle I_1 \rangle$	$\langle I_2 \rangle$	$\langle I_3 \rangle$	$I_1:I_2:I_3$	Aspect ratio	Elongation
β-Cd	105.8	24.7±1.52	29.1±1.14	52.0±2.10	1.0:1.2:2.1	0.83±0.05	1.09±0.05
β-Cd:NP/O1	107.9	25.2±1.22	29.5±1.09	53.3±1.44	1.0:1.2:2.2	0.82±0.05	1.08±0.04
β-Cd:NP(OH) <sub>2</sub> /O1	107.9	24.7±1.13	29.9±1.12	53.2±1.42	1.0:1.2:2.2	0.81±0.04	1.10±0.04
β-Cd:NPCH <sub>3</sub> /O1	108.0	25.0±1.16	29.6±1.07	53.4±1.36	1.0:1.2:2.1	0.82±0.04	1.09±0.04
β-Cd:NPOH/O1	107.7	24.8±1.19	29.8±1.10	53.2±1.43	1.0:1.2:2.1	0.81±0.04	1.10±0.04
β-Cd:NPSO <sub>3</sub> <sup>-</sup> /O2	107.7	24.5±1.35	29.9±1.10	53.2±1.36	1.0:1.2:2.2	0.81±0.05	1.11±0.05
β-Cd:NPNH <sub>3</sub> <sup>+</sup> /O1	107.7	24.2 ±1.26	30.3±1.20	53.2±1.38	1.0:1.3:2.2	0.80±0.07	1.12±0.05

the same type of information and can be determined based on the two closest principal moments,  $I_1$  and  $I_2$  from

$$aspect\ ratio = \frac{I_1}{I_2}, \quad (3.1)$$

and

$$elongation = \sqrt{\frac{I_2}{I_1}} \quad (3.2)$$

respectively.  $I_1$  is the moment of inertia along x- or y-components with the minimum value and  $I_2$  is the maximum value over the two moments of inertia. The *aspect ratio* defined as a function

of the second largest principal moment  $I_2$  and the smallest orthogonal component  $I_1$ , varies from 0.80 to 0.83, indicating a significant deviation from a perfect doughnut-like shape and suggesting elongated structures. From the *elongation* values it can be observed that the charged derivatives promote a higher deformation of the host cavity. This is consistent with the averaged moments of inertia analyzed in each system and the dominant conformations for the inclusion complexes identified by geometric cluster analysis (see Figure 3.4).

### 3.3.5 Thermodynamics

Expression (2.22) is used for the calculation of the association constants for the inclusion complexes and combines the host/guest interaction as measured from the PMF. The latter weights each value of the inclusion coordinate and also the complex volume, established on the basis of the center of mass positioning related to each guest molecule inside the cavity.

In Table 3.3, the estimated standard free energies of binding considering (i) the most favorable orientation of the guest and (ii) the center of mass and two additional reference points of the guest molecule, S1 and S2 (see Figure 3.1), and (iii) the respective association constants, for the inclusion complexes between  $\beta$ -Cd and naphthalene derivatives, are summarized.

Standard deviations of the estimated association constants are also provided. It is worth mentioning that the trend followed by the PMF is generally the same in terms of free-energy,  $\Delta G_{bind}$ . For the most favorable orientation,  $\Delta G_{bind}$  follows the order NP < 2,3-NP(OH)<sub>2</sub> < 2-NPCH<sub>3</sub> < 2-NPOH < 2-NPSO<sub>3</sub><sup>-</sup> < 2-NPNH<sub>3</sub><sup>+</sup>, indicating the most stable complexes as those more hydrophilic, especially if charged. The exception is 2,3-NP(OH)<sub>2</sub>, only slightly more stable than NP. For this complex, the preferred orientation as estimated by the PMF is reversed on the basis of free-energy. It is the only instance in which this happens, and corresponds to a minute difference between the two orientations, both in terms of PMF and free-energy. This behavior will be discussed below.

Table 3.3: Binding free energies ( $\text{kJ mol}^{-1}$ ) and association constants characterizing the complexation of NP derivatives by  $\beta$ -Cd in aqueous solution.

Complex*	$-\Delta G_{bind}^{COM}$	$-\Delta G_{bind}^{S1}$	$-\Delta G_{bind}^{S2}$	$K_{bind}^{COM}$	$K_{bind}^{S1}$	$K_{bind}^{S2}$	$-\Delta G_{bind}^{exp}$	$K_{bind}^{exp}$
$\beta$ Cd-NP/O1	12.0	13.0	15.9	$128 \pm 33$	$191 \pm 27$	$605 \pm 99$	15.8[36]	186
								$377 \pm 35$ [37]
								608[36]
								$630 \pm 40$ [27]
$\beta$ -Cd:NP(OH) <sub>2</sub> /O1	13.1	15.1	16.3	$194 \pm 34$	$435 \pm 56$	$703 \pm 102$	13.0[28]	$188 \pm 9$ [28]
	(-0.9)	(0.8)	(-1.1)					
$\beta$ -Cd:NPCH <sub>3</sub> /O1	16.5	19.6	21.0	$787 \pm 202$	$2726 \pm 430$	$4842 \pm 826$	–	$700 \pm 100$ [27]
	(-3.2)	(-3.4)	(-5.0)					
$\beta$ -Cd:NPOH/O1	17.0	21.7	19.7	$950 \pm 236$	$6310 \pm 1078$	$2852 \pm 437$	–	699[29]
	(-6.1)	(-5.9)	(-2.6)				14.2[28]	$311 \pm 11$ [28]
$\beta$ -Cd:NPSO <sub>3</sub> <sup>-</sup> /O2	17.7	21.8	22.6	$1276 \pm 304$	$6684 \pm 1358$	$9234 \pm 2013$	14.7[30]	$381 \pm 25$ [30]
	(-4.8)	(-8.0)	(-8.5)				30.7[38]	$2.34 \times 10^5$ [38]
								$480 \pm 20$ [39]
								$220 \pm 30$ [39]
$\beta$ -Cd:NPNH <sub>3</sub> <sup>+</sup> /O1	24.7	24.4	27.5	$2.1 \times 10^4 \pm 5.5 \times 10^3$	$1.9 \times 10^4 \pm 4.5 \times 10^3$	$6.7 \times 10^4 \pm 1.7 \times 10^4$	–	$10^3 - 10^4$ [31]
	(-13.2)	(-7.6)	(-13.4)					$428 \pm 22$ [30]



\*  $K_{bind}$  and  $\Delta G_{bind}$  are the calculated association constant and the binding free-energy, respectively.  $K_{bind}^{exp}$  and  $\Delta G_{bind}^{exp}$  denote the experimental results taken for naphthalene and 2-methylnaphthalene[27], 2-naphthol and 2,3-dinaphthol[28, 40, 41], 2-naphthalenesulfonate[30, 38], 2-aminonaphthalene[31]. Reproduced from ref. [16] with permission from the PCCP Owner Societies.

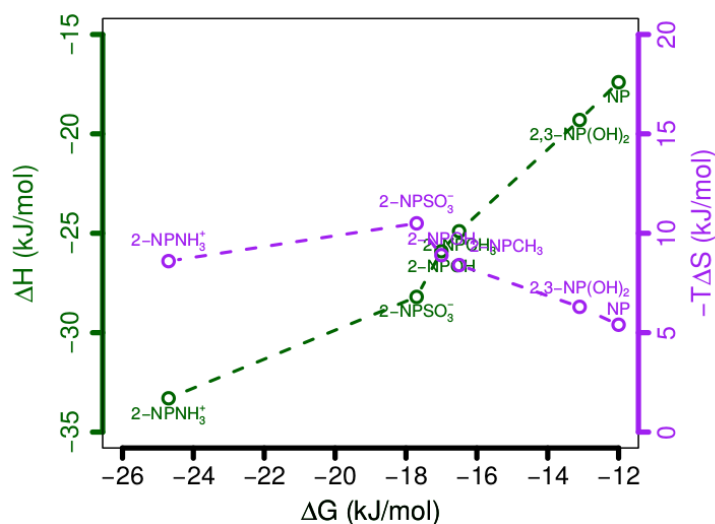


Figure 3.5: Free energy ( $\Delta G$ ), enthalpy ( $\Delta H$ ) and entropy ( $T\Delta S$ ) contributions for the complex formation of  $\beta$ -Cd with NP derivatives for the most favorable orientations (2,3-NP(OH)<sub>2</sub>, 2-NPCH<sub>3</sub>, 2-NPOH and 2-NPNH<sub>3</sub><sup>+</sup>, O1; 2-NPSO<sub>3</sub><sup>-</sup>, O2). Reproduced from ref. [16] with permission from the PCCP Owner Societies.

The stability of these complexes can be attributed to the enthalpic contribution, with entropy consistently decreasing upon complex formation (Table 3.4 and Figure 3.5). From Table 3.4 and Figure 3.5, the inclusion complex that is more strongly favored in enthalpic terms is 2-NPNH<sub>3</sub><sup>+</sup>, followed by 2-NPSO<sub>3</sub><sup>-</sup> and 2-NPOH. This contribution is smaller in the remaining systems, especially for NP and 2,3-NP(OH)<sub>2</sub>. In all cases there is an entropic penalty to inclusion. This increases in increasing order of stability, reaching a maximum with the sulfonate derivative, but it decreases with the amine to a value similar to that found in the methyl substituted naphthalene.

Table 3.4: Enthalpy and entropy changes ( $\text{kJ mol}^{-1}$ ), for inclusion complex formation of  $\beta$ -Cd and naphthalene derivatives at 300 K.

Complex*	$-\Delta H_{bind}^{COM}$	$-\Delta H_{bind}^{S1}$	$-\Delta H_{bind}^{S2}$	$-T\Delta S_{bind}^{COM}$	$-T\Delta S_{bind}^{S1}$	$-T\Delta S_{bind}^{S2}$	$-\Delta H^{exp}$ ( $\text{kJ mol}^{-1}$ )	$-\Delta S^{exp}$ ( $\text{J mol}^{-1}\text{K}^{-1}$ )
$\beta$ -Cd:NP/O1	17.4	18.2	19.9	5.4	5.2	4.0	$18\pm 2$ [36]	$9\pm 5$ [36]
$\beta$ -Cd:NP(OH) <sub>2</sub> /O1	19.3	19.9	19.9	6.3	4.8	3.7	—	—
$\beta$ -Cd:NPCH <sub>3</sub> /O1	24.9	24.7	25.6	8.4	5.1	4.6	—	—
$\beta$ -Cd:NPOH/O1	25.9	25.8	25.4	8.9	4.1	5.7	24.3	$38\pm 3$
							$26.8\pm 9$	$11.3\pm 0.9$
$\beta$ -Cd:NPSO <sub>3</sub> <sup>-</sup> /O2	28.2	28.4	27.9	10.5	6.5	5.3	$26.4\pm 1.4$ [30]	$39.1\pm 3.8$ [30]
							$29.3$ [38]	$11.7\pm 1.1$
$\beta$ -Cd:NPNH <sub>3</sub> <sup>+</sup> /O1	33.3	32.7	33.4	8.6	8.3	5.8	—	—

\*  $\Delta H_{bind}$  and  $T\Delta S_{bind}$  are the calculated enthalpy and entropy changes, respectively.  $\Delta H^{exp}$  and  $\Delta S^{exp}$  denote the experimental results taken from refs.[30, 36, 38].

Reproduced from ref. [16] with permission from the PCCP Owner Societies.

In order to evaluate if the displacement of the guest inside the cavity is adequately measured through the positioning of the center of mass, so as to estimate the volume of inclusion on the basis of  $r(\xi)$ , two additional reference points (S1 and S2) were considered. This reflects the two extremes of the molecule, S1 and S2, as depicted in Figure 3.1. Note that in previous work by other authors several estimates have been made, including fixed values.[13, 42, 43] It is seen that the estimate based on the center of mass is the best for establishing the free-energy difference (or the association constant) within the cylindrical approximation. In fact, the use of points closer to the extreme of the molecule tends, generally, to overestimate stability in relation to the experimental results (Table 3.4). A possible explanation is that the points S1 and S2 are associated to incomplete rotations inside the cavity, while the center of mass more accurately represents the motion of the molecule.

### 3.3.6 Interaction components

Simulations in which host and guest are apart, and simulations in the equilibrium situation, for which the complex is formed, allow a simple analysis of the change in the energy components upon inclusion. Results are summarized in Table 3.5.

Irrespective of the characteristics of the host, a common trend is visible: desolvation penalizes the host(guest)-solvent interaction, as indicated by their positive change, and favors solvent-solvent interaction. However, the latter is not sufficient to compensate the former and the entropy component also reflects a penalty upon inclusion. In fact, complex formation seems to be essentially a result of an increased host-guest interaction, that implies a substantial decrease in the energy (ranging from -88 to  $-213\text{kJ mol}^{-1}$ ). Also, it is apparent that the Cd conformation adopts a more favorable set-up upon inclusion. This is probably related to collapsed situations, and makes a reference system difficult to select for the separated system. The energy components in Table 5 also indicate that the solvent-solvent (negative) and solvation terms (positive) are significantly higher for the charged systems, and do not substantially differ among the hydrophobic and more hydrophilic systems.

Table 3.5: Individual interaction component change ( $\text{kJ mol}^{-1}$ ) for the inclusion process of naphthalene derivatives in  $\beta$ -Cd, considering the most favorable orientation. Reproduced from ref. [16] with permission from the PCCP Owner Societies.

Complex	$\Delta H_{\text{host}}$	$\Delta H_{\text{guest}}$	$\Delta H_{\text{host-host}}$	$\Delta H_{\text{guest-guest}}$	$\Delta H_{\text{sol-sol}}$	$\Delta H_{\text{host-guest}}$	$\Delta H_{\text{host-sol}}$	$\Delta H_{\text{guest-sol}}$
$\beta$ -Cd:NP/O1	-9.4	0.2	-22.9	0.0	-74.7	-88.1	108.2	48.7
$\beta$ -Cd:NP(OH) <sub>2</sub> /O1	-6.0	0.4	-19.9	1.8	-71.8	-100.0	104.3	58.9
$\beta$ -Cd:NPCH <sub>3</sub> /O1	-9.9	-0.3	-16.0	-0.1	-56.4	-95.4	104.3	54.6
$\beta$ -Cd:NPOH/O1	-5.8	0.0	-20.7	0.1	-75.4	-93.6	106.0	56.3
$\beta$ -Cd:NPSO <sub>3</sub> <sup>-</sup> /O2	-5.1	0.6	-7.9	-7.1	-151.6	-212.8	170.2	180.7
$\beta$ -Cd:NPNH <sub>3</sub> <sup>+</sup> /O1	-7.9	0.5	-28.2	-8.6	-125.1	-134.6	156.9	112.5

### 3.3.7 Inclusion and solvation

The inclusion of the NP derivatives into the Cd cavity promotes the release of water molecules from the cavity. This process is governed by the relative size of the Cd cavity and guests and, for the systems under analysis, complete removal of 4 water molecules is done upon inclusion. This is visible in Figure 3.6, close to  $r = 0.35$  nm, which approximately covers the whole interior of the Cd, and represents the running coordination number, which measures the number of water molecules at a distance  $r$  from a group or point. In this case,  $r=0$ , represents the center of mass of the Cd. In Figure 3.7

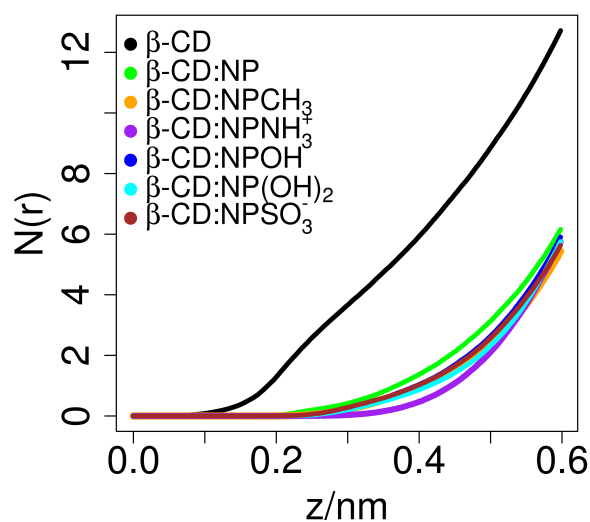


Figure 3.6: Coordination number for water molecules from the center of the  $\beta$ -Cd cavity in aqueous solution and in the corresponding binary systems. Reproduced from ref. [16] with permission from the PCCP Owner Societies.

the running coordination numbers for naphthalene and derivatives, before and after inclusion, are presented for both studied orientations. The amount of solvent decreases upon complexation, and

this decrease is visible in the immediate vicinity of the group. In the other, the amount of solvent does not suffer a significant alteration in the immediate vicinity. A further distinction can be made in terms of the complexes in which a difference in orientation promotes a difference in hydration. For the hydrophobic guests, NP and 2-NPCH<sub>3</sub>, complexation promotes a drastic desolvation. For 2,3-

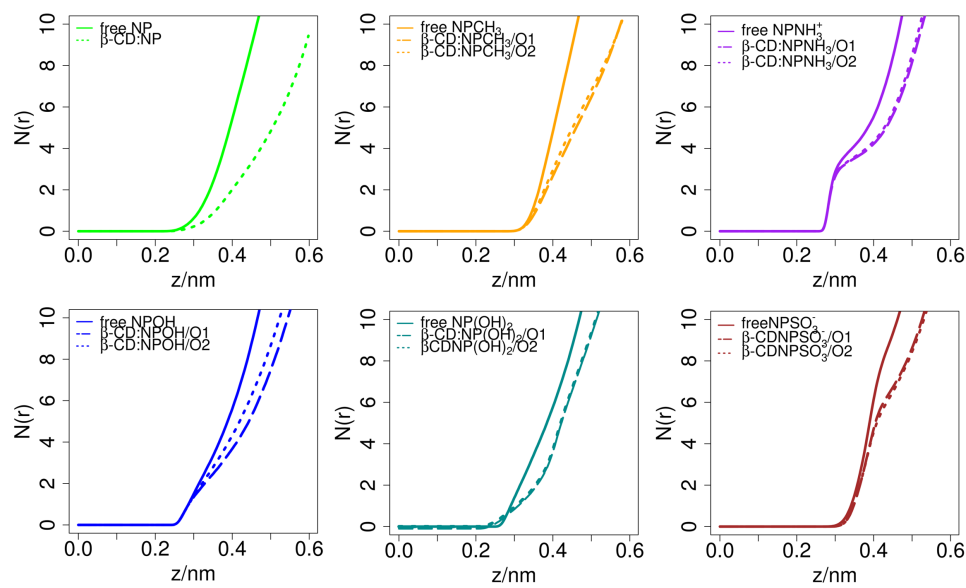


Figure 3.7: Running coordination number of water molecules per substituent group as a function of distance. Reproduced from ref. [16] with permission from the PCCP Owner Societies.

NP(OH)<sub>2</sub>, inclusion also promotes desolvation, but to a lesser extent. In the remaining systems, the inclusion process naturally affects the solvation of the substituents, but at longer distance from the group. For this, solvation is slightly higher when the group is closer to the larger portal.

### 3.3.8 A closer look at the hydroxyl derivatives

The complexes with hydroxyl substituted NPs, 2-NPOH and 2,3-NP(OH)<sub>2</sub> display significant differences in stability, being the monosubstituted naphthalene clearly more stable. Also, the disubstituted hydroxyl derivative displays a behavior very close to naphthalene, in terms of stability, PMF well depth, inclusion degree and thermodynamical quantities.

The higher stability of the complex with 2-NPOH over that with 2,3-NP(OH)<sub>2</sub> is, at least partially, associated to solvation effects. It is clear in Figure 3.7 that the amount of water molecules around the hydroxyl groups in 2,3-NP(OH)<sub>2</sub> decreases upon complexation, and this decrease is visible in

the immediate vicinity of each hydroxyl group. In 2-NPOH, no significant change for the solvated hydroxyl group is observed in the immediate vicinity. These observations imply effects of release of water molecules from the group, in addition to those that are expelled from the cavity, and are compatible with the fact that the entropic penalty is lower for 2,3-NP(OH)<sub>2</sub>; however the enthalpy contribution is also less negative. This is also compatible with the angle the guest axis makes with the Cd axis, which is clearly higher for 2-NPOH than for 2,3-NP(OH)<sub>2</sub>. This observation may be ascribed to the asymmetry of the 2-NPOH molecule, and a tendency to further expose the group to the solvent.

The  $\Delta G_{bind}^{COM}$  values for 2,3-NP(OH)<sub>2</sub> display a difference of less than 1 kJ mol<sup>-1</sup>, which suggests that the positioning of the groups relative to the two portals is irrelevant, although some differences are clearly visible in the PMF profiles. Three dominant conformations for the free and bonded states of 2,3-NP(OH)<sub>2</sub> at 300 K, in aqueous solution, were identified by geometrical cluster analysis and include both inward and outward arrangements of the hydrogen atoms, and a conformation in which one hydroxylic hydrogen is pointing toward the neighboring hydroxyl group (see Figure 3.8) forming an intramolecular hydrogen bond. For simplicity, this arrangement will be denoted as intermediate. It should be noted that the inward and outward arrangements result from the interaction between both hydroxyl groups with the solvent molecules, upon complexation.

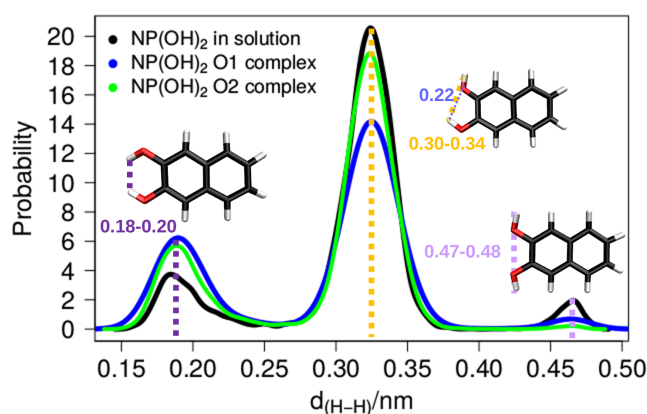


Figure 3.8: Distribution of distances between hydrogen atoms of adjacent hydroxyl groups in 2,3-NP(OH)<sub>2</sub>. Dominant conformations (accounting for more than 95% of the occurrences) of 2,3-NP(OH)<sub>2</sub> in solution or included in the  $\beta$ -Cd cavity for both orientations, are depicted in the inset. These conformations were sampled during the MD simulations in the equilibrium state, at 300 K, and identified by geometric cluster analysis.[24] Reproduced from ref. [16] with permission from the PCCP Owner Societies.

Inspection of Figure 3.8 shows that the outward arrangement is present for the molecule free in solution, but is nearly completely absent upon inclusion. Also, the prevalence of the intermediate conformation is higher for the free molecule, and slightly decreases upon complexation, being replaced by the inward pointing arrangement. In this arrangement, a water molecule is shared by the two hydroxyl groups.

The effects of substitution of hydrogens at the adjacent carbons by hydroxyl groups (e.g. in hydroxyl-substituted derivatives of naphthol and anthrol systems[44]) and subsequent formation of intramolecular hydrogen bonds have been discussed in the literature in terms of free-energy and enthalpy changes.[44–46] Solvation energies are dependent on the relative orientation of the two hydroxyl groups and the strength of this hydrogen bond, i.e., the intramolecular hydrogen bond enthalpy,[44, 47, 48]. Also, intramolecular hydrogen bonds have been identified using computational calculations[44] and part of the intramolecular hydrogen bond enthalpy results from the minimization of repulsion of the oxygen lone pairs at hydroxyl groups, when the -OH group adopts an inward orientation. Water bridges have also been recognized as players in connecting adjacent hydroxyl groups.[49] Note the excellent agreement found for the association constant between the present calculations and experiment, for both 2-NPOH and 2,3-NP(OH)<sub>2</sub>, which also validates the differences between the two systems identified in the MD results.

### 3.4 Overview

This work has shown that, for a variety of naphthalene derivatives (which offer an hydrophobic part with roughly the length of the  $\beta$ -Cd cavity), the association constant tends to increase with substitution. This increase may be attributed to a deeper inclusion of the hydrophobic moiety in the cavity, relative to the unsubstituted compound (as seen for 2,3-NP(OH)<sub>2</sub>, 2-NPCH<sub>3</sub>, 2-NPOH, or more drastically 2-NPNH<sub>3</sub><sup>+</sup>), but 2-NPSO<sub>3</sub><sup>-</sup> is not deeply included and yet displays one of the largest association constants. The charged groups promote the higher association constants, with orientations that vary with the group. In general, the more hydrophilic are the groups, the higher is the association constant. This can be due to the synergistic effect of encapsulating the hydrophobic core of the guest into the



Cd, while at the same time keeping the hydrophilic groups in contact with the solvent.

The substituent affects the positioning of the hydrophobic part, but does not suffer desolvation, except for 2-NPCH<sub>3</sub>, in which desolvation of the hydrophobic group is observed. This is particularly clear in the charged compounds: the overall tendency is to displace the included molecule out of P2 (orientation O2, 2-NPSO<sub>3</sub><sup>-</sup>), or into P1 (orientation O1, 2-NPNH<sub>3</sub><sup>+</sup>), thus favoring exposition of the group to the solvent. In the case of 2-NPOH, this exposition results also from the angle in which the molecule is included, relative to the  $\beta$ -Cd axis. 2,3-NP(OH)<sub>2</sub> displays an example in which guest conformation is affected by inclusion, resulting in an overall behavior closer to that found in naphthalene than that of any other of the compounds.

For this set of systems, the cylindrical approximation used in the calculation of association constants and thermodynamic quantities provided excellent agreement with the experimental determinations, showing that the entropic component acts as a penalty for inclusion, which is lower when groups suffer desolvation (systems NP, 2,3-NP(OH)<sub>2</sub>). However, this pattern is not clear, and 2-NPCH<sub>3</sub> has an entropic penalty close to that found for 2-NPNH<sub>3</sub><sup>+</sup> and 2-NPOH, indicating a more complex behavior. The most favorable free-energy differences correspond to the most favorable enthalpic components, with the entropic term playing a lesser role in the energetic discrimination of the systems.

### 3.5 Concluding remarks

The use of naphthalene derivatives clearly affects the inclusion parameters allowing at least to double the free-energy difference relative to the inclusion of the unsubstituted molecule, or increase the association constant more than 100-fold. In this study, the association constant is increased irrespective of the nature of the substituent group (hydrophobic, hydrophilic and positively or negatively charged), with a tendency to have larger constants for more hydrophilic modifications. Drastic desolvation of the substituent group is not observed, except for the hydrophobic compound (2-NPCH<sub>3</sub>) and (2,3-NP(OH)<sub>2</sub>). The positioning of the hydrophobic backbone inside the cavity is clearly affected by the presence of the substituent which, in general, tends to emphasize inclusion. Entropy opposes inclusion, but constitutes a smaller term compared to the favorable enthalpic component.

The molecules studied in this work have a common included backbone (the two naphthalene rings). However, for a proper estimation of the association constants, substituents effects must be taken into account even if these substitutions do not appear to geometrically affect inclusion. This may also be relevant in supramolecular systems, in which a common guest group/moiety may coexist with different spacers or polymers (as in the case of systems containing zip gels). It is also seen that accurate predictions are available from MD, although further situations must be systematically assessed: presence of substitutes in the Cd, and varying cavity volume. The latter may constitute a significant difficulty in the context of the use of the cylindrical approximation, within the more general "flexible molecule" approximation, for estimating the complex volume.

Several driving forces have been reported to play an important role in the interaction between cyclodextrin and a guest molecule. In this work, the host-guest interactions have been recognized as the major driving force for the inclusion complexation of  $\beta$ -Cd with  $\beta$  substituted NP derivatives, which is accompanied by negative changes in enthalpy and a relatively small entropic penalty.

## References

- [1] Scott Loethen, JongMok Kim, and David H. Thompson. "Biomedical Applications of Cyclodextrin Based Polyrotaxanes". *Polymer Reviews* 47.3 (2007), pp. 383–418. ISSN: 1558-3724. DOI: [10.1080/15583720701455145](https://doi.org/10.1080/15583720701455145).
- [2] Benguo Liu et al. "Physiochemical Properties of the Inclusion Complex of Puerarin and Glucosyl- $\beta$ -Cyclodextrin". *Journal of Agricultural and Food Chemistry* 60.51 (2012), pp. 12501–12507. DOI: [10.1021/jf304447x](https://doi.org/10.1021/jf304447x).
- [3] Lingzhi Zhang, Jinping Zhou, and Lina Zhang. "Structure and properties of  $\beta$ -cyclodextrin/cellulose hydrogels prepared in NaOH/urea aqueous solution". *Carbohydrate Polymers* 94.1 (2013), pp. 386–393. ISSN: 0144-8617. DOI: <https://doi.org/10.1016/j.carbpol.2012.12.077>.
- [4] Jianxiang Zhang and Peter X. Ma. "Cyclodextrin-based supramolecular systems for drug delivery: Recent progress and future perspective". *Advanced Drug Delivery Reviews* 65.9 (2013), pp. 1215–1233. ISSN: 0169-409X.

- [5] Esmat Jalalvandi et al. “Cyclodextrin-polyhydrazine degradable gels for hydrophobic drug delivery”. *Materials Science & Engineering C-Materials for Biological Applications* 69 (2016), pp. 144–153. ISSN: 0928-4931.
- [6] Enguerran Vanquelef et al. “R.E.D. Server: a web service for deriving RESP and ESP charges and building force field libraries for new molecules and molecular fragments”. *Nucleic Acids Research* 39.2 (2011), W511–W517. DOI: [10.1093/nar/gkr288](https://doi.org/10.1093/nar/gkr288).
- [7] Berk Hess et al. “GROMACS 4: Algorithms for highly efficient, load-balanced, and scalable molecular simulation”. *Journal of Chemical Theory and Computation* 4.3 (2008), pp. 435–447. ISSN: 1549-9618.
- [8] David van der Spoel, Paul J. van Maaren, and Carl Caleman. “GROMACS molecule and liquid database”. *Bioinformatics* 28.5 (2012), pp. 752–753. DOI: [10.1093/bioinformatics/bts020](https://doi.org/10.1093/bioinformatics/bts020).
- [9] Kresten Lindorff-Larsen et al. “Improved side-chain torsion potentials for the Amber ff99SB protein force field”. *Proteins: Structure, Function, and Bioinformatics* 78.8 (2010), pp. 1950–1958. DOI: [10.1002/prot.22711](https://doi.org/10.1002/prot.22711).
- [10] Christine Cézard et al. “Molecular dynamics studies of native and substituted cyclodextrins in different media: 1. Charge derivation and force field performances”. *Physical Chemistry Chemical Physics* 13.33 (2011), pp. 15103–15121. DOI: [10.1039/C1CP20854C](https://doi.org/10.1039/C1CP20854C).
- [11] Viktor Hornak et al. “Comparison of multiple amber force fields and development of improved protein backbone parameters”. *Proteins-Structure Function and Bioinformatics* 65.3 (2006), pp. 712–725. ISSN: 0887-3585.
- [12] Trang Truc Nguyen, Man Hoang Viet, and Mai Suan Li. “Effects of Water Models on Binding Affinity: Evidence from All-Atom Simulation of Binding of Tamiflu to A/H5N1 Neuraminidase”. *The Scientific World Journal* 2014 (2014), pp. 1–14. ISSN: 1537-744X. DOI: [10.1155/2014/536084](https://doi.org/10.1155/2014/536084).
- [13] Haiyang Zhang et al. “Quantification of Solvent Contribution to the Stability of Noncovalent Complexes”. *Journal of Chemical Theory and Computation* 9.10 (2013), pp. 4542–4551. ISSN: 1549-9618. DOI: [10.1021/ct400404q](https://doi.org/10.1021/ct400404q).

- [14] Jirasak Wong-ekkabut and Mikko Karttunen. “The good, the bad and the user in soft matter simulations”. *Biochim. Biophys. Acta* 1858.10 (2016), pp. 2529–2538. DOI: [10.1016/j.bbamem.2016.02.004](https://doi.org/10.1016/j.bbamem.2016.02.004).
- [15] B. Hess et al. “LINCS: A linear constraint solver for molecular simulations”. *Journal of Computational Chemistry* 18.12 (1997), pp. 1463–1472. ISSN: 0192-8651.
- [16] Tânia F. G. G. Cova, Sandra C. C. Nunes, and Alberto A. C. C. Pais. “Free-energy patterns in inclusion complexes: the relevance of non-included moieties in the stability constants”. *Physical Chemistry Chemical Physics* 19.7 (2017), pp. 5209–5221. ISSN: 1463-9076. DOI: [10.1039/C6CP08081B](https://doi.org/10.1039/C6CP08081B).
- [17] G. Filippini, C. Bonal, and P. Malfreyt. “How does the dehydration change the host-guest association under homogeneous and heterogeneous conditions?” *Physical Chemistry Chemical Physics* 16.18 (2014), pp. 8667–8674. ISSN: 1463-9076. DOI: [10.1039/C4CP00108G](https://doi.org/10.1039/C4CP00108G).
- [18] Parisa Ahmadi and Jahan B. Ghasemi. “3D-QSAR and docking studies of the stability constants of different guest molecules with beta-cyclodextrin”. *Journal of Inclusion Phenomena and Macrocyclic Chemistry* 79.3-4 (2014), pp. 401–413. ISSN: 1388-3127.
- [19] Y. Izadmanesh and Jahan B. Ghasemi. “Thermodynamic study of beta-cyclodextrin-dye inclusion complexes using gradient flow injection technique and molecular modeling”. *Spectrochimica Acta Part a-Molecular and Biomolecular Spectroscopy* 165 (2016), pp. 54–60. ISSN: 1386-1425.
- [20] F. Mirrahimi, M. Salahinejad, and Jahan B. Ghasemi. “QSPR approaches to elucidate the stability constants between beta-cyclodextrin and some organic compounds: Docking based 3D conformer”. *Journal of Molecular Liquids* 219 (2016), pp. 1036–1043. ISSN: 0167-7322.
- [21] Sunil S. Jambhekar and Philip Breen. “Cyclodextrins in pharmaceutical formulations I: structure and physicochemical properties, formation of complexes, and types of complex”. *Drug Discovery Today* 21.2 (2016), pp. 356–362. ISSN: 1359-6446. DOI: <https://doi.org/10.1016/j.drudis.2015.11.017>.

- [22] K. Harata and H. Uedaira. "Circular-Dichroism Spectra of Beta-Cyclodextrin Complex with Naphthalene Derivatives". *Bulletin of the Chemical Society of Japan* 48.2 (1975), pp. 375–378. ISSN: 0009-2673.
- [23] G. C. Catena and F. V. Bright. "Thermodynamic Study on the Effects of Beta-Cyclodextrin Inclusion with Anilino-naphthalenesulfonates". *Analytical Chemistry* 61.8 (1989), pp. 905–909. ISSN: 0003-2700.
- [24] X. Daura et al. "Peptide folding: When simulation meets experiment". *Angewandte Chemie-International Edition* 38.1-2 (1999), pp. 236–240. ISSN: 1433-7851.
- [25] A. Jakalian et al. "Fast, efficient generation of high-quality atomic Charges. AM1-BCC model: I. Method". *Journal of Computational Chemistry* 21.2 (2000), pp. 132–146. ISSN: 0192-8651. DOI: [10.1002/\(Sici\)1096-987x\(20000130\)21:2<132::Aid-Jcc5>3.3.Co;2-G](https://doi.org/10.1002/(Sici)1096-987x(20000130)21:2<132::Aid-Jcc5>3.3.Co;2-G).
- [26] A. Jakalian, D. B. Jack, and C. I. Bayly. "Fast, efficient generation of high-quality atomic charges. AM1-BCC model: II. Parameterization and validation". *Journal of Computational Chemistry* 23.16 (2002), pp. 1623–1641. ISSN: 0192-8651.
- [27] M. Fujiki, T. Deguchi, and I. Sanemasa. "Association of Naphthalene and Its Methyl-Derivatives with Cyclodextrins in Aqueous-Medium". *Bulletin of the Chemical Society of Japan* 61.4 (1988), pp. 1163–1167. ISSN: 0009-2673.
- [28] Yoshimi Sueishi, Naoya Inazumi, and Tadashi Hanaya. "NMR spectroscopic characterization of inclusion complexes of hydroxy-substituted naphthalenes with native and modified beta-cyclodextrins". *Journal of Inclusion Phenomena and Macrocyclic Chemistry* 64.1-2 (2009), pp. 135–141. ISSN: 1388-3127.
- [29] J. vanStam et al. "2-naphthol complexation by beta-cyclodextrin: Influence of added short linear alcohols". *Journal of Physical Chemistry* 100.51 (1996), pp. 19959–19966. ISSN: 0022-3654.
- [30] J. Nishijo and Y. Ushiroda. "Interaction of 2-naphthalenesulfonate with beta-cyclodextrin: Studies with calorimetry and proton nuclear magnetic resonance spectroscopy". *Chemical & Pharmaceutical Bulletin* 46.11 (1998), pp. 1790–1796. ISSN: 0009-2363.

- [31] Subhadeep Saha et al. “NMR, surface tension and conductivity studies to determine the inclusion mechanism: thermodynamics of host-guest inclusion complexes of natural amino acids in aqueous cyclodextrins”. *New Journal of Chemistry* 40.1 (2016), pp. 651–661. ISSN: 1144-0546.
- [32] V. G. Avakyan et al. “The role of intra- and intermolecular hydrogen bonds in the formation of beta-cyclodextrin head-to-head and head-to-tail dimers. The results of ab initio and semiempirical quantum-chemical calculations”. *Russian Chemical Bulletin* 50.2 (2001), pp. 206–216. ISSN: 1066-5285.
- [33] D. P. Tieleman, D. van der Spoel, and H. J. C. Berendsen. “Molecular dynamics simulations of dodecylphosphocholine micelles at three different aggregate sizes: Micellar structure and chain relaxation”. *Journal of Physical Chemistry B* 104.27 (2000), pp. 6380–6388. ISSN: 1089-5647.
- [34] Ana Figueiras et al. “Interaction of omeprazole with a methylated derivative of beta-cyclodextrin: phase solubility, NMR spectroscopy and molecular simulation”. *Pharmaceutical Research* 24.2 (2007), pp. 377–389. ISSN: 0724-8741. DOI: [10.1007/s11095-006-9161-8](https://doi.org/10.1007/s11095-006-9161-8).
- [35] Haiyang Zhang et al. “Investigation of the Inclusions of Puerarin and Daidzin with beta-Cyclodextrin by Molecular Dynamics Simulation”. *Journal of Physical Chemistry B* 114.14 (2010), pp. 4876–4883. ISSN: 1520-6106.
- [36] Inigo X. Garcia-Zubiri, Gustavo Gonzalez-Gaitano, and Jose Ramon Isasi. “Application of automated docking to the binding of naphthalenes to beta CD in water: correlation with spectrofluorimetric data”. *Journal of Inclusion Phenomena and Macrocyclic Chemistry* 57.1-4 (2007), pp. 265–270. ISSN: 1388-3127.
- [37] C. H. Evans, M. Partyka, and J. Van Stam. “Naphthalene complexation by beta-cyclodextrin: Influence of added short chain branched and linear alcohols”. *Journal of Inclusion Phenomena and Macrocyclic Chemistry* 38.1-4 (2000), pp. 381–396. ISSN: 1388-3127.
- [38] Y. Inoue et al. “Thermodynamics of Molecular Recognition by Cyclodextrins .1. Calorimetric Titration of Inclusion Complexation of Naphthalenesulfonates with Alpha-Cyclodextrin,

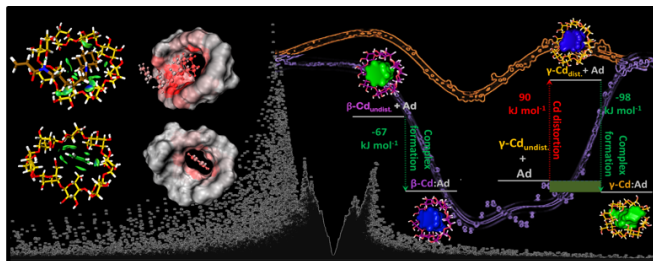
- Beta-Cyclodextrin, and Gamma-Cyclodextrin - Enthalpy Entropy Compensation”. *Journal of the American Chemical Society* 115.2 (1993), pp. 475–481. ISSN: 0002-7863.
- [39] S. Hamai and H. Watanabe. “Capillary electrophoretic study on the formation of inclusion complexes between beta-cyclodextrin and 1- and 2-naphthalenesulfonates”. *Bunseki Kagaku* 46.6 (1997), pp. 495–498. ISSN: 0525-1931.
- [40] S. Hamai. “Association of Inclusion-Compounds of Beta-Cyclodextrin in Aqueous-Solution”. *Bulletin of the Chemical Society of Japan* 55.9 (1982), pp. 2721–2729. ISSN: 0009-2673.
- [41] S. Hashimoto and J. K. Thomas. “Fluorescence Study of Pyrene and Naphthalene in Cyclodextrin Amphiphile Complex-Systems”. *Journal of the American Chemical Society* 107.16 (1985), pp. 4655–4662. ISSN: 0002-7863.
- [42] Gaelle Filippini et al. “Energetic Competition Effects on Thermodynamic Properties of Association between beta-CD and Fc Group: A Potential of Mean Force Approach”. *Journal of Physical Chemistry C* 116.42 (2012), pp. 22350–22358. ISSN: 1932-7447.
- [43] Haiyang Zhang et al. “Cooperative Binding of Cyclodextrin Dimers to Isoflavone Analogues Elucidated by Free Energy Calculations”. *The Journal of Physical Chemistry C* 118.13 (2014), pp. 7163–7173. ISSN: 1932-7447. DOI: [10.1021/jp412041d](https://doi.org/10.1021/jp412041d).
- [44] Hans-Gert Korth and Peter Mulder. “Anthrone and Related Hydroxyarenes: Tautomerization and Hydrogen Bonding”. *Journal of Organic Chemistry* 78.15 (2013), pp. 7674–7682. ISSN: 0022-3263.
- [45] A. C. C. Pais et al. “Solvation of alkane and alcohol molecules. Energy contributions”. *Physical Chemistry Chemical Physics* 3.18 (2001), pp. 4001–4009. ISSN: 1463-9076.
- [46] R. A. Klein. “Ab initio conformational studies on diols and binary diol-water systems using DFT methods. Intramolecular hydrogen bonding and 1 : 1 complex formation with water”. *Journal of Computational Chemistry* 23.6 (2002), pp. 585–599. ISSN: 0192-8651.
- [47] H. G. Korth, M. I. de Heer, and P. Mulder. “A DFT study on intramolecular hydrogen bonding in 2-substituted phenols: Conformations, enthalpies, and correlation with solute parameters”. *Journal of Physical Chemistry A* 106.37 (2002), pp. 8779–8789. ISSN: 1089-5639.

- [48] Grzegorz Litwinienko et al. “Intramolecular and Intermolecular Hydrogen Bond Formation by Some Ortho-Substituted Phenols: Some Surprising Results from an Experimental and Theoretical Investigation”. *Journal of Physical Chemistry A* 113.22 (2009), pp. 6275–6288. ISSN: 1089-5639.
- [49] J. W. Brady and R. K. Schmidt. “The Role of Hydrogen-Bonding in Carbohydrates - Molecular-Dynamics Simulations of Maltose in Aqueous-Solution”. *Journal of Physical Chemistry* 97.4 (1993), pp. 958–966. ISSN: 0022-3654.





# Chapter 4



## Host Flexibility and Space Filling

Factors affecting the thermodynamic signatures and stability of  $\beta$ - and  $\gamma$ -Cd complexes are detailed at the atomic level. The MD/PMF-based method is combined with the description of the nature and strength of the inter-partner affinity. Naphthalene, adamantane and lycorine derivatives are used as models of drug-leading structures. Guest size affects Cd-guest contact and the inclusion degree, inducing Cd deformation, which opposes inclusion. Complexation depends on the available Cd cavity volume, as guest fitting variations and the enthalpy penalty from Cd deformation impact on the binding constants (promoting a reduction of up to  $10^4$ ). The often neglected Cd deformation plays, thus, an important role in the interaction behavior of larger cavity Cd-based systems, being crucial in carbohydrate-mediated recognition phenomena. It corresponds to an increase in energy of ca.  $90 \text{ kJ mol}^{-1}$  in the simpler analyzed model system.

### 4.1 Context and relevant issues

The intrinsic and versatile properties of cyclodextrins (Cds) have credited these cyclic oligosaccharides as effective components for developing nanostructures to improve solubilization, transport and targeting of therapeutic agents ([1–12]). There is currently a great interest in the theoretical prediction and screening design of Cd supramolecular nanoassemblies with superior properties and tailored functionalities, providing attractive strategies for drug encapsulation/conjugation and formulation scale-up ([2, 13–18]). Due to experimental limitations, geometric characterization, preferred inclusion path-

ways, and the stabilizing interactions that govern the molecular architecture of Cd-based complexes are poorly understood ([19]). The hydrophilic outer surface and the hydrophobic cavity of natural Cds (with diameters of 0.47-0.53, 0.60-0.65 and 0.75-0.83 nm for  $\alpha$ -Cd,  $\beta$ -Cd and  $\gamma$ -Cd, respectively) ([2, 20]), award these hosts the ability of interacting, in aqueous solution, with adequately sized guest molecules and forming host-guest inclusion complexes stabilized by noncovalent interactions ([1, 2, 19, 21]). The driving forces leading to complex formation include hydrophobic, van der Waals and dipole-dipole interactions ([1]). The favorable free-energy change related with desolvation of the hydrophobic moieties of the binding partners was primarily attributed to the favorable entropy change resulting from the release of water molecules at the inter-partner interfaces ([19, 22, 23]). MD simulations in water and PMF calculations have suggested that the replacement of high-energy water in host cavities by guest molecules is the main enthalpic driving force for the complex formation; at the same time, desolvation of the host cavity promotes the formation of new hydrogen bonds, and favorable energy changes (up to 10.5 kJ mol<sup>-1</sup>) ([19, 22, 24]). A large gain in free-energy is thus attained from the enthalpy compensation of water-water interactions in the bulk. In systems containing  $\beta$ -Cd, it has been observed that the binding constant ( $K_{bind}$ ) increases, in general, as the cavity is increasingly filled by the guest. Also, the guest volume has been expressed by the number of carbon atoms of the respective hydrophobic segment. Increasing this number decreases energy (ca. -3 kJ mol<sup>-1</sup> per carbon) and increases complex stability ([1, 25]). This effect can be explained by the more intense of hydrophobic, van der Waals and dispersion interactions ([1]).

Some efforts have been made for providing preliminary evidences and rationales on the affinity of Cd towards different guests, anticipating or avoiding extensive experiments. Results from molecular modeling have suggested the need for constructing models to reach feasible structures of the complexes, considering information on the preferred inclusion mode ([19, 26]), the size of the Cd cavity and also the host/guest stoichiometry ([27–30]).

Accurately assessing the flexibility of Cds and consequent cavity size represents in general a challenge in molecular simulations ([28]). *Ab initio* approaches are time consuming, and quantum semi-empirical methods (e.g. CNDO, AM1 and PM3) are commonly used in the theoretical studies of Cds. The semi-empirical PM3 methods are often combined with *ab initio* methods. Due to the improved description of hydrogen bonds and steric effects in the PM3 method, a better performance in the con-

formational study of supramolecular systems, including Cd-based complexes can be achieved, when compared to AM1. However, higher levels of theory have also been employed in the description of Cd chemistry, including DFT ([28]).

It should be noted that successfully designing and employing Cd conjugates requires a comprehensive understanding of the relation between conformation, energy, solvation, recognition behavior and function.([1, 19, 23, 31–33]) The ability of Cds to form selectively host-guest inclusion complexes depends on a proper fit of the guest molecule into the Cd cavity ([19, 25, 34, 35]). In spite of some agreement that the hydrophobic effect is the major driving force within the factors that govern Cd-guest binding in water, a deeper knowledge of the effect of the full size of guest and Cd cavity on the binding mode and on the interaction strength, is still missing ([32–37]). Especially, there is no quantitative understanding of the joint influence of guest substitution and Cd cavity size over the thermodynamic signatures and association/binding constants of the resulting complexes.

Free-energy calculations provide most ingredients to tackle this issue, yielding an explicit description of the binding energetics ([19, 38–40]). Robust and accurate MD based methods, including umbrella-sampling and the cylindrical approximation for the calculation of binding constants, have provided new information that have been correlated with available experimental observations. Accurate predictions are now available from MD, including the effect of variations in guest substituents ([1, 19]). The increasing interest in Cd hosts is explained by their (i) superior affinity towards amphiphilic guests, (ii) distinct role as drug carriers and (iii) multifunctional character in polymeric drug delivery systems ([1, 2, 19]). Bearing in mind that, in most cases, the host cavity cannot fully accommodate the guest, the designed free-energy oriented method (described in Chapters 2 and 3) has been employed for estimating binding constants of inclusion complexes between  $\beta$ -Cd and different naphthalene derivatives with pendant hydrophobic and hydrophilic groups ([19]). In these complexes, the guest molecule alters the structure of the host, leading to relevant cooperative effects, when compared to bulk solvated molecules. The inclusion process is generally governed by individual or complementary interactions, such as relatively weak NCI, including hydrophobic, van der Waals and electrostatic interactions,  $\pi$ - $\pi$  stacking, hydrogen bonding and also by stronger ionic and dipolar interactions. More recently, it has been demonstrated ([1]) that the binding constant ( $K_{bind}$ ) for Cd-based complexes can reach  $10^{28}$   $\text{kJ mol}^{-1}$  ([1]). The modulation of the nature of the interaction sites in Cd-based poly-

mer networks was performed imposing hyaluronic acid derivatives as amphiphilic substituents, for mimicking the network junction nodes. The relevant thermodynamics signatures and the stabilizing/destabilizing noncovalent interactions within the complexes were duly assessed, indicating that the presence of the amphiphilic chains boosted the interaction behavior and increased the binding constant more than 200-fold. Host-guest interactions, desolvation effects, host fit and guest orientation dominated the stability of the junction nodes ([1, 31]). Note, in this context, that previous work suggested, in a straightforward manner, that the ideal proportion of occupancy for a host-guest complex is ca. 55% ([25, 36]).

The present work deals with the question whether (and how) the accessible cavity volume for guest molecules of different natures and sizes determines the intimate conformations and stability of the complexes. Is the effect comparable to that observed with guest size and structural complexity? The interaction patterns and the leading factors affecting the thermodynamic signatures and stability of inclusion complexes between  $\beta$ - and  $\gamma$ -Cds and different model guests are detailed, combining our previously designed MD/PMF-based procedure ([19]) and the Independent Gradient Method (IGM) of Lefebvre et al. ([41]). The latter method is based on the analysis of the electronic charge density of the binding partners and the respective gradients, and allows visualizing and quantifying those regions of stabilizing/stabilizing noncovalent interactions.

The host and guest molecules are selected as models of common building blocks for obtaining higher order structures. The necessity to explain the function of Cds in all details and strands arises from their multiple applications ([42–44]).

Both  $\beta$ - and  $\gamma$ -Cds are employed due to their suitable dimensions and circular structures, which allow assessing the effect of the cavity size and flexibility, especially in the latter. Naphthalene (Np) and adamantane (Ad) provide two different rigid hydrophobic backbones, allowing to explore the effect of guest substitution on the binding process. The adamantyl moiety possesses a bulky and symmetrical diamond-like structure with unique features (e.g. size, lipophilicity) for fitting perfectly in cavities of several host molecules, including Cds. Np and Ad derivatives containing aldehydic chains serve as practical molecular examples and leading structures of an extensive series of promising therapeutic agents, as well as function as model building blocks in supramolecular structures and self-assembled systems for basic chemical and pharmaceutical investigations ([45–50]). Another interesting guest is

anhydrolycorine, a lycorine derivative that possesses a planar-like structure of five enclosed rings and displays several biological properties and anti-tumor activity ([51, 52]).

Complexation of these model guests is sensitive to alterations in the available cavity volume, as the fit variations into the cavity of  $\beta$ - and  $\gamma$ -Cds have a direct impact on the respective binding constants. The calculated thermodynamic quantities allow explaining the effects of using imposed features in the interaction patterns and complex configuration of this type of systems.

#### 4.1.1 System construction and simulation details

The energy patterns and binding affinities for  $\beta$ - and  $\gamma$ -Cds in the presence of several guests of different structural complexity are characterized using MD simulations and free-energy calculations. As the similarity and size of the Cd cavities favor equilibrium free-energy approaches, steered molecular dynamics with center of mass pulling and umbrella sampling are employed, as suggested previously ([Zhang2010, 53–57]) for obtaining the free-energy profiles and binding affinity estimates.

Based on the preferred binding mode reported in similar systems, simulations are performed in one direction, from bulk water to the Cd cavity, through the secondary Cd portal.

The PMF dictates the degree and motion rate of binding, and the selectivity. The coordinate  $\xi$  represent the geometrical coordinate  $\xi(r)$  along which the PMF values may vary. To ensure the adequate sampling of unfavorable states over the MD trajectory, umbrella sampling ([58, 59]) is used and each system is computed under a window biasing potential,  $w(\xi)$ , which improves the sampling in adjacent regions of the reaction coordinate  $\xi$ . Several biased window simulations are required to construct the PMF profile over the selected region (further details are given in ref. [19]).

The stability constants are addressed using the "flexible molecule" approximation, in which the accessible cavity volume is defined by a cylindrical region, weighted by the PMF values. The guest motion is regulated by the positioning of the respective center of mass ([60, 61]).

The basic coordinates of  $\beta$ - and  $\gamma$ -Cds were extracted from the RCSB protein data bank (PDB codes: 1DMB and 5MKA, respectively). The starting geometries of the guest molecules (naphthalene - Np, adamantane - Ad, 2-aminonaphthalene - NpNH<sub>3</sub><sup>+</sup>, naphthalene and adamantane substituted with a pendant aldehydic (Ald) chain - NpAld and AdAld, and anhydrolycorine - Anh) were created in

Pymol (Version 1.7.7.2) and optimized with the semi-empirical Antechamber/SQM method. Partial charges for both host and guest molecules were generated using the R.E.D.D. Server ([62]).

A cubic box of  $7.5 \times 7.5 \times 7.5 \text{ nm}^3$  was employed for each system containing one Cd molecule and one guest, solvated with approximately 13700 water molecules. Cds were centered in the simulation box with the cavity axis parallel to the  $z$ -axis. The reaction coordinate  $\xi_z$  is defined by the  $z$ -distance between the center of mass (COM) of the carbon atoms of the hydrophobic moiety of the guest backbone and that of the central glycosidic oxygen atoms of Cds.

MD simulations were performed using the GROMACS package (version 4.6.5) ([63, 64]) and the all-atom amber99sb ([65–68]) forcefield, under periodic boundary conditions and with a NPT ensemble. TIP3P water was used for modelling aqueous solvation. In all simulations, the temperature and pressure were kept unchanged, at 300 K and 1 bar, by the coupling constants of 0.5 ps and 1 ps, respectively. An equilibration run of 500 ps was performed prior to each production run, maintaining the pressure at 1 bar with the Berendsen barostat. During the production runs, no pressure coupling was applied to maintain the size of the simulation box unchanged. A cutoff of 0.9 nm was employed for Lennard-Jones interactions and electrostatic interactions were assessed using the PME method ([31, 69]). The LINCS algorithm ([70]) was used for applying constraints in bond lengths of both host and guest molecules. A detailed description of the simulation procedure is given in refs. ([1, 19, 31]).

A set of independent simulations were carried out via umbrella sampling, ensuring that these configurations were closer to the equilibrated states. The optimized parameters (e.g. force constants) for umbrella sampling, construction of the PMF profiles and the analysis of the thermodynamic patterns associated to the binding process were taken from previous studies of the authors ([1, 19]). Specifically, for each system, a series of initial configurations was obtained from a periodic pulling, performed after equilibration, resorting to a steered molecular dynamics approach. This allows modulating the formation of 1:1 complexes.

Each configuration corresponds to a position within which the guest molecule evolves towards inclusion, and then separates from the Cd molecule ( $\beta$ - and  $\gamma$ -Cd), using an umbrella biasing potential. This allows restraining the guest (Np, NpAld, Ad, AdAld,  $\text{NpNH}_3^+$  and Anh) to accurately sample the configurational space in the defined region, along the inclusion pathway. In each system, the COM

of the glycosidic atoms of the Cd molecules were harmonically immobilized using an isotropic force constant of  $1000 \text{ kJ mol}^{-1} \text{ nm}^{-1}$ , and a free xy motion for the guest molecules was allowed. The COM of the reference carbon atoms of the guest molecules was pulled through the Cd cavity with a steering force of  $2000 \text{ kJ mol}^{-1} \text{ nm}^{-1}$ , from the secondary to the primary Cd portal, along the z-axis over 500 ps and with a pulling rate of  $0.01 \text{ nm ps}^{-1}$ .

The initial ( $\xi_i$ ) and final ( $\xi_f$ ) values of the reaction coordinate were set to extreme values of  $\xi_i = 1.5 \text{ nm}$  and  $\xi_f = -2.5 \text{ nm}$ . The guest molecules were sampled ca. 4 nm covering the  $[\xi_i, \xi_f]$  interval with ca. 100 neighboring windows separated by 0.03 nm, which were employed as starting configurations for the independent simulations in umbrella sampling. A total of 12 systems were inspected and analyzed following this procedure.

The respective PMF profiles were constructed as a function of the inclusion coordinate, combining all the individual potentials via a periodic version of WHAM ([71]). Statistical uncertainties from the variance of the PMFs were calculated resorting to the bootstrap procedure of trajectories on umbrella histograms ([19, 72]).

In order to establish proper references for the calculations and subsequent analysis of structural and desolvation effects, 20 independent simulations were performed during 5 ns, after a pre-equilibration of 500 ps. These correspond to the equilibrium states of the complexes (minima in the PMF profiles), and the single solvated host and guest molecules.

Prior to NCI analysis, geometric clustering ([73]) was performed for selecting a representative structure of each complex from the ensemble of structures in the equilibrium state, sampled during the MD simulations. Clusters were determined from the RMSD of the atom positions between all pairs of Cd structures. For each Cd structure, the number of neighbors was calculated for RMSD values of 0.25 nm.

Quantum chemical calculations were performed using the Orca electronic structure package (version 4.0.0.2) ([74]). Geometries were optimized at the DFT level using the TPSS meta-GGA functional ([75]) with the Def2-SVP ([76]) polarized double- $\xi$  basis set. Dispersion interactions were included with Grimme's D3 dispersion correction ([77, 78]) and solvent (water) effects were included using the polarisable continuum model (PCM) ([79]). The geometries optimized at this TPSS-D3-PCM/Def2-SVP level were then used in single point energy calculations with the hybrid TPSS0 functional which



is known to yield accurate energetics for weakly-bound systems such as inclusion complexes as well as covalent molecules ([80]). In order to enhance the reliability of the TPSS0 energies, the multiply-polarised triple- $\xi$  basis sets Def2-TZVP and Def2-TZVPP were used ([76]). Dispersion and solvent effects were included with the D3 and PCM methods as in the geometry optimizations. Due to the size of the systems being studied and the large number of degrees of freedom involved no vibrational (zero-point) corrections were applied to the final energies.

### 4.1.2 Visualization of noncovalent interactions

Evaluation of the noncovalent interactions within  $\beta$ - and  $\gamma$ -Cd complexes was performed based on the IGM proposed by Lefebvre et al. ([41]), and using the IGMPLOT software (version 1.0). IGM is controlled by the topological characteristics of the electronic charge density,  $\rho$ , of each system. The method utilizes quantities related to the first and second derivatives of the density, in addition to  $\rho$ .  $\delta g^{inter}$  is the IGM descriptor given by the difference between the first derivatives of the charge densities for the total system and the fragments,

$$\delta g^{inter} = |\nabla \rho^{IGM,inter}| - |\nabla \rho| \quad (4.1)$$

$\delta g^{inter} > 0$  reflects the presence of noncovalent interactions. The magnitude of the descriptor at a point in space allows inferring on the strength of the interaction.

$\nabla \rho^{IGM,inter}$  is obtained (in the following case for the x-direction) from sums over all the  $N$  atoms in the different fragments, denoted as  $A$  and  $B$ ,

$$\left( \frac{\delta \rho}{\delta x} \right)^{IGM,inter} = \left| \sum_{i=1}^{N_A} \frac{\delta \rho_i}{\delta x} \right| + \left| \sum_{i=1}^{N_B} \frac{\delta \rho_i}{\delta x} \right| \quad (4.2)$$

The pre-computed atomic charge densities are used in IGMPLOT for constructing a pro-molecular density which produces a minimal effect on the noncovalent interactions, since very little relaxation of the charge density occurs in these extremely low-density regions, following the formation of covalent

bonds. Although it is possible to identify NCI regions using the  $\delta g^{inter}$  value, a second derivative (Laplacian) of the density  $\nabla^2\rho$  is required, for discriminating favorable/unfavorable NCIs. Information on the stabilizing ( $\lambda_2 < 0$ ) or destabilizing ( $\lambda_2 > 0$ ) interactions can be obtained, by decomposing the Laplacian term into  $\nabla^2\rho = \lambda_1 + \lambda_2 + \lambda_3$  ( $\lambda_1 \leq \lambda_2 \leq \lambda_3$ ), the three eigenvalues of maximal variation. Stronger interactions such as hydrogen bonds display larger (negative) values of  $sign(\lambda_2)\rho$ . van der Waals forces, are weak NCI associated with  $sign(\lambda_2)\rho$ , displaying values close to zero. The coordinates of the Cd complexes at the minima of the PMF profiles were extracted from the simulations at equilibrium. Solvent molecules were removed and the complexes were dissociated into the respective binding components.([1]) The isosurface volumes for the  $\delta g^{inter}$  colored by the value of  $sign(\lambda_2)\rho$  at each point on the surface allows representing in space the NCI, indicating both the extent and (de)stabilizing nature of the interactions. Visual Molecular Dynamics software version 1.9.2 was used for the preparation and representation of the systems and isosurface graphics ([81]). To clearly inspect the relative differences between the complexes, the isosurface representations were combined with the values of the same two descriptors, allowing to compare and evaluate quantitatively the types and strengths of NCI within the  $\beta$ - and  $\gamma$ -Cd.

## 4.2 Results

### 4.2.1 PMF and thermodynamics

The analysis of PMF profiles presented in Figure 4.1 allows comparing the different systems. Also included are the representative conformations of the inclusion complexes extracted from the lowest energy states (minima of the PMFs), showing the most favorable arrangement of the binding partners upon complexation. The inclusion complexes between  $\beta/\gamma$ -Cd and naphthalene and adamantane are used as reference systems. The substituted Np and Ad, and also  $NpNH_3^+$  and Anh are used for evaluating the effect of guest nature and size on the binding affinity of Cd with different cavity sizes. Figure 4.1 and Table 4.1 summarize the main results concerning the calculation of the potential of mean force for the different systems under study. It can be seen that both host and guest molecules possessing different imposed features influence significantly the inclusion behavior and the interaction

patterns, as suggested by the different shapes and well depths of the PMF profiles. However, a more pronounced difference is observed between  $\beta$ - and  $\gamma$ -Cd systems.

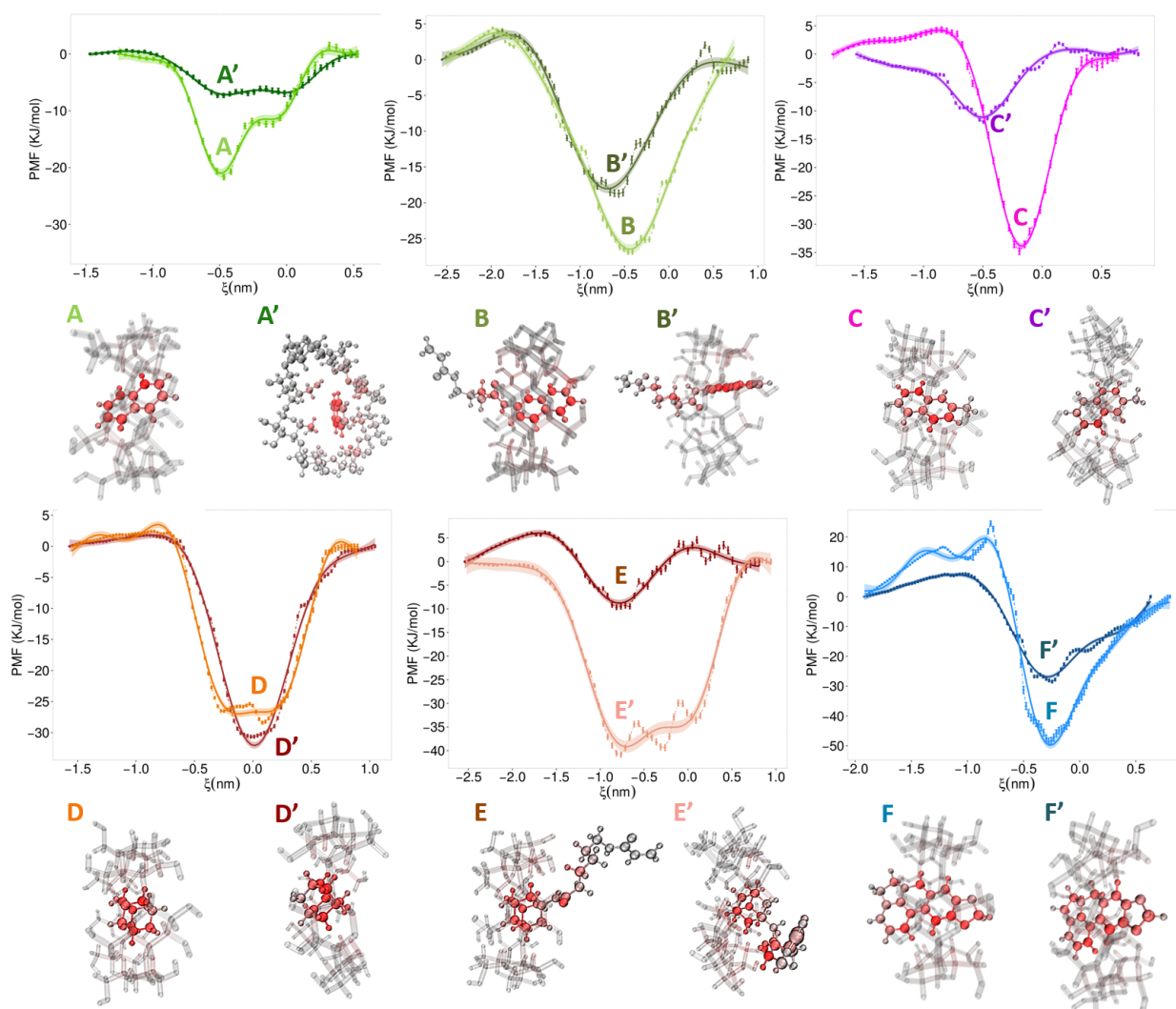


Figure 4.1: Free-energy profiles for the formation of  $\beta$ - and  $\gamma$ -Cd based inclusion complexes calculated from the integration of the mean forces (solid curves) and from the WHAM procedure (dashed curves). The curves are vertically aligned to have the Cd cavity positioned at  $\xi_z = 0.0$  nm. The error bars represent the statistical uncertainties estimated with bootstrap analysis. Also included are the structures of the complexes sampled from the A-F and A'-F' minima in the PMFs.

The well-depth is, in general, markedly higher for the  $\beta$ -Cd than for the  $\gamma$ -Cd counterpart. The only exception is observed in the Ad, for which the PMF is of comparable depth, slightly deeper in the case of the  $\gamma$ -Cd. The  $\beta$ -Cd values are found in the range  $23 - 49 \text{ kJ mol}^{-1}$ , while for the latter we can observe values contained in the interval  $7.4 - 30.7 \text{ kJ mol}^{-1}$ . As previously observed ([1, 19]) for Np and Ad included in  $\beta$ -Cd, well depth increases with substitution in both Np and Ad, irrespective of the type of substituent. The trend is not clear when  $\gamma$ -CD is the host.

Table 4.1: Minimum depth ( $-\Delta G_{PMF}$ ) and position ( $\xi_{z0}$ ), and width at half height (FWHM) extracted from the PMF profiles of the inclusion complexes between  $\beta$ - and  $\gamma$ -Cd and the model guests (Np, NpAld, Ad, AdAld, NpNH<sub>3</sub><sup>+</sup> and Anh).

Guest	$-\Delta G_{PMF}$		FWHM		$\xi_{z0}$	
	$\beta$ -Cd	$\gamma$ -Cd	$\beta$ -Cd	$\gamma$ -Cd	$\beta$ -Cd	$\gamma$ -Cd
Np	23.1	7.4	0.63	0.95	-0.47	0.03
NpAld	26.9	18.7	1.05	1.02	-0.46	-0.56
Ad	28.4	30.7	0.90	0.66	0.08	-0.02
AdAld	40.8	9.7	1.46	0.56	-0.76	-0.81
NpNH <sub>3</sub> <sup>+</sup>	34.8	12.0	0.48	0.50	-0.19	-0.49
Anh	48.6	28.5	0.65	0.72	-0.28	-0.25

The width at half height for  $\beta$ - and  $\gamma$ -Cds differ in some cases (Np, Ad and AdAld systems), while for the others the difference is much lower. Except for the  $\beta$ -Cd:AdAld system, typical values are in the vicinity of or below 1 nm. Ald substituents promote a slight enlargement of the width, more marked in the case of  $\beta$ -Cd. This indicates that, in the latter, the fit of guest to host is tighter and molecule length directly impacts upon the PMF well width.

The degree of inclusion for the minimum value of the PMF varies with the system, with the substituent in the case of the modified Np and Ad systems, and with the host, but an overall trend is not readily apparent. Direct inspection of the PMF profile indicates that, when present, entrance and exit potential barriers are shallow, with the exception of the  $\gamma$ -Cd:Anh system, in which an exit barrier of ca. 20 kJ mol<sup>-1</sup> is observed.

The thermodynamic parameters derived from Equations ( 2.22-2.25) are given in Table 4.2. These are used for the calculation of the binding thermodynamics and constants and combines the host-guest interaction as measured from the PMF profiles.

As could have been anticipated, the value of  $\Delta G_{bind}^0$  follows the same trend as the PMF: the deeper the PMF profile, the more negative is the free-energy of binding. The enthalpic contribution dominates, but the entropic component cannot generally be discarded. Binding constants are always higher in the  $\beta$ -Cd complex, with the exception of Ad, consistent with the PMF values. Values found for the binding constant are in the range 128 – 6.1 × 10<sup>6</sup> M<sup>-1</sup> and 98 – 1.6 × 10<sup>4</sup> M<sup>-1</sup> respectively for the  $\beta$ - and  $\gamma$ -Cd systems.

Table 4.2: Binding free energies ( $\text{kJ mol}^{-1}$ ) and binding constants characterizing the complexation of  $\beta$ - and  $\gamma$ -Cds in aqueous solution, at 300 K.

Guest	$-\Delta G_{bind}^0$		$-\Delta H_{bind}^0$		$T\Delta S_{bind}^0$		$K_{bind}$	
	$\beta$ -Cd	$\gamma$ -Cd	$\beta$ -Cd	$\gamma$ -Cd	$\beta$ -Cd	$\gamma$ -Cd	$\beta$ -Cd	$\gamma$ -Cd
Np	12.0	11.4	17.4	3.4	-5.4	-8.0	$128 \pm 33^*$	$98 \pm 62$
NpAld	17.2	15.9	20.4	14.3	-3.2	-1.6	$1007 \pm 145$	$591 \pm 39$
Ad	19.7	23.7	15.6	29.4	-4.1	-5.6	$2666 \pm 654$	$1.4 \times 10^4 \pm 972$
AdAld	39.0	10.7	39.5	2.4	-0.5	-8.3	$6.1 \times 10^6 \pm 9.0 \times 10^5$	$74 \pm 8.5$
NpNH <sub>3</sub> <sup>+</sup>	24.7	14.7	33.3	3.6	-8.6	-11.2	$2.1 \times 10^4 \pm 5.5 \times 10^3^*$	$379 \pm 37$
Anh	36.4	24.2	45.2	25.6	-8.8	-1.5	$2.2 \times 10^6 \pm 9.8 \times 10^4$	$1.6 \times 10^4 \pm 1.7 \times 10^3$

\*  $K_{bind}$  values obtained from ([1, 19]).

## 4.2.2 Solvation

The inclusion of guest molecules into Cds promote, as expected, the liberation of water molecules from the cavities. This phenomenon is ruled by the relative size of the interacting molecules, as suggested in Figures 4.2 and 4.3, at  $r \approx 0.35\text{nm}$ . At this distance from the center of mass of each Cd or guest molecule ( $r = 0$ ), the whole cavity and guest backbone is covered. This allows estimating the number of water molecules at a distance  $r$  from the Cd cavity center or from a reference guest group. The solvation profiles can be inferred by the running coordination numbers depicted in Figures 4.2, 4.3 for the Cd cavities and for the guest molecules.

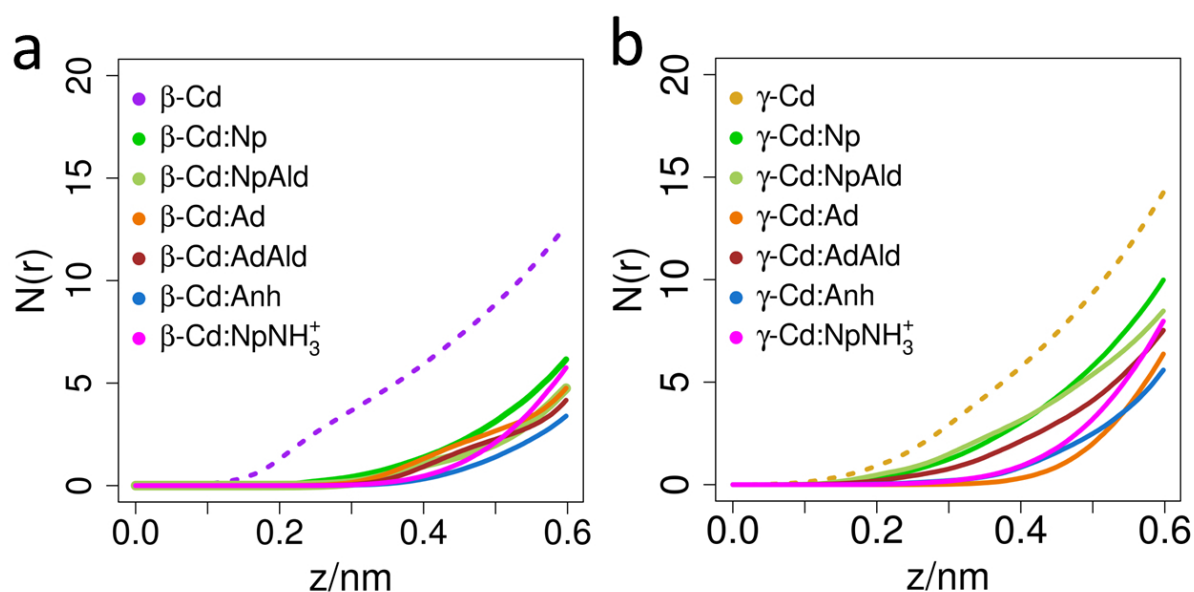


Figure 4.2: Coordination number for water molecules from the center of the (a)  $\beta$ -Cd and (b)  $\gamma$ -Cd cavities in aqueous solution and in the corresponding inclusion complexes.

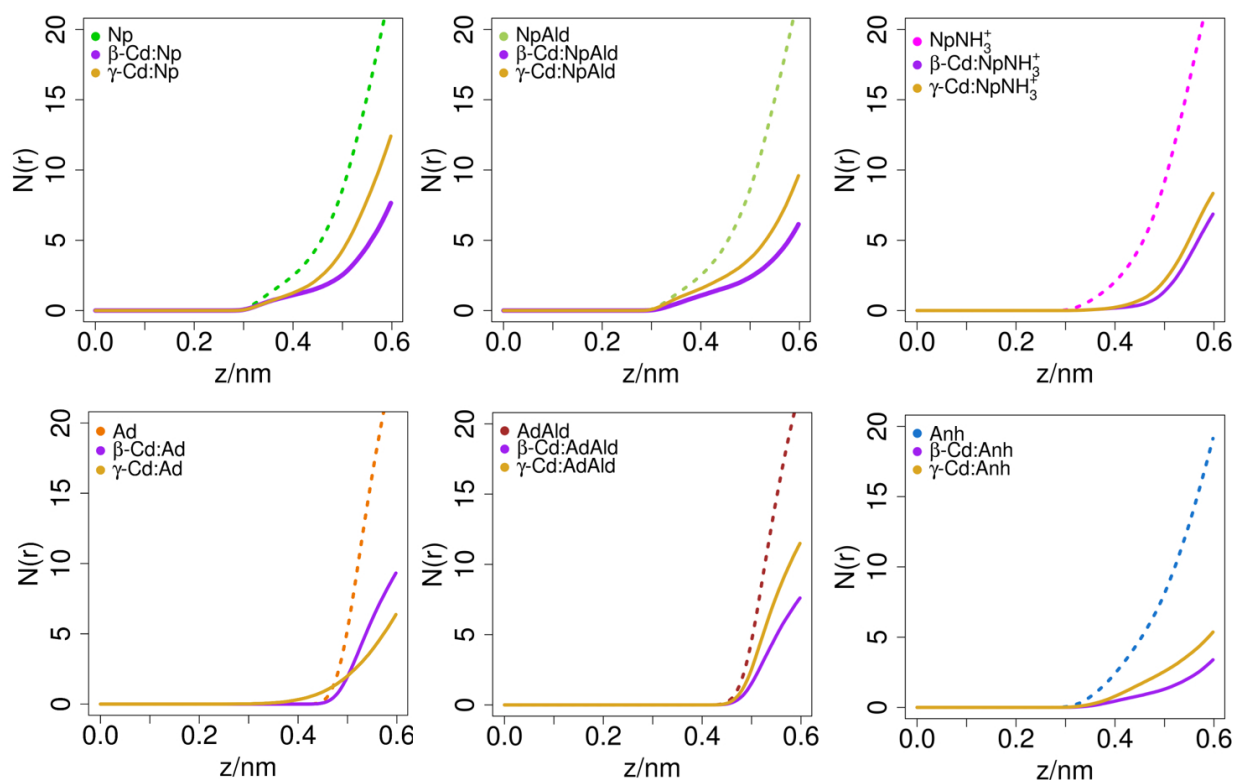


Figure 4.3: Running coordination number of water molecules relative to each guest molecule as a function of distance.

Overall, the amount of solvent in the Cd cavity and in the immediate vicinity of the guest molecules decreases upon the complex formation. In Figure 4.2, the set of curves is delimited above by Np corresponding to the system with lower degree of desolvation, thus also corresponding to a lower binding constant, and below by Anh in  $\beta$ -Cd, and Ad and Anh in  $\gamma$ -Cd systems, corresponding to the highest binding constants. Anh is the larger guest, which is also consistent with a stronger desolvation, and displays high binding constants for both cyclodextrins. It should be stated, however, that in spite of these observations, the correlation desolvation/binding constant is poor, and other factors intervene in the interaction, as previously remarked ([1, 19]). From Figure 4.3 it is also clear that inclusion determines desolvation of the guest, and that desolvation is more intense for  $\beta$ -Cd, except for a single instance, Ad. It is also apparent, from the change in the slope of the curves, that the larger guest, Anh, is the one that loses a larger amount of water.

### 4.2.3 Cd conformation and host-guest contact

In the following, the conformational change of the  $\beta$ - and  $\gamma$ -Cd backbones upon complexation with Np, NpAld, Ad, AdAld, NpNH<sub>3</sub><sup>+</sup> and Anh is detailed, for evaluating distorted structures over the course of the simulations. The distortion phenomena of the Cd cavity has been previously observed in similar systems ([19]). Depending on different binding modes and different guests, the Cd cavity can be dynamically stretched and compressed. In  $\beta$ -Cd complexes, a larger deformation of the cavity is, in general, characterized by a higher degree of inclusion and stronger host-guest interactions. The average overall conformation of each Cd in each complex is summarized in Table 4.3. Also included are the free solvated Cd molecules. Deformation of the Cd cavities is assessed by inspecting the principal moments of inertia (MOI), denoted as  $I_1$ ,  $I_2$  and  $I_3$  ([19, 82, 83]).

Table 4.3: Summary of the total and averaged moments of inertia,  $I_1$ ,  $I_2$  and  $I_3$ , and aspect ratio and elongation values for the  $\beta$ - and  $\gamma$ -Cd backbone, upon inclusion at the equilibrium state. Standard deviations of the estimated parameters are also provided.

	Cd	Np	NpAld	Ad	AdAld	NPNH <sub>3</sub> <sup>+</sup>	Anh
$\beta$ -Cd							
$I_{tot}$	132	142	157	159	158	142	141
$\langle I_1 \rangle$	185 ± 11	188 ± 8	200 ± 2	197 ± 6	198 ± 6	182 ± 8	188 ± 8
$\langle I_2 \rangle$	214 ± 8	216 ± 8	212 ± 2	216 ± 5	215 ± 5	223 ± 8	216 ± 7
$\langle I_3 \rangle$	233 ± 11	237 ± 7	345 ± 3	346 ± 5	345 ± 5	337 ± 7	337 ± 8
$I_1 : I_2 : I_3$	1.0:1.2:1.8	1.0:1.2:1.8	1.0:1.1:1.7	1.0:1.1:1.8	1.1:1.1:1.8	1.1:1.2:1.9	1.0:1.2:1.8
Aspect ratio	0.87 ± 0.07	0.87 ± 0.06	0.94 ± 0.01	0.91 ± 0.03	0.92 ± 0.04	0.82 ± 0.06	0.87 ± 0.06
Elongation	0.93 ± 0.04	1.07 ± 0.04	1.03 ± 0.01	1.05 ± 0.03	1.04 ± 0.02	1.11 ± 0.04	1.07 ± 0.04
Asymmetry	0.24 ± 0.03	0.24 ± 0.03	0.20 ± 0.01	0.22 ± 0.02	0.22 ± 0.03	0.26 ± 0.02	0.24 ± 0.03
$\gamma$ -Cd							
$I_{tot}$	999	1007	1074	986	1027	1008	1033
$\langle I_1 \rangle$	235 ± 20	224 ± 16	262 ± 3	246 ± 12	234 ± 16	242 ± 11	253 ± 11
$\langle I_2 \rangle$	302 ± 16	316 ± 14	314 ± 3	289 ± 10	315 ± 15	300 ± 14	300 ± 13
$\langle I_3 \rangle$	463 ± 23	467 ± 16	499 ± 4	450 ± 15	4785 ± 23	466 ± 15	480 ± 13
$I_1 : I_2 : I_3$	1.0:1.3:2.0	1.0:1.4:2.1	1.0:1.2:1.9	1.0:1.2:1.8	1.0:1.3:2.0	1.0:1.2:1.9	1.0:1.2:1.9
Aspect ratio	0.78 ± 0.09	0.71 ± 0.06	0.83 ± 0.01	0.85 ± 0.06	0.75 ± 0.08	0.81 ± 0.07	0.84 ± 0.07
Elongation	0.88 ± 0.06	1.19 ± 0.06	1.10 ± 0.01	1.09 ± 0.04	1.16 ± 0.06	1.12 ± 0.05	1.10 ± 0.05
Asymmetry	0.29 ± 0.05	0.33 ± 0.04	0.27 ± 0.01	0.25 ± 0.03	0.31 ± 0.04	0.28 ± 0.03	0.28 ± 0.03

It should be noted, that the values of the  $z$ -component ( $I_3$ ), averaged over the simulation trajectory, exceed both  $x$ - and  $y$ - components ( $I_1$  and  $I_2$ , respectively). The Cd cavities are positioned symmetrically along  $I_3$ , at the center of the truncated cone, as illustrated in Figure 4.4. The MOI ratios found for  $\beta$ -Cd accommodating the different guests are 1.0:1.1:1.7, 1.0:1.1:1.7, 1.0:1.2:1.8, and 1.1:1.2:1.9, and for  $\gamma$ -Cd are 1.0:1.2:1.8, 1.0:1.2:1.9, 1.0:1.3:2.0, and 1.0:1.4:2.1 (see Table 4.3). In the absence of a guest molecule,  $\beta$ -Cd cavity displays a similar deformation degree as that observed for the complexes with Np and Anh (1:1.2:1.8). However, the latter two guests promote disparate affinities, with

a relative  $\Delta G_{bind}^0$  difference of ca. 1/3. This suggests that the guest size determines the complex stability in systems containing  $\beta$ -Cd, as the distortion of cavity is not significant. For the complexes containing NpAld, Ad and AdAld the values slightly differ, with the most balanced ratio attributed to AdAld. In  $\beta$ -Cd:AdAld, the  $\beta$ -Cd cavity is less distorted displaying two similar components ( $I_1$  and  $I_2$ ) and also possesses the most favorable interactions ( $\Delta G_{bind}^0=39.0 \text{ kJ mol}^{-1}$ ).  $\beta$ -Cd:AdAld was also identified previously, as one of the two complexes possessing deeper and larger PMF wells. For  $\gamma$ -Cd-based systems, only in  $\gamma$ -Cd:AdAld the Cd cavity presents similar deformation relative to the empty host (1.0:1.3:2.0). The less balanced ratio is displayed by  $\gamma$ -Cd:Np and  $\gamma$ -Cd:AdAld (1.0:1.4:2.1 and 1.0:1.3:2.0, respectively) corresponding to the narrower PMF profiles and to the less stable complexes ( $K_{bind}$  of 98 and 74 for  $\gamma$ -Cd:Np and  $\gamma$ -Cd:AdAld, respectively). This indicates that in  $\gamma$ -Cd systems, the host deformation compromises inclusion and binding. In contrast to  $\beta$ -Cd, the stability of  $\gamma$ -Cd complexes is ruled more by Cd cavity size than guest size. Deformation of the Cd cavity can be further inspected by calculating the aspect ratio and the elongation values, also summarized in Table 4.3. These parameters are shape factors determined based on the closest principal moments,  $I_1$  and  $I_2$ , and can be translated in two proportional relationships between the latter two components (see Figure 4.4). It is clear that the deformation observed in the  $\beta$ -Cd is less significant than that

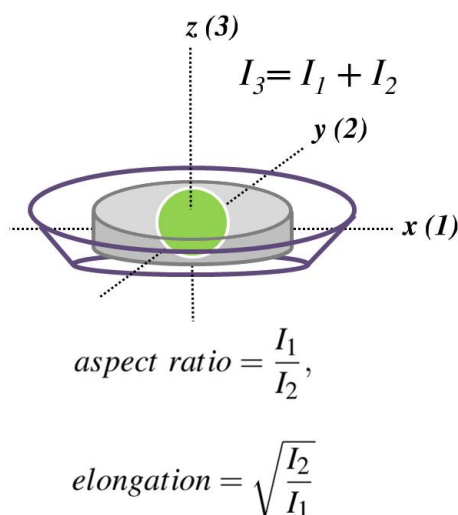


Figure 4.4: Illustrative representation of a typical model reflecting the calculation of the moments of inertia, denoted as  $I_1$ ,  $I_2$  and  $I_3$ , which are averaged over the course of the simulations. The cavities of  $\beta$ - and  $\gamma$ -Cds are positioned symmetrically along the z-component,  $I_3$ . Also described are the aspect ratio and the elongation parameters, used for evaluating the distortion degree of Cds based on  $I_1$  and  $I_2$ .



for the  $\gamma$ -Cd, and this can be ascribed to the larger diameter and larger cavity volume of the latter. Also, the aspect ratios observed in the  $\beta$ -Cd display a small variation among systems, in contrast to  $\gamma$ -Cd. In the latter, deformation decreases in the order of  $\text{Np} > \text{AdAld} > \text{NpNH}_3^+ > \text{NpAld} > \text{Ad} > \text{Anh}$ . Somewhat counterintuitively, the first system corresponds to the most solvated  $\gamma$ -Cd cavity, and the latter to one of the least solvated. This suggests that Cd deformation promotes a higher Cd-guest contact, but does not necessarily govern the amount of water molecules that are expelled from the cavity.

Direct inspection of intermolecular signatures of the Cd complexes at equilibrium states and in the most representative conformations (extracted from geometric clustering) allows inferring on the type and strength of the Cd-guest interactions as a function of the respective electronic charge densities. Areas of low density, corresponding to stabilizing/destabilizing noncovalent interactions between  $\beta$ - and  $\gamma$ -Cd and guest molecules are decoupled and represented by 3D IGM isosurfaces (Figure 4.5). The volume of the interacting regions reflects the extent of the interactions. Blue and red indicate stronger stabilizing/destabilizing interactions (respectively), green denotes weak van der Waals-type interactions. Attractive, repulsive interactions, and weakly repulsive or attractive forces are thus colored in blue, red and green, respectively. In the 3D convex surfaces a volume cutoff of  $\delta g_{inter} = 0.05$  a.u. and a color coding in the range of  $-0.1 \leq \text{sign}(\lambda_2)\rho \leq 0.1$  a.u. are employed. In the latter,  $\text{sign}(\lambda_2)\rho$  corresponds to the second eigenvalue extracted from principal components analysis of the Hessian of the charge density,  $\rho$  (see ref. ([41]) for details). Also included are the corresponding 2D scatter plots, in which each point refers solely to interaction scenarios. Specifically, these represent the total IGM interaction points for  $\delta g_{inter} \leq 0.1$  in the region of  $-0.2 \leq \text{sign}(\lambda_2)\rho \leq 0.2$ . In each system, 35 Å spheres centered on the complexes were used, for providing similar values of grid points and allowing the relative comparison between the Cd complexes. The favorable nature of the Cd-guest interactions is reflected by the asymmetry of the peaks. In all cases the peaks on the positive, destabilizing side of the plot are smaller than the corresponding peaks on the negative, stabilizing side showing that the balance of noncovalent forces in the complex are in overall favoring the complex formation. The reference systems containing Np and Ad molecules display weak stabilizing noncovalent forces such as van der Waals and London dispersion forces with both  $\beta$ - and  $\gamma$ -Cds. These are represented by discrete regions of enhanced interactions (3D isosurfaces) and by solid peaks (2D scatter

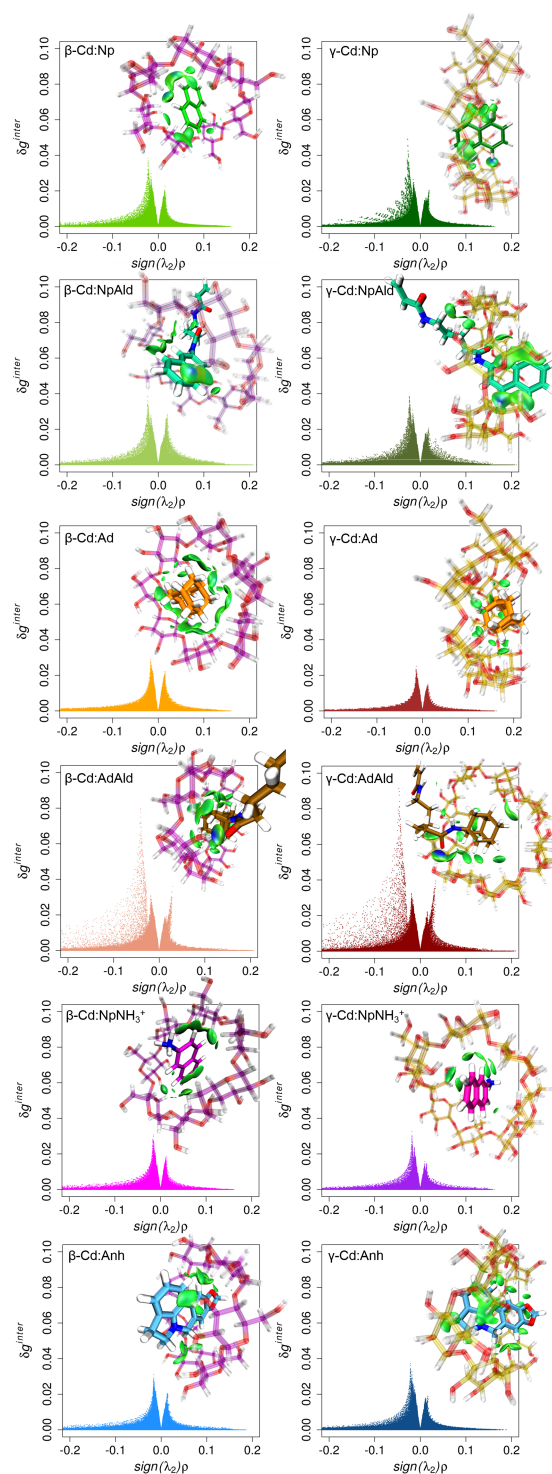


Figure 4.5: A composed view of the IGMPlot isosurfaces and 2D scatter plots for each  $\beta$ - and  $\gamma$ -Cd complex, corresponding to structures in lower energy states (local minima sampled from the PMF profiles). Stabilizing/destabilizing noncovalent interactions are represented in blue/red and van der Waals forces are colored in green (volume cutoff of  $\delta g_{inter} = 0.05$ ; color coding:  $-0.1 \leq \text{sign}(\lambda_2)\rho \leq 0.1$ ).

plots) at  $\text{sign}(\lambda_2)\rho \approx -0.02$ , suggesting some specificity in the nature of binding. This specificity is enhanced by the presence of the Ald substituents. In the Anh systems the van der Waals interactions are similar, although slightly enhanced in  $\gamma\text{-Cd:Anh}$ .

In addition the architectures of the  $\beta\text{-}/\gamma\text{-Cd:Np}$ ,  $\beta\text{-}/\gamma\text{-Cd:NpAld}$ ,  $\beta\text{-}/\gamma\text{-Cd:NpNH}_3^+$  and  $\beta\text{-}/\gamma\text{-Cd:Anh}$  complexes (Figure 4.5) exhibit propensity to establish hydrophobic C-H $\cdots$ C-H interactions and C-H $\cdots\pi$  dispersion interactions. For the former, the C-H bonds belong to the glucopyranose units of Cds and the aromatic rings of the naphthalene backbones. For the C-H $\cdots\pi$  interactions, the glucopyranose units of Cds are the C-H donors and the electron-rich naphthyl rings are the  $\pi$  systems.

These interactions can also be identified in the more intense peaks on the left, at  $\text{sign}(\lambda_2)\rho \approx -0.03$ . Such weak attractive forces have been recognized as important driving forces in the inclusion process of similar systems involving cyclodextrins and aromatic guests ([84–88]).

The latter type have also been observed in more complex systems involving supramolecular carbohydrates and aromatic moieties, such as carbohydrate-binding proteins ([89–92]). The structural predisposition and ability of glucopyranose units for establishing carbohydrate-aromatic interactions has been recently observed and attributed to a favorable parallel stacking geometry ([93–95]).

Typical energies in the range of 6.3–10.5 kJ mol<sup>-1</sup> have been reported in systems involving aliphatic and aromatic C-H groups as hydrogen donor and the C6 aromatic ring as C-H acceptor ([94, 96]).

In Figure 4.5 a clear difference between Ad and AdAld systems can be observed. In both  $\beta\text{-}$  and  $\gamma\text{-Cd:AdAld}$  complexes the aldehydic chain provide a more effective inclusion (Figure 4.1) and desolvation of the adamantyl moiety (see Figure 4.3), thus increasing the adamantyl group-Cd hydrophobic interaction and decreasing the adamantyl moiety-solvent interaction. Due to the polar nature of the Cd hosts, stronger hydrogen-bonding interactions are also established in complexes between AdAld and both  $\beta\text{-}$  and  $\gamma\text{-Cds}$ . In addition to noncovalent forces derived from the interaction between the adamantyl moiety and the methine groups of the Cd cavity, both  $\beta\text{-}$  and  $\gamma\text{-Cd:AdAld}$  complexes are stabilized by a hydrogen bond (corresponding to large volumes with a blue center), between the C=O groups of the Ald chain and the hydroxyl groups present in the Cd larger portals. Water molecules can also significantly affect these Cd-guest interactions, due to variations in the hydrophobic/hydrophilic interactions with the solvent along the association/dissociation of the binding partners.

The hydrogen-bonding is also discriminated in 2D scatter plots, identified by large diffuse peaks with

the respective maxima at  $\text{sign}(\lambda_2)\rho \approx -0.05$ .

The IGM-based model also allows decomposing individual atomic contributions ( $\delta g_{at}$ ), and estimating the impact of a specific Cd or guest atom in the intermolecular region between the binding partners. This complementary scheme is presented in Figure 4.6, in which the atoms of the complex are depicted in a gray-to-red color scheme, depending on the respective contribution to the iso-surfaces of Figure 4.5 (grey if there is no contribution to the interaction and red for the highest relative contribution). This approximation provides an accurate estimation of the contribution (expressed in a percentage score) of each atom in the pro-molecular electron density gradient, presented in the featured peaks of the  $\delta g_{inter}$  2D scatter plots.

From Figure 4.6, different contact patterns are observed, resulting from distinct contributions of the inter-partner atoms, either in the flat iso-surfaces representing the hydrophobic, van der Waals and dispersion interactions or in the well-defined larger volumes (blue center) corresponding to hydrogen bonds. Identifying individual atom contributions in the formation of inclusion complexes is important for understanding the molecular determinants of Cd-guest recognition.

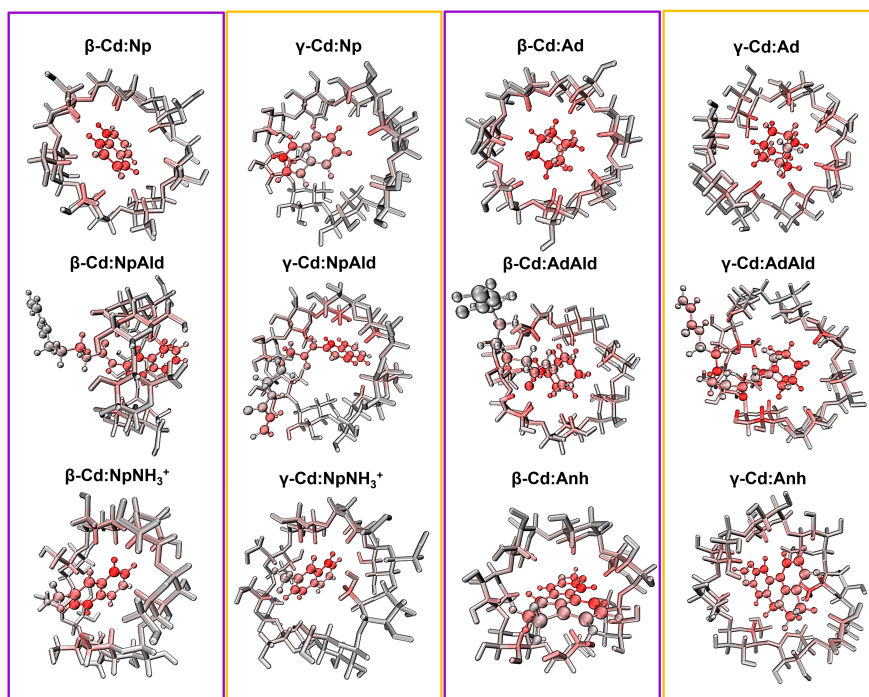


Figure 4.6: An overview of the individual atomic contributions to the Cd-guest noncovalent interactions discriminated in the iso-surfaces included in Figure 4.5. A relative score (%) is attributed to each atom, which is colored using a gray-to-red color gradient, according to this percentage. Gray: no contribution to the noncovalent interaction, red: significant relative contribution to the Cd-guest interaction.

### 4.3 Discussion

Overall, the present work indicates, for each guest, higher binding constants for the  $\beta$ -Cd, with only one exception, Ad. Common sense dictates that this must be dependent on the guest, but other systems ([97]) (see Figure 4.7) have shown the same overall behavior. In this latter work, of experimental

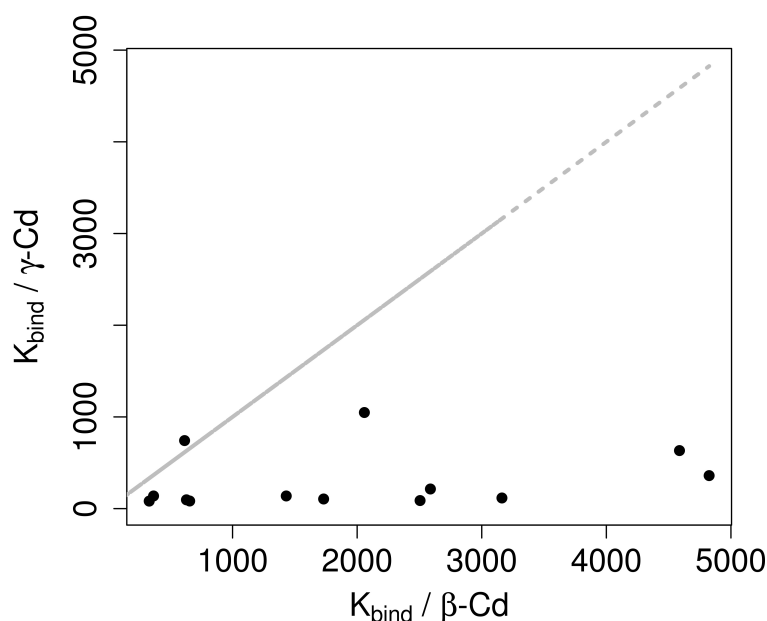


Figure 4.7: Stability constants ( $M^{-1}$ ) extracted from ([97]), showing that 1:1 complexes between  $\beta$ -Cd and several terpenes are, in general, more stable than those with  $\gamma$ -Cd.

nature, again only one exception was found for a set of 14 guests. Naturally, these guests have one thing in common, which is being able to form inclusion complexes with the  $\beta$ -Cd, which limits their size. As such, one is not inspecting a general behavior, rather is looking at the behavior of guests for which the part included in the  $\gamma$ -Cd does not fill the respective cavity.

Why is Ad an exception, forming more stable inclusion complexes with the larger Cd? One observation is that this Cd is more efficient in promoting the desolvation of the guest, while the latter, in turn, induces a strong desolvation of the Cd cavity. Another aspect is that this guest promotes one of the smallest distortions in the larger Cd. Tests conducted at the DFT level in PCM indicate that distortion significantly penalizes binding. This is illustrated in Figure 4.8 for Ad, in both  $\beta$ - and  $\gamma$ -Cd. In the latter, deformation causes an increase in energy of ca.  $90 \text{ kJ mol}^{-1}$ , while host-guest interaction lowers by ca.  $98 \text{ kJ mol}^{-1}$ , with a net decrease of  $\approx 8 \text{ kJ mol}^{-1}$  upon inclusion (this in the order of

magnitude of the PMF well depth). In fact, there is a strong inverse correlation between distortion and

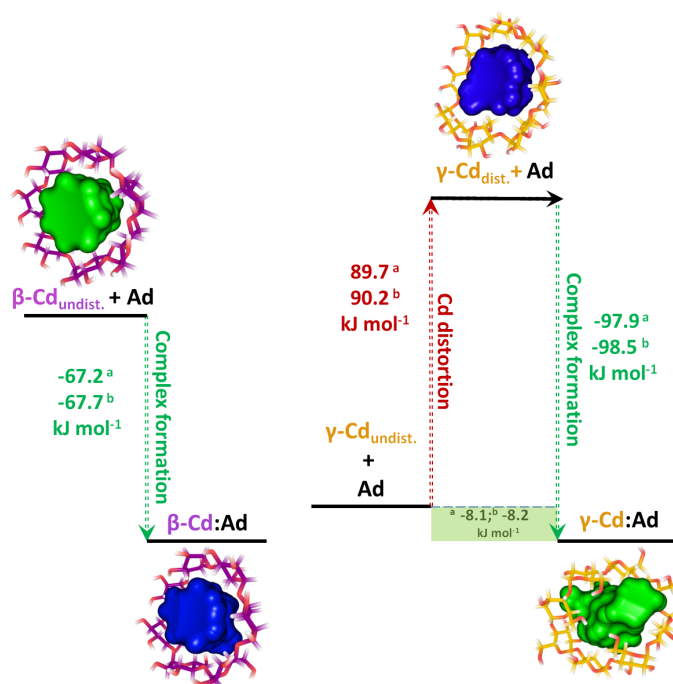


Figure 4.8: Schematic illustration of the proposed thermodynamic cycle corresponding to the formation of 1:1 complexes between  $\beta$ - and  $\gamma$ -Cds and adamantane. The estimated energy differences were estimated using the hybrid DFT TPSS0 level with D3 dispersion corrections and PCM water. The triple-zeta polarized Def2-TZVP (a) and the related Def2-TZVPP (b) with further polarization functions are the two large basis sets used to check the convergence of the energies.

binding constant for the  $\gamma$ -Cd. With no exception, the higher the distortion, the lower is the constant. Distortion is not significant for the  $\beta$ -Cd and the current guests, so this argument does not apply to this Cd. In this case, and as previously remarked, substitution with consequent enlargement of the guest molecule promotes large binding constants.

With regard to desolvation, the pattern is far from clear but observations suggest that a high desolvation of the cavity may correspond to a high constant, while a low desolvation is associated to low constants. Finally, the largest guest considered in this work, and recalling that they are all smaller than the  $\gamma$ -CD cavity, promotes the higher constant in the larger Cd and, still, a high constant in the smaller. Note that, in the former, the size of the guest minimizes distortion.

In summary, it is apparent that host/guest contact and distortion both play an important role in inclusion. The system tends to increase the former, which favors inclusion, at the expense of the latter, which opposes inclusion.

## 4.4 Concluding remarks

Although there exist extensive experimental and theoretical studies concerning Cd complexation, a comprehensive description of the effect of Cd cavity size and conformation on the formation of inclusion complexes, especially at the atomic level, is still lacking. MD simulation and free-energy calculations were used in this work as tools for bridging this gap. Consistent with previous studies, our calculations also suggested that the complexes of  $\gamma$ -Cd are less stable than the  $\beta$ -Cd complexes. The stability of complexes with Np and Ad derivatives were determined and compared with that of the single Np and Ad molecules used as references.

The estimated stability of inclusion complexes between  $\beta$ -Cd and  $\gamma$ -Cd and the model guests, is highly affected by the host conformation, the fit and orientation of the guest into the cavity, the size and nature of the guest moieties and by desolvation effects. As best models, the interactions among  $\beta$ - and  $\gamma$ -Cds and naphthalene, adamantane and also lycorine derivatives are selected.

It was shown that  $\beta$ -Cd is, in general, more effective than  $\gamma$ -Cd in encapsulating Np, Ad and Anh, and that the Cd cavity size difference plays a more important role than the guest size in the stability of the inclusion complexes. The binding constants of  $\beta$ -Cd-based complexes increase monotonically as the size of the guest increases, while those of  $\gamma$ -Cd show higher stability with decreasing degree of substitution. Solvation patterns suggest that the improved stability of the  $\beta$ -Cd complexes as compared with  $\gamma$ -Cd is also due to the higher desolvation degree in both host cavity and guest backbone. The cavity size and propensity to deform has a significant effect on the strength of the interactions, and a series of different findings prove that this phenomenon is the basis for the stability of different Cd-based complexes.

The estimate of the inclusion thermodynamic signatures and binding constants must be complemented with information on the enthalpy penalty associated to collapsed host structures, in order to obtain a reliable description of the binding process.

## References

- [1] Tânia F. G. G. Cova et al. “Drastic Stabilization of Junction Nodes in Supramolecular Structures Based on Host-Guest Complexes”. *Macromolecules* 51.7 (2018), pp. 2732–2741. DOI: [10.1021/acs.macromol.8b00154](https://doi.org/10.1021/acs.macromol.8b00154).
- [2] Tânia FGG Cova et al. “Combining cellulose and cyclodextrins: fascinating designs for materials and pharmaceuticals”. *Frontiers in chemistry* 6 (2018), p. 271.
- [3] R. Sierpe et al. “Construction of 6-thioguanine and 6-mercaptopurine carriers based on  $\beta$ -cyclodextrins and gold nanoparticles”. *Carbohydrate Polymers* 177 (2017), pp. 22–31. ISSN: 0144-8617. DOI: <https://doi.org/10.1016/j.carbpol.2017.08.102>.
- [4] Magdalena Ceborska et al. “Comparative study of molecular recognition of folic acid subunits with cyclodextrins”. *Carbohydrate Polymers* 184 (2018), pp. 47–56. ISSN: 0144-8617. DOI: <https://doi.org/10.1016/j.carbpol.2017.12.031>.
- [5] Elham Einafshar et al. “New cyclodextrin-based nanocarriers for drug delivery and phototherapy using an irinotecan metabolite”. *Carbohydrate Polymers* 194 (2018), pp. 103–110. ISSN: 0144-8617. DOI: <https://doi.org/10.1016/j.carbpol.2018.03.102>.
- [6] Riham Gharib et al. “Liposomes incorporating cyclodextrin-drug inclusion complexes: Current state of knowledge”. *Carbohydrate Polymers* 129.Supplement C (2015), pp. 175–186. ISSN: 0144-8617. DOI: <https://doi.org/10.1016/j.carbpol.2015.04.048>.
- [7] Eva Pinho et al. “Cyclodextrins as encapsulation agents for plant bioactive compounds”. *Carbohydrate Polymers* 101 (2014), pp. 121–135. ISSN: 0144-8617. DOI: <https://doi.org/10.1016/j.carbpol.2013.08.078>.
- [8] Pollyana S.S. Lima et al. “Inclusion of terpenes in cyclodextrins: Preparation, characterization and pharmacological approaches”. *Carbohydrate Polymers* 151 (2016), pp. 965–987. ISSN: 0144-8617. DOI: <https://doi.org/10.1016/j.carbpol.2016.06.040>.
- [9] Qi-Da Hu, Gu-Ping Tang, and Paul K. Chu. “Cyclodextrin-Based Host-Guest Supramolecular Nanoparticles for Delivery: From Design to Applications”. *Accounts of Chemical Research* 47.7 (2014), pp. 2017–2025. DOI: [10.1021/ar500055s](https://doi.org/10.1021/ar500055s).



- [10] Valentina et al. “Linear polymers of  $\beta$  and  $\gamma$ -cyclodextrins with a polyglutamic acid backbone as carriers for doxorubicin”. *Carbohydrate Polymers* 177 (2017), pp. 355–360. ISSN: 0144-8617. DOI: <https://doi.org/10.1016/j.carbpol.2017.08.103>.
- [11] Ruslan R. Kashapov et al. “Controlling the binding of hydrophobic drugs with supramolecular assemblies of  $\beta$ -cyclodextrin”. *Colloids and Surfaces A: Physicochemical and Engineering Aspects* 527 (2017), pp. 55–62. DOI: [10.1016/j.colsurfa.2017.05.026](https://doi.org/10.1016/j.colsurfa.2017.05.026).
- [12] Thorsteinn Loftsson. “Drug solubilization by complexation”. *International Journal of Pharmaceutics* 531.1 (2017), pp. 276–280. DOI: [10.1016/j.ijpharm.2017.08.087](https://doi.org/10.1016/j.ijpharm.2017.08.087).
- [13] Yinjuan Chen et al. “Gas-phase complexation of  $\alpha$ -/ $\beta$ -cyclodextrin with amino acids studied by ion mobility-mass spectrometry and molecular dynamics simulations”. *Talanta* 186 (2018), pp. 1–7. ISSN: 0039-9140. DOI: <https://doi.org/10.1016/j.talanta.2018.04.003>.
- [14] Qiaomei Sun et al. “Mechanism and structure studies of cinnamaldehyde/cyclodextrins inclusions by computer simulation and NMR technology”. *Carbohydrate Polymers* 194 (2018), pp. 294–302. ISSN: 0144-8617. DOI: <https://doi.org/10.1016/j.carbpol.2018.04.055>.
- [15] Francisco Torrens and Gloria Castellano. “Computational Study of Nanosized Drug Delivery from Cyclodextrins, Crown Ethers and Hyaluronan in Pharmaceutical Formulations”. *Current Topics in Medicinal Chemistry* 15.18 (2015), pp. 1901–1913. DOI: [10.2174/156802661566615050614561](https://doi.org/10.2174/156802661566615050614561).
- [16] Petko Ivanov, Emanouil Atanassov, and Carlos Jaime. “Computational study on the conformations of CD38 and inclusion complexes of some lower-size large-ring cyclodextrins”. *Journal of Molecular Structure* 1056.33 (2014), pp. 238–245. DOI: [10.1016/j.molstruc.2013.10.048](https://doi.org/10.1016/j.molstruc.2013.10.048).
- [17] Christopher B. Rodell, Joshua E. Mealy, and Jason A. Burdick. “Supramolecular Guest-Host Interactions for the Preparation of Biomedical Materials”. *Bioconjugate Chemistry* 26.12 (2015), pp. 2279–2289. DOI: [10.1021/acs.bioconjchem.5b00483](https://doi.org/10.1021/acs.bioconjchem.5b00483).
- [18] Iurii Antoniuk et al. “Host-guest interaction and structural ordering in polymeric nanoassemblies: Influence of molecular design”. *International Journal of Pharmaceutics* 531.2 (2017), pp. 433–443. DOI: [10.1016/j.ijpharm.2017.02.061](https://doi.org/10.1016/j.ijpharm.2017.02.061).

- [19] Tânia F. G. G. Cova, Sandra C. C. Nunes, and Alberto A. C. C. Pais. “Free-energy patterns in inclusion complexes: the relevance of non-included moieties in the stability constants”. *Physical Chemistry Chemical Physics* 19.7 (2017), pp. 5209–5221. ISSN: 1463-9076. DOI: [10.1039/C6CP08081B](https://doi.org/10.1039/C6CP08081B).
- [20] Wanda Sliwa and Tomasz Girek, eds. *Cyclodextrins: Properties and Applications*. 1st ed. Germany: Wiley-VCH, 2017.
- [21] Daniel Prochowicz, Arkadiusz Kornowicz, and Janusz Lewiński. “Interactions of Native Cyclodextrins with Metal Ions and Inorganic Nanoparticles: Fertile Landscape for Chemistry and Materials Science”. *Chemical Reviews* 117.22 (2017), pp. 13461–13501. DOI: [10.1021/acs.chemrev.7b00231](https://doi.org/10.1021/acs.chemrev.7b00231).
- [22] Frank Biedermann, Werner M. Nau, and Hans-Jörg Schneider. “The Hydrophobic Effect Revisited-Studies with Supramolecular Complexes Imply High-Energy Water as a Noncovalent Driving Force”. *Angewandte Chemie International Edition* 53.42 (2014), pp. 11158–11171. ISSN: 1521-3773. DOI: [10.1002/anie.201310958](https://doi.org/10.1002/anie.201310958).
- [23] Silvia Angelova et al. “ $\alpha$ -Cyclodextrin: How Effectively Can Its Hydrophobic Cavity Be Hydrated?” *The Journal of Physical Chemistry B* 121.39 (2017), pp. 9260–9267. DOI: [10.1021/acs.jpcc.7b04501](https://doi.org/10.1021/acs.jpcc.7b04501).
- [24] Mahendra Nath Roy et al. “Host-guest inclusion complexes of  $\alpha$  and  $\beta$ -cyclodextrins with  $\alpha$ -amino acids”. *RSC Adv.* 4 (80 2014), pp. 42383–42390. DOI: [10.1039/C4RA07877B](https://doi.org/10.1039/C4RA07877B).
- [25] Corinne LD Gibb and Bruce C Gibb. “Binding of cyclic carboxylates to octa-acid deep-cavity cavitand”. *Journal of computer-aided molecular design* 28.4 (2014), pp. 319–325.
- [26] S. Lu et al. “Cyclodextrin type dependent host-guest interaction mode with phthalocyanine and their influence on photodynamic activity to cancer”. *Carbohydrate Polymers* 148 (2016), pp. 236–242. ISSN: 0144-8617. DOI: <https://doi.org/10.1016/j.carbpol.2016.04.062>.
- [27] M. Fermeglia et al. “Host-guest inclusion complexes between anticancer drugs and  $\beta$ -cyclodextrin: computational studies”. *Carbohydrate Polymers* 53.1 (2003), pp. 15–44. ISSN: 0144-8617. DOI: [https://doi.org/10.1016/S0144-8617\(03\)00011-0](https://doi.org/10.1016/S0144-8617(03)00011-0).

- [28] Adrian Fifere et al. “Theoretical study on  $\beta$ -cyclodextrin inclusion complexes with propiconazole and protonated propiconazole”. *Beilstein journal of organic chemistry* 8 (2012), p. 2191.
- [29] Deepak Kumar et al. “Analysis of Molecular Interaction of Drugs within  $\beta$ -Cyclodextrin Cavity by Solution-State NMR Relaxation”. *The Journal of Physical Chemistry B* 121.13 (2017), pp. 2864–2872. DOI: [10.1021/acs.jpcc.6b11704](https://doi.org/10.1021/acs.jpcc.6b11704).
- [30] Haiyang Zhang et al. “Cooperative Binding of Cyclodextrin Dimers to Isoflavone Analogues Elucidated by Free Energy Calculations”. *The Journal of Physical Chemistry C* 118.13 (2014), pp. 7163–7173. ISSN: 1932-7447. DOI: [10.1021/jp412041d](https://doi.org/10.1021/jp412041d).
- [31] Lingzhi Zhang, Jinping Zhou, and Lina Zhang. “Structure and properties of  $\beta$ -cyclodextrin/cellulose hydrogels prepared in NaOH/urea aqueous solution”. *Carbohydrate Polymers* 94.1 (2013), pp. 386–393. ISSN: 0144-8617. DOI: <https://doi.org/10.1016/j.carbpol.2012.12.077>.
- [32] Lajos Szente et al. “Cyclodextrins: Assessing the Impact of Cavity Size, Occupancy, and Substitutions on Cytotoxicity and Cholesterol Homeostasis”. *Molecules* 23.5 (2018), p. 1228.
- [33] George Pistolis and Ioanna Balomenou. “Cyclodextrin Cavity Size Effect on the Complexation and Rotational Dynamics of the Laser Dye 2,5-Diphenyl-1,3,4-oxadiazole: From Singly Occupied Complexes to Their Nanotubular Self-Assemblies”. *The Journal of Physical Chemistry B* 110.33 (2006), pp. 16428–16438. DOI: [10.1021/jp062003p](https://doi.org/10.1021/jp062003p).
- [34] P. Mura et al. “Effects of the Host Cavity Size and the Preparation Method on the Physicochemical Properties of Ibuprofen-Cyclodextrin Systems”. *Drug Development and Industrial Pharmacy* 25.3 (1999), pp. 279–287. DOI: [10.1081/DDC-100102172](https://doi.org/10.1081/DDC-100102172).
- [35] Carolyn Vargas et al. “Extracavity Effect in Cyclodextrin/Surfactant Complexation”. *Langmuir* 34.20 (2018), pp. 5781–5787. DOI: [10.1021/acs.langmuir.8b00682](https://doi.org/10.1021/acs.langmuir.8b00682).
- [36] Sandro Mecozzi and Jr. Julius Rebek. “The 55% Solution: A Formula for Molecular Recognition in the Liquid State”. *Chemistry - A European Journal* 4.6 (1998), pp. 1016–1022. DOI: [10.1002/\(SICI\)1521-3765\(19980615\)4:6<1016::AID-CHEM1016>3.0.CO;2-B](https://doi.org/10.1002/(SICI)1521-3765(19980615)4:6<1016::AID-CHEM1016>3.0.CO;2-B).
- [37] Sophie Fourmentin et al. “Space filling of  $\beta$ -cyclodextrin and  $\beta$ -cyclodextrin derivatives by volatile hydrophobic guests”. *Beilstein journal of organic chemistry* 9 (2013), p. 1185.

- [38] Chipot. Christophe. “Frontiers in free-energy calculations of biological systems”. *Wiley Interdisciplinary Reviews: Computational Molecular Science* 4.1 (2013), pp. 71–89. DOI: [10.1002/wcms.1157](https://doi.org/10.1002/wcms.1157).
- [39] Qianqian Zhao et al. “Research advances in molecular modeling in cyclodextrins”. *Current Pharmaceutical Design* 23.3 (2017), pp. 522–531.
- [40] Haohao Fu et al. “New Coarse Variables for the Accurate Determination of Standard Binding Free Energies”. *Journal of Chemical Theory and Computation* 13.11 (2017), pp. 5173–5178. DOI: [10.1021/acs.jctc.7b00791](https://doi.org/10.1021/acs.jctc.7b00791).
- [41] Corentin Lefebvre et al. “Accurately extracting the signature of intermolecular interactions present in the NCI plot of the reduced density gradient versus electron density”. *Physical Chemistry Chemical Physics* 19.27 (2017), pp. 17928–17936. ISSN: 1463-9076. DOI: [10.1039/C7CP02110K](https://doi.org/10.1039/C7CP02110K).
- [42] Helmut Ritter. “Superstructures with cyclodextrins: Chemistry and applications”. *Beilstein Journal of Organic Chemistry* 8 (2012), pp. 1303–1304. ISSN: 1860-5397.
- [43] Tingting Cai et al. “Self-healable tough supramolecular hydrogels crosslinked by poly-cyclodextrin through host-guest interaction”. *Carbohydrate Polymers* 193 (2018), pp. 54–61. ISSN: 0144-8617. DOI: <https://doi.org/10.1016/j.carbpol.2018.03.039>.
- [44] E. M. Martin Del Valle. “Cyclodextrins and their uses: a review”. *Process Biochemistry* 39.9 (2004), pp. 1033–1046. ISSN: 1359-5113. DOI: [https://doi.org/10.1016/S0032-9592\(03\)00258-9](https://doi.org/10.1016/S0032-9592(03)00258-9).
- [45] M. D. Altintop et al. “Synthesis and evaluation of naphthalene-based thiosemicarbazone derivatives as new anticancer agents against LNCaP prostate cancer cells”. *Journal of Enzyme Inhibition and Medicinal Chemistry* 31.3 (2016), pp. 410–416. DOI: [10.3109/14756366.2015.1031126](https://doi.org/10.3109/14756366.2015.1031126).
- [46] E Ma et al. “MS-5, a Naphthalene Derivative, Induces the Apoptosis of an Ovarian Cancer Cell Caov-3 by Interfering with the Reactive Oxygen Species Generation.” *Biomolecules & therapeutics* (2018).

- [47] Liang Yan et al. “ $\beta$ -Cyclodextrin-and adamantyl-substituted poly (acrylate) self-assembling aqueous networks designed for controlled complexation and release of small molecules”. *Beilstein journal of organic chemistry* 13 (2017), p. 1879.
- [48] Adela Štimac et al. “Adamantane in drug delivery systems and surface recognition”. *Molecules* 22.2 (2017), p. 297.
- [49] Maxime Grillaud and Alberto Bianco. “Multifunctional adamantane derivatives as new scaffolds for the multipresentation of bioactive peptides”. *Journal of Peptide Science* 21.5 (2014), pp. 330–345. DOI: [10.1002/psc.2719](https://doi.org/10.1002/psc.2719).
- [50] Guy Lamoureux and Graciela Artavia. “Use of the Adamantane Structure in Medicinal Chemistry”. *Current Medicinal Chemistry* 17.26 (2010), pp. 2967–2978. ISSN: 0929-8673/1875-533X. DOI: [10.2174/092986710792065027](https://doi.org/10.2174/092986710792065027).
- [51] Yafei Guo et al. “Inclusion complexes of anhydrolycorine with cyclodextrins: preparation, characterization, and anticancer activity”. *Canadian Journal of Chemistry* 94.6 (2016), pp. 575–582. DOI: [10.1139/cjc-2015-0462](https://doi.org/10.1139/cjc-2015-0462).
- [52] Maomao He et al. “Biological and pharmacological activities of amaryllidaceae alkaloids”. *RSC Adv.* 5 (21 2015), pp. 16562–16574. DOI: [10.1039/C4RA14666B](https://doi.org/10.1039/C4RA14666B).
- [53] S. Kumar et al. “The Weighted Histogram Analysis Method for Free-Energy Calculations on Biomolecules .1. The Method”. *Journal of Computational Chemistry* 13.8 (1992), pp. 1011–1021. ISSN: 0192-8651.
- [54] M. Souaille and B. Roux. “Extension to the weighted histogram analysis method: combining umbrella sampling with free energy calculations”. *Computer Physics Communications* 135.1 (2001), pp. 40–57. ISSN: 0010-4655.
- [55] P. Virnau and M. Muller. “Calculation of free energy through successive umbrella sampling”. *Journal of Chemical Physics* 120.23 (2004), pp. 10925–10930. ISSN: 0021-9606.
- [56] Haiyang Zhang et al. “Molecular Recognition in Different Environments:  $\beta$ -Cyclodextrin Dimer Formation in Organic Solvents”. *The Journal of Physical Chemistry B* 116.42 (2012), pp. 12684–12693. ISSN: 1520-6106. DOI: [10.1021/jp308416p](https://doi.org/10.1021/jp308416p).

- [57] Ruyin Cao and Shanshan Wu. “In silico properties characterization of water-soluble  $\gamma$ -cyclodextrin bi-capped C60 complex: Free energy and geometrical insights for stability and solubility”. *Carbohydrate Polymers* 124.Supplement C (2015), pp. 188–195. ISSN: 0144-8617. DOI: <https://doi.org/10.1016/j.carbpol.2015.02.014>.
- [58] G. M. Torrie and J. P. Valleau. “Monte-Carlo Free-Energy Estimates Using Non-Boltzmann Sampling - Application to Subcritical Lennard-Jones Fluid”. *Chemical Physics Letters* 28.4 (1974), pp. 578–581. ISSN: 0009-2614.
- [59] G. M. Torrie and J. P. Valleau. “Nonphysical sampling distributions in Monte Carlo free-energy estimation: Umbrella sampling”. *Journal of Computational Physics* 23.2 (1977), pp. 187–199. ISSN: 0021-9991. DOI: [https://doi.org/10.1016/0021-9991\(77\)90121-8](https://doi.org/10.1016/0021-9991(77)90121-8).
- [60] Huan-Xiang Zhou and Michael K. Gilson. “Theory of Free Energy and Entropy in Noncovalent Binding”. *Chemical Reviews* 109.9 (2009), pp. 4092–4107. ISSN: 0009-2665. DOI: [10.1021/cr800551w](https://doi.org/10.1021/cr800551w).
- [61] Djurre H. De Jong et al. “Determining equilibrium constants for dimerization reactions from molecular dynamics simulations”. *Journal of Computational Chemistry* 32.9 (2011), pp. 1919–1928. ISSN: 0192-8651. DOI: [10.1002/jcc.21776](https://doi.org/10.1002/jcc.21776).
- [62] Enguerran Vanquelef et al. “R.E.D. Server: a web service for deriving RESP and ESP charges and building force field libraries for new molecules and molecular fragments”. *Nucleic Acids Research* 39.2 (2011), W511–W517. DOI: [10.1093/nar/gkr288](https://doi.org/10.1093/nar/gkr288).
- [63] Berk Hess et al. “GROMACS 4: Algorithms for highly efficient, load-balanced, and scalable molecular simulation”. *Journal of Chemical Theory and Computation* 4.3 (2008), pp. 435–447. ISSN: 1549-9618.
- [64] David van der Spoel, Paul J. van Maaren, and Carl Caleman. “GROMACS molecule and liquid database”. *Bioinformatics* 28.5 (2012), pp. 752–753. DOI: [10.1093/bioinformatics/bts020](https://doi.org/10.1093/bioinformatics/bts020).
- [65] Kresten Lindorff-Larsen et al. “Improved side-chain torsion potentials for the Amber ff99SB protein force field”. *Proteins: Structure, Function, and Bioinformatics* 78.8 (2010), pp. 1950–1958. DOI: [10.1002/prot.22711](https://doi.org/10.1002/prot.22711).

- [66] Christine Cézard et al. “Molecular dynamics studies of native and substituted cyclodextrins in different media: 1. Charge derivation and force field performances”. *Physical Chemistry Chemical Physics* 13.33 (2011), pp. 15103–15121. DOI: [10.1039/C1CP20854C](https://doi.org/10.1039/C1CP20854C).
- [67] Viktor Hornak et al. “Comparison of multiple amber force fields and development of improved protein backbone parameters”. *Proteins-Structure Function and Bioinformatics* 65.3 (2006), pp. 712–725. ISSN: 0887-3585.
- [68] Trang Truc Nguyen, Man Hoang Viet, and Mai Suan Li. “Effects of Water Models on Binding Affinity: Evidence from All-Atom Simulation of Binding of Tamiflu to A/H5N1 Neuraminidase”. *The Scientific World Journal* 2014 (2014), pp. 1–14. ISSN: 1537-744X. DOI: [10.1155/2014/536084](https://doi.org/10.1155/2014/536084).
- [69] Jirasak Wong-ekkabut and Mikko Karttunen. “The good, the bad and the user in soft matter simulations”. *Biochim. Biophys. Acta* 1858.10 (2016), pp. 2529–2538. DOI: [10.1016/j.bbamem.2016.02.004](https://doi.org/10.1016/j.bbamem.2016.02.004).
- [70] B. Hess et al. “LINCS: A linear constraint solver for molecular simulations”. *Journal of Computational Chemistry* 18.12 (1997), pp. 1463–1472. ISSN: 0192-8651.
- [71] Jochen S. Hub, Bert L. de Groot, and David van der Spoel. “*q<sub>w</sub>ham*-A Free Weighted Histogram Analysis Implementation Including Robust Error and Autocorrelation Estimates”. *Journal of Chemical Theory and Computation* 6.12 (2010), pp. 3713–3720. ISSN: 1549-9618. DOI: [10.1021/ct100494z](https://doi.org/10.1021/ct100494z).
- [72] Fangqiang Zhu and Gerhard Hummer. “Convergence and error estimation in free energy calculations using the weighted histogram analysis method”. *Journal of Computational Chemistry* 33.4 (2012), pp. 453–465. DOI: [10.1002/jcc.21989](https://doi.org/10.1002/jcc.21989).
- [73] Xavier Daura et al. “Peptide Folding: When Simulation Meets Experiment”. *Angewandte Chemie International Edition* 38.1-2 (2004), pp. 236–240. DOI: [10.1002/\(SICI\)1521-3773\(19990115\)38:1/2<236::AID-ANIE236>3.0.CO;2-M](https://doi.org/10.1002/(SICI)1521-3773(19990115)38:1/2<236::AID-ANIE236>3.0.CO;2-M).
- [74] Frank Neese. “The ORCA program system”. *Wiley Interdisciplinary Reviews: Computational Molecular Science* 2.1 (2012), pp. 73–78.

- [75] Jianmin Tao et al. “Climbing the density functional ladder: Nonempirical meta-generalized gradient approximation designed for molecules and solids”. *Physical Review Letters* 91.14 (2003), p. 146401.
- [76] Florian Weigend and Reinhart Ahlrichs. “Balanced basis sets of split valence, triple zeta valence and quadruple zeta valence quality for H to Rn: Design and assessment of accuracy”. *Physical Chemistry Chemical Physics* 7.18 (2005), pp. 3297–3305.
- [77] Lars Goerigk and Stefan Grimme. “A thorough benchmark of density functional methods for general main group thermochemistry, kinetics, and noncovalent interactions”. *Physical Chemistry Chemical Physics* 13.14 (2011), pp. 6670–6688.
- [78] Stefan Grimme, Stephan Ehrlich, and Lars Goerigk. “Effect of the damping function in dispersion corrected density functional theory”. *Journal of computational chemistry* 32.7 (2011), pp. 1456–1465.
- [79] R. Cammi and J. Tomasi. “Nonequilibrium solvation theory for the polarizable continuum model: A new formulation at the SCF level with application to the case of the frequency-dependent linear electric response function”. *International Journal of Quantum Chemistry* 56.29 (1995), pp. 465–474. DOI: [10.1002/qua.560560850](https://doi.org/10.1002/qua.560560850).
- [80] Uma R Fogueri et al. “The melatonin conformer space: benchmark and assessment of wave function and DFT methods for a paradigmatic biological and pharmacological molecule”. *The Journal of Physical Chemistry A* 117.10 (2013), pp. 2269–2277.
- [81] Pettersen Eric et al. “UCSF Chimera - A visualization system for exploratory research and analysis”. *Journal of Computational Chemistry* 25.13 (2004), pp. 1605–1612. ISSN: 1096-987X. DOI: [10.1002/jcc.20084](https://doi.org/10.1002/jcc.20084).
- [82] V. G. Avakyan et al. “The role of intra- and intermolecular hydrogen bonds in the formation of beta-cyclodextrin head-to-head and head-to-tail dimers. The results of ab initio and semiempirical quantum-chemical calculations”. *Russian Chemical Bulletin* 50.2 (2001), pp. 206–216. ISSN: 1066-5285.

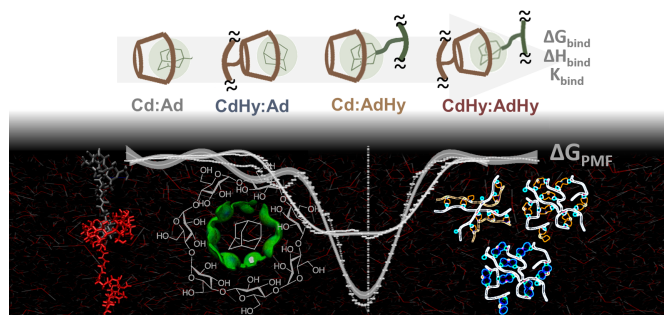


- [83] D. P. Tieleman, D. van der Spoel, and H. J. C. Berendsen. “Molecular dynamics simulations of dodecylphosphocholine micelles at three different aggregate sizes: Micellar structure and chain relaxation”. *Journal of Physical Chemistry B* 104.27 (2000), pp. 6380–6388. ISSN: 1089-5647.
- [84] Kazuaki Harata. “The Structure of the Cyclodextrin Complex. XII. Crystal Structure of  $\alpha$ -Cyclodextrin-1-Phenylethanol (1:1) Tetrahydrate”. *Bulletin of the Chemical Society of Japan* 55.5 (1982), pp. 1367–1371. DOI: [10.1246/bcsj.55.1367](https://doi.org/10.1246/bcsj.55.1367).
- [85] Kazuaki Harata et al. “The Structure of the Cyclodextrin Complex. XVI. Crystal Structure of Heptakis(2,3,6-tri-O-methyl)- $\beta$ -cyclodextrin-p-Iodophenol (1:1) Complex Tetrahydrate”. *Bulletin of the Chemical Society of Japan* 56.6 (1983), pp. 1732–1736. DOI: [10.1246/bcsj.56.1732](https://doi.org/10.1246/bcsj.56.1732).
- [86] Kazuaki Harata. “The X-ray structure of an inclusion complex of heptakis(2,6-di-O-methyl)- $\beta$ -cyclodextrin with 2-naphthoic acid”. *J. Chem. Soc., Chemical Communications* (6 1993), pp. 546–547. DOI: [10.1039/C39930000546](https://doi.org/10.1039/C39930000546).
- [87] Kazuaki Harata. “Complex formation of hexakis (2, 6-di-O-methyl)- $\alpha$ -cyclodextrin with substituted benzenes in aqueous solution”. *Journal of inclusion phenomena and molecular recognition in chemistry* 13.1 (1992), pp. 77–86.
- [88] Thomas Steiner and Katrin Geller. “Aromatic molecules included into and contacting the outer surface of cyclomaltohexaose ( $\alpha$ -cyclodextrin): crystal structure of  $\alpha$ -cyclodextrin-(benzyl alcohol)2-hexahydrate”. *Carbohydrate Research* 260.1 (1994), pp. 27–38. ISSN: 0008-6215. DOI: [https://doi.org/10.1016/0008-6215\(94\)80019-7](https://doi.org/10.1016/0008-6215(94)80019-7).
- [89] Mirzaei Masoud et al. “On the Importance of C-/ $\pi$  and C-H $\cdots$ H-C Interactions in the Solid State Structure of 15-Lipoxygenase Inhibitors Based on Eugenol Derivatives”. *ChemPhysChem* 16.10 (2015), pp. 2260–2266. DOI: [10.1002/cphc.201500287](https://doi.org/10.1002/cphc.201500287).
- [90] Vojtěch Spiwok. “CH/ $\pi$  interactions in carbohydrate recognition”. *Molecules* 22.7 (2017), p. 1038.

- [91] M. Muraki. “The Importance of CH/ $\pi$ ; Interactions to the Function of Carbohydrate Binding Proteins”. *Protein Peptide Letters* 9.3 (2002), pp. 195–209. ISSN: 0929-8665/1875-5305. DOI: [10.2174/0929866023408751](https://doi.org/10.2174/0929866023408751).
- [92] Arijit Banerjee et al. “Molecular bases of cyclodextrin adapter interactions with engineered protein nanopores”. *Proceedings of the National Academy of Sciences* 107.18 (2010), pp. 8165–8170. ISSN: 0027-8424. DOI: [10.1073/pnas.0914229107](https://doi.org/10.1073/pnas.0914229107).
- [93] Ester Jimenez-Moreno et al. “A thorough experimental study of CH/ $\pi$  interactions in water: quantitative structure-stability relationships for carbohydrate/aromatic complexes”. *Chem. Sci.* 6 (11 2015), pp. 6076–6085. DOI: [10.1039/C5SC02108A](https://doi.org/10.1039/C5SC02108A).
- [94] Motohiro Nishio et al. “CH- $\pi$  hydrogen bonds in biological macromolecules”. *Physical Chemistry Chemical Physics* 16 (25 2014), pp. 12648–12683. DOI: [10.1039/C4CP00099D](https://doi.org/10.1039/C4CP00099D).
- [95] Motohiro Nishio. “CH/ $\pi$  hydrogen bonds in crystals”. *CrystEngComm* 6 (27 2004), pp. 130–158. DOI: [10.1039/B313104A](https://doi.org/10.1039/B313104A).
- [96] Motohiro Nishio. “The CH/ $\pi$  hydrogen bond in chemistry. Conformation, supramolecules, optical resolution and interactions involving carbohydrates”. *Physical Chemistry Chemical Physics* 13 (31 2011), pp. 13873–13900. DOI: [10.1039/C1CP20404A](https://doi.org/10.1039/C1CP20404A).
- [97] A. Ciobanu, D. Landy, and S. Fourmentin. “Complexation efficiency of cyclodextrins for volatile flavor compounds”. *Food Research International* 53.1 (2013), pp. 110–114. ISSN: 0963-9969. DOI: <https://doi.org/10.1016/j.foodres.2013.03.048>.



# Chapter 5



## Network Stabilization

The critical role of solvent, enthalpic and entropic contributions in complexes between different hyaluronic acid derivatives bearing monomeric  $\beta$ -cyclodextrin and adamantene moieties are assessed combining the previously designed free-energy oriented method and a recently proposed density-based noncovalent interaction analysis. This establishes the relevant thermodynamics signatures and identifies the stabilizing/destabilizing noncovalent interactions within the complexes used as models for the junction points. It is observed that structural variations promote major changes in the thermodynamic variables. The presence of the amphiphilic chains emphasizes inclusion and drastically increases the binding constant (to ca.  $10^{28}$ ). A comprehensive thermodynamic scheme is thus provided, in which host-guest interactions, host conformation and solvation play the leading roles. These results have direct implications for the rational design of supramolecular materials with specific properties based on these host-guest systems.

### 5.1 General aspects

The interaction of Cd with guest molecules has been extensively investigated[1], but there is no assessment of the effect of amphiphilic substituents when moving towards supramolecular Cd assemblies, in which host-guest inclusion complexes act as junction nodes in transient networks. [2] A quantitative understanding of the effect of substitution on the complex stability is still missing. [3] The effect of polymer pendant modification over the thermodynamic signatures and association/binding

constants of the partner junction sites, has not been addressed so far, in the context of network stabilization. [4] In the continuing effort to develop improved nanostructure-based networks constructed from polysaccharides and using noncovalent interactions, the specific recognition between Cd and Ad, each grafted to a Hy side chain is investigated. This is done by characterizing the energy patterns associated with the formation of 1:1 inclusion complexes between these hyaluronic acid derivatives bearing monomeric Cd and Ad moieties. [4, 5] Such an approach is expected to provide improved networks with properties comparable to those based on other polysaccharide derivatives. [4, 6–8] The key factors affecting the thermodynamic signatures of inclusion complexes between Hy derivatives are presented along with a precise first-principles description of the NCI including their spatial distribution features. The analysis of the NCI is carried out using the recently developed Independent Gradient Method of Lefebvre and co-workers. [9] This method allows the visualization of regions of low charge density corresponding to stabilising/destabilising NCI, based on the analysis of the electronic charge density of the interacting molecules and its gradients, similar to the original NCI method of Johnson et al. [10, 11]. A novel feature is that it permits a quantitative comparison of the strength of NCI interactions through the calculation of the IGM descriptor,  $\delta_g$ , which corresponds directly to the charge density gradient(s) in real-space (for details see refs. [4, 9]).

## 5.2 Model and computational details

Figure 5.1 presents a schematic illustration of the targeted networks in which Cd/Ad complexes play the role of junction points between the Hy chains. [4] These junction points influence the long time dynamics, governed by the degree of substitution, the number of junction points per chain, and the motion of network chains (see e.g. [12, 13]). In the present work, the key parameters controlling the dynamics and stability of the inclusion complexes used as building block for noncovalent networks are elucidated. Investigation of the relative importance of the structural components of the complexes is performed by varying the structural complexity as the presence of the Hy chain in both host and guest molecules may influence the thermodynamics of inclusion.

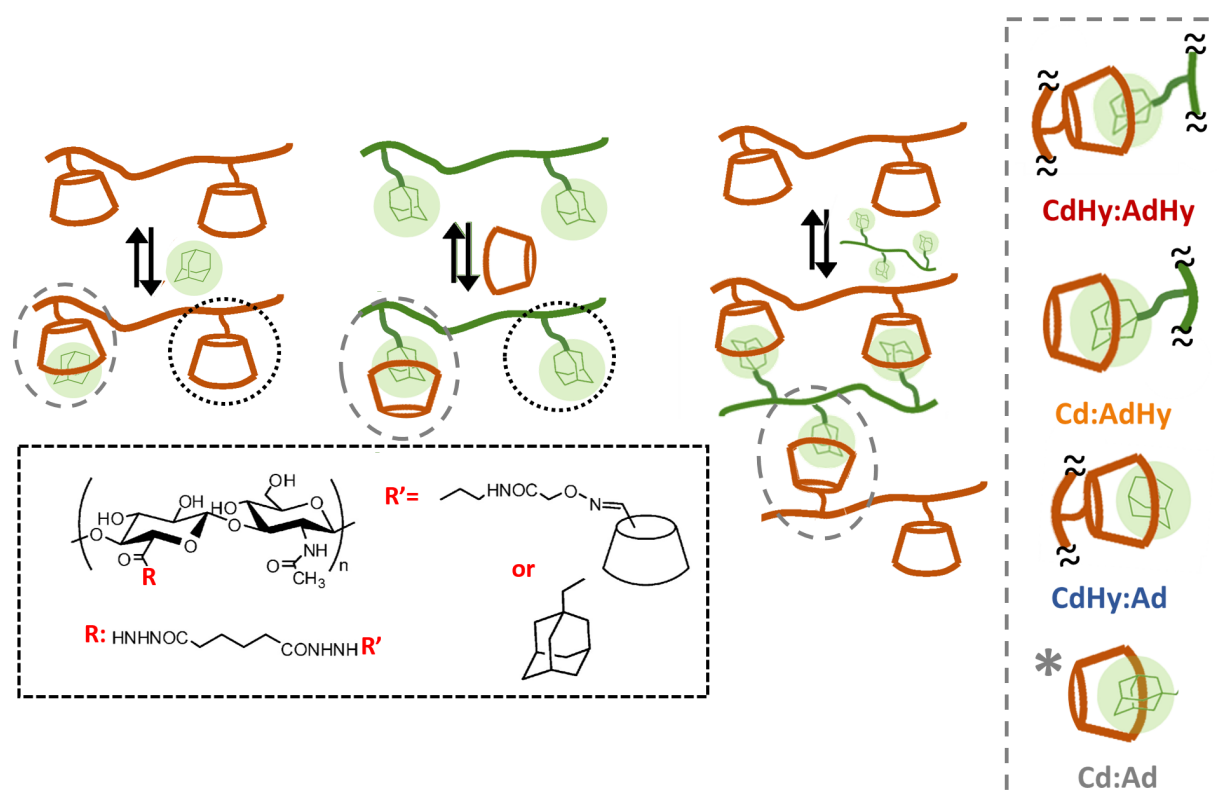


Figure 5.1: Schematic representation of the system components including (top) the targeted networks in which Cd/Ad complexes play the role of junction points and (bottom) the chemical structure of the hyaluronic acid derivatives. Also included (right) are the inclusion complexes used as models of the network junction points, with increasing structural complexity. The Cd:Ad complex is used as a reference system. Reproduced with permission from ref. [4]. Copyright (2018) American Chemical Society.

### 5.2.1 Binding constants

Experimental studies on host-guest interactions usually provide information on stoichiometry and affinity, and/or estimates of free-energy, enthalpy, entropy changes and heat capacity. Such changes in binding interactions are rarely identified as changes in affinity as a consequence of the enthalpy-entropy compensation, from which the enthalpy released from an improved favorable association is offset by an entropic penalty. However, such changes can be inspected by measuring the binding enthalpy. The thermodynamics of inclusion is described essentially by two components of the standard Gibbs free-energy,  $\Delta G_{bind}^0$ , the standard enthalpy,  $\Delta H_{bind}^0$ , and the standard entropy  $\Delta S_{bind}^0$ , which are determined for the entire inclusion process.[4] The binding affinity is derived numerically from the association constant,  $K_{bind}$ , defined in Eq.( 2.22), Chapter 2 (further details are given in refs. [3, 4,

14]). The interval over which host and guest molecules associate and dissociate provides the limits of integration. Eq.(2.22) weighs each value of the inclusion coordinate and the complex volume, established on the basis of the COM positioning related to each Ad backbone inside the cavity. The values of  $K_{bind}$  for the complexes between the hyaluronic acid derivatives are computed using a cylindrical approximation [3]. This approach allows determination of the available volume for the Ad/AdHy guests upon inclusion. This volume is constrained to a small cylinder able to sample most of the movements of guest molecules along the  $xy$  plane of the Cd cavity. The PMF is thus defined in the cylindrical region where the  $\xi_z$  coordinate is oriented along the axis of the cavity and the cylinder. Integrating the PMF over  $z$  is equivalent to integrating over the whole cylinder. It is also possible to calculate the standard free-energy of binding,  $\Delta G_{bind}^0$ , the standard enthalpy,  $\Delta H_{bind}^0$ , and entropy  $T\Delta S_{bind}^0$  (see Chapter 2).

### 5.2.2 Charge density interaction analysis

Investigation of the NCI within the Cd/Ad complexes was carried out with the IGM[9] as implemented in the IGMPLOT software (version 1.0). The IGM depends on the topological characteristics of the electronic charge density,  $\rho$ , of the system under study. The method employs, in addition to  $\rho$ , quantities related to the first and second derivatives of the density. The IGM descriptor  $\delta g^{inter}$  is given by the difference between the first derivatives of the charge densities for the total system. Further details on the NCI analysis are given in Chapter 2 and refs. [4, 9]. IGMPLOT uses pre-computed atomic charge densities to construct a pro-molecular density which although differing from the relaxed bonded density can be shown to have a minimal effect on the NCI's since very little relaxation of the charge density occurs in these extremely low-density regions following covalent bond formation. This has the added benefit of being much faster for large systems where first-principles calculation of electronic charge densities would be computationally demanding. Furthermore, decomposition into fragment densities is trivial for the pro-molecular approach but can be problematic with first-principles electronic structure methods. Although it is possible to identify NCI regions using the value of  $\delta g^{inter}$  it is necessary to progress to the second derivative (Laplacian) of the density  $\nabla^2\rho$  in order to differentiate between types (favorable/unfavorable) of NCI. When the Laplacian is decomposed

into its three eigenvalues of maximal variation,  $\nabla^2\rho = \lambda_1 + \lambda_2 + \lambda_3$  ( $\lambda_1 \leq \lambda_2 \leq \lambda_3$ ), it is found that the sign and magnitude of the second eigenvalue provides information on whether an interaction is bonding/stabilizing ( $\lambda_2 < 0$ ) or non-bonding/destabilizing ( $\lambda_2 > 0$ ). Weak NCI such as van der Waals forces are associated with  $\text{sign}(\lambda_2)\rho$  approaching zero whilst stronger interactions such as hydrogen bonds will display larger (negative) values of  $\text{sign}(\lambda_2)\rho$ .

## 5.3 Computational methodology

### 5.3.1 System components and molecular dynamics simulation setup

The starting geometries of Hy derivatives (Figure 5.1) were constructed using Pymol (Version 1.7.7.2) and optimized with the semi-empirical Antechamber/SQM method. Partial charges were generated using the R. E. D. D. Server. [15] The initial coordinates of the Cd backbone were extracted from the RCSB protein data bank (PDB code: 1DMB). MD simulations were performed with the GROMACS package (version 4.6.5) [16, 17] using the all-atom amber99sb [18, 19] forcefield to describe both host and guest molecules. Aqueous solvation was modelled using the TIP3P water model. Periodic boundary conditions were used in combination with a NPT ensemble. A coupling constant of 0.5 ps was employed to maintain the temperature at 300 K and a coupling constant of 1 ps was applied to keep the pressure at 1 bar. Prior to each production run, an equilibration of 500 ps in which the pressure is maintained at 1 bar with the Berendsen barostat was performed. The box size was kept unchanged with no pressure coupling, during the production runs. A cutoff of 0.9 nm was used for calculating the Lennard-Jones interactions. Electrostatic interactions were evaluated using the PME method. [14, 20] Constraints were applied for bond lengths of host and guest molecules with the LINCS algorithm. [21] Further details of the simulation procedure are described in Refs. [3, 14]. In each system, the Cd backbone was centred in the simulation box with the cavity axis of Cd parallel to the  $z$ -axis. Each system was solvated with ca. 13000 water molecules in a cubic box of  $7.5 \times 7.5 \times 7.5$  nm. After equilibration, a periodic pulling simulation was carried out allowing the distance to be larger than half the box size, to modulate the formation of 1:1 complexes.



### 5.3.2 Biasing procedure

The fundamental steps for optimizing the procedure in (i) umbrella sampling, (ii) construction of the PMF profiles and (iii) the analysis of the thermodynamic aspects of inclusion were already designed in a previous work [3], in which the modulation of Cd-based inclusion complexes and the identification of free-energy patterns were carried out, by imposing different guest substituents on a naphthalene backbone. In the present work, a series of initial configurations were generated, each corresponding to a location within which the adamantane moiety evolves towards inclusion in, and then separates from the host molecule (Cd and CdHy), using an umbrella biasing potential. This restraint allows the guest (Ad and AdHy) to sample the configurational space in a defined region along the inclusion pathway. Specifically, the reaction coordinate  $\xi_z$  is set as the distance in the  $z$  direction between the centre of mass (COM) of the carbon atoms of the Ad backbone and that of the central glycosidic oxygen (GO) atoms of Cd. In each system, the Cd backbone is centred in the simulation box with the cavity axis of Cd parallel to the  $z$ -axis. The COM of the GO atoms of the Cd backbone was harmonically restrained with an isotropic force constant of  $1000 \text{ kJ mol}^{-1} \text{ nm}^{-1}$  and used as an immobile reference. A steering force of  $2000 \text{ kJ mol}^{-1} \text{ nm}^{-1}$  was applied to the COM of the carbon atoms of the Ad backbone for pulling the guest molecule through the Cd cavity from the secondary to the primary portal, along the  $z$ -axis over 480 ps and with a pulling rate of  $0.01 \text{ nm ps}^{-1}$ . The results from the pulling process were used both to establish the initial configurations and to estimate the force constants to be applied in each window in the actual umbrella sampling (for details see Ref. [3]). The initial ( $\xi_i$ ) and final ( $\xi_f$ ) values of the reaction coordinate were set to  $\xi_i = 1.5 \text{ nm}$  and  $\xi_f = -2.0 \text{ nm}$  for systems containing the natural Ad moiety, and  $\xi_i = 1.0 \text{ nm}$  and  $\xi_f = -3.5$  for systems with AdHy guest, respectively. The guest molecules were sampled approximately 3.5 and 4.5 nm covering the entire  $[\xi_i, \xi_f]$  intervals. In these intervals ca. 120 adjacent windows were selected, with an imposed distance of 0.03 nm between adjacent positions, and were used as starting configurations for umbrella sampling simulations. All the systems regarding the hyaluronic derivatives were inspected and analyzed following this scheme.

### 5.3.3 Construction of the free-energy profiles

In order to calculate the PMF for each system, multiple simulations were performed corresponding to adjacent umbrella windows, using different position values of  $\xi_z$  for the harmonic force centre. The mean force, as a function of  $\xi_z$  position, was calculated in each window, and potentials were derived using an unbiasing procedure. [3] Those potentials were combined using a periodic version of WHAM [22]), which minimizes the discrepancy between each umbrella window, in regions where the windows overlap. The PMF profiles were established as a function of the inclusion coordinate. The more negative is the value of the free-energy ( $\Delta G_{PMF}$ ), the more favorable the interaction. The bootstrap procedure of trajectories based on umbrella histograms was used to calculate the statistical uncertainties from the variance of the PMFs. [3, 4, 23]

### 5.3.4 Equilibrium, references and energy decomposition

In order to establish appropriate references for free-energy calculations and subsequent energy decomposition, 10 independent simulations were performed, corresponding to the equilibrium states of the complexes and the completely separate state between host and guest molecules. At equilibrium, the Ad moiety or the Hy amphiphilic chain are included in the Cd cavity. The equilibrium properties, structure and dynamics of these systems were calculated over the 5 ns simulation runs after the systems were equilibrated for 500 ps. A relevant aspect that still obscures the rationalization of the experimentally observed enthalpy and entropy parameters is the fact that both are global terms, composed by several individual contributions. It has been shown [3, 14] that the rationale for enthalpy optimization is essentially based on the misleading premise that the measured observed enthalpy is governed by direct host-guest interactions. This simplistic assumption neglects other important factors that affect the dynamics and complexity of host-guest binding and the respective thermodynamic attributes, including host and guest conformational changes, and solvation/desolvation effects. A detailed analysis of the enthalpy change (Eq.(5.1)) can be performed for simulations in the equilibrium state (corresponding to systems containing the inclusion complexes and systems in which the host and guest molecules are dissociated), by estimating the van der Waals contributions, and decompos-

ing the electrostatic components. However, in the GROMACS package the latter interactions are evaluated using the particle mesh Ewald (PME) method, which combines the long-range energies for the pair-pair contributions (host-guest (HG), host-solvent (HS), guest-solvent (GS), host-host (HH), guest-guest (GG), and solvent-solvent (SS)) into a global expression for the reciprocal sum. The latter can be further decomposed by re-running the reference systems (complexes and free components) with different charge layouts, as described in Refs. [3, 14]. The global enthalpy is decomposed in individual contributions as follows,

$$\Delta H = \Delta H_H + \Delta H_G + \Delta H_{HH} + \Delta H_{GG} + \Delta H_{HG} + \Delta H_{HS} + \Delta H_{GS} + \Delta H_{SS} \quad (5.1)$$

$\Delta H_H$  and  $\Delta H_G$  refer to bonded interactions, including the bond and dihedral angles. The other six terms correspond to intra- and intermolecular non-bonded interactions. As the bond lengths are constrained, and the bond lengths and angles in the rigid water model TIP3P are fixed during the simulations, the bond stretching terms of host and guest molecules equals to zero and the bonded interactions do not exist. Lennard-Jones and Coulomb contributions are summed for the estimation of energy terms corresponding to non-bonded interactions.

### 5.3.5 NCI calculations

Cartesian coordinates of the minima in the calculated PMF were taken from the MD simulations of all systems described above. After removal of solvent the complexes were split into their host and guest components and analysis of noncovalent interactions between the components analysed using version 1.0 of the IGMPLOT software.[9] Spatial representations of the NCI were obtained by plotting isosurface volumes for the  $\delta g^{inter}$  coloured by the value of  $sign(\lambda_2)\rho$  at each point on the surface, indicating both the extent and (de)stabilizing nature of the interactions. UCSF Chimera version 1.12 was used for the preparation of all isosurface graphics.[24] Whilst these plots are able to provide a rapid qualitative overview of the NCI, it can be difficult to clearly detect differences between two systems. For this reason the isosurface plots were complimented by graphical plots of the same two descriptors which permit much better quantitative analysis and comparison of the types and strengths

of NCI within the various complexes.

## 5.4 Results and discussion

### 5.4.1 Free-energy profiles and favorable interactions

In the following, the analysis of PMF profiles presented in Figures 5.2 and 5.3 permits direct comparison between the different systems. The inclusion complex between natural  $\beta$ -Cd and Ad serves as a reference, while the substituted host and guest molecules are used to assess the different features that are imposed. From Figures 5.2 and 5.3 it can be seen that substituents clearly affect the inclusion process and the interaction behaviour, as indicated by the different shapes and well depths. Also included in Figures 5.2 and 5.3 are the representative 3D IGM isosurfaces showing areas of low charge density corresponding to stabilizing/destabilizing NCI between host and guest molecules. In these 3D molecular images a volume cut-off of  $\delta g_{inter} = 0.05$  is used and the colour coding corresponds to the range of  $-0.1 \leq sign(\lambda_2)\rho \leq 0.1$ . In the latter,  $sign(\lambda_2)\rho$  is the second eigenvalue obtained from principle components analysis of the Hessian of the charge density,  $\rho$ . [9]

Table 5.1 summarizes the main descriptive parameters of the PMF profiles and includes, for each system, the minimum depth and respective position, and the width at half height. The range of profile depths is 28-165 kJ mol<sup>-1</sup>, with the extreme values corresponding to the reference system, Cd:Ad, with non-substituted molecules and the system with both host and guest bearing the polymer chain, CdHy:AdHy. The latter is almost 6 times deeper than for the reference system. It is clear that these substituents have a significant effect on the PMF profile, with tendency to make it deeper relative to that of non-substituted components.

Examining the PMF profiles in more detail, and considering the most prevalent conformations in the equilibrium state, it is also informative to investigate the binding in the present host-guest systems using non-empirical methods depending on their electronic charge densities, in order to decouple the types of interaction and rationalize the respective strengths. In the reference system, Figure 5.2 (bottom, A), since both molecules are neutral, the only form of interaction expected between host

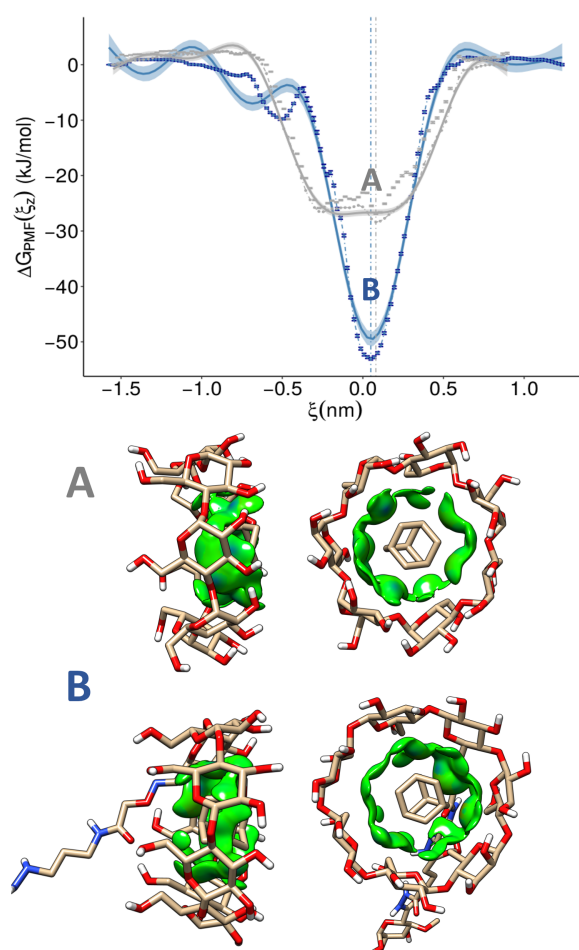


Figure 5.2: (Top) Free energy profiles for the formation of inclusion complexes involving non-substituted Ad moieties: (A) Cd:Ad and (B) CdHy:Ad, calculated from the integration of the mean forces (solid curves) and from the WHAM approach (dashed curves), both presenting a high degree of overlap. All curves are vertically aligned to have the Cd cavity positioned at  $\xi_z = 0.0$  nm. The error bars represent the statistical uncertainties estimated with bootstrap analysis. (Bottom) IGM-Plot isosurfaces (side and top views) for the (A) reference system, Cd:Ad, and (B) CdHy:Ad, for complex structures sampled from the A/B minima in the upper plot. Blue/red indicates stabilizing/destabilizing noncovalent interactions and green indicates weak vdW-type interactions (volume cut-off of  $\delta g_{inter} = 0.05$ , color coding:  $-0.1 \leq \text{sign}(\lambda_2)\rho \leq 0.1$ ). Reproduced with permission from ref. [4]. Copyright (2018) American Chemical Society.

and guest are weak noncovalent forces such as van der Waals and London (dispersion) forces. Due to the polar nature of the Cd host, stronger hydrogen-bonding interactions are conceivable with the substituted Ad derivatives. The presence of water can also significantly modify these host-guest interactions, due to variations in the hydrophobic/hydrophilic interactions with the solvent as the host and guest molecules approach each other.

In Figures 5.2 and 5.3 (bottom), the volume of the interacting regions can be taken as an indication of the extent of interaction. Green denotes weak vdW-type interactions whilst blue and red indicate

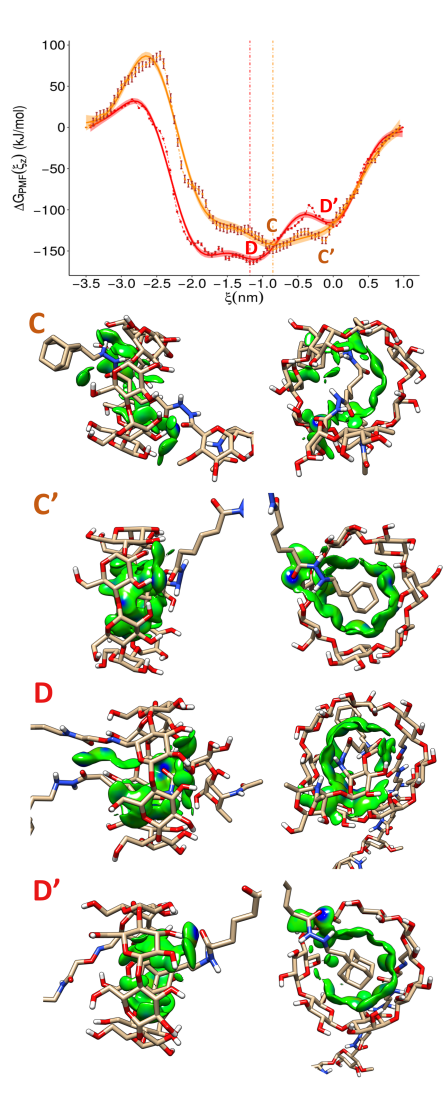


Figure 5.3: A composed view of the PMF profiles for the inclusion complexes between (orange) natural Cd and substituted guest AdHy, Cd:AdHy, and (red) substituted host and guest molecules, CdHy:AdHy. Also included are the 3D molecular images for the equilibrium states of Cd:AdHy (C and C') and CdHy:AdHy (D and D') complexes, showing different types and strengths of noncovalent interactions between host and guest molecules (for details see Figure 5.2). Reproduced with permission from ref. [4]. Copyright (2018) American Chemical Society.

Table 5.1: Summary of the main features assessed from the PMF profiles of the inclusion complexes between hyaluronic acid derivatives, including the minimum depth ( $\text{kJ mol}^{-1}$ ) and position (nm), and width at half height. Reproduced with permission from ref. [4]. Copyright (2018) American Chemical Society.

Complex	$-\Delta G_{PMF}$	FWHM	$\xi_z$
Cd:Ad	28.4	0.90	0.08
Cd:AdHy	148.9	2.25	-0.85
CdHy:Ad	53.1	0.44	0.05
CdHy:AdHy	164.5	2.55	-1.18

stronger stabilising/destabilising interactions (respectively). An interesting feature is that the 3D isosurface images show discrete regions of enhanced interactions which indicates that even with the most simple reference Cd:Ad system there exists specificity in the nature of the encapsulation of the guest within the host cavity. The specificity is increased, as is to be expected, by the inclusion of the Hy substituents. In Figure 5.2 a clear difference between A and B minima is observed. In the latter, the CdHy host provides a more complete cavity for the Ad guest, shielding it from the bulk solvent and thereby diminishing the Ad-solvent hydrophobic interaction.

In the complexes containing the substituted guests, Cd:AdHy and CdHy:AdHy, the deepest minima (Figure 5.3, C and D), display configurations in which a strong interaction between host and guest chains is clearly visible. In the second minima (Figure 5.3, C' and D'), the configurations of both complexes display the Ad moiety included in the Cd cavity. In addition to the noncovalent forces, and suggesting a significant interaction between the guest adamantyl group and the methine groups of the Cd cavity, both complexes are stabilized by a hydrogen bond, between the NH and C=O groups of the guest chain and the hydroxyl groups present in the Cd larger portal. These hydrogen bonds are identified by large volumes with blue centres (Figure 5.3, C' and D'). All these observations point to amphiphilic nature of the guest molecules, determined by substitution in the hyaluronic acid chain, being those that form inclusion complexes with the most favorable interactions.

Further details on the nature and strength of the interactions are provided in the 2D scatter plots, presented in Figure 5.4 (bottom). These show the total IGM interaction points for  $\delta g_{inter} \leq 0.1$  and in the region  $-0.2 \leq \text{sign}(\lambda_2)\rho \leq 0.2$ . In each of the systems studied 35 Å spheres centred on the complexes were employed providing identical numbers of grid points for the analyses so the contents of these 2D plots can be directly compared with one another. The strong hydrogen bond seen in the upper left isosurface plots in Figure 5.4 is observed as a large diffuse peak with its maximum at

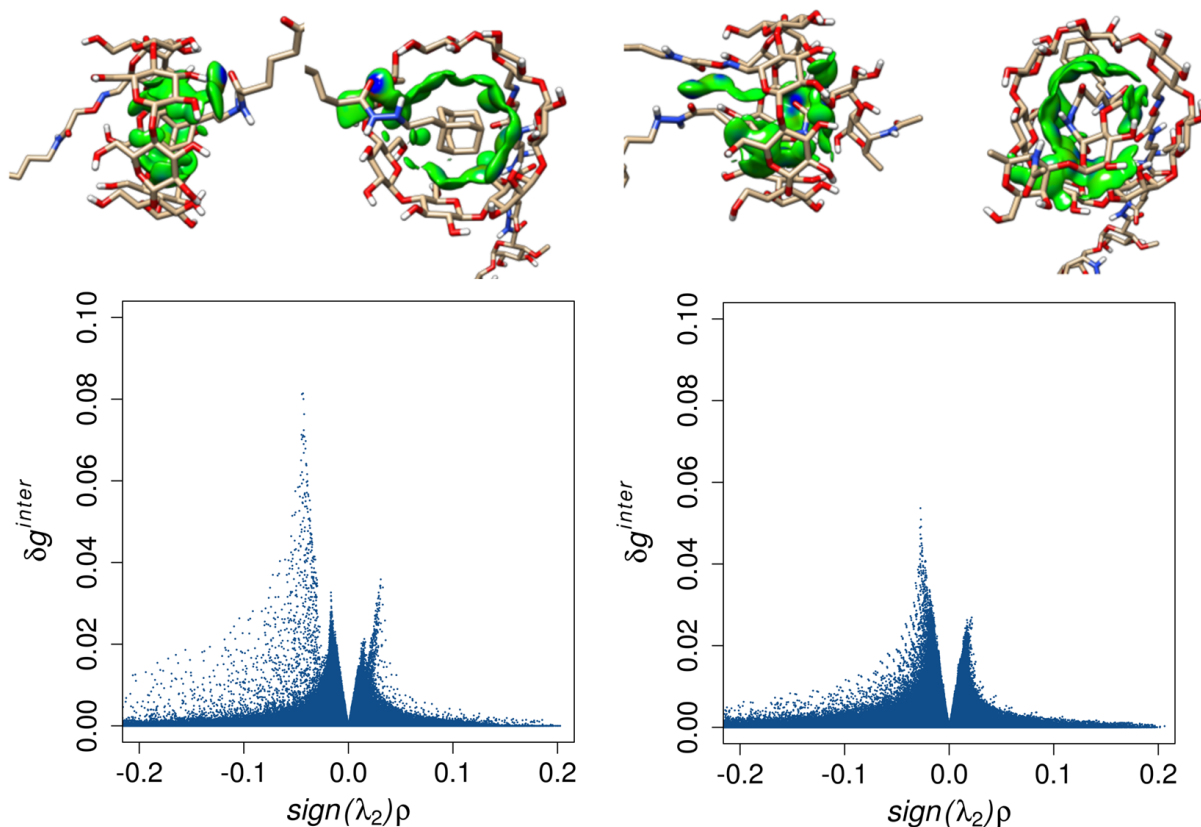


Figure 5.4: IGMPlot isosurfaces (top) and 2D scatter plots (bottom) for the CdHy:AdHy system, corresponding to the deepest minimum (left) and to the higher-lying local minimum (right) of the corresponding PMF profiles, depicted in Figure 5.3, D and D', respectively. Reproduced with permission from ref. [4]. Copyright (2018) American Chemical Society.

$sign(\lambda_2)\rho \approx -0.05$  in the lower left scatter plot. The solid peak at  $sign(\lambda_2)\rho \approx -0.02$  corresponds to weakly stabilising van der Waals-type interactions.

It is interesting to note that in the second PMF minimum on the right of Figure 5.4 the van der Waals interactions remain similar, although slightly enhanced, and another polar interaction (weaker than the Hydrogen-bond in the structure on the left) can be seen at  $sign(\lambda_2)\rho \approx -0.03$ . This interaction is identifiable as two regions of blue coloration in the isosurface plots on the right of the figure with one arising from the interaction of the AdHy tail with the CdHy macrocycle and the other occurring between the AdHy and CdHy tails.

In the 2D scatter plots the favorable nature of the host-guest interactions can be seen in the asymmetry of the peaks. In all cases the peaks on the positive, destabilising side of the plot are smaller than the corresponding peaks on the negative, stabilising side showing that the balance of noncovalent forces in the complex are in overall favor of complex formation.



## 5.4.2 Thermodynamics and interaction components

The thermodynamic parameters derived from the cylindrical model are given in Table 5.2. Eq.( 2.22) is used for the calculation of the binding constants and combines the host/guest interaction as measured from the PMF profiles. It can be seen that substitution has a significant effect in the thermodynamic signatures of the inclusion complexes and the trend followed by the PMF ( $\Delta G_{PMF}$ ) is generally the same in terms of  $\Delta G_{bind}^0$ ,  $\Delta H_{bind}^0$  and  $K_{bind}$ , following the order Cd:Ad < CdHy:Ad << Cd:AdHy < CdHy:AdHy. This indicates that the most stable complexes are those with the substituted guest, AdHy, displaying association constants much higher than that found for the binding of natural Cd and Ad. The complex Cd:Ad displays a binding constant of  $2666 \pm 25$ , within the typical range,  $10^3$ - $10^5$  M<sup>-1</sup> [5, 25, 26], for complexes between Ad derivatives and  $\beta$ -Cd. Substitution with Hy chain increases binding strength, as also found experimentally [12, 13].

The unfavorable entropy found for the CdHy:Ad and CdHy:AdHy interactions is probably due to a restriction of mobility and freedom of host and guest molecules upon inclusion, as the presence of the polymer chain may influence the degree of inclusion and provides additional interaction sites, conferring an increased structural rigidity to the complexes. The presence of the polymer chain in Cd appears to slightly enhance the binding constant, in complexes with non-substituted and substituted guests. This can be related to a more pronounced hydrophobic character for the Ad moiety and the possibility of occurring favorable intermolecular chain-chain interactions.

Table 5.2: Binding free energies, enthalpy and entropy changes (kJ mol<sup>-1</sup>), and association constants for the complex formation between hyaluronic acid derivatives, at 300K and in aqueous solution. Standard deviations of the estimated association constants are also provided. Reproduced with permission from ref. [4]. Copyright (2018) American Chemical Society.

Complex	$-\Delta G_{PMF}$	$-\Delta G_{bind}^0$	$-\Delta H_{bind}^0$	$T\Delta S_{bind}^0$	$K_{bind}$
Cd:Ad	28.4	19.7	15.6	-4.1	$2666 \pm 25$
Cd:AdHy	148.9	147.8	147.8	-0.04	$5.4 \times 10^{25} \pm 23$
CdHy:Ad	53.1	39.8	51.7	11.9	$8.5 \times 10^6 \pm 24$
CdHy:AdHy	164.5	161.3	163.4	2.1	$1.2 \times 10^{28} \pm 34$

In general, complex formation is accompanied by negative changes in enthalpy and a relatively small entropic penalty. The stability of inclusion complexes can be attributed to the enthalpic contribution,

with entropy decreasing upon formation of CdHy:Ad and CdHy:AdHy (Table 5.2). The inclusion complexes that are more strongly favored in enthalpic terms are Cd:AdHy (-147.8 kJ mol<sup>-1</sup>) and CdHy:AdHy (-163.4 kJ mol<sup>-1</sup>) both containing the substituted guest molecule. This contribution is smaller in the remaining systems including the natural Ad guest. In complexes with the substituted Cd, there is an entropic penalty to inclusion. This penalty reaches a maximum in the CdHy:Ad complex. Entropy opposes inclusion, as experimentally observed [12, 13], but constitutes a small contribution to the overall stability compared to the favorable enthalpic component. The estimates for  $\Delta H^0$  are close to those found in supramolecular assemblies [13], once the availability for complexation is taken into consideration. For example, the predicted  $\Delta H^0$  values for each node are of the order of 150 kJ mol<sup>-1</sup>, while experimental determinations halve this value, pointing only to 59% of availability for complexation (see Table 3 and text of Ref. [13]).

The global enthalpy change is now decomposed into individual components, as described in Eq. (5.1) and combines estimates of van der Waals contributions and individual electrostatic components (Table 5.3). It is apparent that the complex formation is governed essentially by increased host-guest ( $\Delta H_{HG}$ ) and solvent-solvent ( $\Delta H_{SS}$ ) interactions, and also by favorable conformational changes of Cd ( $\Delta H_{HH}$ ), which implies a substantial decrease in energy. The latter term suggests that the Cd adopts a more favorable conformation upon inclusion, as addressed in Ref. [3]. Desolvation penalizes the host/guest-solvent interactions ( $\Delta H_{HS}$  and  $\Delta H_{GS}$ , respectively), as indicated by their positive change, and favors solvent-solvent interactions ( $\Delta H_{SS}$ ). However, the latter does not compensate for either  $\Delta H_{HS}$  or  $\Delta H_{GS}$ .

Table 5.3: Individual interaction changes (kJ mol<sup>-1</sup>) for the inclusion process between hyaluronic acid derivatives. Reproduced with permission from ref. [4]. Copyright (2018) American Chemical Society.

Complex	$-\Delta H_H$	$\Delta H_G$	$\Delta H_{HH}$	$\Delta H_{GG}$	$\Delta H_{SS}$	$\Delta H_{HG}$	$\Delta H_{HS}$	$\Delta H_{GS}$	$\Delta H_T$
Cd:Ad	-16.0	0.2	-85.1	-0.1	-104.2	-167.2	302.2	11.6	-58.6
Cd:AdHy	-5.6	4.13	-18.9	21.4	-140.2	-121	127.2	37.1	-96
CdHy:Ad	1.6	-2.4	-25.3	0.04	-76.1	-105.7	111.4	47.7	-57.8
CdHy:AdHy	12.6	0.44	-51.4	-10.8	-285	-204.6	240.4	119.3	-177

### 5.4.3 Analysis of substitution effects

The host/guest affinity, and the respective dependence on hyaluronic acid substitution is now to be addressed in a systematic way. Note that this implies assessing the main effect of each of the imposed substitutions, and also the interaction between substitution in host and guest. Simply, the effect of substituting the host must be evaluated both with a non- and a substituted guest, and vice-versa. The effects are described in terms of  $\Delta\Delta G_{bind}$  (Figure 5.5). This emphasizes the effect of host and guest substitution on the final energy. Table 5.2 indicates that Cd:AdHy and CdHy:AdHy complexes, both containing the substituted guest display the most favorable energies. The presence of the Hy chain in the Ad moiety results in a lower Gibbs free-energy and a higher association constant compared to the reference Cd:Ad. Table 5.2 also suggests that there is a main effect of Cd substitution: the presence of the polymer chain in both Cd and Ad results in lower  $\Delta\Delta G_{bind}$  than just one-way partner substitution. Figure 5.5 presents the  $\Delta\Delta G_{bind}$  difference between all possible featured states corresponding to the (i) reference system with non-substituted (N) Cd and Ad (NN), (ii) substituted (S) Cd in CdHy:Ad (SN) and CdHy:AdHy (SS) and (iii) substituted Ad in Cd:AdHy (NS) and CdHy:AdHy (SS). The picture is very clear: substituting the guest is the key action for obtaining a much more stable complex (with a much higher binding constant), either with the substituted or the non-substituted host. Substitution on the host promotes only a moderate impact upon the energy, slightly higher if the guest is already substituted. Note, however, that this slight impact upon the energy translates into a 220 fold increase in the binding constant.

All these observations can be summarized using a DoE-like approach, in which  $H/G = -1$  codes for unsubstituted and  $H/G = +1$  for substituted, yielding

$$\Delta X = s_0 + s_H H + s_G G + s_{HG} HG \quad (5.2)$$

where  $\Delta X$  represents the energy differences depicted in Table 5.4,  $s_0$  is the overall average of the determinations, which would ideally correspond to the value in the absence of substitution effects, and  $s_H H$ ,  $s_G G$ , and  $s_{HG} HG$  are, respectively, the model coefficients corresponding to the main effects of substituting host (H), guest (G), and to the interaction term (HG). It is seen for  $\Delta G_{bind}^0$  that the main effect of substituting the guest is ca. 7 times that of substituting the host, and that the interaction

term is small and potentiates the main effect of host/guest in the absence of substitution for guest/host, respectively. A similar trend is found for  $\Delta G_{PMF}$ , and  $\Delta H_{bind}^0$ . In contrast, the effect upon  $\Delta S_{bind}^0$  stems mainly from substituting the host.

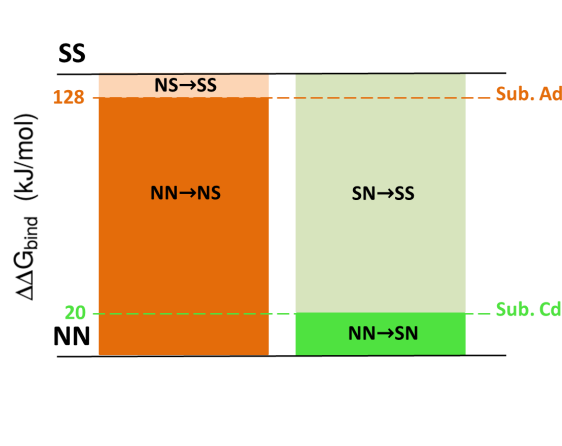


Figure 5.5: Estimated  $\Delta\Delta G_{bind}$  differences between the inclusion complexes corresponding to the reference system Cd:Ad (NN), Cd:AdHy (NS), CdHy:Ad (SN) and CdHy:AdHy (SS). Reproduced with permission from ref. [4]. Copyright (2018) American Chemical Society.

Table 5.4: Coefficient values obtained from a simple factorial design, reflecting the significance of the main substitution effects. Reproduced with permission from ref. [4]. Copyright (2018) American Chemical Society.

Energy component	$s_0$	$s_H$	$s_G$	$s_{HG}$
$T\Delta S_{bind}^0$	2.5	4.5	-1.4	-3.4
$\Delta G_{bind}^0$	-92.2	-8.4	-62.4	1.7
$\Delta H_{bind}^0$	-94.6	-12.9	-61.0	5.1
$\Delta G_{PMF}$	-98.7	-10.1	-58.0	2.3

## 5.5 Concluding remarks

The modulation of the interaction between hyaluronic acid derivatives provides general rules to identify the forces that govern the thermodynamics of binding in supramolecular nanostructures cross-linked by host-guest complexes. The main driving forces of binding are host-guest interactions, i.e., van der Waals interactions and intermolecular hydrogen bonding. The favorable conformation adopted by the host molecule upon inclusion also contributes to decrease the total energy. Desolvation effects, contributions that are often neglected, oppose binding. The most favorable free-energy differences display greatest correspondence with changes in enthalpy, with entropy playing a lesser

role in the energetic profile of the complexes. The presence of the amphiphilic chains enhances inclusion behavior and drastically increases the binding constant ( $> 10^{28}$ ). Stability of the inclusion complexes is greatly affected by host-guest interactions, desolvation effects, host fit and guest orientation. The cylindrical approximation and the thermodynamic quantities indicate that the entropic component acts as a penalty for inclusion, when the Cd is substituted with the amphiphilic chain. Strong contribution from desolvation of both host and guest molecules is observed, even for natural Cd and Ad. Measured thermodynamics quantities, when directly comparable, and respective trends are compatible with those found experimentally in related systems.

Modulation of the character of the network interaction sites can be achieved by incorporating amphiphilic substituents, with direct implications for the rational design of supramolecular structures with tailored properties based on these complexes. Detailed analysis of the energetics of the host-guest complexation suggests that conformational changes of the binding partners and solvation-related enthalpy change must be included in the estimation of the binding thermodynamics. From the present study, it follows that the substituted Cd and Ad molecules help to assess the relative importance of the different structural features, allowing for systematic prediction of binding free energies. Free-energy calculations represent an effective alternative route to access the thermodynamics underlying the inclusion processes and provide a logical connection between experimental and computational studies. The present approach can be adopted for obtaining a detailed understanding of the mechanisms governing soft associations in nanogel materials and other nanostructures such as targeted nanoparticles.

## References

- [1] Wanda Sliwa and Tomasz Girek, eds. *Cyclodextrins: Properties and Applications*. 1st ed. Germany: Wiley-VCH, 2017.
- [2] Ruslan R. Kashapov et al. "Controlling the binding of hydrophobic drugs with supramolecular assemblies of  $\beta$ -cyclodextrin". *Colloids and Surfaces A: Physicochemical and Engineering Aspects* 527 (2017), pp. 55–62. DOI: [10.1016/j.colsurfa.2017.05.026](https://doi.org/10.1016/j.colsurfa.2017.05.026).

- [3] Tânia F. G. G. Cova, Sandra C. C. Nunes, and Alberto A. C. C. Pais. “Free-energy patterns in inclusion complexes: the relevance of non-included moieties in the stability constants”. *Physical Chemistry Chemical Physics* 19.7 (2017), pp. 5209–5221. ISSN: 1463-9076. DOI: [10.1039/C6CP08081B](https://doi.org/10.1039/C6CP08081B).
- [4] Tânia F. G. G. Cova et al. “Drastic Stabilization of Junction Nodes in Supramolecular Structures Based on Host-Guest Complexes”. *Macromolecules* 51.7 (2018), pp. 2732–2741. DOI: [10.1021/acs.macromol.8b00154](https://doi.org/10.1021/acs.macromol.8b00154).
- [5] Keivan Sadrerafi, Ellen Moore, and Mark Lee. “Association constant of  $\beta$ -cyclodextrin with carboranes, adamantane, and their derivatives using displacement binding technique”. *Journal of Inclusion Phenomena and Macrocyclic Chemistry* 83.1-2 (2015), pp. 159–166. DOI: [10.1007/s10847-015-0552-5](https://doi.org/10.1007/s10847-015-0552-5).
- [6] Pietro Matricardi et al. “Interpenetrating Polymer Networks polysaccharide hydrogels for drug delivery and tissue engineering”. *Advanced Drug Delivery Reviews* 65.9 (2013), pp. 1172–1187. DOI: [10.1016/j.addr.2013.04.002](https://doi.org/10.1016/j.addr.2013.04.002).
- [7] Namdev B. Shelke et al. “Polysaccharide biomaterials for drug delivery and regenerative engineering”. *Polymers for Advanced Technologies* 25.5 (2014), pp. 448–460. DOI: [10.1002/pat.3266](https://doi.org/10.1002/pat.3266).
- [8] Youming Deng et al. “Injectable in situ cross-linking chitosan-hyaluronic acid based hydrogels for abdominal tissue regeneration”. *Scientific Reports* 7.2699 (2017). DOI: [10.1038/s41598-017-02962-z](https://doi.org/10.1038/s41598-017-02962-z).
- [9] Corentin Lefebvre et al. “Accurately extracting the signature of intermolecular interactions present in the NCI plot of the reduced density gradient versus electron density”. *Physical Chemistry Chemical Physics* 19.27 (2017), pp. 17928–17936. ISSN: 1463-9076. DOI: [10.1039/C7CP02110K](https://doi.org/10.1039/C7CP02110K).
- [10] Erin R. Johnson et al. “Revealing Noncovalent Interactions”. *Journal of the American Chemical Society* 132.18 (2010), pp. 6498–6506. ISSN: 0002-7863. DOI: [10.1021/ja100936w](https://doi.org/10.1021/ja100936w).

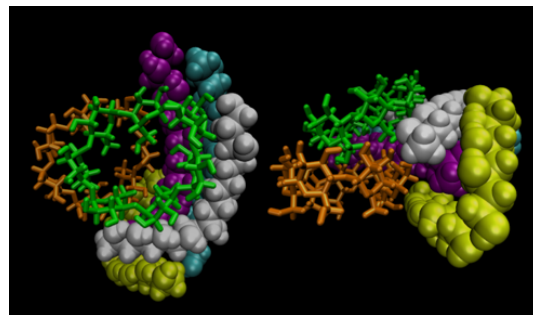
- [11] Contreras-García Julia et al. “NCIPLLOT: A Program for Plotting Noncovalent Interaction Regions”. *Journal of Chemical Theory and Computation* 7.3 (2011), pp. 625–632. DOI: [10.1021/ct100641a](https://doi.org/10.1021/ct100641a).
- [12] Aurélia Charlot et al. “Controlled synthesis and inclusion ability of a hyaluronic acid derivative bearing beta-cyclodextrin molecules”. *Biomacromolecules* 7.3 (2006), pp. 907–913. DOI: [10.1021/bm0507094](https://doi.org/10.1021/bm0507094).
- [13] Aurélia Charlot and Rachel Auzély-Velty. “Synthesis of Novel Supramolecular Assemblies Based on Hyaluronic Acid Derivatives Bearing Bivalent  $\beta$ -Cyclodextrin and Adamantane Moieties”. *Macromolecules* 40.4 (2007), pp. 1147–1158. DOI: [10.1021/ma062322e](https://doi.org/10.1021/ma062322e).
- [14] Lingzhi Zhang, Jinping Zhou, and Lina Zhang. “Structure and properties of  $\beta$ -cyclodextrin/cellulose hydrogels prepared in NaOH/urea aqueous solution”. *Carbohydrate Polymers* 94.1 (2013), pp. 386–393. ISSN: 0144-8617. DOI: <https://doi.org/10.1016/j.carbpol.2012.12.077>.
- [15] Enguerran Vanquelef et al. “R.E.D. Server: a web service for deriving RESP and ESP charges and building force field libraries for new molecules and molecular fragments”. *Nucleic Acids Research* 39.2 (2011), W511–W517. DOI: [10.1093/nar/gkr288](https://doi.org/10.1093/nar/gkr288).
- [16] Berk Hess et al. “GROMACS 4: Algorithms for highly efficient, load-balanced, and scalable molecular simulation”. *Journal of Chemical Theory and Computation* 4.3 (2008), pp. 435–447. ISSN: 1549-9618.
- [17] David van der Spoel, Paul J. van Maaren, and Carl Caleman. “GROMACS molecule and liquid database”. *Bioinformatics* 28.5 (2012), pp. 752–753. DOI: [10.1093/bioinformatics/bts020](https://doi.org/10.1093/bioinformatics/bts020).
- [18] Kresten Lindorff-Larsen et al. “Improved side-chain torsion potentials for the Amber ff99SB protein force field”. *Proteins: Structure, Function, and Bioinformatics* 78.8 (2010), pp. 1950–1958. DOI: [10.1002/prot.22711](https://doi.org/10.1002/prot.22711).
- [19] Christine Cézard et al. “Molecular dynamics studies of native and substituted cyclodextrins in different media: 1. Charge derivation and force field performances”. *Physical Chemistry Chemical Physics* 13.33 (2011), pp. 15103–15121. DOI: [10.1039/C1CP20854C](https://doi.org/10.1039/C1CP20854C).

- [20] Jirasak Wong-ekkabut and Mikko Karttunen. “The good, the bad and the user in soft matter simulations”. *Biochim. Biophys. Acta* 1858.10 (2016), pp. 2529–2538. DOI: [10.1016/j.bbamem.2016.02.004](https://doi.org/10.1016/j.bbamem.2016.02.004).
- [21] B. Hess et al. “LINCS: A linear constraint solver for molecular simulations”. *Journal of Computational Chemistry* 18.12 (1997), pp. 1463–1472. ISSN: 0192-8651.
- [22] Jochen S. Hub, Bert L. de Groot, and David van der Spoel. “*qwham*-A Free Weighted Histogram Analysis Implementation Including Robust Error and Autocorrelation Estimates”. *Journal of Chemical Theory and Computation* 6.12 (2010), pp. 3713–3720. ISSN: 1549-9618. DOI: [10.1021/ct100494z](https://doi.org/10.1021/ct100494z).
- [23] Fangqiang Zhu and Gerhard Hummer. “Convergence and error estimation in free energy calculations using the weighted histogram analysis method”. *Journal of Computational Chemistry* 33.4 (2012), pp. 453–465. DOI: [10.1002/jcc.21989](https://doi.org/10.1002/jcc.21989).
- [24] Pettersen Eric et al. “UCSF Chimera - A visualization system for exploratory research and analysis”. *Journal of Computational Chemistry* 25.13 (2004), pp. 1605–1612. ISSN: 1096-987X. DOI: [10.1002/jcc.20084](https://doi.org/10.1002/jcc.20084).
- [25] Mikhail V. Rekharsky and Yoshihisa Inoue. “Complexation Thermodynamics of Cyclodextrins”. *Chemical Reviews* 98.5 (1998), pp. 1875–1918. DOI: [10.1021/cr970015o](https://doi.org/10.1021/cr970015o).
- [26] Christopher B. Rodell, Joshua E. Mealy, and Jason A. Burdick. “Supramolecular Guest-Host Interactions for the Preparation of Biomedical Materials”. *Bioconjugate Chemistry* 26.12 (2015), pp. 2279–2289. DOI: [10.1021/acs.bioconjchem.5b00483](https://doi.org/10.1021/acs.bioconjchem.5b00483).





# Chapter 6



## Aggregation of Cyclodextrins

The simulation of host-guest systems involving Cd molecules and aggregates is already offering ways to explore a set of favorable events at different scales. The aggregation behavior and the interaction patterns of Cds, modified with both hydrophobic and hydrophilic groups, have been investigated by atomistic simulations in non-polar solvents and in water [1, 2] Although most studies involving amphiphilic Cds have been conducted in aqueous solutions, the use of non-polar solvents is also important in preparative and characterization procedures, as suggested in ref. [1]. In the latter, dynamic light scattering observations demonstrated that Cds can form well defined aggregates in non-polar solvents (e.g. dichloromethane) displaying a hydrodynamic radius of ca. 80 nm and low polydispersity. [1]

Electrostatic, dipolar, and dispersion forces have been recognized as playing a definite role in the formation and stabilization of these aggregates. The formation of even larger structures (such as micelles, vesicles, membranes and nanoparticles) based on these smaller aggregates, and their potential uses in pharmaceutical formulations have also been suggested. [3]

### 6.1 Controversial experimental evidence

The aggregation of single Cds and Cd-guest complexes, in water, has been described in a number of recent studies. [4–10] Despite the efforts for understanding the factors that govern inclusion/binding with guest molecules, the precise manner in which Cd molecules aggregate and the cooperative effects

underlying this phenomenon is much less studied and still far from consensual.

The classical assumption states that inclusion complexes between Cds and guest molecules are always formed in "ideal" solutions, with individual complexes, independent of each other. However, the treatment of the interaction between system components is oversimplified, since Cds can form both inclusion and non-inclusion complexes and water-soluble aggregates. In some cases, the aggregation results in the opalescence of aqueous Cd solutions. However, the reduced diameter of the aggregates is smaller than the wavelength of visible light and, more often, the formation of clear solutions is promoted. The first reference to the occurrence of self-aggregation dates back to 1983, when Miyajima and co-workers [11], based on viscosity and activity coefficient data of aqueous solutions of  $\alpha$ - and  $\gamma$ -cyclodextrins, suggested the occurrence of dimers or larger aggregates. These authors have also pointed out that such aggregates are acting as "structure making" [12] by tightening water-water hydrogen bonding. Ten years later, Hausler and Muller-Goymann [13] have observed that at concentrations above 50 % (w/w) hydroxypropyl(HP)- $\beta$ -Cd self-aggregates, leading to an increase in the solution viscosity. They also found that the addition of chaotropic solutes (e.g., urea and NaCl) tends to decrease the viscosity of solutions as a consequence of Cd disaggregation. A similar observation was found for  $\gamma$ -Cd (10 % m/v) solutions [14], at physiological pH. In both works, the self-aggregation of Cd monomers is justified by intermolecular H-bonding interactions promoted by the hydrophilic rims. [13, 14] Coleman et al. [15] extended their studies to  $\beta$ -Cd, the less soluble of all native Cds, and found that the addition of water structure-breaking solutes or an increase of the solution pH (at values higher than 12.5) in order to ionize the -OH groups, lead to an increase in solubility. This evidence led them to hypothesize that the solubility of Cds is related with interactions between Cd aggregates and the water through the formation of two chains of hydrated  $\beta$ -Cd molecules forming a rod-like aggregate. These authors also argue that the structure of water has an important role on the aggregation/dissociation of Cds. The quantification of size and mass percentage of aggregates was only made possible, in a systematic manner, during the last decade. It has been concluded, by using photon correlation spectroscopy (PCS), that in a 12 mM Cd aqueous solution, large polydisperse aggregates of 200-300 nm in size were formed [16]; however, the respective mass percentage is quite small when compared to that of free Cd. For example, the mass contribution of  $\alpha$ -Cd aggregates is ca. 0.8 % (0.096 mM) assuming coils, or 0.001 % (0.12  $\mu$ M) considering spheres. [16] For other

Cds, the mass contribution of aggregates is also residual, i.e., 0.0011 % (0.13  $\mu\text{M}$ ) for  $\beta$ -Cd [17], and 0.02 % (0.154 mM) for  $\gamma$ -Cd solutions. [14] He et al. [17] found a bimodal distribution in dynamic-light scattering (DLS) data of  $\alpha$ -,  $\beta$ - and  $\gamma$ -Cd aqueous solutions, with mean hydrodynamic radii of less than 1 nm and higher than 60 nm for the fast and slow components (attributed to monomer and aggregated Cds, respectively). This has been revisited by Puskás et al. [18] by using the same technique. However, contrarily to previous work, only  $\gamma$ -Cd aggregates have been confirmed. In other studies [19, 20], the formation of Cd aggregates of globular shape, at  $[\beta\text{-Cd}]=3$  mM, with a minimum hydration radius of ca. 90 nm, was reported, based on data from different techniques, including DLS, cryo-TEM and electron spin resonance (ESR) probe spectroscopy. However, at higher Cd concentrations these particles coexist with other structures as large as a few micrometres. These aggregates tend to increase with Cd concentration suggesting cooperative aggregate-aggregate interactions. In addition, Rao and Geckeler [21] have concluded that the formation of  $\beta$ -Cd supramolecules can also occur in aqueous solutions at room temperature. By increasing the stirring time and the concentration from 4 to 10 mM it was possible to follow the formation of cage-like structures (with an average size of 7.5 nm), after 5 hours stirring, evolving to channelled structures (with 260 nm length) after 72 hours stirring. The thermodynamic parameters of  $\beta$ -Cd self-assembly have been studied, assuming that Cds behave as colloids. [22] For that, the scattering intensity of a set of  $\beta$ -Cd solutions of different concentrations has been measured; by plotting the scattering intensity as a function of  $\beta$ -Cd concentration, two different regimes were observed below and above the critical aggregation concentration ( $c_{ac}=1.6$  mM): at  $c < c_{ac}$  only monomers (the occurrence of small aggregates cannot be also neglected) exist in solution. However, at  $c > c_{ac}$  the scattering intensity increases linearly with  $\beta$ -Cd concentration, indicating the presence of two different set of aggregates of 60.0 nm and 120 nm in size. Using the pseudo-phase model, the free energy of aggregation was calculated to be  $-15.95$   $\text{kJ mol}^{-1}$ , at 298.15 K. From the dependence of the  $c_{ac}$  value on the temperature, the variation of the aggregation enthalpy and, consequently, the aggregation entropy (at 298.15 K) were estimated to be  $-26.48$   $\text{kJ mol}^{-1}$  and  $-35.32$   $\text{J K}^{-1} \text{mol}^{-1}$ , respectively. These values for thermodynamic parameters suggest that: a) aggregation is enthalpy-driven, and b) aggregates are formed by non-covalent interactions. [23] Following the same approach, the  $c_{ac}$  values of  $\alpha$ -,  $\beta$ - and  $\gamma$ -Cds were also measured by using a permeability technique, based on dialysis membranes with molecular weight-cut off higher

than 2 kDa. [5, 24] Inspecting the flux of Cds as a function of concentration, two different regimes have been found which was attributed to the formation of aggregates. The calculated values for the  $cac$  of  $\alpha$ -,  $\beta$ - and  $\gamma$ -Cds are 12.2, 6.1 and 7.2 mM, respectively. Recently, a thermodynamic study [25] using isodesmic and K2-K self-assembly models was performed on Cd derivatives (HP- $\beta$ -Cd, HP- $\gamma$ -Cd and sulfobutylether(SBE)- $\beta$ -Cd). The isodesmic model assumes that the Gibbs energy and equilibrium constant (K) are equal in each addition of a monomer to an aggregate (for details see ref. [25]). The K2-K model is a modified version of the former, in which the K value of the first step of the self-assembly is different from those of the remaining steps. The respective  $cac$  values and aggregate sizes were also determined, using DLS and  $^1\text{H}$ NMR and TEM, respectively. These Cds displayed similar  $cac$  values of ca. 2 % (m/v). Three different groups of particle sizes were also identified based on correlation functions: (i) a group with ca. 1 nm corresponds to a single Cd molecule, (ii) a group with size values ranging from ca. 30 nm to 60 nm for HP- $\gamma$ -Cd and from ca. 10-70 nm for SBE- $\beta$ -Cd and from ca. 100 nm to 200 nm for HP- $\beta$ -Cd, and (iii) a small group with larger aggregates attaining 1  $\mu\text{m}$ , for  $\beta$ -Cd derivatives, and from ca. 140 nm to 1  $\mu\text{m}$  for HP- $\gamma$ -Cd. It was shown that aggregation results from some cooperative contributions, with the first step of the aggregation being less favorable than the subsequent ones. A thermodynamic analysis indicated that the aggregation process was spontaneous, exothermic and associated to an entropy loss. The calculated standard free energies range from  $-7.1 \text{ kJ mol}^{-1}$  for SBE- $\beta$ -Cd to  $-10.6$  for HP- $\gamma$ -Cd), the enthalpy values were  $-20.6$ ,  $-27.5$  and  $-46.3 \text{ kJ mol}^{-1}$  for HP- $\beta$ -Cd, SBE-  $\beta$ -Cd and HP- $\gamma$ -Cd, respectively. [25] The dynamics of Cds in aqueous solution has been fully assessed using different NMR techniques by Valente et al. [26, 27]. The analysis of  $^1\text{H}$ NMR self-diffusion of deuterium solutions of Cds shows that, for all three natural Cds, diffusion coefficients depend linearly on the Cd volume fraction, suggesting that these molecules are behaving as non-aggregate hard spheres. A similar conclusion was reached from the analysis of the dependence of mutual diffusion coefficients on Cds concentration. [28–30] A more sensitive parameter, related to the volume of the diffusing particle, is the transverse magnetization relaxation time  $T_2$ , or the spin-spin relaxation rate  $R_2$  ( $=1/T_2$ ). In a perfectly homogeneous magnetic field, the  $R_2$  relaxation rate can be measured directly from the free induction decay in the time domain or the full width at half height of the resonance in the frequency domain. The dependence of  $R_2$  as a function of Cd volume showed that no aggregation occurs. However, the presence of more transient aggregates

cannot be excluded for cases in which the lifetime of the aggregate is short compared to the respective tumbling time. The presence of very large aggregates, not visible in the NMR spectra on account of their slow rotational tumbling, cannot also be ruled out. A different, but complementary aspect is related to the mechanism of interaction. For further insight, the aggregation of  $\alpha$ -,  $\beta$ - and  $\gamma$ -Cds, in aqueous solutions was addressed by focusing on the Cd-Cd interactions using deuterium relaxation rates ( $R_1$ ) for deuterium labelled Cds. In this particular case, the dependence of  $T_1$  ( $=1/R_1$ ) on the Cd concentration, for all Cds, was explained by the equilibrium between monomeric and dimeric Cds and, again, no evidence in favour of large aggregates of Cds involving a non-negligible fraction was found. [27] The formation of aggregates in aqueous solutions containing Cds can be promoted by the presence of guest compounds, which upon inclusion can also contribute to understand and predict the Cd aggregation behavior. The structure and nature of the guest molecule can thus affect the Cd aggregation process. Cd-guest complexes are, most often, simply formed by one guest molecule and one Cd molecule. However, ternary complexes are also frequently described [31] where water-soluble polymers [32, 33], metal ions, or organic salts [34] are used to potentiate some Cd effect. The coexistence of inclusion and non-inclusion complexes in aqueous solutions containing Cds has been documented and associated with the formation of aggregates based on these complexes. The first evidence for aggregation with complexes involving Cds and lipophilic guests was reported by Mele and co-workers [35] in 1998. Later studies [36], with contradictory or ambiguous results fostered further investigation on this phenomenon. The formation of Cd-guest based aggregates in the nanosize range has been confirmed by DLS and TEM analyses, and associated to a negative deviation from linearity. This type of aggregation occurred for a Cd concentration of ca. 10 % (wt/vol). [36] The self-association of Cd complexes can explain the observed decrease in the activity coefficient with increasing Cd concentration, and the dependence of the complex stoichiometry on the method applied. Several model compounds [36] have been recently used to investigate the effect of the physicochemical properties of the guest molecules on the Cd aggregation behavior. For instance, the impact of a set of esters of para-hydroxybenzoic acid, differing in the side chain length, on HP- $\beta$ -Cd aggregation was recently evaluated resorting to permeation experiments, DLS and MS. The number and size of Cd aggregates ( $<200$  nm) increased in the presence of longer guests. However, no clear relation was found between the extent of aggregate formation and the Cd concentration. The pre-micellar asso-

ciation of inclusion complexes of cationic surfactants and  $\beta$ -Cd followed by micellar association of the inclusion complexes, has also been suggested based on NMR studies. In addition, micelle-like assemblies with diameters exceeding 200 nm have been observed in aqueous solutions containing trans- $\beta$ -carotene and  $\beta$ -Cd and  $\gamma$ -Cd. [4] The structure and size of these Cd aggregates is clearly affected by water molecules and hydration shells. [4] Although the ability of Cds to self-assemble to form aggregates is well documented, it has also been shown that the aggregates are very unstable. Attempts to stabilize nanosize self-assembled Cd aggregates of the native Cds, and their hydrophilic and monomeric derivatives have not been successful so far.

## 6.2 Common arrangements in Cd aggregates

There are two typical crystal structures for native Cds: cages and channels (see Figure 6.1). [37, 38] The cage arrangement occurs when Cds are grouped crosswise, displaying a herringbone pattern (Figure 6.1a), or are aligned in adjacent layers leading to a brick-like pattern (Figure 6.1b). In both cases, the formation of inclusion complexes is prevented, as the Cd cavities are blocked on both portals by neighboring Cds. The channel-type assembly is observed if the Cds are stacked in columns so that cavities are aligned to produce channels (Figure 6.1c). While the channel arrangement can be converted into a cage structure by water sorption/desorption cycles, with an intermediated amorphous state, the latter usually results from rapid recrystallization of Cds. After reaching sorption equilibrium, Cd molecules undergo a slow rearrangement to the cage structure with defined water content. [38] Similar patterns are generally found in the crystal structures of Cd inclusion complexes. [38] When the entire guest molecule is small enough to be included inside a single Cd cavity, cage-type structures are formed. On the other hand, a channel-type structure is observed in the presence of long-chain molecules as guests (e.g. polymers). Rusa and co-workers [4, 39] have reported the encapsulation of poly( $\epsilon$ -caprolactone) and poly(L-lactic acid) into  $\alpha$ - and  $\gamma$ -Cds. The inclusion of a polymeric structure inside the Cd cavity induces the formation of channel-like structures, being those with  $\alpha$ -Cd more stable due to the increase of hydrophobic Cd-polymer interactions. By using an appropriate experimental procedure, the authors were able to produce a solid-state channel packing of Cds containing only water molecules inside the cavities [40] The same group has also observed the inclusion

of poly(vinyl alcohol) (PVA) into Cd by taking advantage of the freezing-thawing process for PVA gelation. [41] In this process, the gelation of PVA-containing composites occurs taking into account two different types of cross-linking: (i) the hydrogel-bonding naturally observed during the freezing-thawing process and (ii) the Cd-Cd aggregation resulting from channel-type arrangements. [41]

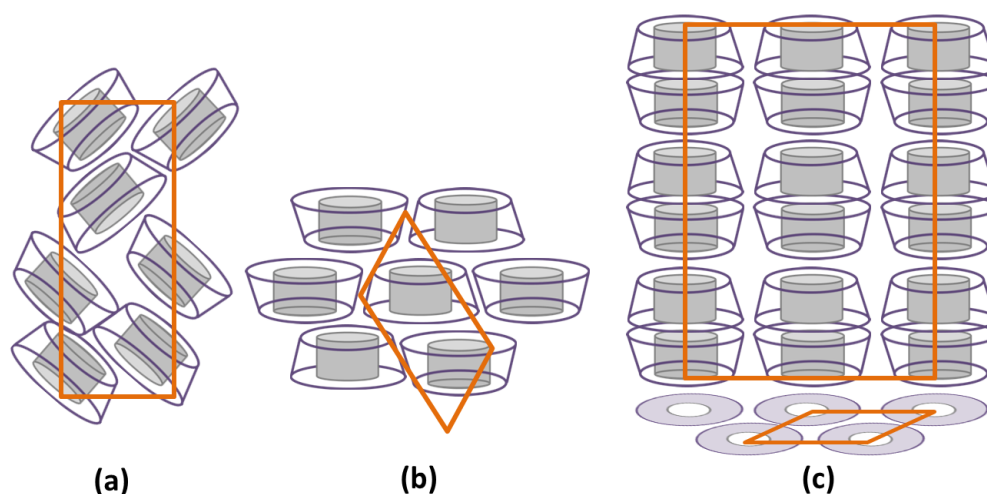


Figure 6.1: Schematic representation of packing structures of (a) cage-type; (b) layer-type Cd; and (c) head-to-tail channel-type Cd crystals. Adapted with permission from ref. [38]. Copyright (2018) American Chemical Society.

## 6.3 Applications of Cd aggregates

As already mentioned in previous sections, a variety of Cd-based aggregates can be formed under different conditions (e.g. concentration, solvent medium, and temperature). These include native and modified Cds, inclusion complexes and the respective aggregates and also rotaxanes and polyrotaxanes, nanotubes, and other high-order structures, such as nanospheres and network aggregates. [42] The potential use of these self-assembled nanomaterials have been explored for advanced applications, ranging from drug stabilization and drug delivery [43], selective binding [44] and controlled adsorption [44]. In pharmaceutical and biomedical fields it is expected that such applications may include (i) the nanoencapsulation of drugs in the hydrophobic interchain volumes and nanocavities of modified Cds, which can be used as drug carriers or pharmaceutical excipients, (ii) anticancer phototherapy, (iii) gene delivery, and (iv) protection of unstable active components through the for-



mation of inclusion complexes. [42] Several interesting examples of these potential applications have been focused on amphiphilic Cds, which allow to easily modulate both hydrophobic/hydrophilic and self-assembly properties, by grafting different substituents on the portals of native Cds. [42, 45] For instance, supramolecular assemblies based on Cd/porphyrin nanoassemblies have been studied in vitro [46] as potential nanotherapeutics in A375 human melanoma cells. Other micellar structures and spherical vesicles based on Cd-perylene conjugates have been designed to be included in fluorescence sensory and photoresponsive materials, photoinduced electron transfer systems and organic electronic devices. [47] The self-aggregation of amphiphilic Cds have also been explored for drug delivery applications, as they are able to capture selectively drug molecules, displaying enhanced solubilization capacity. [43] The affinity of amphiphilic Cds for incorporation in model and biological membranes has also been investigated and explored for preparation of functionalized lipid membranes and improved biomimetic systems. [45, 48, 49] A broader range of potential applications of Cd aggregates are compiled in recent publications such as refs. [42] and [45], and references therein.

## 6.4 Computational results

Irrespective of the disparate observations, the self-aggregation capability must be affected by the type of Cd present in the aqueous solution. While the aggregates of  $\alpha$ -Cd and  $\gamma$ -Cd can be completely removed by standard filtering procedures, the formation of  $\beta$ -Cd aggregates (at least as dimers, or possibly larger aggregates) persists in solution, displaying fast aggregation kinetics. This suggests that the hydrophilic Cd portals play a definite role in the aggregation process. [16] The disruption of hydrogen bond networks by ionization (or functionalization) increases solubility and may suppresses aggregation. The presence of aggregates in solutions containing structure-breaking solutes, in which the solubility of  $\beta$ -Cd is enhanced, has provided new insights into this unusual behavior. The low solubility of  $\beta$ -Cd has been explained by the presence of aggregates and the respective unfavorable interaction with the hydrogen bond network of bulk water. [15] Note that aspects pertaining to the binding energy in the solid state cannot be disregarded. The relevance of understanding the mechanistic details of the Cd aggregation phenomena encompasses either controlling/preventing the formation of aggregates (that preclude the development of specific formulations and the product development)

or designing novel formulation strategies. Computer simulations have been used to rationalize the experimental findings concerning recognition [50], inclusion [22, 50–52], and aggregation [1, 2, 8, 53, 54]. The cooperative binding of at least two Cd monomers to a guest molecule has been considered the driving force responsible for self-assembly processes in the construction of Cd-based nanoarchitectures. [51] For aggregation processes without using guests, the assembly is usually driven by the hydrophilic portals (in native Cds) and by interactions between substituent chains of Cd derivatives with the neighboring cavities of other Cds. [51] The orientational patterns of inter-glucopyranose hydrogen bonds at the secondary portal of  $\beta$ -Cd and the respective effect on the Cd structure and dimer binding/stability in polar and non-polar solvents have been explored by Spoel et al. [50] in the presence of various guest molecules. It was demonstrated, based on MD simulations and free energy calculations, that polar solvents with stronger hydrogen bond accepting abilities can easily disrupt intermolecular hydrogen bonds, resulting in less stable dimers. Also, the guest models included in the channel-type cavity increases the binding affinity between Cd monomers, particularly in polar solvents. [50] Using a similar computational approach, the authors have explored the effect of three different dimerization modes of  $\beta$ -Cd molecules and the presence of isoflavone drug analogues in the construction of Cd-based nanostructured materials. It was demonstrated that the cooperative binding of Cd cavities to guest molecules favors the dimerization process and, consequently, the overall stability and assembly of the Cd nanostructures. It was also proved that the desolvation of Cd dimers and entropy changes upon complexation cooperatively contribute to the binding process. [51] Another study [8] focused on the spontaneous adsorption of native Cds and the respective aggregates, and the related dependence on temperature. It was found that the adsorption of both individual Cds and small Cd aggregates (ca. 20 molecules) to the solution/air interface is negligible. The solute-solute interactions were significantly larger for  $\beta$ -Cd than for  $\alpha$ -Cd at 298 K, and the dependence of these interactions on temperature was more relevant for the smaller Cd, which displayed a more favorable aggregation at 283 K than at 298 K. The dynamic exchange of hydrogen bonds between the Cd hydroxyl groups and the neighboring water molecules, indicated a much larger occupancy for individual intramolecular hydrogen bonds in  $\beta$ -Cd. In what follows, the Cd-Cd interactions [27], for deuterium labelled Cds, in aqueous solutions are further explored by atomistic simulations. Two types of systems are defined, one in which the  $\beta$ -Cd is free in water, and three others in which two  $\beta$ -Cds

are present and may form dimers. In what concerns the latter, these include initial arrangements with proximity of one primary portal and one secondary portal (PS), two primary portals (PP), and two secondary portals (SS), as shown in Figure 6.2.

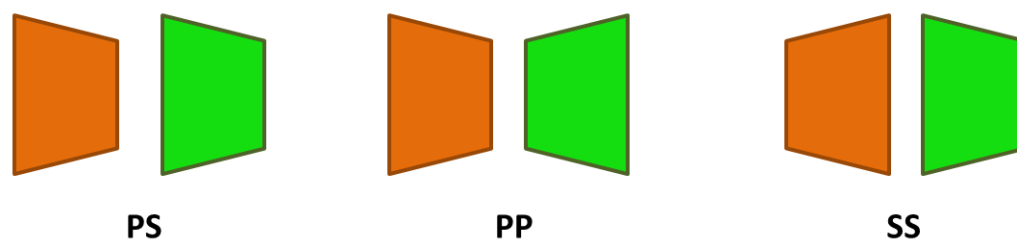


Figure 6.2: Schematic illustration of the pairwise initial arrangements of  $\beta$ -Cds, with facing primary and secondary portals (PS), two primary portals (PP), and two secondary portals (SS), with the colors used to distinguish  $\beta$ -Cd molecules. Reproduced from ref. [3].

The molecular dynamics simulations were performed with GROMACS (version 4.6.5), using the all-atom amber99sb [55] force field and the TIP3P water model. The initial coordinates of the  $\beta$ -Cd were extracted from the RCSB protein data bank (PDB code: 1DMB) and partial charges were generated using the R.E.D.D. Server. [56] In each system, the molecules were accommodated in a cubic box (7.5 nm edge-length) containing approximately 13000 explicit TIP3P water molecules. To obtain a starting configuration, each system was firstly subjected to an energy minimization step. All the calculations were carried out in NPT ensemble with periodic boundary conditions at a constant temperature of 300 K, and a pressure coupling of 1.0 bar, respectively, to V-rescale and Berendsen external baths. A standard time step of 2 fs was used for both equilibration and production runs. A cut-off of 0.9 nm was used for calculating the Lennard-Jones interactions. Electrostatic interactions were evaluated using the particle mesh Ewald method. [57] Constraints were applied for bond lengths with the LINCS algorithm. [58] Equilibrium properties, structure and dynamics of  $\beta$ -Cd systems were calculated for the simulation runs of 50 ns after the systems were equilibrated for 2 ns. Geometric clustering was performed to identify dominant Cd-Cd structures, sampled during the MD simulations. The algorithm for cluster analysis is based on the hierarchical (top-down) approach [59], and allows evaluating the conformational prevalence of each Cd-Cd structure, by determining dominant clusters based on the root mean square deviation of the atom positions between all pairs of structures. For

each Cd-Cd arrangement, the number of neighbouring structures is calculated for RMSD values of 0.35 nm. Figure 6.3 presents the behaviour of Cd-Cd structures in different simulation runs, each corresponding to a different initial arrangement. For each Cd backbone, the COM of the oxygen atoms at the secondary portal (S) was defined as the reference point for evaluating aggregated and non-aggregated structures, and the possible rotation or tilt of the Cd molecules.

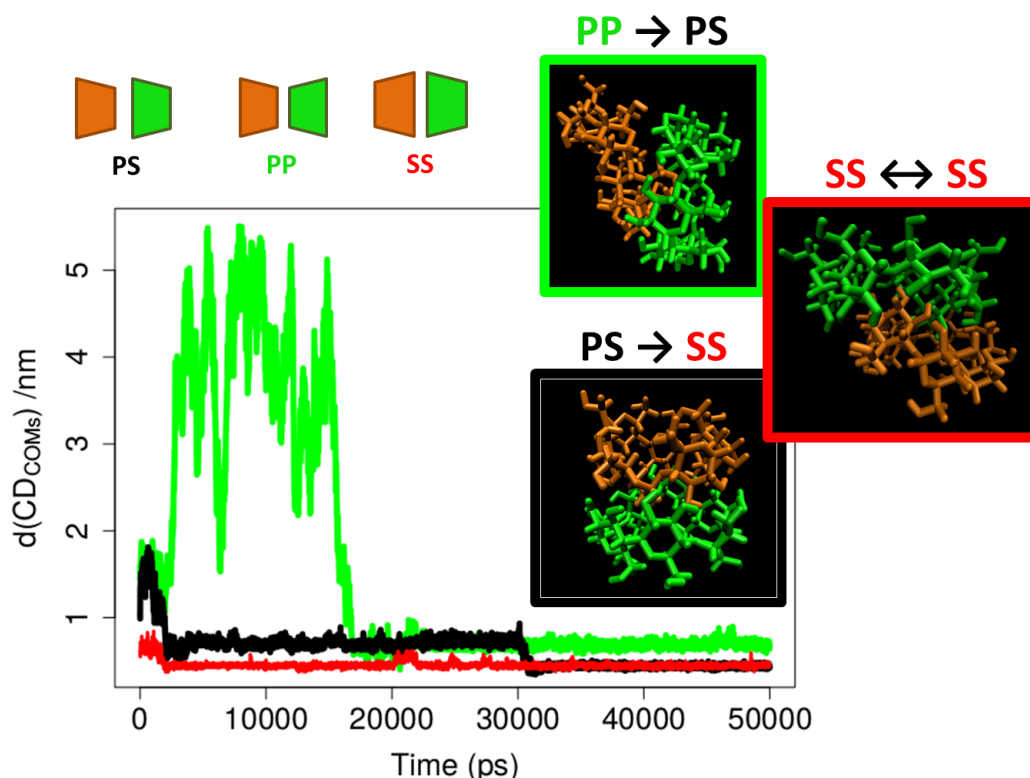


Figure 6.3: Distribution of distances between the centers of mass of  $\beta$ -Cd molecules, defined by the oxygen atoms of the secondary portals. Right panels illustrate the final conformations for the imposed PS, PP and SS initial arrangements of  $\beta$ -Cd molecules, in aqueous solution, sampled during the MD simulations at 300 K and identified by geometric cluster analysis. The colour codes for Cd molecules are as in Figure 6.2, while the initial arrangements are represented in black, green and red, for PS, PP and SS, respectively. Reproduced from ref. [3].

For PS and PP as initial arrangements, a significant evolution is observed in the relative positioning of the two molecules. The PS and PP initial arrangements display an almost complete rotation or a tilt of one molecule with respect to the other, leading to most favourable SS and PS arrangements, respectively. The "intermediate" PS arrangement increases the Cd-Cd interactions through partial inclusion of some P groups in the hydrophobic cavity of the other Cd molecule. The initial SS arrangement prevails over the course of the simulation with a typical COM distance of 0.46 nm. In addition to intramolecular hydrogen bonds, the two Cd molecules can form additional intermolecular

hydrogen bonds, optimizing the Cd-Cd interaction. PS is an intermediate arrangement between the most (SS) and the least stable (PP) arrangements. The PP arrangement of the Cd pair involves weaker interactions between P groups of the two molecules, producing a low prevalence, relatively open aggregate (COM distance of 0.8 nm), suggesting a relatively poor clustering of this dimeric aggregate. Also inspected were the rotational autocorrelation functions (ACF) corresponding to the motion of each Cd, free or mostly in dimer arrangement. Two alternatives were tested for the definition of the molecule fixed rotating vector: defined by the C2-D (see Figure 6.4) bond (vector) and resulting from the use of three atoms (triplet), those of the C2-D bond and the adjacent carbon C3, and defined as the cross product of vectors C3-C2 and C2-D.

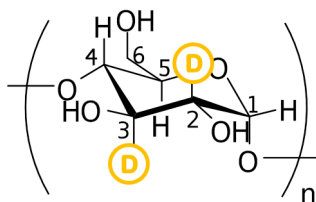


Figure 6.4: Cyclodextrin structures ( $\alpha$ -Cd,  $n=6$ ;  $\beta$ -Cd,  $n=7$  and  $\gamma$ -Cd,  $n=8$ ). Reproduced from ref. [3].

The ACF curves are similar for these two cases, and are represented in Figure 6.5. The curves were fitted from 0 up to 500.0 ps to a one-parameter exponential, and reflect the slower decay for the dimer situation,  $\tau_0=1250$  ps, much larger than for the free Cd,  $\tau_0=448$  ps. These values are of order of magnitude of those experimentally obtained.

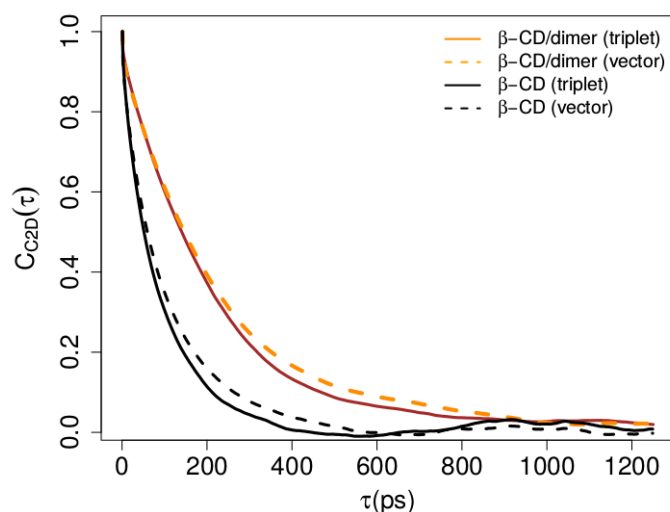


Figure 6.5: Average autocorrelation function of C2-D bond for Cd molecules in the monomeric and dimeric states, in water at 300 K. (black and orange curves, respectively). Reproduced from ref. [3].

The organization of Cd molecules in aggregates when in the presence of guest-entities clearly deserves further attention. As an example of the behaviour found for more complex systems, simulations were performed to study the inclusion complex of  $\beta$ -Cd and PVA molecules in water. The importance of this polymer is related to the ability to form hydrogels exhibiting a high degree of swelling in water that have demonstrated a great potential to act as a matrix for many applications, including drug delivery [60], wound dressing [61], and sensors [62]. More recently, it has been found that such broad applications of PVA result from its ability to behave as an amphiphilic polymer. [63] This latter feature is relevant for studying the ability of Cds for forming host-guest or aggregate complexes. In this example, three molecular dynamics simulations were performed in systems containing two  $\beta$ -Cd (denoted as A and B) molecules with 1 PVA, 2 PVA (A and B), and 10 PVA (A to J) oligomers, respectively. The main results are illustrated in Figure 6.6. Cds are able to form aggregates at early stages of the simulations and PVA seems to promote the formation of Cd dimers ( $Dm_{AB}$ ). Indeed, PVA contains both hydrophilic and hydrophobic groups that may interact either with the outside part of the Cds or form inclusion complexes; the latter is shown by the snapshot in Figure 6.6(b), while the former appears for simulations of 2 Cds with 1 PVA (Figure 6.6(a)) and 2 Cds with 10 PVAs (Figure 6.6(c)). It is also noted that the prevalence of the type of configurations in Figure 6.6(b) and Figure 6.6(c) across the simulation is very high (above 95 %), which is a strong indication that such complexes are stable; for 2 Cds with 1 PVA, even though the prevalence of the typical configuration represented in Figure 6.6(a) is above 50 %, it is much less than in the other two cases. Nonetheless, it is apparent from the distance versus time plot in Figure 6.6(b) that the PVA is able to exit the Cd pocket in some instances and, then, reform the inclusion complex. In turn, it is particularly interesting to notice from the simulation of 2 Cds with 10 PVAs that the concomitant aggregation of the Cds with various molecules of PVA appears to be relatively stable complex, and likely to delay or even prevent the formation of inclusion complexes (not observed during the course of the simulation).

## 6.5 Concluding remarks

Cd aggregation is still a poorly understood phenomenon that requires systematic studies, both from the experimental and computational points of view. Several conflicting evidences are provided experi-

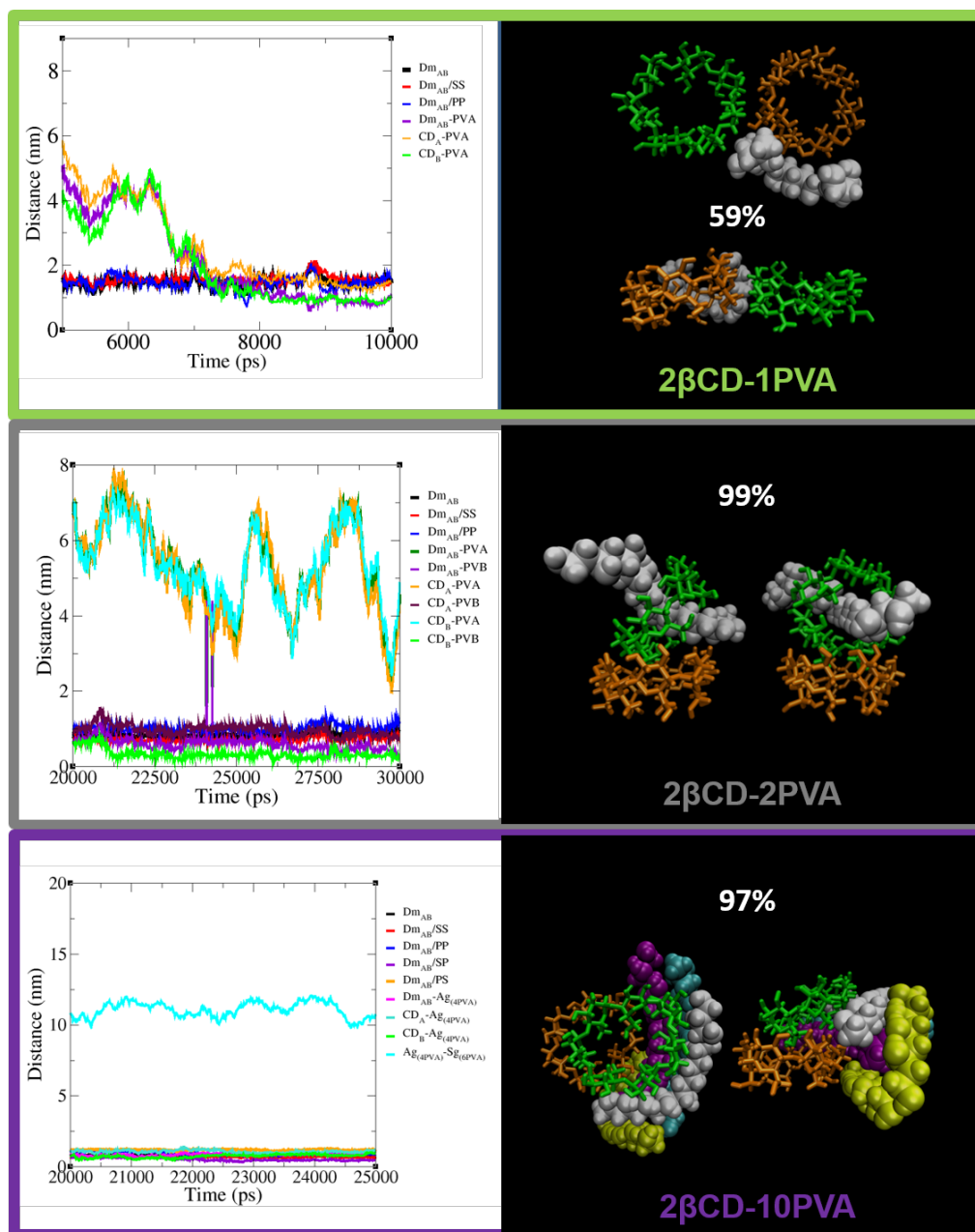


Figure 6.6: Summary of the MD simulations between  $\beta$ -Cd and PVA molecules. Left panels present the measured distances between the center of mass of the groups formed by (i) each  $\beta$ -Cd in the dimer ( $Dm_{AB}$ ), (ii) the secondary-secondary portals (SS), the primary-primary portals ( $Dm_{AB}/PP$ ), the secondary-primary portals (PS),  $Dm_{AB}$ -PVA,  $Dm_{AB}$ -PVB,  $Cd_A$ -PVA,  $Cd_A$ -PVB,  $Cd_B$ -PVA,  $Cd_B$ -PVB,  $Dm_{AB}$ -PVA aggregate ( $Ag(4PVA)$ ),  $Cd_A$ - $Ag(4PVA)$ ,  $Cd_B$ - $Ag(4PVA)$ , and  $Ag(4PVA)$  - 6 separated PVA molecules ( $Sg(6PVA)$ ). Right panels illustrate the 3 dominant conformations (accounting for more than 50 %, panel a, and 90 %, panels b and c, of the occurrences) sampled during the equilibrated parts of the production runs, at 300 K, in aqueous solution. The force field F-85 was used for the Cds. The electrostatic charges of PVA were calculated using the R.E.D. server and the remaining terms generated by acpype. [64] Reproduced from ref. [3].

mentally, calling for a comprehensive explanation of the involved phenomena and detailed, interaction based, mechanistic rationales from computation are still much needed. It is expected that, in the next

years, this subject will benefit from substantial efforts on both grounds.

## References

- [1] Giuseppina Raffaini, Antonino Mazzaglia, and Fabio Ganazzoli. “Aggregation behaviour of amphiphilic cyclodextrins: the nucleation stage by atomistic molecular dynamics simulations”. *Beilstein Journal of Organic Chemistry* 11 (2015), pp. 2459–2473. ISSN: 1860-5397. DOI: [10.3762/bjoc.11.267](https://doi.org/10.3762/bjoc.11.267).
- [2] Giuseppina Raffaini, Fabio Ganazzoli, and Antonino Mazzaglia. “Aggregation behavior of amphiphilic cyclodextrins in a nonpolar solvent: evidence of large-scale structures by atomistic molecular dynamics simulations and solution studies”. *Beilstein Journal of Organic Chemistry* 12 (2016), pp. 73–80. ISSN: 1860-5397. DOI: [10.3762/bjoc.12.8](https://doi.org/10.3762/bjoc.12.8).
- [3] Tânia F.G.G. Cova et al. “Aggregation of Cyclodextrins: Fundamental Issues and Applications”. *Cyclodextrin*. Ed. by Poonam Arora and Neelima Dhingra. Rijeka: IntechOpen, 2018. Chap. 2. DOI: [10.5772/intechopen.73532](https://doi.org/10.5772/intechopen.73532).
- [4] Alexey Ryzhakov et al. “Self-Assembly of Cyclodextrins and Their Complexes in Aqueous Solutions”. *Journal of Pharmaceutical Sciences* 105.9 (2016), pp. 2556–2569. ISSN: 0022-3549. DOI: <https://doi.org/10.1016/j.xphs.2016.01.019>.
- [5] Phennapha Saokham et al. “The self-assemble of natural cyclodextrins in aqueous solutions: Application of miniature permeation studies for critical aggregation concentration (cac) determinations”. *International Journal of Pharmaceutics* 505.1 (2016), pp. 187–193. ISSN: 0378-5173. DOI: <https://doi.org/10.1016/j.ijpharm.2016.03.049>.
- [6] Alaaeddin Alsbaiee et al. “Rapid removal of organic micropollutants from water by a porous  $\beta$ -cyclodextrin polymer”. *Nature* 529.7585 (2016), pp. 190–194. ISSN: 0028-0836. DOI: [10.1038/nature16185](https://doi.org/10.1038/nature16185).
- [7] Hadar Zaman et al. “Characterisation of aggregates of cyclodextrin-drug complexes using Taylor Dispersion Analysis”. *International Journal of Pharmaceutics* 522.1 (2017), pp. 98–109. ISSN: 0378-5173. DOI: <https://doi.org/10.1016/j.ijpharm.2017.02.012>.



- [8] Edgar Mixcoha, José Campos-Terán, and ángel Piñeiro. “Surface Adsorption and Bulk Aggregation of Cyclodextrins by Computational Molecular Dynamics Simulations as a Function of Temperature:  $\alpha$ -CD vs  $\beta$ -CD”. *The Journal of Physical Chemistry B* 118.25 (2014), pp. 6999–7011. ISSN: 1520-6106. DOI: [10.1021/jp412533b](https://doi.org/10.1021/jp412533b).
- [9] David Lucio et al. “Nanoaggregation of inclusion complexes of glibenclamide with cyclodextrins”. *International Journal of Pharmaceutics* 519.1 (2017), pp. 263–271. ISSN: 0378-5173. DOI: <https://doi.org/10.1016/j.ijpharm.2017.01.028>.
- [10] Prasun Ghosh et al. “Modulation of Small Molecule Induced Architecture of Cyclodextrin Aggregation by Guest Structure and Host Size”. *The Journal of Physical Chemistry C* 115.43 (2011), pp. 20970–20977. ISSN: 1932-7447. DOI: [10.1021/jp206299y](https://doi.org/10.1021/jp206299y).
- [11] Miyajima Koichiro, Sawada Masahiro, and Nakagaki Masayuki. “Viscosity B-Coefficients, Apparent Molar Volumes, and Activity Coefficients for  $\alpha$ - and  $\gamma$ -Cyclodextrins in Aqueous Solutions”. *Bulletin of the Chemical Society of Japan* 56.12 (1983), pp. 3556–3560. DOI: [10.1246/bcsj.56.3556](https://doi.org/10.1246/bcsj.56.3556).
- [12] Yizhak Marcus. “Effect of Ions on the Structure of Water: Structure Making and Breaking”. *Chemical Reviews* 109.3 (2009), pp. 1346–1370. ISSN: 0009-2665. DOI: [10.1021/cr8003828](https://doi.org/10.1021/cr8003828).
- [13] Olaf Häusler and Christel C. Müller-Goymann. “Properties and Structure of Aqueous Solutions of Hydroxypropyl-beta-Cyclodextrin”. *Starch - Stärke* 45.5 (1993), pp. 183–187. ISSN: 1521-379X. DOI: [10.1002/star.19930450508](https://doi.org/10.1002/star.19930450508).
- [14] Lajos Szente, Jozsef Szejtli, and Georg L. Kis. “Spontaneous Opalescence of Aqueous  $\gamma$ -Cyclodextrin Solutions: Complex Formation or Self-Aggregation?” *Journal of Pharmaceutical Sciences* 87.6 (1998), pp. 778–781. ISSN: 0022-3549. DOI: <https://doi.org/10.1021/js9704341>.
- [15] Anthony W. Coleman et al. “Aggregation of cyclodextrins: An explanation of the abnormal solubility of  $\beta$ -cyclodextrin”. *Journal of inclusion phenomena and molecular recognition in chemistry* 13.2 (1992), pp. 139–143. ISSN: 1573-1111. DOI: [10.1007/bf01053637](https://doi.org/10.1007/bf01053637).

- [16] G. González-Gaitano et al. “The Aggregation of Cyclodextrins as Studied by Photon Correlation Spectroscopy”. *Journal of Inclusion Phenomena and Macrocyclic Chemistry* 44.1 (2002), pp. 101–105. ISSN: 1573-1111. DOI: [10.1023/A:1023065823358](https://doi.org/10.1023/A:1023065823358).
- [17] Aihua Wu, Xinghai Shen, and Yongke He. “Investigation on  $\gamma$ -cyclodextrin nanotube induced by N,N'-diphenylbenzidine molecule”. *Journal of Colloid and Interface Science* 297.2 (2006), pp. 525–533. ISSN: 0021-9797. DOI: <https://doi.org/10.1016/j.jcis.2005.11.014>.
- [18] István Puskás et al. “Characterization and control of the aggregation behavior of cyclodextrins”. *Journal of Inclusion Phenomena and Macrocyclic Chemistry* 75.3 (2013), pp. 269–276. ISSN: 1573-1111. DOI: [10.1007/s10847-012-0127-7](https://doi.org/10.1007/s10847-012-0127-7).
- [19] Massimo Bonini et al. “Self-Assembly of  $\beta$ -Cyclodextrin in Water. Part 1: Cryo-TEM and Dynamic and Static Light Scattering”. *Langmuir* 22.4 (2006), pp. 1478–1484. ISSN: 0743-7463. DOI: [10.1021/la052878f](https://doi.org/10.1021/la052878f).
- [20] Simona Rossi et al. “Self-Assembly of  $\beta$ -Cyclodextrin in Water. 2. Electron Spin Resonance”. *Langmuir* 23.22 (2007), pp. 10959–10967. ISSN: 0743-7463. DOI: [10.1021/la7011638](https://doi.org/10.1021/la7011638).
- [21] J. P. Rao and Kurt E. Geckeler. “Cyclodextrin Supramacromolecules: Unexpected Formation in Aqueous Phase under Ambient Conditions”. *Macromolecular Rapid Communications* 32.5 (2011), pp. 426–430. ISSN: 1521-3927. DOI: [10.1002/marc.201000630](https://doi.org/10.1002/marc.201000630).
- [22] Tânia F. G. G. Cova, Sandra C. C. Nunes, and Alberto A. C. C. Pais. “Free-energy patterns in inclusion complexes: the relevance of non-included moieties in the stability constants”. *Physical Chemistry Chemical Physics* 19.7 (2017), pp. 5209–5221. ISSN: 1463-9076. DOI: [10.1039/C6CP08081B](https://doi.org/10.1039/C6CP08081B).
- [23] Mrinmoy De et al. “Biomimetic Interactions of Proteins with Functionalized Nanoparticles: A Thermodynamic Study”. *Journal of the American Chemical Society* 129.35 (2007), pp. 10747–10753. ISSN: 0002-7863. DOI: [10.1021/ja071642q](https://doi.org/10.1021/ja071642q).
- [24] Phennapha Saokham and Thorsteinn Loftsson. “A New Approach for Quantitative Determination of  $\gamma$ -Cyclodextrin in Aqueous Solutions: Application in Aggregate Determinations and Solubility in Hydrocortisone/ $\gamma$ -Cyclodextrin Inclusion Complex”. *Journal of Pharmaceutical*

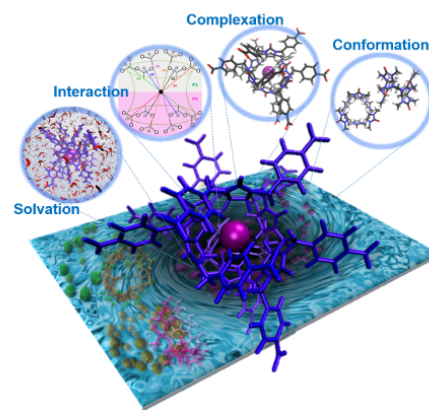
- Sciences* 104.11 (2015), pp. 3925–3933. ISSN: 0022-3549. DOI: <https://doi.org/10.1002/jps.24608>.
- [25] Thao Thi Do, Rob Van Hooghten, and Guy Van den Mooter. “A study of the aggregation of cyclodextrins: Determination of the critical aggregation concentration, size of aggregates and thermodynamics using isodesmic and K2-K models”. *International Journal of Pharmaceutics* 521.1 (2017), pp. 318–326. ISSN: 0378-5173. DOI: <https://doi.org/10.1016/j.ijpharm.2017.02.037>.
- [26] Artur J. M. Valente, Rui A. Carvalho, and Olle Söderman. “Do Cyclodextrins Aggregate in Water? Insights from NMR Experiments”. *Langmuir* 31.23 (2015), pp. 6314–6320. ISSN: 0743-7463. DOI: [10.1021/acs.langmuir.5b01493](https://doi.org/10.1021/acs.langmuir.5b01493).
- [27] A. J. M. Valente et al. “Molecular Dynamics of Cyclodextrins in Water Solutions from NMR Deuterium Relaxation: Implications for Cyclodextrin Aggregation”. *Langmuir* 33.33 (2017), pp. 8233–8238. ISSN: 0743-7463. DOI: [10.1021/acs.langmuir.7b01923](https://doi.org/10.1021/acs.langmuir.7b01923).
- [28] A. A. S. T. Ribeiro, B. A. C. Horta, and R. B. de Alencastro. “MKTOP: A program for automatic construction of molecular topologies”. *Journal of the Brazilian Chemical Society* 19 (2008). DOI: [10.1590/s0103-50532008000700031](https://doi.org/10.1590/s0103-50532008000700031).
- [29] Ana C. F. Ribeiro et al. “Binary Mutual Diffusion Coefficients of Aqueous Solutions of  $\beta$ -Cyclodextrin at Temperatures from 298.15 to 312.15 K”. *Journal of Chemical & Engineering Data* 51.4 (2006), pp. 1368–1371. ISSN: 0021-9568. DOI: [10.1021/je060092t](https://doi.org/10.1021/je060092t).
- [30] Ana C. F. Ribeiro et al. “Some Transport Properties of  $\alpha$ -Cyclodextrin Aqueous Solutions at (298.15 and 310.15) K”. *Journal of Chemical & Engineering Data* 53.3 (2008), pp. 755–759. ISSN: 0021-9568. DOI: [10.1021/je700598v](https://doi.org/10.1021/je700598v).
- [31] Jia He et al. “Cooperative Recruitment of Amphotericin B Mediated by a Cyclodextrin Dimer”. *The Journal of Physical Chemistry C* 118.41 (2014), pp. 24173–24180. ISSN: 1932-7447. DOI: [10.1021/jp507325j](https://doi.org/10.1021/jp507325j).
- [32] A. Figueiras et al. “New insight into the discrimination between omeprazole enantiomers by cyclodextrins in aqueous solution”. *Journal of Inclusion Phenomena and Macrocyclic Chemistry* 62.3-4 (2008), pp. 345–351. ISSN: 0923-0750. DOI: [10.1007/s10847-008-9477-6](https://doi.org/10.1007/s10847-008-9477-6).

- [33] Ana Figueiras et al. “Molecular interaction governing solubility and release profiles in supramolecular systems containing fenbufen, pluronics and cyclodextrins”. *Journal of Inclusion Phenomena and Macrocyclic Chemistry* 81.3-4 (2015), pp. 395–407. ISSN: 1388-3127.
- [34] Kun Li et al. “Inclusion complexes of organic salts with small beta-cyclodextrin as organocatalysts for CO<sub>2</sub> cycloaddition with epoxides”. *RSC Advances* 7.24 (2017), pp. 14721–14732. DOI: [10.1039/C7RA00416H](https://doi.org/10.1039/C7RA00416H).
- [35] Andrea Mele, Raniero Mendichi, and Antonio Selva. “Non-covalent associations of cyclomaltooligosaccharides (cyclodextrins) with trans- $\beta$ -carotene in water: evidence for the formation of large aggregates by light scattering and NMR spectroscopy”. *Carbohydrate Research* 310.4 (1998), pp. 261–267. ISSN: 0008-6215. DOI: [https://doi.org/10.1016/S0008-6215\(98\)00193-1](https://doi.org/10.1016/S0008-6215(98)00193-1).
- [36] Jef Stappaerts et al. “The impact of guest compounds on cyclodextrin aggregation behavior: A series of structurally related parabens”. *International Journal of Pharmaceutics* 529.1 (2017), pp. 442–450. ISSN: 0378-5173. DOI: <https://doi.org/10.1016/j.ijpharm.2017.07.026>.
- [37] Yifeng He et al. “Cyclodextrin-based aggregates and characterization by microscopy”. *Micron* 39.5 (2008), pp. 495–516. ISSN: 0968-4328. DOI: <https://doi.org/10.1016/j.micron.2007.06.017>.
- [38] Rebeca Hernández et al. “Controlling PVA Hydrogels with  $\gamma$ -Cyclodextrin”. *Macromolecules* 37.25 (2004), pp. 9620–9625. ISSN: 0024-9297. DOI: [10.1021/ma048375i](https://doi.org/10.1021/ma048375i).
- [39] Cristian C. Rusa, Justin Fox, and Alan E. Tonelli. “Competitive Formation of Polymer-Cyclodextrin Inclusion Compounds”. *Macromolecules* 36.8 (2003), pp. 2742–2747. ISSN: 0024-9297. DOI: [10.1021/ma021755o](https://doi.org/10.1021/ma021755o).
- [40] Cristian C. Rusa et al. “Inclusion Compound Formation with a New Columnar Cyclodextrin Host”. *Langmuir* 18.25 (2002), pp. 10016–10023. ISSN: 0743-7463. DOI: [10.1021/la0262452](https://doi.org/10.1021/la0262452).
- [41] Adina Papancea et al. “PVA-DNA Cryogel Membranes: Characterization, Swelling, and Transport Studies”. *Langmuir* 24.1 (2008), pp. 273–279. ISSN: 0743-7463. DOI: [10.1021/la702639d](https://doi.org/10.1021/la702639d).

- [42] Leïla Zerkoune, Angelina Angelova, and Sylviane Lesieur. “Nano-Assemblies of Modified Cyclodextrins and Their Complexes with Guest Molecules: Incorporation in Nanostructured Membranes and Amphiphile Nanoarchitectonics Design”. *Nanomaterials* 4.3 (2014), p. 741. ISSN: 2079-4991.
- [43] R. Auzély-Velty et al. “Micellization of Hydrophobically Modified Cyclodextrins. 1. Micellar Structure”. *Langmuir* 16.8 (2000), pp. 3727–3734. ISSN: 0743-7463. DOI: [10.1021/la991361z](https://doi.org/10.1021/la991361z).
- [44] Teng Wang et al. “Structural Characterization of Micelles Formed of Cholesteryl-Functionalized Cyclodextrins”. *Langmuir* 27.1 (2011), pp. 91–97. ISSN: 0743-7463. DOI: [10.1021/la103288j](https://doi.org/10.1021/la103288j).
- [45] Wanda Sliwa and Tomasz Girek. *Cyclodextrins: Properties and Applications*. John Wiley & Sons, 2016. ISBN: 3527695281.
- [46] Antonino Mazzaglia et al. “Supramolecular Assemblies Based on Complexes of Nonionic Amphiphilic Cyclodextrins and a meso-Tetra(4-sulfonatophenyl)porphine Tributyltin(IV) Derivative: Potential Nanotherapeutics against Melanoma”. *Biomacromolecules* 14.11 (2013), pp. 3820–3829. ISSN: 1525-7797. DOI: [10.1021/bm400849n](https://doi.org/10.1021/bm400849n).
- [47] Bang-Ping Jiang, Dong-Sheng Guo, and Yu Liu. “Self-Assembly of Amphiphilic Perylene-Cyclodextrin Conjugate and Vapor Sensing for Organic Amines”. *The Journal of Organic Chemistry* 75.21 (2010), pp. 7258–7264. ISSN: 0022-3263. DOI: [10.1021/jo1014596](https://doi.org/10.1021/jo1014596).
- [48] Wanda Sliwa and Tomasz Girek, eds. *Cyclodextrins: Properties and Applications*. 1st ed. Germany: Wiley-VCH, 2017.
- [49] Martin Bauer et al. “Insertion properties of cholesteryl cyclodextrins in phospholipid membranes: a molecular study”. *Soft Matter* 8.4 (2012), pp. 942–953. ISSN: 1744-683X. DOI: [10.1039/C1SM06346D](https://doi.org/10.1039/C1SM06346D).
- [50] Haiyang Zhang et al. “Molecular Recognition in Different Environments:  $\beta$ -Cyclodextrin Dimer Formation in Organic Solvents”. *The Journal of Physical Chemistry B* 116.42 (2012), pp. 12684–12693. ISSN: 1520-6106. DOI: [10.1021/jp308416p](https://doi.org/10.1021/jp308416p).

- [51] Haiyang Zhang et al. “Cooperative Binding of Cyclodextrin Dimers to Isoflavone Analogues Elucidated by Free Energy Calculations”. *The Journal of Physical Chemistry C* 118.13 (2014), pp. 7163–7173. ISSN: 1932-7447. DOI: [10.1021/jp412041d](https://doi.org/10.1021/jp412041d).
- [52] Lingzhi Zhang, Jinping Zhou, and Lina Zhang. “Structure and properties of  $\beta$ -cyclodextrin/cellulose hydrogels prepared in NaOH/urea aqueous solution”. *Carbohydrate Polymers* 94.1 (2013), pp. 386–393. ISSN: 0144-8617. DOI: <https://doi.org/10.1016/j.carbpol.2012.12.077>.
- [53] Xinzhe Zhu, Guozhong Wu, and Daoyi Chen. “Molecular dynamics simulation of cyclodextrin aggregation and extraction of Anthracene from non-aqueous liquid phase”. *Journal of Hazardous Materials* 320.Supplement C (2016), pp. 169–175. ISSN: 0304-3894. DOI: <https://doi.org/10.1016/j.jhazmat.2016.08.015>.
- [54] Haiyang Zhang, Tianwei Tan, and David Van der Spoel. “Generalized Born and Explicit Solvent Models for Free Energy Calculations in Organic Solvents: Cyclodextrin Dimerization”. *Journal of Chemical Theory and Computation* 11.11 (2015), pp. 5103–5113. ISSN: 1549-9618.
- [55] David van der Spoel, Paul J. van Maaren, and Carl Caleman. “GROMACS molecule and liquid database”. *Bioinformatics* 28.5 (2012), pp. 752–753. DOI: [10.1093/bioinformatics/bts020](https://doi.org/10.1093/bioinformatics/bts020).
- [56] Enguerran Vanquelef et al. “R.E.D. Server: a web service for deriving RESP and ESP charges and building force field libraries for new molecules and molecular fragments”. *Nucleic Acids Research* 39.2 (2011), W511–W517. DOI: [10.1093/nar/gkr288](https://doi.org/10.1093/nar/gkr288).
- [57] Jirasak Wong-ekkabut and Mikko Karttunen. “The good, the bad and the user in soft matter simulations”. *Biochimica Et Biophysica Acta-Biomembranes* 1858.10 (2016). SI, pp. 2529–2538. ISSN: 0005-2736.
- [58] B. Hess et al. “LINCS: A linear constraint solver for molecular simulations”. *Journal of Computational Chemistry* 18.12 (1997), pp. 1463–1472. ISSN: 0192-8651.
- [59] X. Daura et al. “Peptide folding: When simulation meets experiment”. *Angewandte Chemie-International Edition* 38.1-2 (1999), pp. 236–240. ISSN: 1433-7851.

- [60] Subhaseema Das and Usharani Subuddhi. “Exploring poly(vinyl alcohol) hydrogels containing drug-cyclodextrin complexes as controlled drug delivery systems”. *Journal of Applied Polymer Science* 131.11 (2014), n/a–n/a. ISSN: 1097-4628. DOI: [10.1002/app.40318](https://doi.org/10.1002/app.40318).
- [61] Jianbo Zhou et al. “Preparation and characterization of electrospun polyvinyl alcoholstyrylpyridinium/ $\beta$ -cyclodextrin composite nanofibers: Release behavior and potential use for wound dressing”. *Fibers and Polymers* 17.11 (2016), pp. 1835–1841. ISSN: 1875-0052. DOI: [10.1007/s12221-016-6716-0](https://doi.org/10.1007/s12221-016-6716-0).
- [62] Lei Ouyang et al. “Preparation of a native small beta-cyclodextrin modified plasmonic hydrogel substrate and its use as a surface-enhanced Raman scattering scaffold for antibiotics identification”. *Journal of Materials Chemistry C* 3.29 (2015), pp. 7575–7582. ISSN: 2050-7526. DOI: [10.1039/C5TC01368B](https://doi.org/10.1039/C5TC01368B).
- [63] Matti Knaapila et al. “Incorporation of a Cationic Conjugated Polyelectrolyte CPE within an Aqueous Poly(vinyl alcohol) Sol”. *Macromolecules* 49.23 (2016), pp. 9119–9131. ISSN: 0024-9297. DOI: [10.1021/acs.macromol.6b01895](https://doi.org/10.1021/acs.macromol.6b01895).
- [64] Frederico B. De Sousa et al. “Superstructure based on small beta-CD self-assembly induced by a small guest molecule”. *Physical Chemistry Chemical Physics* 14.6 (2012), pp. 1934–1944. ISSN: 1463-9076. DOI: [10.1039/C2CP22768A](https://doi.org/10.1039/C2CP22768A).



## Chapter 7

# Properties and Patterns in Bambusurils

The recently discovered glycoluril-based macrocycles, bambusurils, have been recognized as effective anion containers and electron donors, playing an important role in a variety of systems with technological and biological relevance. The potential use of bambusurils in energy-storage systems and in processes related to ion-channel diseases are undoubtedly examples of emerging applications. [1, 2] Their multifaceted properties are, so far, very little explored and recent efforts have set the basis for a better understanding of the binding behavior of bambusuril derivatives, able to form stable complexes with various anionic molecules. In what follows the key advances pertaining to bambusurils, including structural variations, methods of synthesis and corresponding physical and chemical properties are summarized. The main factors affecting the stability and structure of the respective inclusion complexes are outlined. Challenges regarding computational approaches for predicting properties of these host-guest systems are also discussed. Computational insight is particularly valuable to improve and fine-tune the conformation and ion affinity of bambusurils, being crucial to reinforce anion recognition properties.

### 7.1 Anion-receptors: properties and relevant issues

Macrocycles formed by glycoluril units have been used in functional structures involving host-guest interactions. [1–3] These cyclic molecules, that function as anion receptors, are essential in a variety of systems with technological and biological relevance. Bambusurils consist of 2,4-dimethylglycoluril



units, adopting alternate conformations, interconnected by one methylene bridge. [2] Their interior acts as anion receptor, but little is known about the binding properties of their portals. In spite of the importance of these systems, only a few studies on the preparation methods are available in the literature, the most recent ones dating from 6 years ago.

For many years the field of noncovalent anion coordination chemistry was only sporadically studied. Even the first edition of *Comprehensive Supramolecular Chemistry* series [4, 5] devoted only a single chapter fully to anion binding. This subject, which has attained in the last 10 years an impressive degree of diversity and complexity, has been developed at an unusually rapid pace following the initial findings on the molecular recognition of small anionic species. A variety of receptors for anionic species have been investigated in detail in areas of particular importance such as organocatalysis and in the development of new sensors and sensing arrays for anionic agents. [6] Several comprehensive publications have provided a full account of the advances in the field (see e.g. [6–11]). The chemistry of anion receptors cannot be dissociated from host-guest and supramolecular interactions, which have also led to a huge variety of applications. [6, 12]

Although the concepts underlying "receptor" or "host" often have different meanings, both terms can be used to describe complexes that are composed of two or more entities (molecules or ions) that are held together in unique structural relationships by interactions of noncovalent nature. For instance, the development of anion transporters to promote the translocation of anions across lipid membranes is an emerging field, contributing to improve the mechanisms involved in ion channel diseases such as cystic fibrosis. [13] In parallel, the use of anions to template self-assembled structures has also significantly progressed, and has been recently revisited. [14] Subsequently, the synthesis of anion-templated rotaxanes and catenanes [10, 14] have provided new systems of the same type, again making a direct connection to host-guest supramolecular systems. Recently, rotaxanes forming strong complexes with halides in water through a combination of halogen and hydrogen bonding have also been investigated. [10, 15] The recognition and monitoring of anions is of paramount importance in maintaining balances and neutrality in biological mechanisms, including those connected to ion-channel diseases. In these systems, compatibility with aqueous media is mandatory; however, in some cases, water may hinder the binding affinity. This has fostered the development of new host-anion systems, but the establishment of tools to rationalize the relation between structural

variations of the new synthetic anion receptors and their affinity, with different anions, still remains necessary. In fact, anions are generally strongly hydrated [7, 16], and possess a great range of hydrophilicity/hydrophobicity and multiple protonation equilibria that causes difficulties in their recognition. Due to their strong hydration, they interact weakly by electrostatic interactions with positively charged hosts. Anions also possess a huge variety of geometries (spherical, linear, etc.), thus requiring a higher degree of design and complementarity to prepare selective and specific receptors. The design of water-soluble receptors for anions is particularly challenging and significant advances have been made, taking advantage of specific effects such as the hydrophobic effect, C-H hydrogen and halogen bonding. [7] The nature of the solvent plays a fundamental role in the selectivity and strength of the anion binding process. Electrostatic interactions are particularly important in stabilizing anions in solution and generally dominate over other recognition forces. A potential anion receptor must compete effectively with the solvent environment. Neutral anion receptors possess directional modes of interaction via hydrogen-bonds, which allow stabilizing their complexes with bound anions. The use of these interactions provides an increased selectivity for a particular anion, and minimizes the competition effect in the presence of a counter ion. A neutral receptor that binds anions solely through hydrogen-bonding interactions is less likely to win the competition with the solvation shell surrounding the anion, and hence may only be effective as an anion receptor in solvents in which the anion interacts more weakly (e.g. organic solvents). Charged receptors, on the other hand, can benefit from electrostatic effects and thus may be more effective in the presence of water or other polar protic solvents. Note that, the anion receptor also faces competition from the counterion of the target anion. Additionally, host solvation, hydrophobicity, and Hofmeister effects [7, 15, 17] also affect the selectivity of the receptor. Anion receptors that disrupt the Hofmeister series regular order are usually able to bind the target anion selectively. The most popular hosts for recognition of anions in aqueous solution, are naturally those of cationic nature. The interaction occurs through electrostatic attraction and hydrogen bonding. [18, 19] A few strategies have been used to counteract the strong interactions between anions and their hydration shells. [15, 16, 20] Examples of receptors that are neutral or possess a low charge and function in organic/aqueous mixtures are uncommon and those that operate in pure water are in fact, very scarce. [7, 8] These receptors are often classified according to the nature of the interaction with the anion, including hydrogen and halogen bonds [21–24] and anion- $\pi$  inter-

actions. [25] In fact, the role of anion- $\pi$  interactions has been discussed, and a survey of synthetic supramolecular examples for this type of complexes has been included in the Protein Data Bank. An example of these type of anion receptors is the bambusuril (BU[n]s) family, which have been pointed as effective ion caging agents [2] and transporters [26], and electron donors in photoinduced electron transfer processes. [3] The results already obtained with benzoates and tosylates [27] and dialkyl phosphates [28] seem to point towards the feasibility of obtaining interesting supramolecular structures, possibility that further motivates exploring the potential of BUs in energy-storage systems, such as optoelectronic devices. [3] Fiala et al. [3] have reported a new photoactive crystalline material in which dodecabenzylbambus[6]uril plays an interesting and innovative role as reducing agent in the photoreduction of methyl viologen ( $MV^{2+}$ ) in the presence of hexafluorophosphate. As previously observed by the same group [27, 28] the stabilization of the complex of ( $Bn_{12}BU[6]$ ),  $MV^{2+}$  and two hexafluorophosphate ( $PF_6^-$ ) ions is ensured by one water molecule placed in the center of the cavity, between the  $PF_6^-$  ions. These complexes adopt a layered structure in which the BU molecules interact by weak hydrogen bonds (for details see ref. [3]). The mechanistic details of one-electron transfer from BU to  $MV^{2+}$  and the formation and nature of the radical ion pair were provided resorting to a combined approach based on experimental (spectral and cyclic voltammetry data) and computational techniques (quantum-chemical calculations). In the next section, a comparison between the structure and binding affinity of the methyl-substituted bambus[6]uril,  $Me_{12}BU[6]$ , containing six glycoluril monomers and two other hosts (cucurbit[6]uril, CB[6], and hemicucurbit[6]uril, hmCB[6]) derived from the same building block is provided.

## 7.2 Structure and binding affinity

The cyclic structure [29–32] of the glycoluril-based receptors, BU[n]s, discovered by Sindelar and co-workers and illustrated in Figure 7.1 (panel a), possesses dimethylglycoluril units, adopting alternate conformations, interconnected by methylene bridges. [30, 31, 33] The development of the glycoluril building block and its derivatives is an important linking thread between the bambusuril and cucurbit[n]uril (CB[n]s) families. [34–38] Interestingly, although the latter have similar glycoluril building blocks, the different arrangement of these units makes them hosts for cationic and neu-

tral species. Other related macrocyclic molecules, formed of  $n$  methylene-linked imidazolidin-2-one units, have been called hemicucurbit[ $n$ ]urils [39–41] (hmCB[ $n$ ]s,  $n=6, 12$ ), as their structures feature the arrangement obtained when the corresponding cucurbit[ $n$ ]uril is cut in half along the equator (Figure 7.1, panel a). These hmCBs can also bind anionic guests. Some of the structural features of CBs and hmCBs have been combined to produce the cyclic hexamer bambus[6]uril, methyl-substituted bambus[6]uril (Me<sub>12</sub>BU[6]). [34] In spite of being characterized by high steric constraints imposed by their subunits, the latter differ from CB[6] by enhanced overall structural flexibility, conferred by the "single stranded" arrangement of their glycoluril units, in contrast with the significantly rigid structure of the "double stranded" CBs molecules. The parent containers, hmCBs, are devoid of these steric effects, and are highly flexible. [34, 40] BUs and hmCBs are both flexible and present good solubility in organic solvents. However, BUs bind halide anions with higher affinity and selectivity than hmCBs. [34] From panel b (Figure 7.1) it is worth to note the differences between the charge density of each macrocycle, compatible with the differential binding affinity.

Electrostatic potential profiles thus confirm that in Me<sub>12</sub>BU[6], the positive potential is present inside the core due to the inward methine hydrogens. The presence of only one row of methylene bridges confers to the cavity an increased flexibility and adaptability to the size of the anion. [31, 42] Using electronic structure calculations, at the DFT level, Sundararajan and co-workers [34] have investigated the type of interactions present in host-guest complexes formed between halides (iodide, bromide and chloride) and Me<sub>12</sub>BU[6]. The calculations showed that, among the complexes with hmCB[6] and Me<sub>12</sub>BU[6], chloride complexes possess the largest relaxation energies (ca. 8.6 kcal mol<sup>-1</sup> and 12.5 kcal mol<sup>-1</sup>, respectively). This indicates that the host molecules have large structural reorganizations when the size of the halide ion is small, due to strong electrostatic and hydrogen bonding interactions. The possible binding sites of the halide ions were then revealed by the LUMO of the three empty hosts (Figure 7.1, panel c). [34] In hmCB[6] and in BU[6], the twelve methine hydrogens create a positive potential at the core, whereas in CB[6], a positive potential is created by methine hydrogens oriented outwards the CB[6] cavity. The central core region of hmCB[6] and BU[6] is, therefore, more suitable for the inclusion of anions, such as halides. However, CB[6] can be a better binding site for cations, such as metal ions, and anion binding can occur only outside the cavity. In comparison to hmCB[6] and BU[6], inclusion of a halide ion to CB[6] does not lead to any significant

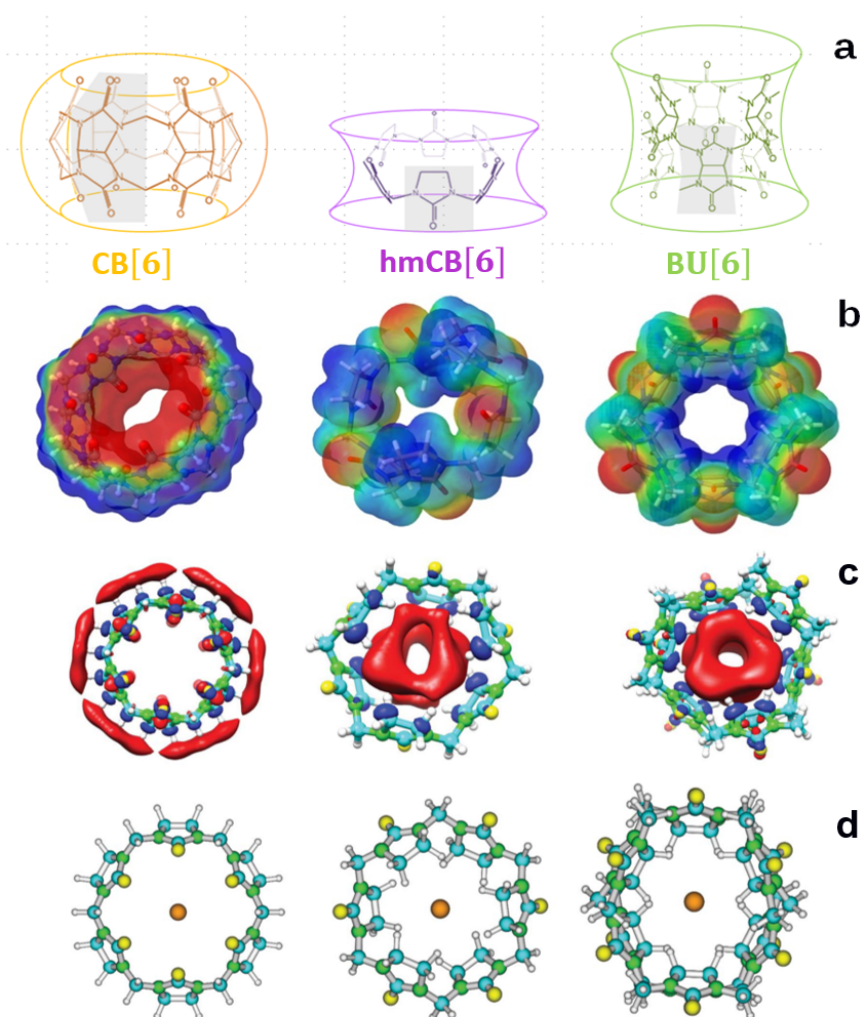


Figure 7.1: (a) Molecular structures of bare CB[6] (left), hmCB[6] (middle) and BU[6] (right) molecules. The shaded parts highlight one of the repeating units. (b) Electrostatic potential profiles of CB[6] (left), hmCB[6] (middle) and BU[6]. ESPs are mapped on electron density isosurfaces at the HF/6-31G(d) level of theory. The carbonyl oxygen atoms of the macrocycles are negatively charged and are colored in red, while positive regions are depicted in blue. (c) Lowest unoccupied molecular orbitals of CB[6] (left), hmCB[6] (middle) and BU[6] (right). (d) Optimized structures of a halide encapsulated in CB[6] (left), hmCB[6] (middle) and BU[6] (right) (color code: yellow refers to oxygen, bright blue to carbon, green to nitrogen, brown to halide ion and pale white to hydrogen). Reproduced from ref. [1].

geometrical change (for details see Figure 7.1, panel d, and ref. [34]). As expected, the anionic portals in CB[6] hinder the inclusion of anions. The calculated binding energies also confirm that inclusion by hmCB[6] and BU[6] is favored. In addition to the electrostatic contribution, the twelve methine hydrogens of the glycoluril units pointing inside the core, promote the formation of hydrogen bonds with halide ions. In contrast, inclusion by CB[6] is largely unfavorable irrespective of the nature of

the halide ions. [34]

The convex arrangement of glycoluril units in BUs, dictate that the methine hydrogen atoms point inwards. In this typical conformation, the methine hydrogens form a pocket with the possibility of establishing  $\text{CH}\cdots\text{X}$  interactions. The internal diameter and the respective height of  $\text{Me}_{12}\text{BU}[6]$  may reach a typical maximum of 6.4 Å and 12.7 Å, respectively. [31] The binding modes of  $\text{BU}[6]$  and their arrangement in the solid-state have been established [33] using X-ray diffraction and the measured parameters are summarized in Figure 7.2. The values in the inset correspond to the typical heights and diameters of the host in various  $\text{BU}[6]$ -anion complexes, with the latter increasing with the increasing of the anion size.

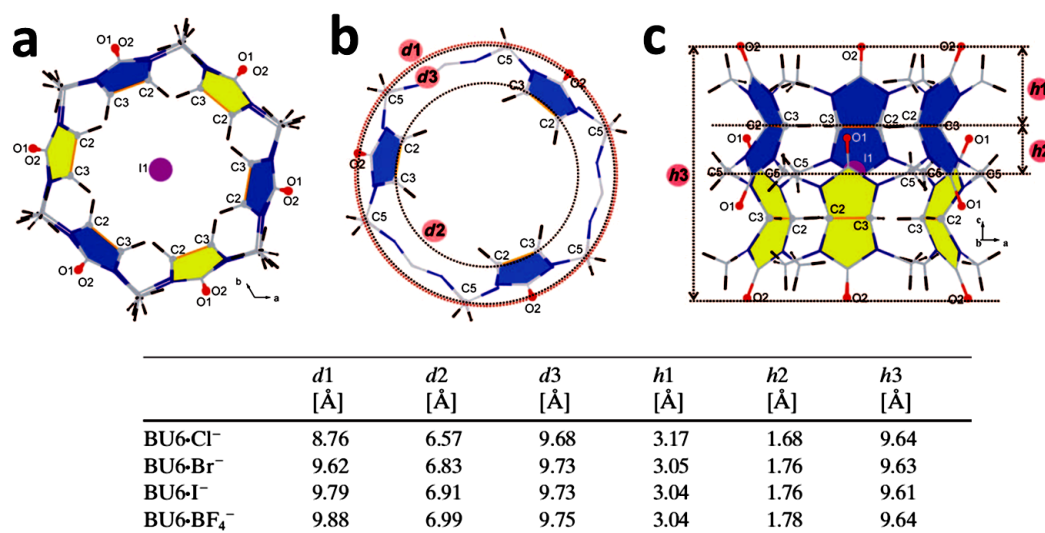
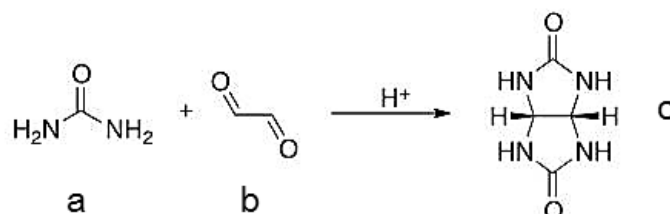


Figure 7.2: Crystal structure of the complex between  $\text{BU}[6]$  and iodide including the measured (b) diameters and (c) heights. The glycoluril units of the host displayed on the upper (blue) and lower positions (yellow) are symmetric related and are at the same distance to the central anion. Reproduced from ref. [1].

## 7.3 Synthesis and properties

Glycoluril (systematic name: tetrahydro[4,5-d]imidazole-2,5(1H,3H)-dione, Scheme 7.1c) was first prepared in 1865 [43], and since then has become a fundamental building-block for the preparation and assembly of supramolecular molecules [44–51], such as bambusurils and cucurbiturils. [47, 51–

55], and also molecules used as acyclic hosts (e.g. glycoluril oligomers [54, 56–59], molecular clips [46, 60–65], and capsules [56, 66]). The potential of glycoluril as key unit of supramolecular constructs is due to their intrinsic geometry, chemical nature and ability to form noncovalent interactions [46, 67, 68]. The suitability of this bicyclic product (c) of the reaction of glyoxal (b) with two equivalents of urea (a) has been a relevant topic covered in refs. [44, 46, 49, 69].

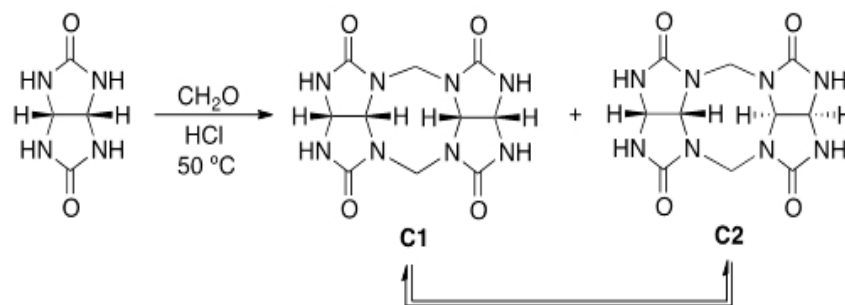


Scheme 7.1: Preparation of glycoluril (c) used for the synthesis of important cyclic and acyclic host molecules. This bicyclic product is obtained from the reaction of glyoxal (b) with two equivalents of urea (a). Reproduced from ref. [1].

The mechanistic details for the preparation of BUs are scarce, in contrast to what happens for CBs. However, part of this mechanism is likely to be similar to that found in the latter, especially in what concerns the cyclo-oligomerization (see below). CBs are obtained from an acid-catalyzed condensation reaction of glycoluril and formaldehyde, in which participate methylene bridged glycoluril oligomers. A molar ratio of 1:2 between glycoluril and formaldehyde is required to ensure the synthesis of the macrocycle. [46, 48, 52, 53, 67] Using less than 2 equivalents of formaldehyde, a mixture of oligomers is obtained, intermediates of the synthesis of the macrocycle. Thus, the CBs synthesis can be explained by a mechanism based on a step-growth cyclo-oligomerization. The stepwise addition of the glycoluril to the end of the growth oligomer chain affords oligomer (e.g. hexamer) that can undergo direct cyclization to give CB[n] macrocycles by the condensation with 2 equivalents of formaldehyde.

The reaction of glycoluril with one equivalent of formaldehyde affords glycoluril dimer C1, (C-shaped form) the dimer with the relative orientation of the pairs of methine C-H groups observed in the macrocycle and no evidence for the formation of diastereoisomer C2 (S-shaped form) is observed. This selectivity was explained considering the thermodynamic preference for C1, which is in agreement with model studies carried out with C1 and C2 derivatives bearing CO<sub>2</sub>Et groups. [54] Nevertheless, in the synthesis of CB, glycoluril reacts initially with two equivalent of formaldehyde to

afford a mixture of diastereomers C1 and C2 which can undergo interconversion via an intramolecular process 60 (Scheme 7.2). Further oligomerization of the dimer, followed by macrocyclization affords



Scheme 7.2: General preparation of methylene bridged glycoluril dimers. Reproduced from ref. [1].

CB. However, Sindelar et al. [44] demonstrated that for substituted glycolurils the imerization process involves the initial synthesis of the S-shaped dimer which undergoes isomerization into its C-shaped diastereoisomeric. [44]

Bambusurils are prepared by acid-catalyzed reaction of the appropriate 2,4-disubstituted glycoluril  $c'$  with formaldehyde  $d$  (Figure 7.3). In these glycoluril building blocks, only two nitrogens of the same imidazolidin-2-one ring are available for the reaction with formaldehyde resulting in the synthesis of bambus[6]uril where the glycoluril units are connected by one methylene bridge.

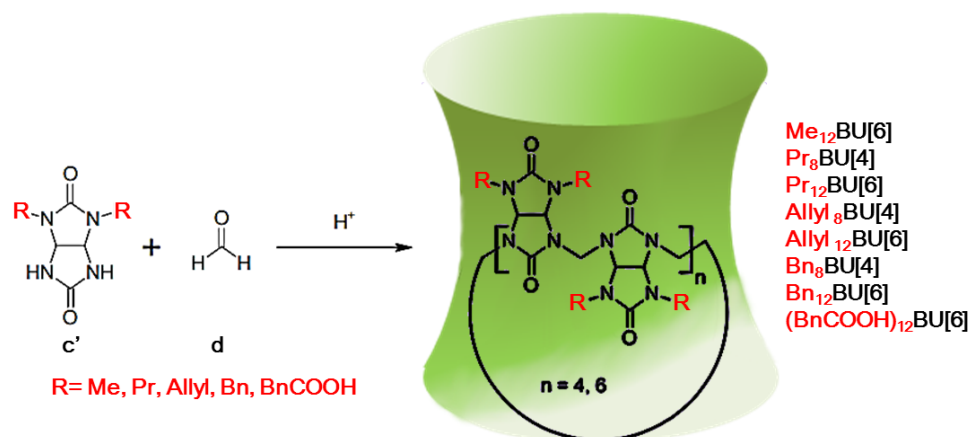


Figure 7.3: General synthesis of bambusuril derivatives from the acidic-catalyzed condensation between 2,4-disubstituted glycoluril ( $c'$ ) and formaldehyde ( $d$ ). Reproduced from ref. [2].

So far, bambusuril derivatives have been prepared from disubstituted glycoluril building block containing aliphatic residues (methyl [30, 31, 33], propyl and allyl [32] groups) and aromatic substituents



(benzyl and benzoyl [27, 29] groups). Depending on the substitution, it is possible to tune the properties of the macrocycle backbone, such as, solubility and molecular affinity. At this point it should be stressed that BUs derivatives (Figure 7.3) result from peripheral substitutions, in which the disubstituted glycoluril units, containing aliphatic or aromatic substituents are used to construct the macrocycle, while BU analogs [26, 70, 71], in which the portal or equatorial oxygen atoms of the carbonyl groups are replaced by different heteroatoms (e.g sulfur [71] and nitrogen [70]) requires the reaction of glycoluril analogs (e.g. monothio glycoluril). Figure 7.4 presents the structures of BUs derivatives, panels (a) to (c), and sulfur-based BUs analogs, panel (d).

The preparation of the methyl substituted BU,  $\text{Me}_{12}\text{BU}[6]$ , was first described in 2010 [31] by Sindelar and co-workers, and consisted of an acid-catalyzed condensation between 2,4-dimethylglycoluril and formaldehyde. During the synthesis, the chloride anion from HCl was used as a template and the macrocycle was formed as a 1:1 complex, in which the chloride anion was bound in the middle part of the cavity. The  $\text{Me}_{12}\text{BU}[6]\text{-Cl}$  complex was soluble in a chloroform-methanol mixture (1:1), but also in the water-acetonitrile mixture (1:1). The stability of the complex hampered the dissociation to obtain the anion-free  $\text{Me}_{12}\text{BU}[6]$ . The chloride anion was substituted only by bromide or iodide anions, which were able to be included inside  $\text{Me}_{12}\text{BU}[6]$  with higher affinity compared to the chloride anion. The oxidation of the iodide anion in the  $\text{Me}_{12}\text{BU}[6]\text{-HI}$  complex allowed the isolation of the anion-free  $\text{Me}_{12}\text{BU}[6]$ , which appeared insoluble in the investigated solvents. [31]  $\text{Me}_{12}\text{BU}[6]$  is a strong anion binder but their synthesis depends on the anion template effect as described in references [31, 72, 73]. This approach is based on the use of the anion of interest as a templating agent to link together the glycoluril units into assemblies that have high selectivity for the templating anion. The latter can be considered as an entity that contains the required features to promote the organization of the building blocks in a specific manner, in a thermodynamically or kinetically driven process. [72] Since the discovery of  $\text{Me}_{12}\text{BU}[6]$ , the synthesis of other derivatives has been reported namely octabenzylbambus[4]uril ( $\text{Bn}_8\text{BU}[4]$ ), dodecabenzylbambus[6]uril ( $\text{Bn}_{12}\text{BU}[6]$ ) and dodecapropylbambus[6]uril ( $\text{Pr}_{12}\text{BU}[6]$ ) [30], obtained from 2,4-dibenzylglycoluril (for  $\text{Bn}_8\text{BU}[4]$  and  $\text{Bn}_{12}\text{BU}[6]$ , Scheme 7.3) or 2,4-dipropylglycoluril (for  $\text{Pr}_{12}\text{BU}[6]$ ) units, respectively. The synthesis of these derivatives has been controlled by anionic templates and has been performed in non-polar solvents, in contrast to the aqueous media used in the synthesis of  $\text{Me}_{12}\text{BU}[6]$ . The microwave

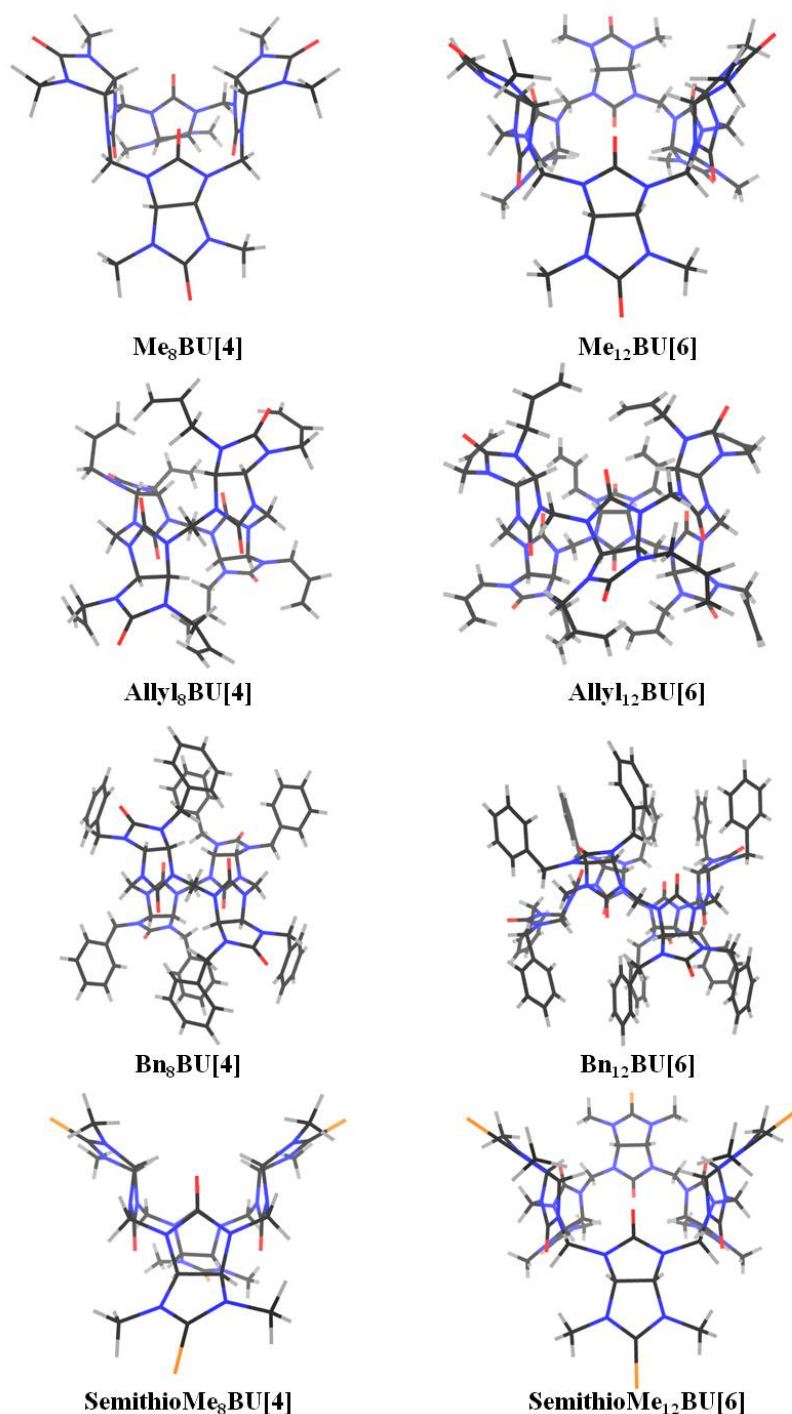
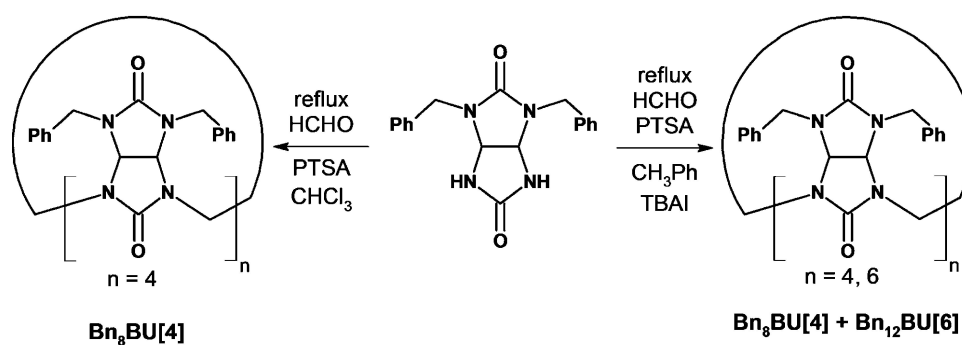


Figure 7.4: Representative structures of some derivatives and analogues of bambusurils. All structures were optimized at the HF/6-31G(d) level, except for the larger molecules (Bn<sub>8</sub> BU[4] and Bn<sub>12</sub> BU[6]), in which the AM1 semiempirical method was employed. Color code: red refers to oxygen; gray to carbon; blue to nitrogen and orange to sulfur atoms. Reproduced from ref. [2].

assisted synthesis of unsaturated bambusurils including the octaallylbambus[4]uril (Allyl<sub>8</sub>BU[4]) and dodecaallylbambus[6]uril (Allyl<sub>12</sub>BU[6]) derivatives has been detailed by Heck and co-workers [32], considering the preliminary preparation of diallylglycoluril, Scheme 7.4. The latter has been reacted

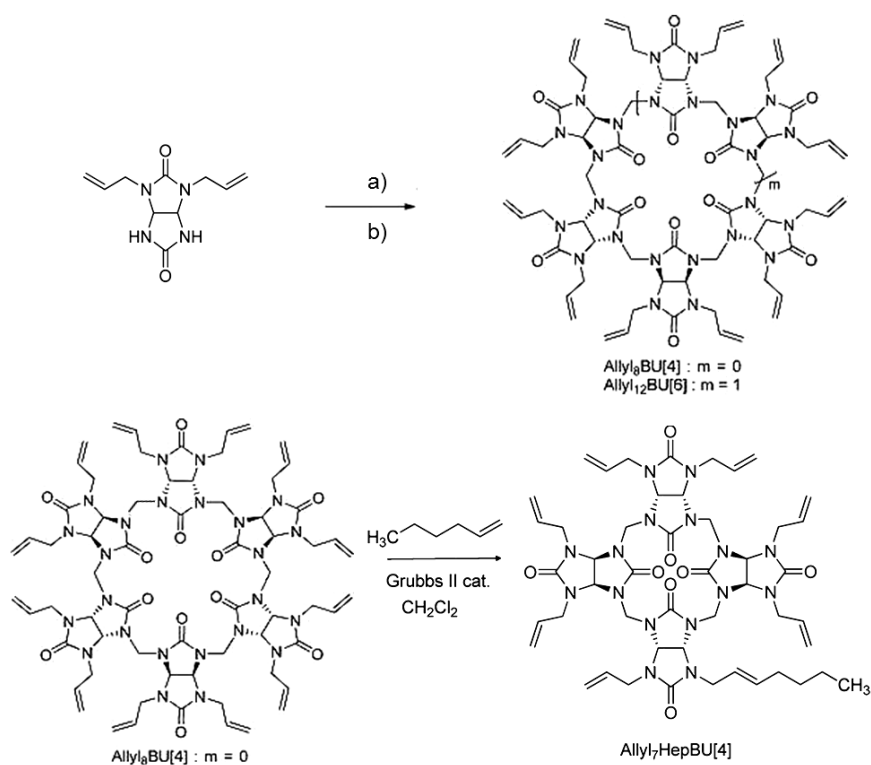


Scheme 7.3: Preparation of Bn<sub>8</sub>BU[4] and Bn<sub>12</sub>BU[6] from 2,4-dibenzylglycoluril and formaldehyde under different conditions. Reproduced from ref. [1].

with formaldehyde under classical conditions to afford BUs bearing diallylglycoluril units. A mono-functionalization of Allyl<sub>8</sub>BU[4] by a cross metathesis reaction [32], using 2 equivalents of hexene and the Hoveyda-Grubbs II catalyst affording Allyl<sub>7</sub>HepBU[4] was also reported (Scheme 7.4). Additionally, the preparation of the propyl derivative Pr<sub>8</sub>BU[4] has been carried out by the hydrogenation reaction of Allyl<sub>8</sub>BU[4] using H<sub>2</sub> over 10 % Pd/C in EtOH.

Other related molecules have also been synthesized using N,N-methyl semithio-glycoluril as building block. Reany, Keinan and co-workers [71], found that this precursor is suitable to react with formaldehyde under various acidic conditions, leading to successful synthesis of the related tetrameric and hexameric macrocycles (Scheme 7.5). These containers, known as semithio-bambusurils (semithio-BUs), have been prepared by the incorporation of sulfur atoms within the backbone of the macrocycle, specifically by the substitution of the carbonyl oxygen atoms. This structure confers a strong binding capability with a broad variety of anions in their interiors, and with metal ions at their sulfur edged portals. As observed in previous works [32], halide anions have also acted as templates, promoting the formation of the semithio-BU[6] macrocycle instead of the semithio-BU[4].

Sindelar and co-workers [29] have prepared a water-soluble bambusuril, functionalized with twelve benzoate groups, (BnCOOH)<sub>12</sub>BU[6], using the synthetic procedure described in Scheme 7.6. This receptor exhibits good solubility in neutral and basic aqueous solutions, being suitable for applications in areas such as biomedicine and analytical chemistry. [29] In the course of the preparation of this review, a new study [70] reporting the synthesis and characterization of a unique BU analog was published. This was obtained through an accessible manner from the corresponding

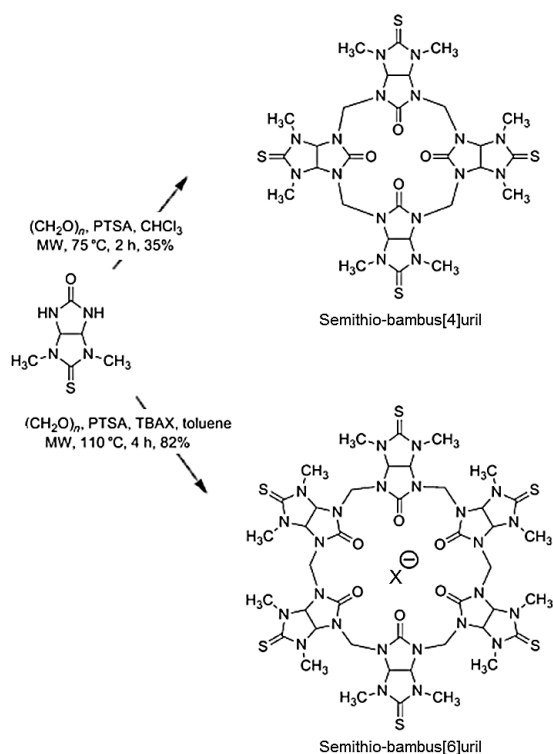


Scheme 7.4: (top) Preparation of allylbambusurils derivatives,  $\text{Allyl}_8\text{BU}[4]$  and  $\text{Allyl}_{12}\text{BU}[6]$ , from diallylglycoluril (top), using optimized conditions a)  $\text{CH}_2\text{O}$ , HCl, PTSA,  $\text{CHCl}_3$ , 0.04 M, MW for  $\text{Allyl}_8\text{BU}[4]$  and b)  $\text{CH}_2\text{O}$ , HCl, PTSA, toluene, 0.01 M, MW, TBAI; (bottom) Cross metathesis reaction of  $\text{Allyl}_8\text{BU}[4]$ . Reproduced from ref. [1].

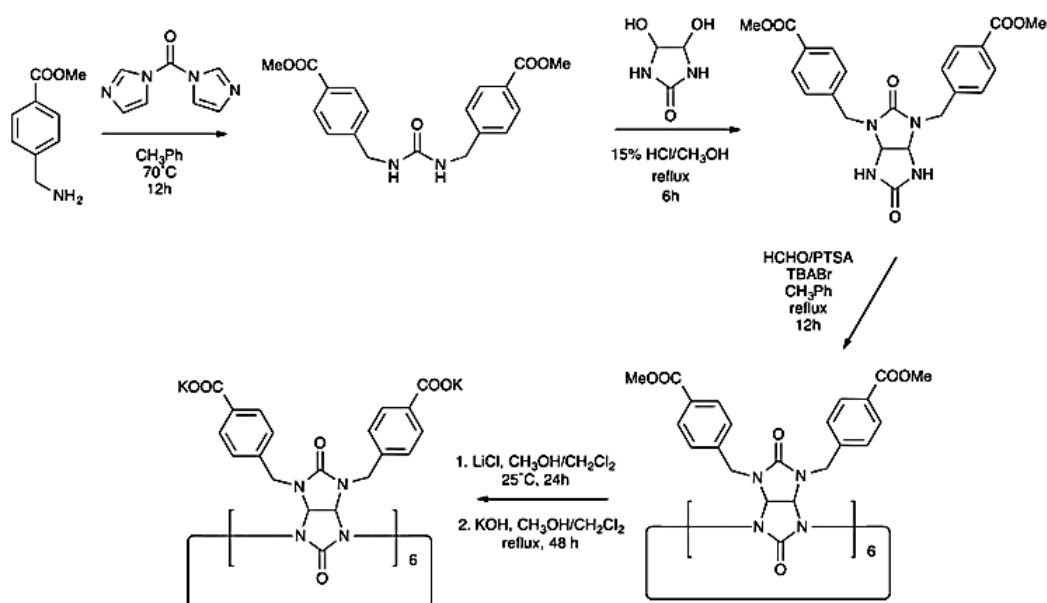
semithio-bambusurils and following a similar strategy used in the synthesis of several dendrimers and calixarenes, that consists on the modification of functional groups in the complete skeleton of the macrocycle. Considering the cyclic hexamer of semithio-BU[6] (1a-c), the neutralized compounds 3'-6' were obtained by the neutralization of the corresponding protonated semiaza-BU[6] (3-6) with Amberlyst A26 (OH - form) (Scheme 7.7). The latter compounds were obtained by the reaction of triflate salts of semi(methyl)sulfonium-bambusurils 2a-c with primary amines.

## 7.4 Complexes

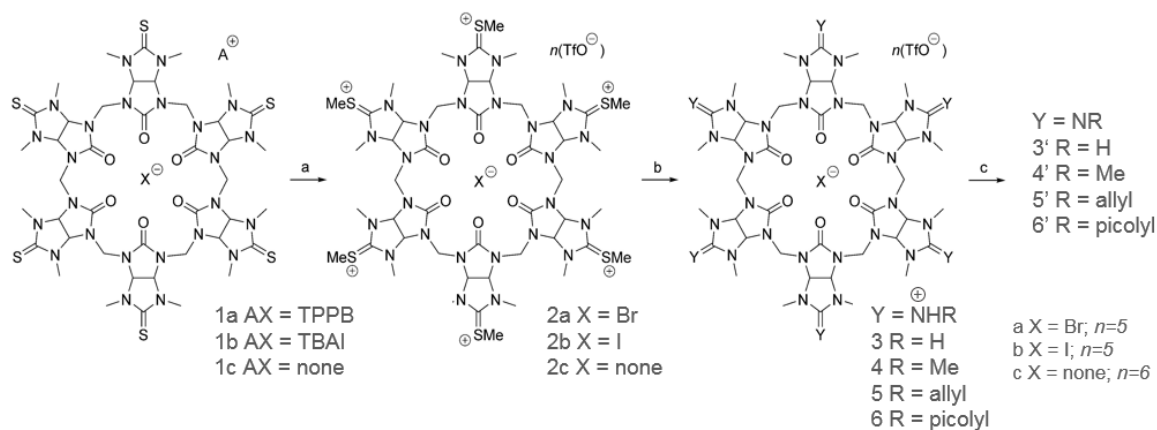
$\text{Me}_{12}\text{BU}[6]$ , binds anions with affinities of up to  $3.0 \times 10^9 \text{ L mol}^{-1}$  in organic solvents. [29] The equilibrium association constants calculated for  $\text{Me}_{12}\text{BU}[6]$  with  $\text{Cl}^-$ ,  $\text{Br}^-$ ,  $\text{BF}_4^-$ ,  $\text{NO}_3^-$  and  $\text{CN}^-$  using solubility measurements, are summarized in ref. [1] (Table S1), in which a general overview of the



Scheme 7.5: Synthesis of semithio-bambus[n]urils ( $n=4, 6$ ),  $\text{X} = \text{Cl}^-$ ,  $\text{Br}^-$ ,  $\text{I}^-$ ,  $\text{ClO}_4^-$ . The methyl-substituted BU[6] reacts with formaldehyde under various acidic conditions, leading to either semithio-BU[4] and semithio-BU[6] (35 and 82 %, respectively). Reproduced from ref. [1].



Scheme 7.6: Synthesis of the water-soluble and benzoyl-functionalised bambusuril macrocycle  $(\text{BnCOOH})_{12}\text{BU}[6]$ . Reproduced from ref. [1].



Scheme 7.7: Synthesis of semiaza-BU[6] (3-6') by the neutralization of the corresponding protonated semiaza-BU[6] (3-6) with Amberlyst A26 (OH<sup>-</sup> form). Reproduced from ref. [1].

reactants employed in each synthesis and the experimental techniques used both to confirm complexation and determine the stability constants are also presented. Although there exists a manifold of methods for the determination of the stability constants of these complexes, most of them require considerable amounts of material, are time-consuming, and can only be applied to systems with one receptor and one (or two) anions. Electrospray ionization mass spectrometry (ESI-MS) have been alternatively used to probe the binding of small anions to Me<sub>12</sub>BU[6], establishing the correlations between anion binding in the condensed phase and the abundance of anion-receptor clusters in gas-phase measurements. [74] The strength of anion binding has been mainly studied based on competition experiments [33]. However, other relevant insights have been provided using the anion-free Me<sub>12</sub>BU[6]. [33] The latter has been used to determine equilibrium association constants of the complexes with various anions and demonstrate the ability to bind halide ions in organic solvents and aqueous media, while still preserving its high affinity and selectivity. The binding of Me<sub>12</sub>BU[6] to halide ions follows the order I<sup>-</sup> > Br<sup>-</sup> > Cl<sup>-</sup> > F<sup>-</sup>. The influence of anion size on the macrocycle structural parameters and the electrochemical behavior of the complex have also been investigated. [33] The presence of twelve weak favorable interaction sites (for the chloride ion) has been confirmed using single crystal structure, and further modifications to this macrocycle have been considered to afford novel materials for various applications. The formation of cationic (Me<sub>12</sub>BU[6] · H<sub>3</sub>O<sup>+</sup> and Me<sub>12</sub>BU[6] · (H<sub>3</sub>O<sup>+</sup>)<sub>2</sub>) [75], neutral, (Me<sub>12</sub>BU[6] · Cs<sup>+</sup> I<sup>-</sup> [76] and Me<sub>12</sub>BU[6] · Na<sup>+</sup> I<sup>-</sup>) [77] and anionic (Me<sub>12</sub>BU[6] · OCN<sup>-</sup>, Me<sub>12</sub>BU[6] · SCN<sup>-</sup> [78] and Me<sub>12</sub>BU[6] · SH<sup>-</sup>) [79] complexes, has been suggested resorting to DFT calculations (see ref. [1], Table S1, in which the estimated binding energies are reported).

Note that the stabilities of the complexes  $\text{Me}_{12}\text{BU}[6] \cdot \text{H}_3\text{O}^+$  and  $\text{Me}_{12}\text{BU}[6] \cdot (\text{H}_3\text{O}^+)_2$  are approximately half those of the corresponding complex species  $\text{CB}[6] \cdot \text{H}_3\text{O}^+$  and  $\text{CB}[6] \cdot (\text{H}_3\text{O}^+)_2$ . The octabenzylbambus[4]uril ( $\text{Bn}_8 \text{BU}[4]$ ) presents similar structural features to those of previously reported  $\text{Me}_{12}\text{BU}[6]$ . However, the small cavity of the  $\text{Bn}_8 \text{BU}[4]$  macrocycle has no affinity for anions. Recent studies carried out by Sindelar and co-workers [27, 80] have elucidated the formation of stable supramolecular complexes of dodecabenzylbambus[6]uril,  $\text{Bn}_{12}\text{BU}[6]$ , with tetrabutylammonium benzoates and tosylates, in the solid state and in wet chloroform solution, mediated by water molecules. Ion-dipole interactions are considered relevant, but the complex formation between these components is also mediated by water molecules, acting as bridges between the two carboxylate and the two sulfonate groups, thus stabilizing the 1:2 complexes. An analogous arrangement has been observed in complexes of  $\text{Me}_{12}\text{BU}[6]$  with diethyl phosphate anions. [28] In those complexes, a water molecule serve as a bridge between two phosphate anions located in oppose portals of the macrocycle, by formation of two  $\text{O}-\text{H} \cdots \text{O}^-$  hydrogen bonds. The first use of two bambus[6]uril derivatives (with 12 benzyl and 12 benzoyl groups) as NMR-active chemosensors, for analyzing multi-anion mixtures, comprise anions with affinities higher than  $10^4 \text{ M}^{-1}$ . This has been applied to environmental pollutants, biologically active anions, species used in ion-pairing catalysis, among others. [80] In particular, the ability of these receptors for recognizing specific components of multianion mixtures in aqueous solutions have been used in conjunction with  $^1\text{H}$ -NMR techniques, in order to construct a system with sensing properties, able for detection and characterization of complex mixtures of inorganic anions. [80]. Inspired by previous studies on the preparation of phosphatethreaded rotaxanes [81, 82], the supramolecular complexes between  $\text{Bn}_{12}\text{BU}[6]$  and several dialkyl phosphates, bearing various alkyl substituents, have been characterized using  $^1\text{H}$ -NMR spectroscopy and X-ray diffraction. [28] Two possible binding modes were proposed, corresponding to internal and external 1:1 complexes. However, only the external complex was formed, precluding the formation of interlocked structures, such as rotaxanes. The complex formation between  $\text{Me}_{12}\text{BU}[6]$  investigated and a complex with 1:2 stoichiometry was obtained in the solid state. Two diethyl phosphate anions were bound at the carbonyl portals of  $\text{Me}_{12}\text{BU}[6]$  and the complex was stabilised by one water molecule, an analogous structure already observed in complexes of  $\text{Bn}_{12}\text{BU}[6]$  with benzoates and tosylates. [27] Quantum mechanical DFT calculations on BUs complexes have proposed the most probable structures of the

complexes with halide ions. [34] The host-guest interactions of these molecules in aqueous environments and in non-polar solvents on the topic [83] focuses on the binding properties of work have also been investigated using thermal calorimetry and  $^1\text{H-NMR}$  data. A recent dodecabenzylbambus[6]uril ( $\text{Bn}_{12}\text{BU}[6]$ ) in the presence of multiple anion mixtures in chloroform, with association constants of up to  $10^{10}\text{ M}^{-1}$ . In aqueous solutions, BUs have been suggested, among others, for the preparation of sensors able to detect the occurrence of abnormal salt concentrations in human body, upon contact with very small amounts of blood or urine. [50, 84] Further interest has grown with the preparation of the first water soluble derivative,  $(\text{BnCOOH})_{12}\text{BU}[6]$ . [2, 29] This molecule, functionalized with twelve benzoate groups, is able to bind anions in buffered water solution with high affinity (stability constants up to  $10^7\text{ M}^{-1}$ ) [29] and high selectivity. The structure and complexation profile of this BU molecule with grafted carboxylate groups have been inspected by  $^1\text{H-NMR}$  titration and isothermal titration calorimetry (ITC). The association constants for the formation of 1:1 complexes between  $(\text{BnCOOH})_{12}\text{BU}[6]$  and various halide ions have been determined through free-energy calculations [2] and competition experiments [29] with another anion (often the chloride ion). The complex is stabilized by multiple weak  $\text{C-H}\cdots\text{anion}$  interactions, resulting in exceptionally strong complexes with various anions in water, even those that are usually weakly associated (e.g.  $\text{PF}_6^-$ ,  $\text{BF}_4^-$  and  $\text{ClO}_4^-$ ). Reany, Keinan and co-workers [71] have prepared new BU derivatives taking advantage of the stability of substituted monothiol-glycolurils to synthesize the semithio-bambusurils (semithio-BU[n]s). These new molecules, including semithio-BU[4] and semithio-BU[6], (Figure 7.4, panel d) differ from the parent BU macrocycles in that half of the carbonyl groups are replaced with thiocarbonyl groups. The resulting modified bambusurils are able to interact with thiophilic metal cations at their sulphur-edged portal, while retaining the ability to bind anions in their interior with high affinity. These observations were also confirmed [70], shortly afterwards, by the same group. In this interesting effort to improve the binding properties of BUs, in comparison with the all-oxygen counterparts, novel binding opportunities were predicted considering the substitution of glycoluril oxygen atoms by other heteroatoms (e.g. nitrogen). This modification alters the molecular electrostatic potential and the binding properties of the macrocycle, as reflected by the different BU analogs, depicted in Figure 7.5. This was explored using DFT calculations on the crystal structures of the model complexes with halide guests (e.g. chloride). The replacement at the portal carbonyls affect the induced dipole



more significantly than substitutions in the equatorial carbonyls. [70] The new portal heteroatoms are thus acting as "electron sinks", conferring interesting capabilities reflected by stronger dipole moments, polarizations and stronger anion binding (see ref. [70]). These molecules open interesting pathways in

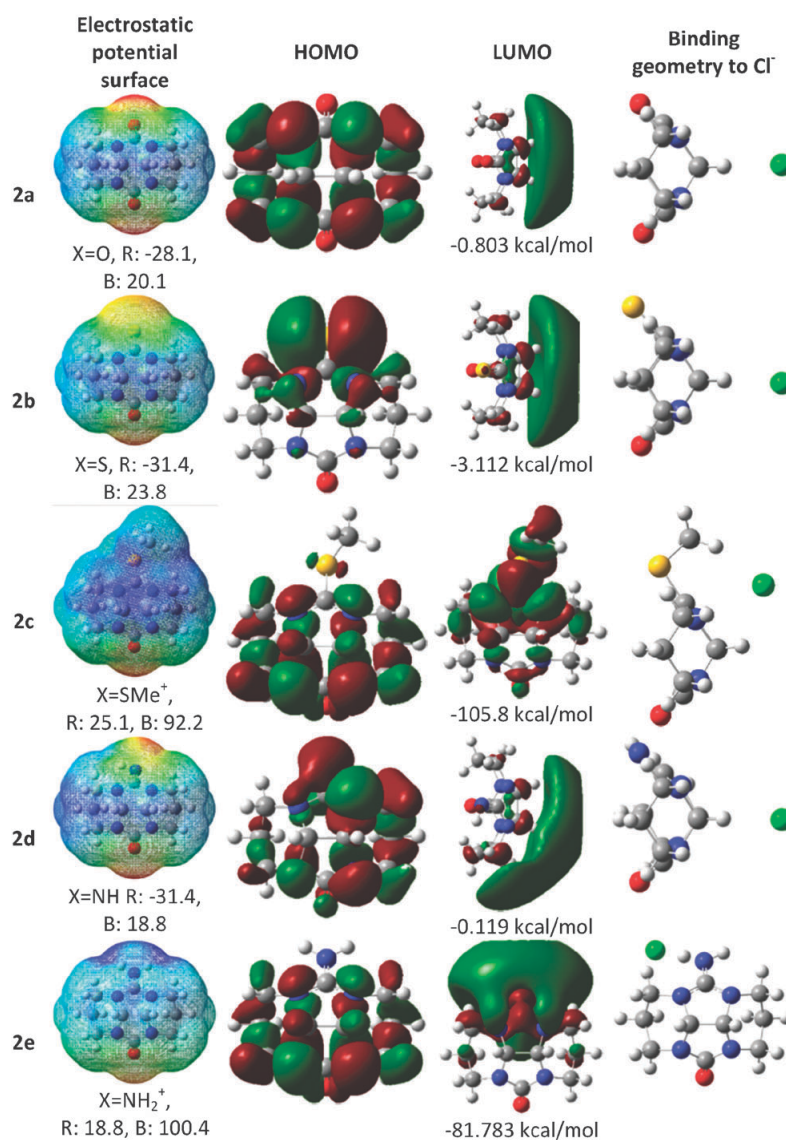


Figure 7.5: Electrostatic potential maps (left) and structure of the HOMO and LUMO (middle) and binding geometries (right) of the different complexes involving glycoluril analogs, 2a-e. Calculations were performed at the M06-2X/6-311+G\*\* level of theory. The electrostatic potential surfaces are presented in kcal mol<sup>-1</sup>, ranging from red (R) to blue (B). Reproduced from ref. [70] published by the PCCP Owner Societies.

both basic and applied science. It has been demonstrated that the formation of the hexameric macrocycle is facilitated by the use of halide anions as templates. Successful synthesis of semithio-BU[6] have been observed [70, 71] not only with tetrabutylammonium salts (TBAX, X=Cl<sup>-</sup>, Br<sup>-</sup>, I<sup>-</sup>, ClO<sub>4</sub><sup>-</sup>), but also with Et<sub>4</sub>NClO<sub>4</sub>, Ph<sub>4</sub>PBR, CsI and Me<sub>4</sub>NI. [71] These thiourea-based BUs can be explored in nanotechnology, including patterning of nanoparticles, in the formation of monolayers on metal

surfaces, as well as in catalysis. The most recent works [26, 70] on the enhanced properties of bambusuril analogs, have predicted that protonated aza-bambusurils are able to bind multiple anions and function as synthetic anion channels, with potential applications in ion transport mechanisms. The substitution of the six portal oxygen atoms in  $\text{Me}_{12}\text{BU}[6]$  by nitrogen atoms leads to the formation of semiaza-bambus[6]urils. Surprisingly, the positive electrostatic potential character of their cavity allows to accommodate multiple anions, due to the capability for overcoming electrostatic repulsion among ions, which is relevant for promoting multiple ion flows. This opens unprecedented opportunities due to the possibility of converting a single anion-host in an ion-channel. It should be noted that other anion receptors with the glycoluril molecular scaffold have been developed, such as those based on diphenylglycoluril and imidazolium rings. The association of the diphenylglycoluril-based receptors with various anions has reflected the shape, size and basicity of the anions. [85–88], Additionally, there are some other related macrocycles such as biotinurils [89], which have emerged recently, and which have sufficient similarities to be mentioned in the context of this review. The synthesis of the macrocyclic 6+6 hexamer of d-biotin with formaldehyde and templated by halide ions, has been reported. [50, 84] This molecule is able to bind mono-charged anionic guests in water with binding constants ranging from  $\log K=1.8$  ( $\text{Cl}^-$ ) to  $\log K=4.5$  ( $\text{SCN}^-$ ). ITC measurements have indicated that anion binding is enthalpically driven, with contributions from the release of high-energy waters present in the cavity (see Refs. [84, 90]). Besides this non-classical hydrophobic effect, it has been suggested (by the single-crystal X-ray structure) that C-H hydrogen-bonding interactions are present between the host and the anion.

## 7.5 Evaluating the ion caging ability

For understanding the bambusuril ion caging ability in aqueous media, MD simulations, including free-energy calculations are performed. Our investigation is focused on three BU derivatives, dodecamethylbambus[6]uril ( $\text{Me}_{12}\text{BU}[6]$ ), dodecabenzylbambus[6]uril,  $\text{Bn}_{12}\text{BU}[6]$ , and dodeca(4-carboxybenzyl)bambus[6]uril,  $(\text{BnCOOH})_{12}\text{BU}[6]$ .

### 7.5.1 General procedure

The exploratory MD simulations were performed with the GROMACS package (version 4.6.5) by using all-atom amber99sb force-field. The starting geometries of the Me<sub>12</sub>BU[6], Bn<sub>12</sub>BU[6] and (BnCOOH)<sub>12</sub>BU[6] hosts were constructed resorting to Avogadro and Pymol (Version 1.7.7.2) and optimized by the semi-empirical Antechamber/SQM method. Electrostatic charges were obtained from AM1-BCC [91, 92] calculations. For the rigid Me<sub>12</sub>BU[6], these methods provide good approximations for its structure in solution. However, some degree of distortion is expected for the benzyl (Bn<sub>12</sub>BU[6]) and carboxybenzyl (BnCOOH)<sub>12</sub>BU[6] derivatives, as has been reported for other flexible hosts, such as cyclodextrins [90]. The distortion/collapse of these flexible hosts may suggest that a high energy is required to fill their cavities and preclude the interior vacuum state [90]. The main idea in what follows is to evaluate *in silico* how the conformation and the hydration pattern of each BU molecule is affected by the presence of bulky substituents and by the formation of the inclusion complexes. For this purpose, five different systems are considered: three of them taken as references, account for the solvation of each single molecule of Me<sub>12</sub>BU[6], Bn<sub>12</sub>BU[6] and (BnCOOH)<sub>12</sub>BU[6], while in the other two the inclusion complexes of the charged host (BnCOO)<sub>12</sub>BU[6] with one and two chloride ions are considered. In each case, the molecules were accommodated in a cubic box (7.5 nm edge-length) containing explicit TIP3P water molecules. All the calculations were carried out in NPT ensemble with periodic boundary conditions at a constant temperature of 298 K, and a pressure coupling of 1.0 bar, respectively, to V-rescale and Berendsen external baths. A standard time step of 2 fs was used for both equilibration and production runs. Non-bonded interactions were computed on the basis of a neighbor list, updated every 10 steps. Long range electrostatic contributions were computed using the particle mesh Ewald (PME) method [93]. For Lennard-Jones energies, a cut-off of 0.9 was applied. To obtain a starting configuration, each system was firstly subjected to an energy minimization step.

Equilibrium properties, structure and dynamics of BU systems were calculated over the 35 ns simulation runs after the systems were equilibrated for 5 ns. The bonds were constrained by the LINCS algorithm [94]. The simulated time was found to be enough to provide a robust statistics for the host solvation and the last 5 ns were subjected to the standard analysis. These include time-dependent

RMSD for (i) all BU atoms and (ii) a defined cavity backbone, excluding the twelve carboxybenzyl groups and geometric clustering performed to identify similar structures, sampled during the MD simulations. The algorithm for geometric cluster analysis is based on the hierarchical (top-down) approach, as described by Daura and coworkers [95], and allows evaluating the conformational prevalence of each BU structure. This simple clustering approach reduces the complexity of the structural information, revealing patterns which are hidden, at the scope of dynamic properties. To find clusters of structures in each MD trajectory,

## 7.5.2 Free-energy calculations

The free-energy profile of the binding process was inspected using a path-based approach based on umbrella sampling with PMF estimation [96]. The host molecule was taken to have a net charge of 12,  $(\text{BnCOO}^-)_{12}\text{BU}[6]$  and was centered in the simulation box with the cavity axis parallel to the z-component. The distance  $d_{\text{Cl-BU}}$  between the COM of the chloride ion and that of the cavity methylene-linkers of the host was defined as the reaction coordinate  $\xi_z$  (see Figure 7.6). The initial (i) and final (f) values of the reaction coordinate were set to  $\xi_{z_i} = 0 \text{ nm}$  and  $\xi_{z_f} = 2.0 \text{ nm}$ , respectively. After equilibration, a periodic pulling simulation was carried out allowing the distance to be larger than half the box size, to modulate a dissociation process of 1:1  $(\text{BnCOO})_{12}\text{BU}[6]:\text{Cl}$  complex. The center of mass of the  $(\text{BnCOO}^-)_{12}\text{BU}[6]$  backbone was harmonically restrained with an isotropic force constant of  $1000 \text{ kJ mol}^{-1} \text{ nm}^{-2}$  and used as an immobile reference for pulling. The ion was moved away from the  $(\text{BnCOO}^-)_{12}\text{BU}[6]$  cavity along the z-axis for 600 ps with a harmonic force constant of  $1000 \text{ kJ mol}^{-1} \text{ nm}^{-2}$  and a pulling rate of  $0.005 \text{ nm ps}^{-1}$ . The guest ion was sampled approximately 2 nm covering the entire  $[\xi_{z_i}, \xi_{z_f}]$  interval. In this interval, ca. 60 windows were selected, with an imposed distance of 0.03 nm between adjacent positions and used as starting configuration for umbrella sampling simulations.

The thermodynamic parameters and the binding affinity associated to the formation of the BU:Cl complexes were estimated using the procedure described in Chapter 2 and ref. [2].

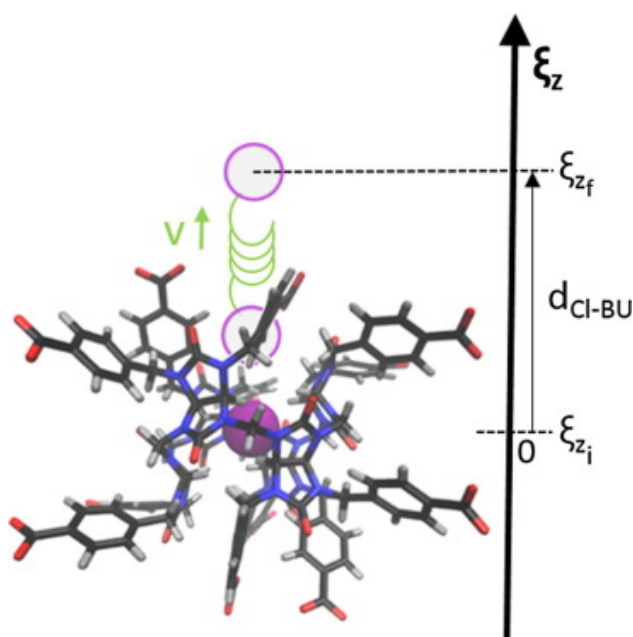


Figure 7.6: Schematic representation of the pathway along which chloride ion is pulled along the z-component, with umbrella sampling. The purple circle indicates where the steering force is applied. Reproduced from ref. [2].

### 7.5.3 Structural stability and cavity size

In what follows, the structural features of bare  $\text{Me}_{12}\text{BU}[6]$ ,  $\text{Bn}_{12}\text{-BU}[6]$  and  $(\text{BnCOOH})_{12}\text{BU}[6]$ , and the relative energy contributions to the formation of the  $(\text{BnCOO})_{12}\text{BU}[6]:\text{Cl}$  complex are detailed.

In the absence of anions and in polar solvents, the conformational and binding studies have been hampered by the low solubility of the macrocycle. The solubility can be tuned by varying the substituents grafted to the nitrogen atoms of the portals. The type of substitution also affects the conformational behavior in solution, as can be seen in Figure 7.7 for the bare  $\text{Me}_{12}\text{BU}[6]$ ,  $\text{Bn}_{12}\text{BU}[6]$  and  $(\text{BnCOOH})_{12}\text{BU}[6]$  hosts. Although regular conformations prevailed for  $\text{Me}_{12}\text{BU}[6]$  and  $\text{Bn}_{12}\text{BU}[6]$ , distorted structures account for ca. 11 and 24 %, respectively. The distortion observed in  $\text{Me}_{12}\text{BU}[6]$  can be attributed to the ability of some glycoluril units to rotate with respect to the cavity plane defined by the methylene-linked groups.  $\text{Me}_{12}\text{BU}[6]$  displays an approximately symmetric arrangement with an open and accessible cavity (see Figure 7.7). In  $\text{Bn}_{12}\text{BU}[6]$  and  $(\text{BnCOOH})_{12}\text{BU}[6]$  the minimization of the steric effects among their bulky phenyl and carboxybenzyl substituents leads to a considerable distortion of the cavity-backbone and structural asymmetry (see Figure 7.8).

Distortion is also expressed in terms of the variation of the "typical diameter" of each molecule,

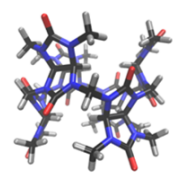
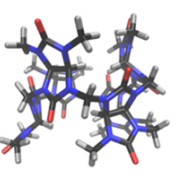
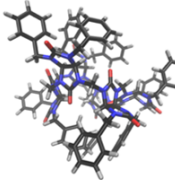
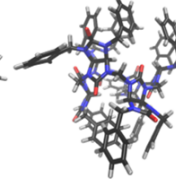
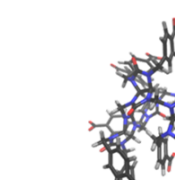
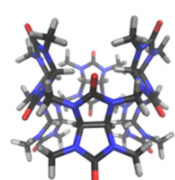
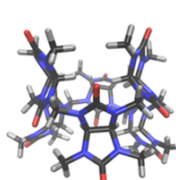
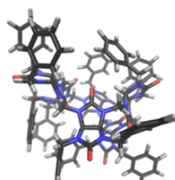
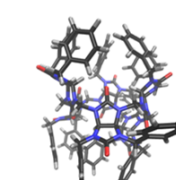
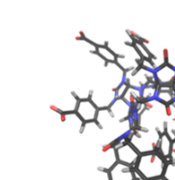
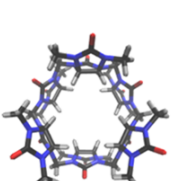
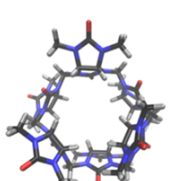
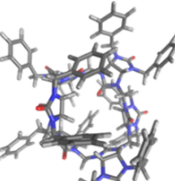
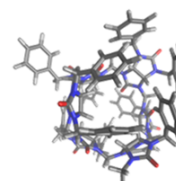
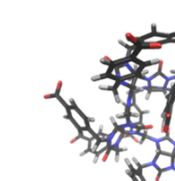
Single-host Conformation	Me <sub>12</sub> BU[6] (%)		Bn <sub>12</sub> BU[6] (%)		(BnCOOH) <sub>12</sub> BU[6] (%)
Side					
Front					
Top					
Prevalence	77.3	10.7	54.5	23.7	99.9

Figure 7.7: Typical conformations for the bare Me<sub>12</sub>BU[6], Bn<sub>12</sub>BU[6], (BnCOOH)<sub>12</sub>BU[6] hosts in aqueous solution, sampled during the MD simulations. The occurrence of each type of conformation is also included. Reproduced from ref. [2].

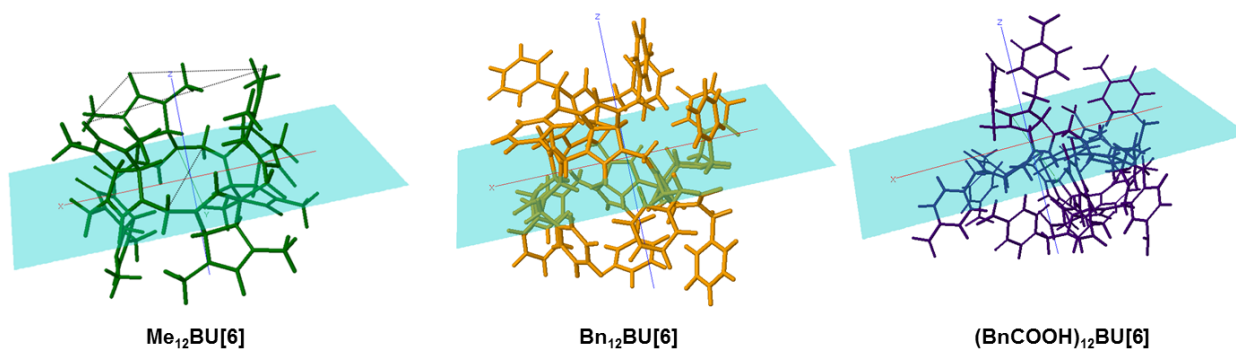


Figure 7.8: Schematic illustration of the structural symmetry present in the bare BU-hosts and reflected by the final arrangement of the six glycoluril units and the methyl (Me<sub>12</sub>BU[6]), phenyl (Bn<sub>12</sub>BU[6]) and carboxybenzyl ((BnCOOH)<sub>12</sub>BU[6]) substituents relative to the plane defined by the cavity methylene-linked groups. Reproduced from ref. [2].

Figure 7.9.

The distance profile of Bn<sub>12</sub>BU[6] shows a broad range of values that include those related to the skewed arrangements (lower distances and less frequent) and the one reflecting the most prevalent

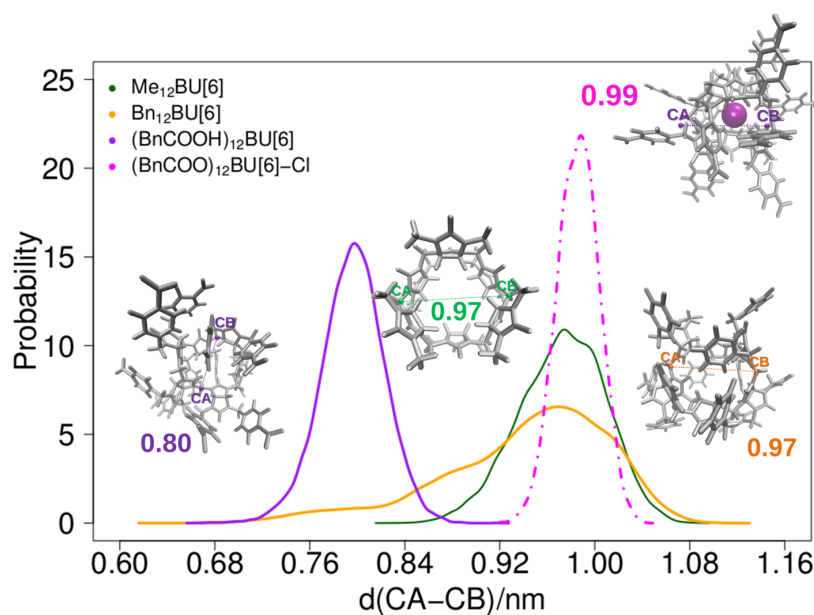


Figure 7.9: Distribution of distances from cavity-carbon CA to cavity-carbon CB in  $\text{Me}_{12}\text{BU}[6]$  (green),  $\text{Bn}_{12}\text{BU}[6]$  (orange),  $(\text{BnCOOH})_{12}\text{BU}[6]$  (purple) and  $(\text{BnCOO})_{12}\text{BU}[6]-\text{Cl}$  (magenta). The cavity-carbon atoms considered for each host, to define the relevant distances, are depicted in the structure of each molecule. Reproduced from ref. [2].

and undistorted arrangement. In  $(\text{BnCOOH})_{12}\text{BU}[6]$ , only one typical distance indicating a permanently collapsed structure is found. When this host is complexed with one chloride ion, collapse is prevented and the cavity diameter increases. In this complex, the chloride ion resides in the center of the electropositive cavity (see Figure 7.10), without water molecules inside, being the cavity hermetically sealed by four carboxybenzyl groups. Sindelar and co-workers [33, 83], have reported the complexation of two chloride ions with  $\text{Bn}_{12}\text{BU}[6]$  positioned above and below the plane of the central ring formed by the methylenelinked groups, mediated by an water molecule between the ions.

Based on these observations it was decided to explore the possibility of a similar 1:2 complex with  $(\text{BnCOO}^-)_{12}\text{BU}[6]$ . A simulation was carried out with the starting configuration presenting two chloride ions inside the  $(\text{BnCOO}^-)_{12}\text{BU}[6]$ . Contrarily to what had been reported for  $\text{Bn}_{12}\text{BU}[6]$ , the chloride ions have left the BU cavity along the simulation. Apparently, the electrostatic repulsion between anions and the carboxybenzyl groups overcome the stabilizing interactions that would favor the complex formation. In fact, the release of the first chloride induced the distortion of the host cavity, and thus prevented the stability of a possible 1:1 complex. Subsequently, the second anion has

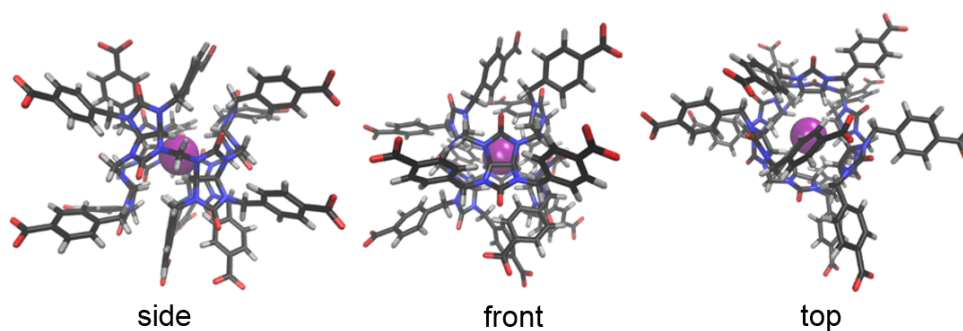


Figure 7.10: Dominant conformation (accounting for more than 94 % of the occurrences) sampled during the last 5 ns of the production run, at 298 K, for the inclusion complex of  $(\text{BnCOO})_{12}\text{BU}[6]:\text{Cl}$  (1:1) in aqueous solution (for details see Figure 7.7) Reproduced from ref. [2].

also escaped from the cavity. Note that increased repulsion, including that of chloride-chloride term and the consequent displacement of the ion towards the portal barriers are likely explanations for the absence of a 1:2 complex.

The formation of the 1:1 complex enhances the symmetry of the host structure with the arrangements of the substituents in the two portals becoming identical, see Figure 7.11, panels (c) and (d). In the solvated host, panels (a) and (b), the distances of the carboxyl group to the center of the cavity differ significantly, reflecting some "random" arrangement of the bulky substituents, and the distance profiles related to each portal (P1 and P2) are clearly different. This structural asymmetry is reverted when the chloride ion is inserted in the cavity, panels (c) and (d).

Figure 7.12 presents the RMSD evolution along the simulation run for the  $(\text{BnCOO})_{12}\text{BU}[6]:\text{Cl}$  complex. Panel (a) indicates a significant difference between the structural fluctuations of the cavity backbone and the all-atoms carboxybenzylsubstituted BU, in the complex. The RMSD values suggest that the structural changes in the  $(\text{BnCOO})_{12}\text{BU}[6]:\text{Cl}$  complex are mainly due to fluctuations in the carboxybenzyl substituents. Positional variations of these groups, highly mobile, seem to play a central role for the overall structure fluctuations of the complex. In panel (b), the distribution of the RMSD values is represented. An almost equilibrated Gaussian distribution of the corresponding RMSDs is observed in both cases.



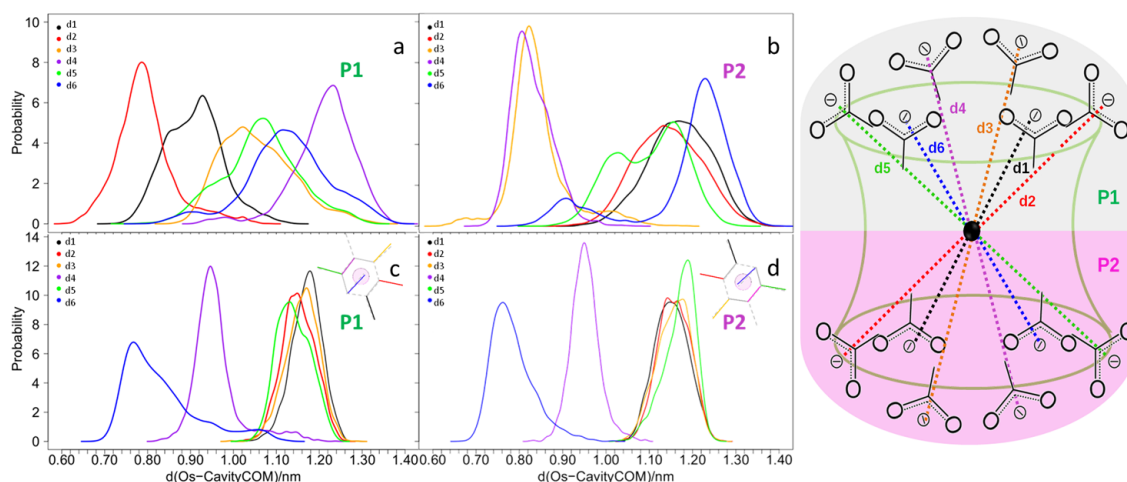


Figure 7.11: Distribution of the distances between the center of mass of the groups formed by the two oxygen atoms in each carboxybenzyl group, and the cavity center of  $(\text{BnCOO}^-)_{12}\text{BU}[6]$ . Panel (a) and (b) refer to portals P1 and P2 in the hydrated host. Panels (c) and (d) correspond to the same portals in the 1:1  $(\text{BnCOO})_{12}\text{BU}[6]:\text{Cl}$  complex. A schematic illustration of the arrangement of each carboxybenzyl group is included in panel (c) and (d), with the colors used to represent the corresponding oxygen atoms. Right panel illustrates the measured distances referred in panels (a)-(d).. Reproduced from ref. [2].

## 7.5.4 Solvation

The solvation of each component of the system can play a key role in the formation and stability of the complex [16], being thus inspected in more detail. To gain insight into the system hydration patterns, the number of water molecules inside the cavity was inspected as a function of the cavity radius. The hydration profile of each BU system (Figure 7.13) shows that, in general, the larger the substituents, the less water molecules are found inside the cavity. In  $\text{Me}_{12}\text{BU}[6]$ , three water molecules are found inside the cavity, one in a more central position and two surrounding the latter. The curve steeply increases outside of the cavity because the volume of the substituents is small, and bulk water starts to be considered. In the  $(\text{BnCOOH})_{12}\text{BU}[6]$  host, prone to a collapse that produces a smaller cavity, this number decreases to one. In  $\text{Bn}_{12}\text{BU}[6]$  a less clear profile is observed, showing that four water molecules reside inside the cavity, without a definite gap between cavity and bulk water. The inclusion of chloride in  $(\text{BnCOO}^-)_{12}\text{BU}[6]$  [9], displaces the single water molecule from the cavity, indicating that the interaction between chloride ion and the host cavity is stronger than with nearby water molecules. In other words, the energy cost for desolvation of both guest and host

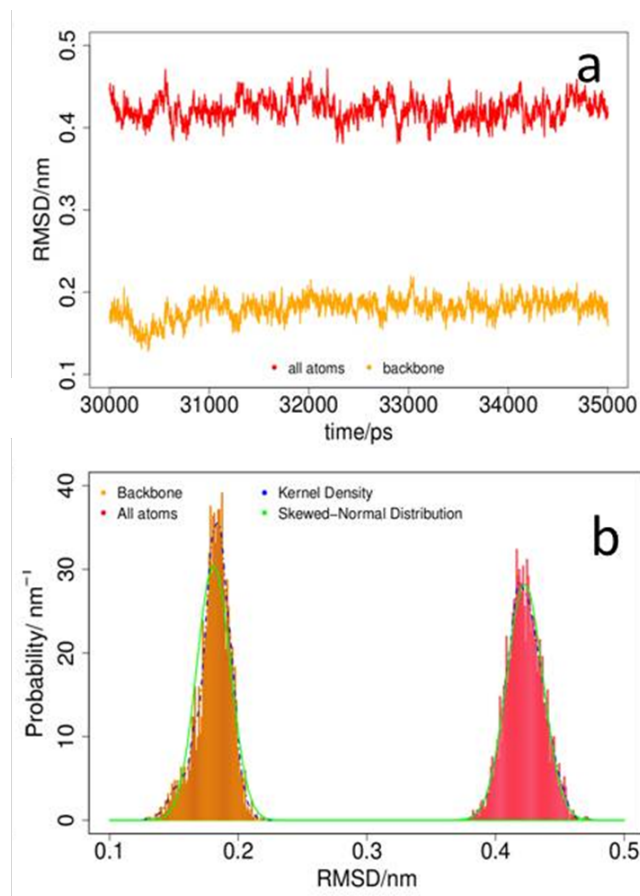


Figure 7.12: Time evolution of RMSD for the simulation of the hydrated  $(\text{BnCOO})_{12}\text{BU}[6]:\text{Cl}$  complex, panel (a). Red lines represent the RMSD considering all atoms of the host; orange lines refer to the RMSD considering only the atoms of the cavity backbone. Panel (b) shows the normalized statistical distributions for the RMSD values considering the cavity-backbone and all atoms of the host. Reproduced from ref. [2].

cavity is compensated by the formation of the inclusion complex. It has been shown [29, 97] that some halide ions, such as fluoride, are much more strongly solvated than others such as chloride and iodide, and the lower binding affinities of the former can be partially attributed to the high desolvation energies.

### 7.5.5 Interaction components

Eq.(2.22) is used for the calculation of the binding constant for the bambusuril-ion complex and incorporates the  $(\text{BnCOO}^-)_{12}\text{BU}[6]/\text{Cl}^-$  interaction as measured from the PMF. The latter weights each value of the reaction coordinate and also the complex volume, established on the basis of the center of mass positioning related to the ion inside the cavity. The estimated standard free-energy of bind-

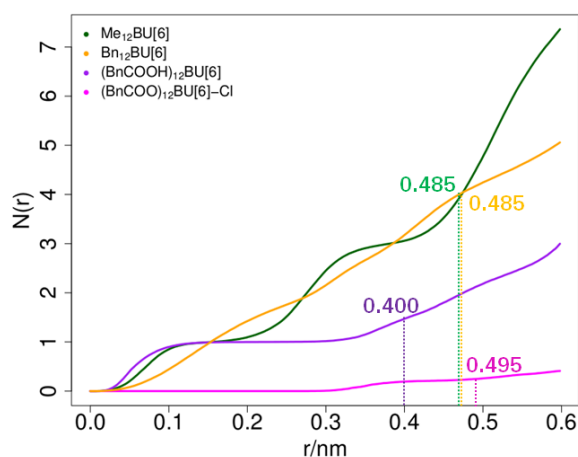


Figure 7.13: Running coordination number of water molecules, calculated from the center of the BUs cavity. The average cavity radius is indicated as a dashed line in each curve. Reproduced from ref. [2].

ing and the respective  $K_{bind}$  are  $-11.7 \text{ kJ mol}^{-1}$  and 112, respectively, pointing to a degree of binding lower than that experimentally [29, 97] determined, and closer to the one based on ITC measurements. The fact that the PMF profile possesses a very pronounced energy barrier for the exit/entry of the chloride in the BU cavity (data not shown), has caused some difficulties in what pertains to the restraining force constants. A gross estimation of this barrier points to  $130 \text{ kJ mol}^{-1}$ . The entropic term favors association, with a  $-T\Delta S^0$  term of  $-7.6 \text{ kJ mol}^{-1}$ , exceeding the also negative enthalpy change ( $-4.1 \text{ kJ mol}^{-1}$ ).

Simulations in the equilibrium state, for which the complex  $(\text{BnCOO})_{12}\text{BU}[6]:\text{Cl}$  is formed and simulations in which host and guest are dissociated, allow a detailed analysis of the enthalpy change, by determining the van der Waals contributions, and decomposing the electrostatic components.

As the latter interactions are treated using the particle mesh Ewald (PME) method, long-range energies for the pair-pair contributions (bambusuril-chloride, BU-Cl, bambusuril-solvent, BU-S chloride-solvent, Cl-S, bambusuril-bambusuril, BU-BU, chloride-chloride, Cl-Cl, and solvent-solvent, S-S) are combined in a global term of the reciprocal sum. This term can be further decomposed by re-running the reference simulations (bonded and non-bonded states) with different charge arrangements, as described in ref. [96]. Results for the main interaction components are summarized in Table 7.1.

The individual interaction component changes for the binding process of chloride in  $(\text{BnCOO}^-)_{12}\text{BU}[6]$  are  $-2.4, 0.0, -107.2, -28.5, -144.6, -59.5, 265.7$  and  $175.4 \text{ kJ mol}^{-1}$ , for  $\Delta H_{BU}, \Delta H_{Cl}, \Delta H_{BU-Cl},$

Table 7.1: Lennard-Jones,  $\Delta H_{LJ}$ , and Coulombic contributions (Coulombic,  $\Delta H_{Coul}$ , and reciprocal sum,  $\Delta H_{Coul_{rec}}$ ) ( $\text{kJ mol}^{-1}$ ) for the interaction between  $(\text{BnCOO}^-)_{12}\text{BU}[6]$  and chloride ion. Reproduced from ref. [2].

Interaction pair	$\Delta H_{LJ}$	$\Delta H_{Coul}$	$\Delta H_{Coul_{rec}}$
BU-BU	-53.7	81.3	-175
Cl-Cl	$7.3 \times 10^4$	0.1	-28.6
S-S	-58.3	-15.0	-71.3
BU-Cl	16.6	-142.2	66.1
BU-S	65.0	-51.7	252.5
Cl-S	-39.5	280.4	-65.6

$\Delta H_{Cl-Cl}$ ,  $\Delta H_{S-S}$ ,  $\Delta H_{BU-Cl}$ ,  $\Delta H_{BU-S}$  and  $\Delta H_{Cl-S}$  respectively. The  $\Delta H_{BU}$  and  $\Delta H_{BU-BU}$  values are compatible with the increased stability of the host backbone in the presence of the anion, promoted by the concerted arrangement of the carboxybenzyl groups (see Figure 7.7) which minimizes the internal electrostatic repulsion. In the collapsed structure, which is the prevalent conformation in the absence of the anion, repulsion increases as the overall distance between these groups tends to decrease (see Figure 7.8). Overall, desolvation opposes complex formation: it is favored by the release of water molecules into bulk water ( $\Delta H_{S-S} < 0$ ), but this term is surpassed by the strong penalties for host and guest desolvation ( $\Delta H_{BU-S}$ ,  $\Delta H_{Cl-S} > 0$ ). Also favorable is the host-guest interaction,  $\Delta H_{BU-Cl}$ . The bonded terms of the binding entities ( $\Delta H_{BU}$  and  $\Delta H_{Cl}$ ) are very small, but the non-bonded counterparts tend to favor BU-Cl complexation. The substantial stabilization provided by the host-guest (both negatively charged) component is surprising, and may be ascribed to direct  $\text{C-H} \cdots \text{Cl}^-$  interactions. In summary, the association and respective enthalpy of chloride to the BU-host is, in any case, relatively weak [29, 97], because the enthalpy cost for desolvation is high when compared to larger halide ions. The release of water molecules from the cavity with the chloride inclusion is expected to result in an entropy gain. However, the reported entropy of binding has not been fully understood [29]. The loss of mobility of the guest, and the loss of conformational freedom in the host upon complexation may contribute to, at least partially, counterbalance the effect of guest desolvation. The overall trend is that the smaller is the guest, the larger is the entropic penalty of binding [29, 98]. Inclusion of the anion cancels ion-water interaction contributions, and respective effects upon the water structure [29, 98]. The molar Gibbs energy of hydration becomes more negative from iodide to fluoride in the series  $\text{I}^-$  ( $-275 \text{ kJ mol}^{-1}$ ),  $\text{Br}^-$  ( $-315 \text{ kJ mol}^{-1}$ ),  $\text{Cl}^-$  ( $-340 \text{ kJ mol}^{-1}$ ),  $\text{ClO}_4^-$  ( $-430 \text{ kJ mol}^{-1}$ ) and  $\text{F}^-$  ( $-465 \text{ kJ mol}^{-1}$ ) ions [99, 100], thus correlating with the decrease of association constants and with the

binding trends, in terms of the Hofmeister effects, found along the same series [29]. However, there is no simple relationship between the size of the anion and the entropic cost of binding, as the number and arrangement of water molecules is dependent on desolvation and also on aspects pertaining to the conformation of the inclusion complex.

## 7.6 Concluding remarks

Water soluble bambusurils can bind and isolate inorganic anions in the center of the hydrophobic cavity, with high affinity and selectivity. The ion caging ability of BUs in aqueous media was explored using MD simulations and free-energy calculations. This provided new insights on the conformation, hydration and energy changes involved in the complexation process between the water-soluble benzoyl-substituted bambus[6]uril, (BnCOOH)<sub>12</sub>BU[6], and chloride ion. The structural features of single dodecamethylbambus[6]uril (Me<sub>12</sub>BU[6]), dodecabenzylbambus[6]uril (Bn<sub>12</sub>BU[6]) and (BnCOOH)<sub>12</sub>BU[6], and the relative energy contributions to the formation of the (BnCOO)<sub>12</sub>BU[6]:Cl complex were detailed. For the latter, the estimated standard free-energy of binding and the respective binding constant were -11.7 kJ mol<sup>-1</sup> and 112, respectively. Anion binding, in water, occurred with complete desolvation of both ion and BU cavity. The ion was hermetically sealed inside the cavity, as a result of a concerted action of both conformation change and desolvation. [2] All the efforts mentioned above reflect the multitude of possibilities that can be explored with bambusurils. In fact, inclusion complexes, in which a ionic guest binds to a neutral or ionic host, can be used as the basis for building an array of interconnections yielding highly complicated, ordered, and rearrangeable structures due to the noncovalent nature of the interaction. However, "the implementation of these constructs towards tackling specific real world issues is still in its infancy" [101], and an approach based in building blocks going towards higher complexity is especially appealing. Host-guest interactions in supramolecular systems, such as those found in the functionalization of surfaces and in hydrogels, are amenable to such an approach and to the best of our knowledge, the properties of BUs and their potential in the formation of supramolecular structures have not been previously addressed in this perspective. In this context, modelling of BU-based supramolecular structures, as well as predicting their properties, become indispensable. The current challenge in the supramolecular chemistry of

bambusurils is to understand the affinity trends of these containers, with a high preference for iodide or hexafluorophosphate over other anions. This is a general pattern in the recognition of chaotropic anions [102] by macrocyclic hosts in water, a direction worth exploring computationally, for example, by studying a series  $\text{Cl}^-$ ,  $\text{Br}^-$ ,  $\text{I}^-$  by Molecular Dynamics calculations. From the theoretical perspective, computer simulations of the bambusuril systems, employing systematic approaches, are almost inexistent and are clearly useful to predict and guide future studies. The variety of possibilities related to the number and type of host and guest molecules suggests that a systematic rationalization of the inclusion complexes is most relevant. BUs suffer, with the exception of  $(\text{BnCOOH})_{12}\text{BU}$ [6], from poor aqueous solubility, thus requiring the use of organic-aqueous solvent mixtures for anion-binding investigations. It is therefore essential to predict the properties of new derivatives and the respective competition behavior in biologically and environmentally relevant aqueous media.

Energy profiles of host-guest inclusion must be established to get insight on the different interacting pairs and modes of interaction (direct host-guest interaction, host-guest interaction from functionalized chains or host-guest interactions mediated by linkers, among others). In fact, these are quite complex systems to tackle computationally. However, relevant information can be gathered from the computational study of small oligomers. Although the models are often quite simplified, effects such as the nature of the groups, type of linker, respective length and geometry can be inspected resorting for example to Molecular Dynamics, in an atomistic perspective, and Monte Carlo simulations, for a coarse-grained approach.

Bambusurils bind to ions and, naturally, can only be used as linkers in the presence of polymers substituted with negative groups. The type of charged group in the polymer must thus be explored, but the results already obtained with benzoates and tosylates [27] and phosphates [3, 28] seem to point towards the feasibility of relevant supramolecular structures.

## References

- [1] Tânia F. G. G. Cova et al. "Properties and patterns in anion-receptors: A closer look at bambusurils". *Journal of Molecular Liquids* 242.Supplement C (2017), pp. 640–652. ISSN: 0167-7322. DOI: <https://doi.org/10.1016/j.molliq.2017.07.065>.

- [2] Tânia F. G. G. Cova et al. “Bambusurils as effective ion caging agents: Does desolvation guide conformation?” *Chemical Physics Letters* 672.Supplement C (2017), pp. 89–96. ISSN: 0009-2614. DOI: <https://doi.org/10.1016/j.cplett.2017.01.029>.
- [3] Tomas Fiala et al. “Bambusuril as a One-Electron Donor for Photoinduced Electron Transfer to Methyl Viologen in Mixed Crystals”. *Journal of the American Chemical Society* 139.7 (2017), pp. 2597–2603. ISSN: 0002-7863. DOI: [10.1021/jacs.6b08589](https://doi.org/10.1021/jacs.6b08589).
- [4] Jerry L Atwood and J-M Lehn. *Comprehensive Supramolecular Chemistry*. Pergamon, 1996. ISBN: 0080427146.
- [5] J. Mendoza and Ch. Seel. “From Chloride Katapinates to Trinucleotide complexes: Developments in Molecular Recognition of Anionic Species”. *Comprehensive supramolecular chemistry*. Ed. by Jerry L Atwood and J-M Lehn. Vol. 2. 1996. Chap. 17, pp. 519–549.
- [6] Nathalie Busschaert et al. “Applications of Supramolecular Anion Recognition”. *Chemical Reviews* 115.15 (2015), pp. 8038–8155. ISSN: 0009-2665. DOI: [10.1021/acs.chemrev.5b00099](https://doi.org/10.1021/acs.chemrev.5b00099).
- [7] M. J. Langton, C. J. Serpell, and P. D. Beer. “Anion Recognition in Water: Recent Advances from a Supramolecular and Macromolecular Perspective”. *Angewandte Chemie International Edition* 55.6 (2016), pp. 1974–87. ISSN: 1521-3773 (Electronic) 1433-7851 (Linking). DOI: [10.1002/anie.201506589](https://doi.org/10.1002/anie.201506589).
- [8] L. A. Joyce, S. H. Shabbir, and E. V. Anslyn. “The uses of supramolecular chemistry in synthetic methodology development: examples of anion and neutral molecular recognition”. *Chemical Society Reviews* 39.10 (2010), pp. 3621–32. ISSN: 1460-4744 (Electronic) 0306-0012 (Linking). DOI: [10.1039/b926224p](https://doi.org/10.1039/b926224p).
- [9] Matthew J. Langton et al. “Halogen bonding in water results in enhanced anion recognition in acyclic and rotaxane hosts”. *Nature Chemistry* 6.12 (2014), pp. 1039–1043. ISSN: 1755-4330. DOI: [10.1038/nchem.2111](https://doi.org/10.1038/nchem.2111).
- [10] Matthew J. Langton and Paul D. Beer. “Rotaxane and Catenane Host Structures for Sensing Charged Guest Species”. *Accounts of Chemical Research* 47.7 (2014), pp. 1935–1949. ISSN: 0001-4842. DOI: [10.1021/ar500012a](https://doi.org/10.1021/ar500012a).

- [11] S. Kubik, C. Reyheller, and S. Stuwe. "Recognition of anions by synthetic receptors in aqueous solution". *Journal of Inclusion Phenomena and Macrocyclic Chemistry* 52.3-4 (2005), pp. 137–187. ISSN: 0923-0750. DOI: [10.1007/s10847-005-0601-6](https://doi.org/10.1007/s10847-005-0601-6).
- [12] Philip A Gale. *Anion Recognition in Supramolecular Chemistry*. Vol. 24. Springer Science & Business Media, 2010. ISBN: 3642154433.
- [13] Jeffery T. Davis et al. "Using small molecules to facilitate exchange of bicarbonate and chloride anions across liposomal membranes". *Nature Chemistry* 1.2 (2009), pp. 138–144. ISSN: 1755-4330. DOI: [10.1038/nchem.178](https://doi.org/10.1038/nchem.178).
- [14] Graeme T. Spence and Paul D. Beer. "Expanding the Scope of the Anion Templated Synthesis of Interlocked Structures". *Accounts of Chemical Research* 46.2 (2013), pp. 571–586. ISSN: 0001-4842. DOI: [10.1021/ar300264n](https://doi.org/10.1021/ar300264n).
- [15] Philip A. Gale et al. "Anion receptor chemistry: highlights from 2011 and 2012". *Chemical Society Reviews* 43.1 (2014), pp. 205–241. ISSN: 0306-0012.
- [16] Punidha Sokkalingam et al. "Binding Hydrated Anions with Hydrophobic Pockets". *Journal of the American Chemical Society* (2015). ISSN: 0002-7863.
- [17] C. L. Gibb et al. "Thermodynamic profiles of salt effects on a host-guest system: new insight into the Hofmeister effect". *The Journal of Physical Chemistry B* 119.17 (2015), pp. 5624–38. ISSN: 1520-5207 (Electronic) 1520-5207 (Linking). DOI: [10.1021/acs.jpccb.5b01708](https://doi.org/10.1021/acs.jpccb.5b01708).
- [18] Ramón Vilar. *Recognition of Anions*. Vol. 129. Structure and Bonding. Springer, 2008, p. 261. ISBN: 978-3-540-79091-4. DOI: [10.1007/978-3-540-79092-1](https://doi.org/10.1007/978-3-540-79092-1).
- [19] Y. Li and A. H. Flood. "Pure C-H hydrogen bonding to chloride ions: a preorganized and rigid macrocyclic receptor". *Angewandte Chemie International Edition* 47.14 (2008), pp. 2649–52. ISSN: 1521-3773 (Electronic) 1433-7851 (Linking). DOI: [10.1002/anie.200704717](https://doi.org/10.1002/anie.200704717).
- [20] Stefan Kubik. "Anion recognition in water". *Chemical Society Reviews* 39.10 (2010), pp. 3648–3663. ISSN: 0306-0012. DOI: [10.1039/b926166b](https://doi.org/10.1039/b926166b).
- [21] Pierangelo Metrangolo et al. "Halogen bonding in supramolecular chemistry". *Angewandte Chemie-International Edition* 47.33 (2008), pp. 6114–6127. ISSN: 1433-7851. DOI: [10.1002/anie.200800128](https://doi.org/10.1002/anie.200800128).



- [22] Julio Caballero et al. “Study of the interaction between progesterone and beta-cyclodextrin by electrochemical techniques and steered molecular dynamics”. *Journal of Physical Chemistry B* 112.33 (2008), pp. 10194–10201. ISSN: 1520-6106.
- [23] Michael G. Chudzinski, Corey A. McClary, and Mark S. Taylor. “Anion Receptors Composed of Hydrogen- and Halogen-Bond Donor Groups: Modulating Selectivity With Combinations of Distinct Noncovalent Interactions”. *Journal of the American Chemical Society* 133.27 (2011), pp. 10559–10567. ISSN: 0002-7863. DOI: [10.1021/ja202096f](https://doi.org/10.1021/ja202096f).
- [24] Valeria Amendola et al. “The Interaction of Fluoride with Fluorogenic Ureas: An ON1-OFF-ON2 Response”. *Journal of the American Chemical Society* 135.16 (2013), pp. 6345–6355. ISSN: 0002-7863. DOI: [10.1021/ja4019786](https://doi.org/10.1021/ja4019786).
- [25] Valeria Amendola et al. “Urea, Squaramide, and Sulfonamide Based Anion Receptors: A Thermodynamic Study”. *Chemistry-A European Journal* 17.21 (2011), pp. 5972–5981. ISSN: 1521-3765.
- [26] Mandeep Singh et al. “Aza-Bambusurils En Route to Anion Transporters”. *Chemistry - A European Journal* (2016), n/a–n/a. ISSN: 1521-3765. DOI: [10.1002/chem.201600343](https://doi.org/10.1002/chem.201600343).
- [27] Vaclav Havel et al. “Water-mediated inclusion of benzoates and tosylates inside the bambusuril macrocycle”. *Chemical Communications* 50.11 (2014), pp. 1372–1374. ISSN: 1359-7345. DOI: [10.1039/c3cc47828a](https://doi.org/10.1039/c3cc47828a).
- [28] Tomas Fiala and Vladimir Sindelar. “Supramolecular complexes of bambusurils with dialkyl phosphates”. *Supramolecular Chemistry* (2016), pp. 1–7. ISSN: 1061-0278. DOI: [10.1080/10610278.2016.1146278](https://doi.org/10.1080/10610278.2016.1146278).
- [29] Mirza Arfan Yawer, Vaclav Havel, and Vladimir Sindelar. “A Bambusuril Macrocycle that Binds Anions in Water with High Affinity and Selectivity”. *Angewandte Chemie-International Edition* 54.1 (2015), pp. 276–279. ISSN: 1433-7851. DOI: [10.1002/anie.201409895](https://doi.org/10.1002/anie.201409895).
- [30] Vaclav Havel et al. “Bambusurils: a New Family of Macrocyclic Anion Receptors”. *Organic Letters* 13.15 (2011), pp. 4000–4003. ISSN: 1523-7060. DOI: [10.1021/ol201515c](https://doi.org/10.1021/ol201515c).
- [31] Jan Svec, Marek Necas, and Vladimir Sindelar. “Bambus[6]uril”. *Angewandte Chemie-International Edition* 49.13 (2010), pp. 2378–2381. ISSN: 1433-7851. DOI: [10.1002/anie.201000420](https://doi.org/10.1002/anie.201000420).

- [32] Julie Rivollier, Pierre Thuery, and Marie-Pierre Heck. "Extension of the Bambus[*n*]uril Family: Microwave Synthesis and Reactivity of Allylbambus[*n*]urils". *Organic Letters* 15.3 (2013), pp. 480–483. ISSN: 1523-7060. DOI: [10.1021/ol303277u](https://doi.org/10.1021/ol303277u).
- [33] Jan Svec et al. "Anion-Free Bambus[6]uril and Its Supramolecular Properties". *Chemistry - A European Journal* 17.20 (2011), pp. 5605–5612. ISSN: 0947-6539. DOI: [10.1002/chem.201003683](https://doi.org/10.1002/chem.201003683).
- [34] Mahesh Sundararajan et al. "Elucidating the structures and binding of halide ions bound to cucurbit 6 uril, hemi-cucurbit 6 uril and bambus[6]uril using DFT calculations". *RSC Advances* 1.7 (2011), pp. 1333–1341. ISSN: 2046-2069. DOI: [10.1039/c1ra00266j](https://doi.org/10.1039/c1ra00266j).
- [35] Khaleel I. Assaf et al. "Water Structure Recovery in Chaotropic Anion Recognition: High-Affinity Binding of Dodecaborate Clusters to  $\gamma$ -Cyclodextrin". *Angewandte Chemie International Edition* 54.23 (2015), pp. 6852–6856. ISSN: 1521-3773. DOI: [10.1002/anie.201412485](https://doi.org/10.1002/anie.201412485).
- [36] Nan Zhao, Gareth O. Lloyd, and Oren A. Scherman. "Monofunctionalised cucurbit 6 uril synthesis using imidazolium host-guest complexation". *Chemical Communications* 48.25 (2012), pp. 3070–3072. ISSN: 1359-7345. DOI: [10.1039/c2cc17433b](https://doi.org/10.1039/c2cc17433b).
- [37] J. W. Lee et al. "Cucurbituril homologues and derivatives: New opportunities in supramolecular chemistry". *Accounts of Chemical Research* 36.8 (2003), pp. 621–630. ISSN: 0001-4842. DOI: [10.1021/ar020254k](https://doi.org/10.1021/ar020254k).
- [38] S. J. Barrow et al. "Cucurbituril-Based Molecular Recognition". *Chemical Reviews* 115.22 (2015), pp. 12320–406. ISSN: 1520-6890 (Electronic) 0009-2665 (Linking). DOI: [10.1021/acs.chemrev.5b00341](https://doi.org/10.1021/acs.chemrev.5b00341).
- [39] H. J. Buschmann, A. Zielesny, and E. Schollmeyer. "Hemicucurbit[6]uril a macrocyclic ligand with unusual complexing properties". *Journal of Inclusion Phenomena and Macrocyclic Chemistry* 54.3-4 (2006), pp. 181–185. ISSN: 0923-0750. DOI: [10.1007/s10847-005-6993-5](https://doi.org/10.1007/s10847-005-6993-5).
- [40] H. J. Buschmann, E. Cleve, and E. Schollmeyer. "Hemicucurbit[6]uril, a selective ligand for the complexation of anions in aqueous solution". *Inorganic Chemistry Communications* 8.1 (2005), pp. 125–127. ISSN: 1387-7003. DOI: [10.1016/j.inoche.2004.11.020](https://doi.org/10.1016/j.inoche.2004.11.020).

- [41] Y. Miyahara et al. "Remarkably facile ring-size control in macrocyclization: Synthesis of hemicucurbit 6 uril and hemicucurbit 12 uril". *Angewandte Chemie-International Edition* 43.38 (2004), pp. 5019–5022. ISSN: 1433-7851. DOI: [10.1002/anie.200460764](https://doi.org/10.1002/anie.200460764).
- [42] Riina Aav et al. "New Chiral Cyclohexylhemicucurbit[6]uril". *Organic Letters* 15.14 (2013), pp. 3786–3789. ISSN: 1523-7060. DOI: [10.1021/ol401766a](https://doi.org/10.1021/ol401766a).
- [43] Von Heinrich Rheiraeck. "Ueber das Verhalten des Allantoïns zu Natrium". *Annalen der Chemie und Pharmacie* 134.2 (1865), pp. 219–228. ISSN: 0075461710990690. DOI: [10.1002/jlac.18651340209](https://doi.org/10.1002/jlac.18651340209).
- [44] Marek Stancl, Zuzana Gargulakova, and Vladimir Sindelar. "Glycoluril Dimer Isomerization under Aqueous Acidic Conditions Related to Cucurbituril Formation". *The Journal of Organic Chemistry* 77.23 (2012), pp. 10945–10948. ISSN: 0022-3263. DOI: [10.1021/jo302063j](https://doi.org/10.1021/jo302063j).
- [45] Robert Behrend, Eberhard Meyer, and Franz Rusche. "I. Ueber Condensationsproducte aus Glycoluril und Formaldehyd". *Justus Liebigs Annalen der Chemie* 339.1 (1905), pp. 1–37. ISSN: 1099-0690. DOI: [10.1002/jlac.19053390102](https://doi.org/10.1002/jlac.19053390102).
- [46] A. E. Rowan, Jaaw Elemans, and R. J. M. Nolte. "Molecular and supramolecular objects from glycoluril". *Accounts of Chemical Research* 32.12 (1999), pp. 995–1006. ISSN: 0001-4842. DOI: [10.1021/ar9702684](https://doi.org/10.1021/ar9702684).
- [47] P. Cintas. "Cucurbiuril - Supramolecular perspectives for an old ligand". *Journal of Inclusion Phenomena and Molecular Recognition in Chemistry* 17.3 (1994), pp. 205–220. ISSN: 0923-0750. DOI: [10.1007/bf00708781](https://doi.org/10.1007/bf00708781).
- [48] Jaaw Elemans, A. E. Rowan, and R. J. M. Nolte. "Self-assembled architectures from glycoluril". *Industrial & Engineering Chemistry Research* 39.10 (2000), pp. 3419–3428. ISSN: 0888-5885. DOI: [10.1021/ie000079g](https://doi.org/10.1021/ie000079g).
- [49] P. A. Gale, S. E. Garcia-Garrido, and J. Garric. "Anion receptors based on organic frameworks: highlights from 2005 and 2006". *Chemical Society Reviews* 37.1 (2008), pp. 151–190. ISSN: 0306-0012. DOI: [10.1039/b715825d](https://doi.org/10.1039/b715825d).
- [50] Micke Lisbjerg et al. "Discovery of a cyclic 6+6 hexamer of D-biotin and formaldehyde". *Chemical Science* 5.7 (2014), pp. 2647–2650. ISSN: 2041-6520. DOI: [10.1039/c4sc00990h](https://doi.org/10.1039/c4sc00990h).

- [51] R. P. Sijbesma and R. J. M. Nolte. "MOLECULAR CLIPS AND CAGES DERIVED FROM GLYCOLURIL". *Supramolecular Chemistry II - Host Design and Molecular Recognition* 175 (1995), pp. 25–56. ISSN: 0342-6793.
- [52] L. Isaacs. "Cucurbit[n]urils: from mechanism to structure and function". *Chemical Communications* 6 (2009), pp. 619–29. ISSN: 1359-7345 (Print) 1359-7345 (Linking). DOI: [10.1039/b814897j](https://doi.org/10.1039/b814897j).
- [53] L. Isaacs. "The Mechanism of Cucurbituril Formation". *Israel Journal of Chemistry* 51.5-6 (2011), pp. 578–591. ISSN: 0021-2148. DOI: [10.1002/ijch.201100022](https://doi.org/10.1002/ijch.201100022).
- [54] Wei-Hao Huang, Peter Y. Zavalij, and Lyle Isaacs. "Cucurbit[n]uril formation proceeds by step-growth cyclo-oligomerization". *Journal of the American Chemical Society* 130.26 (2008), pp. 8446–8454. ISSN: 0002-7863. DOI: [10.1021/ja8013693](https://doi.org/10.1021/ja8013693).
- [55] K. Jansen et al. "Glycoluril derivatives as precursors in the preparation of substituted cucurbit[n]urils". *Designed Monomers and Polymers* 6.1 (2003), pp. 43–55. ISSN: 1385-772X. DOI: [Doi10.1163/156855503321127529](https://doi.org/10.1163/156855503321127529).
- [56] Derick Lucas and Lyle Isaacs. "Recognition Properties of Acyclic Glycoluril Oligomers". *Organic Letters* 13.15 (2011), pp. 4112–4115. ISSN: 1523-7060. DOI: [10.1021/ol201636q](https://doi.org/10.1021/ol201636q).
- [57] A. Chakraborty et al. "Diastereoselective formation of glycoluril dimers: Isomerization mechanism and implications for cucurbit[n]uril synthesis". *Journal of the American Chemical Society* 124.28 (2002), pp. 8297–8306. ISSN: 0002-7863. DOI: [10.1021/ja025876f](https://doi.org/10.1021/ja025876f).
- [58] A. X. Wu et al. "Methylene-bridged glycoluril dimers: Synthetic methods". *Journal of Organic Chemistry* 67.16 (2002), pp. 5817–5830. ISSN: 0022-3263. DOI: [10.1021/jo0258958](https://doi.org/10.1021/jo0258958).
- [59] Wei-Hao Huang, Peter Y. Zavalij, and Lyle Isaacs. "Metal-Ion-Induced Folding and Dimerization of a Glycoluril Decamer in Water". *Organic Letters* 11.17 (2009), pp. 3918–3921. ISSN: 1523-7060. DOI: [10.1021/ol901539q](https://doi.org/10.1021/ol901539q).
- [60] Y. Cotellet et al. "Fused Glycoluril-Tetrathiafulvalene Molecular Clips as Receptors for Neutral Electron Acceptor Guests". *Organic Letters* 16.10 (2014), pp. 2590–2593. ISSN: 1523-7060. DOI: [10.1021/ol500458e](https://doi.org/10.1021/ol500458e).

- [61] Yoann Cotellet et al. "Glycoluril-tetrathiafulvalene molecular clips: on the influence of electronic and spatial properties for binding neutral accepting guests". *Beilstein Journal of Organic Chemistry* 11 (2015), pp. 1023–1036. ISSN: 1860-5397. DOI: [10.3762/bjoc.11.115](https://doi.org/10.3762/bjoc.11.115).
- [62] L. Isaacs. "Stimuli responsive systems constructed using cucurbit[n]uril-type molecular containers". *Accounts of Chemical Research* 47.7 (2014), pp. 2052–62. ISSN: 1520-4898 (Electronic) 0001-4842 (Linking). DOI: [10.1021/ar500075g](https://doi.org/10.1021/ar500075g).
- [63] J. G. Wang et al. "Dimeric packing of molecular clips induced by interactions between pi-systems". *Crystengcomm* 17.12 (2015), pp. 2486–2495. ISSN: 1466-8033. DOI: [10.1039/c4ce02447h](https://doi.org/10.1039/c4ce02447h).
- [64] F. Gharakhani et al. "The interaction energies between glycoluril clip and thiophenol derivatives using density functional theory calculations". *Journal of Sulfur Chemistry* 36.4 (2015), pp. 351–357. ISSN: 1741-5993. DOI: [10.1080/17415993.2015.1028941](https://doi.org/10.1080/17415993.2015.1028941).
- [65] J. G. Wang et al. "X-ray studies of conformation: observation of conformational polymorphism of a glycoluril clip". *Crystengcomm* 17.11 (2015), pp. 2245–2249. ISSN: 1466-8033. DOI: [10.1039/c5ce00066a](https://doi.org/10.1039/c5ce00066a).
- [66] D. Ajami and J. Rebek. "Reversibly Expanded Encapsulation Complexes". *Chemistry of Nanocontainers*. Ed. by M. Albrecht and F. E. Hahn. Vol. 319. Topics in Current Chemistry. Berlin: Springer-Verlag Berlin, 2012, pp. 57–78. ISBN: 978-3-642-28059-7. DOI: [10.1007/128\\_2011\\_290](https://doi.org/10.1007/128_2011_290).
- [67] R. P. Sijbesma et al. "Binding features of molecular clips derived from diphenylglycoluril". *Journal of the American Chemical Society* 115.20 (1993), pp. 8999–9005. ISSN: 0002-7863. DOI: [10.1021/ja00073a015](https://doi.org/10.1021/ja00073a015).
- [68] Galina A. Gazieva and Angelina N. Kravchenko. "Unexpected Formation of Thioglycolurils Precursors". *Journal of Heterocyclic Chemistry* 52.6 (2015), pp. 1858–1863. ISSN: 0022-152X. DOI: [10.1002/jhet.2305](https://doi.org/10.1002/jhet.2305).
- [69] Ningqiang Zhang et al. "Research Progress of Cucurbit(n)uril Application". *Progress in Chemistry* 27.2-3 (2015), pp. 192–211. ISSN: 1005-281X. DOI: [10.7536/pc140910](https://doi.org/10.7536/pc140910).

- [70] Ephrath Solel et al. “Enhanced anion binding by heteroatom replacement in bambusurils”. *Physical Chemistry Chemical Physics* 18.19 (2016), pp. 13180–13185. ISSN: 1463-9076. DOI: [10.1039/C6CP00442C](https://doi.org/10.1039/C6CP00442C).
- [71] Mandeep Singh et al. “Dual-Functional Semithiobambusurils”. *Chemistry - A European Journal* 21.2 (2015), pp. 536–540. ISSN: 0947-6539. DOI: [10.1002/chem.201404210](https://doi.org/10.1002/chem.201404210).
- [72] R. Vilar. “Anion recognition and templation in coordination chemistry”. *European Journal of Inorganic Chemistry* 3 (2008), pp. 357–367. ISSN: 1434-1948. DOI: [10.1002/ejic.200701017](https://doi.org/10.1002/ejic.200701017).
- [73] Helen T. Chifotides and Kim R. Dunbar. “Anion- $\pi$  Interactions in Supramolecular Architectures”. *Accounts of Chemical Research* 46.4 (2013), pp. 894–906. ISSN: 0001-4842. DOI: [10.1021/ar300251k](https://doi.org/10.1021/ar300251k).
- [74] Agnes Revesz et al. “Anion Binding by Bambus[6]uril Probed in the Gas Phase and in Solution”. *Journal of Physical Chemistry A* 115.41 (2011), pp. 11378–11386. ISSN: 1089-5639. DOI: [10.1021/jp205218k](https://doi.org/10.1021/jp205218k).
- [75] Petr Toman, Emanuel Makrlik, and Petr Vanura. “Theoretical study on the protonation of bambus[6]uril”. *Monatshefte Fur Chemie* 143.3 (2012), pp. 373–376. ISSN: 0026-9247. DOI: [10.1007/s00706-011-0682-4](https://doi.org/10.1007/s00706-011-0682-4).
- [76] Petr Toman, Emanuel Makrlik, and Petr Vanura. “Bambus[6]uril as a ditopic ion-pair molecular receptor for Cs<sup>+</sup>I<sup>-</sup>”. *Monatshefte Fur Chemie* 143.10 (2012), pp. 1365–1368. ISSN: 0026-9247. DOI: [10.1007/s00706-012-0806-5](https://doi.org/10.1007/s00706-012-0806-5).
- [77] Emanuel Makrlik, Petr Toman, and Petr Vanura. “Bambus[6]uril as a novel example of a ditopic ion-pair molecular receptor for sodium iodide”. *Monatshefte Fur Chemie* 145.5 (2014), pp. 721–724. ISSN: 0026-9247. DOI: [10.1007/s00706-014-1154-4](https://doi.org/10.1007/s00706-014-1154-4).
- [78] Petr Toman, Emanuel Makrlik, and Petr Vanura. “Theoretical study on the complexation of bambus[6]uril with the cyanate and thiocyanate anions”. *Monatshefte Fur Chemie* 143.7 (2012), pp. 985–988. ISSN: 0026-9247. DOI: [10.1007/s00706-012-0748-y](https://doi.org/10.1007/s00706-012-0748-y).
- [79] Emanuel Makrlik, Petr Toman, and Petr Vanura. “Theoretical study on the complexation of bambus[6]uril with the hydrogen sulfide anion”. *Monatshefte Fur Chemie* 145.6 (2014), pp. 877–879. ISSN: 0026-9247. DOI: [10.1007/s00706-014-1161-5](https://doi.org/10.1007/s00706-014-1161-5).

- [80] Vaclav Havel, Mirza Arfan Yawer, and Vladimir Sindelar. “Real-time analysis of multiple anion mixtures in aqueous media using a single receptor”. *Chemical Communications* 51.22 (2015), pp. 4666–4669. ISSN: 1359-7345. DOI: [10.1039/c4cc10108a](https://doi.org/10.1039/c4cc10108a).
- [81] S. Lee, C. H. Chen, and A. H. Flood. “A pentagonal cyanostar macrocycle with cyanostilbene CH donors binds anions and forms dialkylphosphate 3 rotaxanes”. *Nature Chemistry* 5.8 (2013), pp. 704–710. ISSN: 1755-4330. DOI: [10.1038/nchem.1668](https://doi.org/10.1038/nchem.1668).
- [82] Y. D. Yang et al. “Multicomponent Self-Assembled Metal-Organic[3]Rotaxanes”. *Journal of the American Chemical Society* 137.40 (2015), pp. 12966–76. ISSN: 1520-5126 (Electronic) 0002-7863 (Linking). DOI: [10.1021/jacs.5b07308](https://doi.org/10.1021/jacs.5b07308).
- [83] Vaclav Havel and Vladimir Sindelar. “Anion Binding Inside a Bambus[6]uril Macrocycle in Chloroform”. *Chempluschem* 80.11 (2015), pp. 1601–1606. ISSN: 2192-6506. DOI: [10.1002/cplu.201500345](https://doi.org/10.1002/cplu.201500345).
- [84] Micke Lisbjerg et al. “Anion binding by biotin[6]uril in water”. *Organic & Biomolecular Chemistry* 13.2 (2015), pp. 369–373. ISSN: 1477-0520. DOI: [10.1039/c4ob02211d](https://doi.org/10.1039/c4ob02211d).
- [85] J. Kang, J. H. Jo, and S. In. “Carboxylate anion selective receptor with glycoluril molecular scaffold”. *Tetrahedron Letters* 45.27 (2004), pp. 5225–5228. ISSN: 0040-4039. DOI: [10.1016/j.tetlet.2004.05.040](https://doi.org/10.1016/j.tetlet.2004.05.040).
- [86] J. M. Kang, H. K. Ju, and J. H. Jo. “A new anion receptor with a glycoluril molecular scaffold”. *Supramolecular Chemistry* 16.3 (2004), pp. 175–179. ISSN: 1061-0278. DOI: [10.1080/10610270310001633754](https://doi.org/10.1080/10610270310001633754).
- [87] H. Kim, S. In, and J. M. Kang. “Anion receptor with two imidazolium rings on the glycoluril”. *Supramolecular Chemistry* 18.2 (2006), pp. 141–145. ISSN: 1061-0278. DOI: [10.1080/10610270600564702](https://doi.org/10.1080/10610270600564702).
- [88] J. Kang, S. In, and S. J. Cho. “Anion receptors with glycoluril molecular scaffold”. *Supramolecular Chemistry* 19.4-5 (2007), pp. 243–249. ISSN: 1061-0278. DOI: [10.1080/10610270701358491](https://doi.org/10.1080/10610270701358491).
- [89] Micke Lisbjerg et al. “Biotin[6]uril Esters: Chloride-Selective Transmembrane Anion Carriers Employing C–H···Anion Interactions”. *Journal of the American Chemical Society* 137.15 (2015), pp. 4948–4951. ISSN: 0002-7863. DOI: [10.1021/jacs.5b02306](https://doi.org/10.1021/jacs.5b02306).

- [90] Frank Biedermann, Werner M. Nau, and Hans-Joerg Schneider. “The Hydrophobic Effect Revisited-Studies with Supramolecular Complexes Imply High-Energy Water as a Noncovalent Driving Force”. *Angewandte Chemie-International Edition* 53.42 (2014), pp. 11158–11171. ISSN: 1433-7851. DOI: [10.1002/anie.201310958](https://doi.org/10.1002/anie.201310958).
- [91] A. Jakalian et al. “Fast, efficient generation of high-quality atomic Charges. AM1-BCC model: I. Method”. *Journal of Computational Chemistry* 21.2 (2000), pp. 132–146. ISSN: 0192-8651. DOI: [10.1002/\(Sici\)1096-987x\(20000130\)21:2<132::Aid-Jcc5>3.3.Co;2-G](https://doi.org/10.1002/(Sici)1096-987x(20000130)21:2<132::Aid-Jcc5>3.3.Co;2-G).
- [92] A. Jakalian, D. B. Jack, and C. I. Bayly. “Fast, efficient generation of high-quality atomic charges. AM1-BCC model: II. Parameterization and validation”. *Journal of Computational Chemistry* 23.16 (2002), pp. 1623–1641. ISSN: 0192-8651.
- [93] U. Essmann et al. “A Smooth Particle Mesh Ewald Method”. *Journal of Chemical Physics* 103.19 (1995), pp. 8577–8593. ISSN: 0021-9606. DOI: [10.1063/1.470117](https://doi.org/10.1063/1.470117).
- [94] B. Hess et al. “LINCS: A linear constraint solver for molecular simulations”. *Journal of Computational Chemistry* 18.12 (1997), pp. 1463–1472. ISSN: 0192-8651.
- [95] X. Daura et al. “Peptide folding: When simulation meets experiment”. *Angewandte Chemie-International Edition* 38.1-2 (1999), pp. 236–240. ISSN: 1433-7851.
- [96] Haiyang Zhang et al. “Quantification of Solvent Contribution to the Stability of Noncovalent Complexes”. *Journal of Chemical Theory and Computation* 9.10 (2013), pp. 4542–4551. ISSN: 1549-9618. DOI: [10.1021/ct400404q](https://doi.org/10.1021/ct400404q).
- [97] R. Behrend, E. Meyer, and F. Rusche. “Condensates of glycoluril and formaldehyde”. *Justus Liebigs Annalen Der Chemie* 339.1/3 (1905), pp. 1–37. ISSN: 0075-4617.
- [98] Dor Ben-Amotz and Robin Underwood. “Unraveling water’s entropic mysteries: A unified view of nonpolar, polar, and ionic hydration”. *Accounts of Chemical Research* 41.8 (2008), pp. 957–967. ISSN: 0001-4842. DOI: [10.1021/ar7001478](https://doi.org/10.1021/ar7001478).
- [99] Y. Marcus. “Thermodynamics of solvation of ions.5. Gibbs free-energy of hydration at 298.15 K”. *Journal of the Chemical Society-Faraday Transactions* 87.18 (1991), pp. 2995–2999. ISSN: 0956-5000. DOI: [10.1039/ft9918702995](https://doi.org/10.1039/ft9918702995).
- [100] Y. Marcus. *Ion Properties*. 1st. New York, 1997.



- [101] Shereen Tan et al. “Cyclodextrin-Based Supramolecular Assemblies and Hydrogels: Recent Advances and Future Perspectives”. *Macromolecular Rapid Communications* 35.13 (2014), pp. 1166–1184. ISSN: 1022-1336. DOI: [10.1002/marc.201400080](https://doi.org/10.1002/marc.201400080).
- [102] K. I. Assaf et al. “Water Structure Recovery in Chaotropic Anion Recognition: High-Affinity Binding of Dodecaborate Clusters to gamma-Cyclodextrin”. *Angewandte Chemie International Edition* 54.23 (2015), pp. 6852–6. ISSN: 1521-3773 (Electronic) 1433-7851 (Linking). DOI: [10.1002/anie.201412485](https://doi.org/10.1002/anie.201412485).

# Chapter 8

## Conclusions and Future Prospects

Calculation of binding free-energies through molecular dynamics simulations still represents an intricate computational challenge due to the mathematical complexity of solvated macromolecular systems, often consisting of myriads of atoms. Simulations contribute to the understanding of these complex systems by providing a complementary molecular or atomistic view, which is in general not accessible in experiments. The use of inclusion complexes as building blocks for supramolecular structures/materials provides an important and convenient way for constructing targeted controlled-release drug delivery systems.

Host and guest molecules are selected as models of common building blocks for obtaining higher order structures. The necessity to explain the function of cyclodextrins in all details arises from their multiple applications. The increasing interest in Cd as hosts is explained by their superior affinity towards amphiphilic guests, distinct role as drug carriers and multifunctional character in polymeric drug delivery systems. Bambusurils are also explored due to their recent discovery as transporters and anion receptors, and to their poorly exploited host-guest properties.

The selected guests are practical molecular examples and leading structures of an extensive series of promising therapeutic agents, acting also as model building blocks in supramolecular systems for basic chemical and pharmaceutical applications. Robust and accurate MD based methods, including umbrella-sampling and the cylindrical approximation for the calculation of binding constants in this type of systems, provide new information that is correlated with available experimental observations. Accurate predictions are now available from MD, including the effect of variations in guest substituents and of the available volume in the host cavity.

Complexation of the model guests is sensitive to alterations in the basic backbone and in the available cavity volume, as the fit variations into the host cavity have a direct impact on the respective binding constants.

In summary, the designed computational procedure allows exploring the underlying factors affecting the formation of supramolecular structures based on host-guest associations and is successfully applied to different systems with potential to be used in drug delivery technologies.

The effect of different imposed features on the stability of inclusion complexes between cyclodextrins, bambusurils and several guests is thus investigated in terms of structural, mechanistic and thermodynamic aspects. These have direct implication in guest encapsulation and release from host molecules and include substitution, size, conformation, orientation, flexibility, fit and contact, solvation, and energy.

For a proper estimation of the binding constants, substituent effects must be taken into account even if these substitutions do not appear to geometrically affect inclusion. This may also be relevant in supramolecular systems, in which a common guest group/moiety may coexist with different spacers or polymers, as in the case of systems containing polymeric networks. Additionally, the estimate of the inclusion thermodynamic signatures and binding constants must be complemented with information on the enthalpy penalty associated to distorted host structures, in order to obtain a reliable description of the binding process.

Cd aggregation is also investigated. Several conflicting evidence arise from experiment, requiring a deep explanation of the involved phenomena.

The design of advanced materials based on host-guest complexes is thus a challenging and ingenious proving-ground, from both the academic and commercial points of view. Several approaches are currently introduced to produce Cd derivatives with improved properties that can be applied in different scenarios. However, the broad range of properties and specificities for different target molecules, such as drugs, ensures that one specific type of host and polymer will not always be suitable of effectively interacting and releasing specific molecules, thus requiring new molecular candidates. Comprehensive rationales of the involved interaction mechanisms from computation are still much needed. This means that substantial efforts involving chemical-physics and synthetic organic chemistry, must be combined with work on materials design and characterization, and drug delivery for obtaining prod-

ucts that make a change. Molecular simulations, including free-energy calculations is still a fertile ground for research, from both theoretical and applied perspectives. Among the various challenges in the field of free-energy calculations, the integration of thermodynamics and kinetics through the concomitant determination of potentials of mean force and diffusivities in biased simulations, will benefit from substantial efforts. There is a general consensus that free-energy calculations are an important tool of computational chemistry and structural biology, but some concerns still remain outside academia, mainly dealing with the question of whether or not such methods provide convincing, reliable, useful answers.

The work described in this dissertation is to be expanded with the use of in-house synthesized compounds, with different characteristics, so that both experimental and theoretical, computational, data can be collected and contrasted. This will include terpenes of variable size and cross section, acting as guests for Cds. Larger supramolecular networks, comprising assembled hydrogels, will also be modeled resorting to coarse-grained approaches in which variations in the polymers and "connectors" will be tested. Charge, rigidity, among others, are parameters to be tested in the effect they have on the transient network.

Work on other hosts, including amphiphilic cyclodextrins and cucurbiturils, is also a natural extension of the present work, now taking into account 1:2 (host:guest) stoichiometry, so as to assess the possibility of using these compounds for noncovalent reticulation and surface functionalization. The latter will also be addressed by coarse-grain methods, which implies the development of interaction potentials of high selectivity, so as to model host-guest interactions of different stoichiometry. More specifically, experimental development resorting to lipid nanoparticles including the above surface modification will be complemented with molecular simulations. The objective is to design, optimize and test a system which allows the delivery of up to three anticancer drugs directly at tumor sites. The setup is indeed complex, allowing the prediction of a wide range of structural and thermodynamic properties which can be used to improve the design of the targeted lipid nanoparticles, while promoting non-covalently tunable surfaces with high drug loading capacity and efficiency, tumor selectivity, and an efficient delivery of drugs. Combining three drugs with three different mechanisms in a single nanoparticle is conceptually simple, and can be achieved using green chemistry and sustainable

strategies, i.e. without elaborated synthetic steps or the use of organic solvents. The multi-functional lipid nanoparticle characteristics will be achieved by loading complementary drugs in the nanoparticle core, and by surface modification through threading of hosts, acting as mediators between the nanoparticle surface and the inhibitors for checkpoint targets. The computational results have direct implications in the rational design of the targeted nanoparticles involving host-guest interactions towards the optimal formulation. The selection, *in silico*, of the optimal components and procedures, and of the most stable complexes are ensured by molecular simulations, including PMF calculations and binding affinity estimates. The associations of the nanoparticle components are governed by electrostatics and noncovalent interactions. The most adequate components correspond to those for which the association constants are, in relative terms, the highest possible. These are the basis for the success of the surface modification. These efforts will enable designing and testing this innovative vehicle, increasing the value of the co-encapsulated drugs and the therapeutic efficacy.

*"Let me tell you the secret that has led me to my goal. My strength lies solely in my tenacity. Whether our efforts are, or not, favored by life, let us be able to say, when we come near to the great goal, I have done what I could!"*  
*(Louis Pasteur)*